LASER IONISATION SPECTROSCOPY OF ALKALIS

- APPLICATIONS TO RESONANCE IONISATION MASS SPECTROMETRY

Michael Henry Charles Smyth

Department of Physics and Astronomy

University of Glasgow

ProQuest Number: 10998032

ProQuest 10998032

Published by ProQuest LLC (2018). Copyright of the Dissertation is held by the Author.

ProQuest LLC.
789 East Eisenhower Parkway
P.O. Box 1346
Ann Arbor, MI 48106 – 1346

Acknowledgements

Publications

Wavelength dependence of laser induced ionisation in proportional counters.

K.W.D. Ledingham, C. Raine, K.M. Smith, M.H.C. Smyth, D.T. Stewart, M.Towrie and C.M. Houston

Nucl. Instr. and Meth. <u>A241</u> (1985) 441

Detection of phenol in proportional counter gas by two photon ionisation spectroscopy

M. Towrie, J.W. Cahill, K.W.D. Ledingham, C. Raine, K.M. Smith, M.H.C. Smyth, D.T. Stewart and C.M. Houston

J. Phys. B., Atomic and Molecular Physics <u>19</u> (1986) 1989

Detection of toluene in proportional counter gas by two photon ionisation spectroscopy

S.L.T. Drysdale, K.W.D. Ledingham, C. Raine, K.M. Smith, M.H.C. Smyth, D.T. Stewart, M.Towrie and C.M. Houston

Nucl. Inst. and Meth. <u>A252</u> (1986) 521

Detection of caesium atoms by two photon resonance ionisation spectroscopy

K.W.D. Ledingham, C. Raine, K.M. Smith, M.H.C. Smyth, D.T. Stewart, M.Towrie and C.M. Houston

Proceedings SPIE - Int. Soc. Opt. Eng.

("Laser Applications in Chemistry and Biophysics") 620 (1986)

Investigation of the effect of gas purification on the background laser ionisation in proportional counters

S.L.T. Drysdale, A.P. Land, K.W.D. Ledingham, C. Raine, K.M. Smith, M.H.C. Smyth, D.T. Stewart, M.Towrie and C.M. Houston

ALEPH 86-30   (distr. TPCC-AL) (1986)

Applications of resonant ionisation spectroscopy to accelerator based high energy physics

K.W.D. Ledingham, J.W. Cahill, S.L.T. Drysdale, C. Raine, K.M. Smith, M.H.C. Smyth, D.T. Stewart, M.Towrie and C.M. Houston

"Resonance Ionisation Spectroscopy 1986" Inst. Phys. Conf. Ser. No. 84

Multiphoton transitions in caesium vapour

C.M. Houston, S.L.T. Drysdale, K.W.D. Ledingham, C. Raine, K.M. Smith, M.H.C. Smyth, D.T. Stewart, M.Towrie

"Resonance Ionisation Spectroscopy 1986" Inst. Phys. Conf. Ser. No. 84

Potential of resonant ionisation mass spectroscopy for detecting environmentally important radioactive nuclides

M.H.C. Smyth, S.L.T. Drysdale, R. Jennings, K.W.D. Ledingham, D.T. Stewart, M.Towrie, C.M. Houston, M.S. Baxter, R.D. Scott

"Resonance Ionisation Spectroscopy 1986" Inst. Phys. Conf. Ser. No. 84

Two and three photon ionisation transitions in caesium vapour

C.M. Houston, S.L.T. Drysdale, R. Jennings, A.P. Land, K.W.D. Ledingham, R.P. Singhal, M.H.C. Smyth, D.T. Stewart, M.Towrie

(1988) to be published

The Glasgow resonant ionisation mass spectrometer

M.Towrie, S.L.T. Drysdale, R. Jennings, A.P. Land, K.W.D. Ledingham, P.T. McCombes, R.P. Singhal, M.H.C. Smyth, D.T. Stewart, C.M. Houston, C.J. McLean

Proc. 4th. Int. Symposium on Resonance Ionisation Spectroscopy and Applications 1988, (to be published)

Molecular and collisional processes during three photon ionisation transitions in caesium and rubidium vapours.

M.H.C. Smyth, S.L.T. Drysdale, R. Jennings, A.P. Land, K.W.D. Ledingham, R.P. Singhal, D.T. Stewart, M.Towrie, C.M. Houston

Proc. 4th. Int. Symposium on Resonance Ionisation Spectroscopy and Applications 1988, (to be published)

Application of resonant ionisation mass spectroscopy to depth profiling in III - V
semiconductor devices

C.J. McLean, J.H. Marsh, J.W. Cahill, S.L.T. Drysdale, R. Jennings, A.P. Land, K.W.D.
Ledingham, P.T. McCombes, R.P. Singhal, M.H.C. Smyth, D.T. Stewart, M.Towrie,
Proc. 4th. Int. Symposium on Resonance Ionisation Spectroscopy and Applications1988,
(to be published)

CONTENTS

SUMMARY

Resonance ionisation spectroscopy (RIS) at Glasgow University began as a result of the need to calibrate large gas-filled multiwire proportional counters (MWPCs) currently being built at CERN, specifically the ALEPH time projection chamber.

From this work the direction shifted towards the development of laser ionisation as an analytical tool, with the design of two resonance ionisation time of flight mass spectrometers. The two instruments have slightly different remits. One is particularly suited to surface analysis, the other to trace element detection.

The work outlined in this thesis was intended to help in the design of these time of flight mass spectrometers, by highlighting difficulties likely to be encountered in the resonant ionisation and detection of small numbers of atoms.

In order to prove the potential of resonance ionisation, and also to gain experience in the experimental techniques applicable to resonance ionisation mass spectrometry, initial experiments were carried out on elemental caesium and rubidium in a simple proportional counter.

Chapter 1 outlines the basic theory behind the resonance ionisation technique, and shows its wide applicability to elemental ionisation and detection. A brief historical outline of previous experimental and theoretical work on resonance ionisation traces the development of RIS as an analytical tool, leading to the design and construction of a resonance ionisation time of flight mass spectrometer at Glasgow.

Chapter 2 is a brief description of some of the theoretical aspects of resonance ionisation. A simple population rate equation model is used to derive expressions for the ion yields for a two level atom as a function of atomic and laser parameters. A semi-classical model of the atom-radiation interaction is given, leading to the model of Rabi oscillations between electronic states in an intense laser field. Transitions involving more than one photon are qualitatively described.

The laser systems used for resonance ionisation are described in chapter 3, along with the ion detectors used. Descriptions of the proportional counter, and quadrupole and

time of flight mass spectrometers are given. Chapter 3 concludes with a discussion of the reasoning behind the decision to use caesium and rubidium for the initial experiments with these detectors.

Chapter 4 begins with a brief survey of previous work on the resonance ionisation of alkali metals. The electronic structure of atomic and molecular caesium and rubidium is summarised, and energy level diagrams for these systems are presented.

Experimental work conducted at Glasgow to investigate the background ionisation in proportional counters is reported in chapter 5. These results were deemed important in that they suggested that, at wavelengths below 300 nm, the ionisation of organic impurities in proportional counters, or any ionisation spectrometer, could swamp the resonant ionisation signal of interest, particularly at trace concentration levels. The ionisation of these impurities might therefore be a limiting factor to the sensitivity of resonance ionisation at these UV wavelengths. Two impurities were identified in the proportional counter, phenol and toluene. The origin of phenol was traced to plastic piping used to introduce the buffer gas to the proportional counter. The origin of toluene was not determined.

Chapter 6 reports on the resonance ionisation spectroscopy of caesium and rubidium. Early work concentrated on using a specially designed proportional counter, which was both robust and free from contaminants. One and two photon transitions were investigated. The collisional enhancement of the ionisation of photoexcited Rydberg levels was investigated using a simple model of the process. The proportional counter was also incorporated into a quadrupole mass spectrometer for an early attempt at the resonant ionisation mass spectroscopy of atomic and molecular rubidium.

With the completion of the construction of the time of flight mass spectrometer, the experimental work switched to this instrument. Preliminary results are presented in chapter 7. These have mainly been obtained to date, (due to technical difficulties with the ion gun), with a fairly simple technique of pulsed laser ablation/ionisation of a sample, ions being formed in the ablation process itself and by the nonresonant ionisation of ablated neutrals. Not surprisingly the selectivity of this process is limited although resonant transitions can be distinguished. A brief calculation of the projected sensitivity of the instrument, when operating in its normal mode of pulsed ion bombardment with resonant ionisation, is also presented, and ways in which the

sensitivity may be increased are explored.

The conclusion draws together the results from the work with the proportional counter/quadrupole mass spectrometer, and suggests future experiments, both spectroscopic and analytical, which could be carried out in this instrument, with the addition of a low temperature oven to atomise samples. Experiments could be done to investigate the collisional ionisation of highly excited states, search for autoionisation states in multielectron atoms, investigate the potential of field ionisation as a substitute for photoionisation and also determine the validity of population rate equations to describe resonance ionisation.

Experiments to determine the sensitivity of the time of flight mass spectrometer will shortly be conducted. This instrument promises to revolutionise the detection of trace elements, particularly in surface analysis.

CHAPTER 1

INTRODUCTION

The field of laser induced resonant ionisation is fairly new and expanding fast, primarily due to its proven application in the detection of very small numbers of atoms and molecules. Resonant ionisation is also becoming a spectroscopic technique in its own right. The development of the tunable dye laser marked the beginning of the surge in interest in resonant ionisation, and it has been the ongoing refinements to tunable lasers that has enabled the field itself to expand.

1.1 RESONANT AND NONRESONANT IONISATION

The basic concepts behind the resonant ionisation of atoms (or molecules) are straightforward. Atoms of a particular element have unique bound energy levels and a continuum of unbound energy levels as illustrated in figure 1.1. If the energy of an incident photon is equal to the energy difference between, for example, the ground state of an atom and a higher bound energy state, an electronic transition may occur between these two states. Further transitions from the first excited level to even higher excited levels can occur if further photons of the right energy are incident on the excited atom. Eventually a transition is made into a continuum state and the atom is ionised. This is referred to as resonant ionisation. If the energy of the photon(s) is not equal to the energy separation of the discreet levels in the atom, the probability that the atom will be ionised is considerably reduced. This is non-resonant ionisation, figure 1.2. Since the energy levels of an atom are unique to that element (and to an isotope of that element) the photon energy required to resonantly ionise one particular species of atom will only be sufficient to nonresonantly ionise any other species of atom. It is the large difference between the resonant and nonresonant ionisation probabilities that is the basis of this technique.

From simple population rate equations, described in chapter 2, it can be shown that in order to saturate a typical two photon resonant ionisation process, ie. every irradiated atom is ionised, the photon flux density of laser beam must be of the order 10^{23} photons cm^{-2} sec^{-1}. Conventional monochromatic light sources have photon
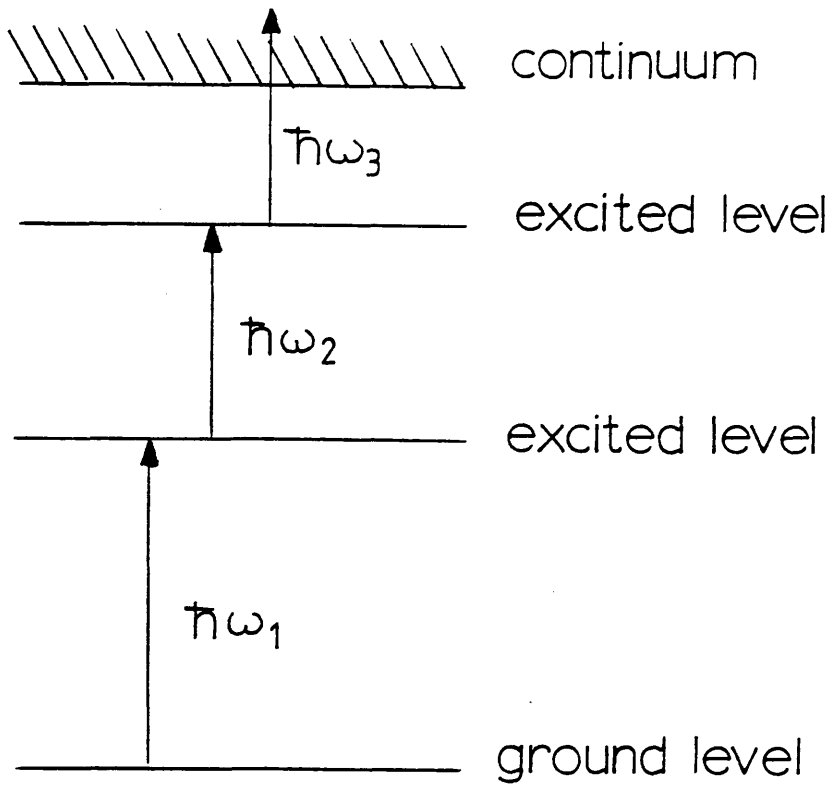
Fig 1.1   Three photon resonant ionisation via two real intermediate levels
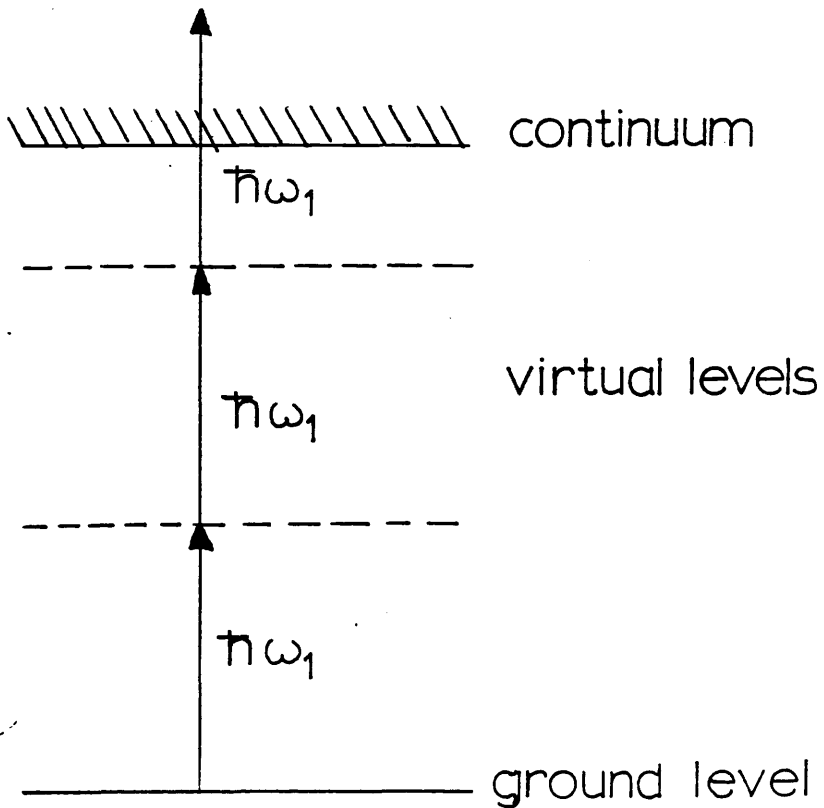
Fig 1.2   Three photon nonresonant ionisation via two virtual levels.

flux densities of the order 10^{16} photons cm^{-2} sec^{-1}, whilst pulsed lasers can deliver pulses of light of the order 10^{28} photons cm^{-2} sec^{-1} and can easily saturate a two photon resonant ionisation process. Pulsed dye lasers are therefore commonly used in resonant ionisation spectroscopy.

Figure 1.3a (1) illustrates the simplest example of resonant ionisation using two photons of the same energy from the one laser. This two step process (excitation step plus ionisation step) requires the intermediate excited state to be more than half-way to the continuum. The maximum photon energy that commercially available dye lasers can produce is about 4 eV so that two step resonant ionisation with one laser is only suitable for atoms with low ionisation potentials around 8 eV. Frequency doubling crystals increase the range of atoms that can be resonantly ionised, figure 1.3a (2).

For atoms with higher ionisation potentials, two or more excitation steps can be used as illustrated in figure 1.3a (3). This process requires two or more independently tunable dye lasers.

An alternative to using real intermediate states is to use virtual states. This technique, as well as increasing the energy difference between the coupled states, also permits electric dipole forbidden transitions, figure 1.3a (5).

Hurst et al (1979b) has listed five basic schemes using just two lasers (figure 1.3a) which enable almost all the elements in the periodic table to be resonantly ionised, figure 1.3b. The notable exceptions are helium and neon which have very high ionisation potentials, and in which the energy difference between the ground state and the first excited state is very large.

1.2 APPLICATIONS OF RESONANCE IONISATION

The spectroscopy of atoms and molecules has been given an extra impetus with the introduction of tunable lasers. Basic spectroscopic research is essential for an understanding of the structure of atoms and molecules. Apart from the pure spectroscopy, resonance ionisation allied to mass analysis has applications in almost any field requiring the detection of small numbers of selected atoms or molecules. In fundamental science this has led to its proposed use in detecting solar neutrinos and the

1. ω_1 ω_1

2. ω_1 $2\omega_1$

3. ω_1, ω_2 ω_2 ω_1

4. ω_1, ω_2 ω_2 $2\omega_1$

5. ω_1 ω_1 virtual level ω_1
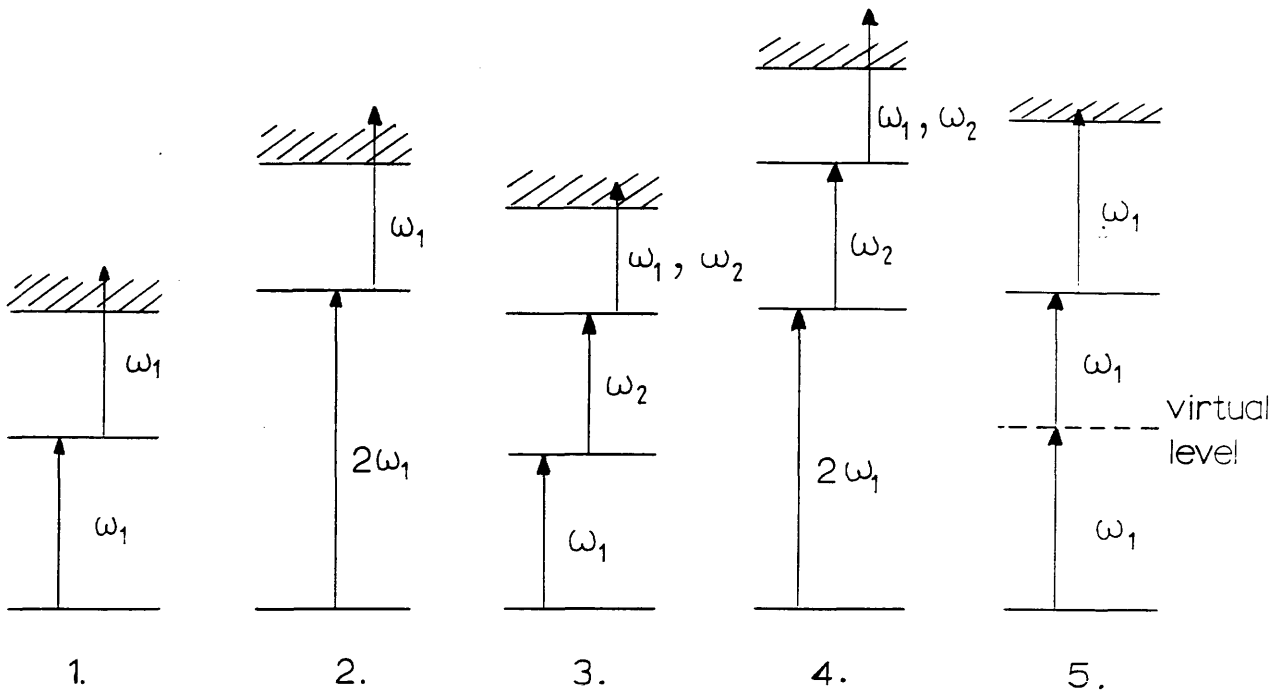
Fig 1.3a Five resonant ionisation schemes using two tunable lasers proposed by Hurst (1979b)

symbol ———— Cs
1 —— RIS scheme

H																	He
5																	
Li	Be											B	C	N	O	F	Ne
2	4											4	5	5	5	5	
Na	Mg											Al	Si	P	S	Cl	Ar
2	3											1	4	5	5	5	5
K	Ca	Sc	Ti	V	Cr	Mn	Fe	Co	Ni	Cu	Zn	Ga	Ge	As	Se	Br	Kr
1	2	2	2	2	2	2	2	2	2	4	4	1	1	5	5	5	5
Rb	Sr	Y	Zr	Nb	Mo	Tc	Ru	Rh	Pd	Ag	Cd	In	Sn	Sb	Te	I	Xe
1	2	3	3	2	2	3	2	2	4	4	4	1	2	4	4	5	5
Cs	Ba	La	Hf	Ta	W	Re	Os	Ir	Pt	Au	Hg	Tl	Pb	Bi	Po	At	Rn
1	2	1	3?	3	3	2	3	3	4	4	4	1	4	4	4	5?	5
Fr	Ra	Ac															
1?	2	3?															

Ce	Pr	Nd	Pm	Sm	Eu	Gd	Tb	Dy	Ho	Er	Tm	Yb	Lu
1	1	1	1?	1	2	1	1	1	1	1	1	2	1
Th	Pa	U	Np	Pu	Am	Cm	Bk	Cf	Es	Fm	Md	No	Lw
		2	1	1	2	1	1	2					

Fig 1.3b Elements which can be ionised using the five schemes. Only helium and neon are excluded.

half-lives of double beta decay, (Chen et al 1980), and naturally ocurring radioisotopes (Moore et al 1985). In applied science the same techniques are being harnessed towards detecting impurities in semiconductors (Bekov et al 1983a), trace elements in biological tissue (Fassett et al 1984b) and radioactive nuclides in the waste from nuclear power stations (Kronert et al 1985, Peuser et al 1985).

LASER IONISATION STUDIES AT GLASGOW UNIVERSITY

Initial research at Glasgow was based around proportional counter detectors. These can be extremely sensitive, are cheap and simple to build and are ideal for ionisation spectroscopy of volatile atoms and molecules. Work concentrated on identifying impurities in proportional counter gas and on determining suitable seeding agents for the purpose of the laser calibration of large multiwire proportional counters at CERN, (Towrie 1987). At the completion of this research it was decided to build a time of flight mass spectrometer, specially designed for resonant ionisation and capable of trace analysis using small samples. Subsequent work has been geared towards that goal.

Preliminary work was concerned with the two and three photon resonant ionisation spectroscopy of caesium vapour. Spectroscopy is essential to the development of RIMS as an analytical tool. It must be used to determine the relative strengths of resonant transitions, the most suitable laser line widths and powers and for determining the energies of autoionisation states in the continuum, if these are to be used to increase the photoionisation cross-section.

Caesium was chosen because its physical properties made it particularly suitable for detection in proportional counters, and because it was felt that detection of the radionuclide isotope ^{135}Cs was of significance to the nuclear power industry (Houston 1986).

My own work carried on the studies with caesium vapour and extended it to the resonant ionisation of rubidium vapour, also in the proportional counter. Rubidium, with two naturally occuring isotopes, lends itself to mass analysis and this was carried out using a quadrupole mass spectrometer. This work progressed to the resonant ionisation of rubidium in the newly built time of flight mass spectrometer. Some early results from this instrument are reported.

6

1.3 HISTORICAL BACKGROUND

This short section attempts to give a brief historical outline of the experimental and theoretical work that has been of influence in the design of the resonant ionisation time of flight mass spectrometer at Glasgow. An outline of some of the early work on the resonant ionisation spectroscopy of alkali metals is given in chapter 4.

PRE-1970's

The advent of powerful Q-switched ruby lasers led to the observation of noble gas breakdown at the focal point of such lasers, (Meyerand 1963,1964, Voronov 1965). Keldysh (1965), Gold and Bebb (1965) and Bebb and Gold (1966) proposed that the initial step in this breakdown was due to multiphoton ionisation of neutral noble gas atoms in the focal volume of the laser pulse. This simultaneous absorption of two photons was first proposed by Goppart-Mayer (1931). Bebb extended his analysis to the two photon ionisation (Bebb 1966) and three photon ionisation (Bebb 1967) of the alkali atoms. Further experimental work on the multiphoton ionisation of hydrogen and the rare gases was carried out by Agostini et al (1968).

RESONANT IONISATION

The introduction of tunable lasers and in particular tunable organic dye lasers marked the beginning of laser ionisation spectroscopy. Resonant ionisation was first reported by Ambartsumyan et al (1971). Using a tunable dye laser pumped by a Q-switched ruby laser they were able to ionise rubidium atoms with two photons, the first step being the $5s_{1/2}$-$5p_{3/2}$ transition. The extension of this technique to molecules was also demonstrated and the more general use of resonant ionisation to selectively ionise atoms and molecules of particular species was noted, (Ambartusumyan et al 1972). The use of an electric field to ionise high lying Rydberg levels of sodium, a technique that effectively increases the ionisation cross-section, was investigated (Ambartsumyan et al 1975). Saturation of the two photon resonant ionisation of helium atoms was demonstrated by Hurst et al (1975), who also coined the phrase Resonance Ionisation Spectroscopy (RIS).

SINGLE ATOM DETECTION

The full potential of the RIS process was demonstrated by Hurst et al (1977) who was able to detect a single caesium atom in a proportional counter. This was extended to detecting a single molecule of caesium iodide by photodissociation of the molecule and saturated resonant ionisation of the caesium atom, (Grossman et al 1977). A more sophisticated resonant ionisation scheme was used by Bekov et al (1978a) in the single atom detection of ytterbium. Using three dye lasers they resonantly excited the ground state atom to a high lying rydberg level which was then field ionised. The elimination of the laser ionisation step effectively reduced the laser power required to saturate the process. The single atom detection of sodium using two excitation steps plus field ionisation was also demonstrated by Bekov et al (1978b).

The widespread applicability of laser induced resonant ionisation to experiments requiring extreme sensitivity was outlined by Hurst et al (1979b). Hurst et al (1979a) also outlined the experimental conditions which would be needed to saturate the process, and reviewed some experiments which demonstrated this. A more recent review of the experimental techniques involved in single atom detection has also been written, (Letokov 1987).

RESONANCE IONISATION MASS SPECTROMETRY (RIMS).

The potential of resonant ionisation of selected atoms coupled with mass analysis was recognised very early in the development of the field. This was probably due to the prospect it held of a cheaper method of separating isotopes to provide fuel for nuclear reactors.

Early work using mass spectrometers in conjunction with resonant ionisation were concerned with molecules and easily ionised atoms, (Antonov et al 1978, Zandee et al 1978, Zandee et al 1979, Boesl et al 1980).

The feasability of a time of flight instrument for the mass analysis was discussed by Beekman et al (1980). Boesl et al (1980) was already using this technique in the ionisation of polyatomic molecules and went on to improve the mass resolution of his instrument by including an electrostatic ion mirror, (Boesl et al 1982). Miller et al

(1982) used resonance ionisation coupled with a magnetic sector mass spectrometer for high precision ratio measurements of lutetium in the presence of ytterbium. Similar work was conducted by Donohue et al (1982).

TRACE ELEMENT DETECTION USING RIMS

The single atom detection capabilities of the resonance ionisation technique together with high transmission mass spectrometers enables the detection of small numbers of selected atoms. When applied to trace element detection this enables the use of smaller samples and/or shorter counting times. The actual method by which trace analysis is attempted using RIMS can vary but involves similar steps; the sample must be vapourised, the neutral atoms resonantly ionised, and the ions mass separated. The design of the mass spectrometer at Glasgow has centred on vapourising the sample using a pulsed ion gun, resonant ionisation by two pulsed dye lasers and time of flight mass analysis, (Towrie et al 1988). This arrangement is essentially similar to a conventional secondary ionisation mass specrometer (SIMS) instrument, but with resonant ionisation of the sputtered neutrals.

Winograd et al (1982) demonstrated the resonant ionisation of neutral atoms sputtered from a solid sample using a high energy argon ion beam. A detection limit of around 1 part per billion was claimed for this arrangement using currently available low repetition rate (30 Hz) lasers and ion sources, Kimock et al (1984). A similar technique but using a magnetic sector mass spectrometer instead of a time of flight instrument was reported by Parks et al (1983) and a detection efficiency of 2 ppb sensitivity was claimed, (Parks et al 1985).

Trace analysis using thermal atomisation from a high temperature filament has also been extensively used. This has been combined with a magnetic sector mass analyser for isotope ratio measurements, Donohue et al (1982), Moore et al (1984, 1985), Fassett et al (1983). Pulsed thermal sources have been used to improve the duty cycle of this technique, Donohue (1984), Fassett (1984a).

An electrothermal graphite atomiser with a time of flight mass analyser has been used extensively for trace analysis at the Institute of Spectroscopy in the USSR, (Bekov et al 1983b, 1985, 1986).

Other methods of increasing the duty cycle have been tried using continuous wave lasers, (Cannon et al 1985, Miller et al 1985), and high repetition copper vapour lasers, (Peuser et al 1985, Kronert et al 1985, Bekov et al 1986).

TRACE ELEMENT DETECTION USING NONRESONANT IONISATION

The use of nonresonant ionisation using a high powered UV laser pulse as a method of trace element detection is also under investigation, (Becker et al 1984, 1985). The advantage of non-resonant ionisation is that a rapid analysis of vapourised atoms can be carried out fairly cheaply using just a single UV laser. However the elemental selectivity of resonant ionisation is lost.

Young et al (1987) has compared the useful ion yields obtainable from these two different techniques, resonant and non resonant ionisation of ion sputtered neutrals.

CHAPTER 2

THEORY

2.1 POPULATION RATE EQUATIONS

INTRODUCTION

Modelling resonant ionisation with population rate equations enables an overall picture of the process to be presented simply and clearly. The inter-relationships between the competing processes of absorption, emission and ionisation, and the dependence of these on the laser parameters can be obtained quite easily. It is also useful for obtaining the conditions necessary to saturate the process whereby every irradiated atom is ionised.

However this model does not give any explanation as to how the global terms used, such as the absorption cross-section, relate to more fundamental physical terms. A quantum mechanical approach is needed for that. It is also invalid for coherent incident light since it assumes that the laser pulse is made up of a superposition of plane waves of random phases, and that there is no interference between the waves. Nevertheless for pulsed lasers with a bandwidth Δv_L the coherence time is approximately $1/\Delta v_L$, which may be very short compared to the pulse length. Typical dye lasers have a bandwidth of ~ 1 cm^{-1} corresponding to a coherence time of $\sim 10^{-11}$ sec. If the overall ionisation process is on a time scale long compared to the coherence time, the effects of the coherence will be small and rate equations will apply, (Kliger 1983)

TWO LEVEL ATOM WITH PHOTOIONISATION FROM THE SECOND LEVEL

Using the example of a two-level atom, (figure 2.1) with the second level connected to the continuum, and with non-radiative relaxation from the second level which does not end at the first level, the rate equations for the three levels can be written down.

$$\frac{dN_0}{dt} = -\sigma_a \Phi N_0 + \Gamma N_1 + \sigma_s \Phi N_1 \qquad (2\cdot1)$$

$$\frac{dN_1}{dt} = \sigma_a \Phi N_0 - \Gamma N_1 - \sigma_s \Phi N_1 - \beta N_1 - \sigma_i \Phi N_1 \qquad (2\cdot2)$$

$$\frac{dN_i}{dt} = \sigma_i \Phi N_1 \qquad (2\cdot3)$$

N_0 = population of level 0 , N_1= population of level 1 , N_i = number of ionised atoms

Φ = photon flux (number of photons cm^{-2} sec^{-1})

σ_a = stimulated absorption cross-section , σ_s = stimulated emission cross-section

σ_i = ionisation cross-section from level 1 to continuum

β = rate of non radiative decay from level 1 not ending on level 0

Γ = spontaneous decay rate from level 1 to 0

The model assumes that the bandwidth of the laser is broader than the frequency width of the stimulated transitions. The coupled rate equations can be solved to give the population of the intermediate N_1 level and the ion yield N_i , at the end of the laser pulse of length T, which has a top hat profile.

$$N_1 = \frac{N_0(0)\ \sigma_a \Phi}{\alpha_2 - \alpha_1} \left[e^{-\alpha_1 t} - e^{-\alpha_2 t} \right] \qquad (2\cdot4)$$

$$\alpha_{1,2} = \frac{k}{2} \pm \frac{1}{2}\sqrt{k^2 - 4\omega^2} \qquad (2\cdot5)$$

$$k = \Gamma + \beta + \Phi(\sigma_a + \sigma_s + \sigma_i) \quad , \quad \omega^2 = \left[\sigma_a \Phi(\beta + \sigma_i \Phi)\right]$$

$$(2\cdot6a,b)$$
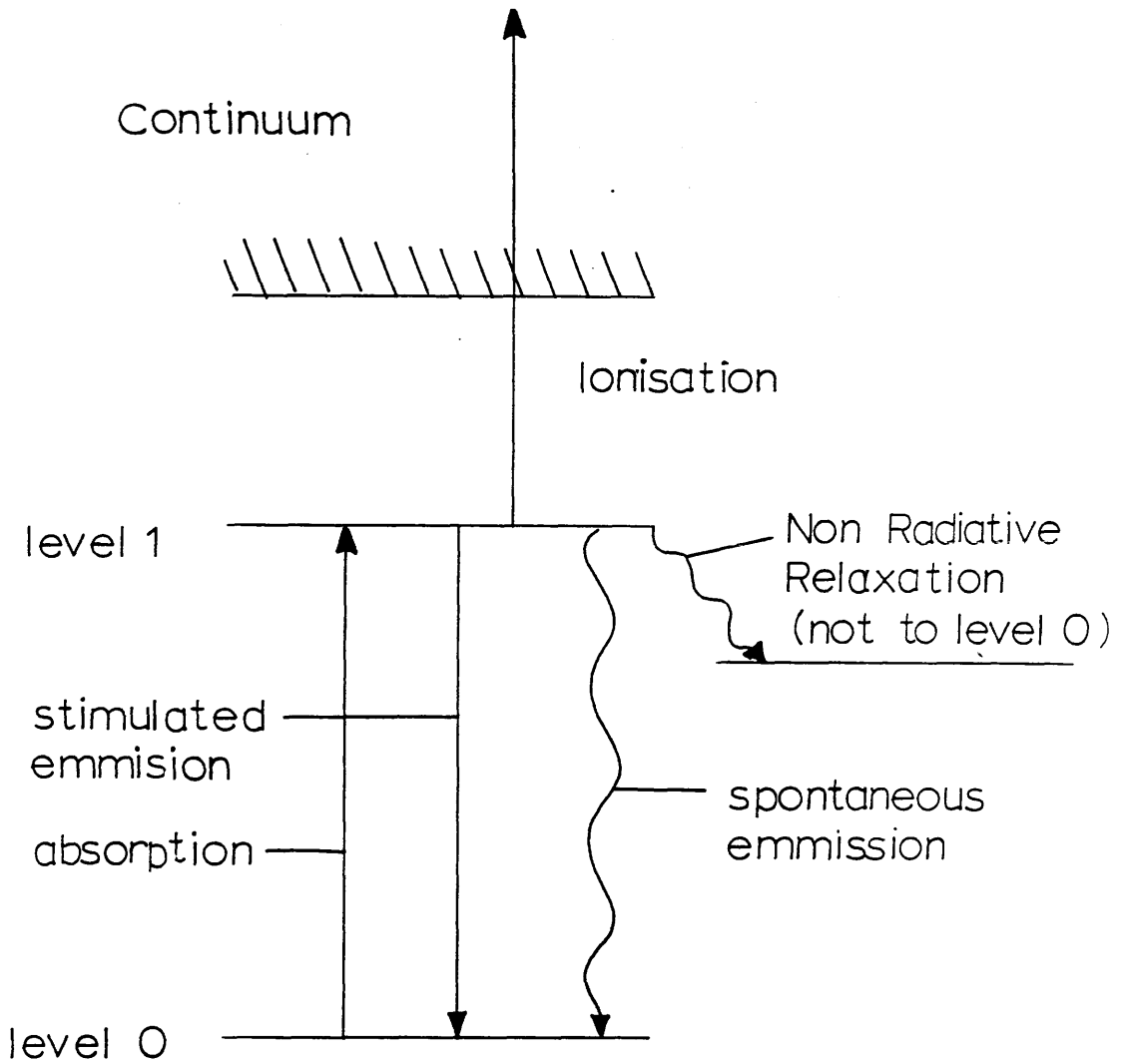
Fig 2.1   Population rate equation model of the two level atom, with ionisation
from the second level.

In order to simplify the equations some assumptions can be made. If the levels are nondegenerate then generally, on resonance, and with the band width of the laser not too large, the cross-sections for absorption and emission will be of similar magitude, and they will both be much larger than the ionisation cross-section, (Hurst et al 1979a).

$$\sigma_a \sim \sigma_s >> \sigma_i \qquad (2\cdot7)$$

If the rate of ionisation is large compared to the non-radiative relaxation rate, $\sigma_i \Phi >> \beta$, and the rate of excitation from level 0 to 1 is large compared to the spontaneous decay rate Γ from 1 to 0, $\sigma_a \Phi >> \Gamma$, then the population of level 1 is,

$$N_1 = \frac{N_0(0)\,\sigma_a \Phi}{\alpha_1} \left[\, e^{-\alpha_2 t} \,\right] \qquad (2\cdot8)$$

and the number of ions is,

$$N_i = \int_{pulselength,\ T} N_1 \sigma_i \Phi \ dt = N_0(0) \qquad (2\cdot9)$$

At the end of the laser pulse T all the irradiated atoms in the state 0 have become ionised.

This is the definition of saturation and is achieved provided,

$$\sigma_i \Phi T \gg 1 \ , \quad \sigma_a \Phi \gg \Gamma \ \text{and} \ \sigma_i \Phi \gg \beta \qquad (2\cdot10a,b,c)$$

The fluence condition $\sigma_i \Phi T >> 1$ is usually the most difficult to meet. Typical values for the terms are, $\sigma_a = \sigma_s = 10^{-14} \ cm^2$, $\sigma_i = 10^{-17} \ cm^2$, $\Gamma = 10^8 \ sec^{-1}$, $\beta = 10^6 \ sec^{-1}$. If the laser has a pulse length of 10 nsec then in order to saturate the ionisation process it must have a fluence $> 1/\sigma_i = 4 \times 10^{-3} \ J \ cm^{-2}$. In general, with pulsed lasers, when the fluence is sufficent to saturate the ionisation step the flux is many times larger than that required to saturate the excitation step.

Fron the original expression for the population of the excited level, N_1, and using conditions $\sigma_a \sim \sigma_s \gg \sigma_i$ and $\sigma_i \Phi \gg \beta$,

$$N_i = \frac{N_0(0)\,\sigma_i \sigma_a \Phi^2}{\alpha_1^2}\left[\,\frac{\alpha_1}{\alpha_2}\{\,1 - e^{-\alpha_2 t}\} - \{\,1 - e^{-\alpha_1 t}\}\,\right]\qquad(2\cdot11)$$

If the fluence is not large enough to saturate the ionisation step, $\sigma_i \Phi T \gg 1$, and if the relaxation rate is negligible compared to the spontaneous decay rate, $\Gamma \gg \beta$, this equation simplifies to,

$$N_i = \frac{N_0(0)}{4\sigma_a}\,\frac{(2\,\sigma_a\phi)^2}{(2\,\sigma_a\phi + \Gamma T)^2}\,\left[\,\Gamma T + 2\sigma_a\phi - 1 + e^{-(\Gamma T + 2\sigma_a\phi)}\,\right]$$

$$(2\cdot12)$$

where $\phi = \Phi T = $ photon fluence (number of photons per cm^2)

At light levels well below those required for saturation, the dependence of the ion yield on laser flux will vary according to whether, over the pulse length T, the spontaneous decay rate from level 1 to 0 is greater or less than the excitation rate from 0 to 1.

LONG PULSE LENGTH

If the pulse length is long compared to the intermediate state life-time, $\Gamma T \gg 1$, and the rate of excitation is less than the spontaneous decay rate, $\sigma_a \Phi \ll \Gamma$, the ionisation yield is,

$$N_i = N_0(0)\,\sigma_i \sigma_a \Phi^2\,\frac{T}{\Gamma}\qquad(2\cdot13)$$

If the excitation step is saturated, $\sigma_a \Phi \gg \Gamma$, then the ion yield becomes,

$$N_i = \frac{1}{2}N_0(0)\,\sigma_i \Phi\,T\qquad(2\cdot14)$$

As the intensity of the light is increased the yield changes from being quadratically dependent on the laser flux to a linear dependence on the laser fluence.

If the pulse length is short compared to the intermediate state lifetime, $\Gamma T \ll 1$, and the excitation step is not saturated, $\sigma_a \Phi \ll \Gamma$, then the ion yield is,

$$N_i = \frac{1}{2} N_0(0) \; \sigma_a \sigma_i \; \Phi^2 T^2 \qquad\qquad (2 \cdot 15)$$

If the excitation is saturated $\sigma_a \Phi \gg \Gamma$,

$$N_i = \frac{1}{2} N_0(0) \; \sigma_i \; \Phi \; T \qquad\qquad (2 \cdot 16)$$

As the laser power is increased the dependence changes from quadratic in fluence to linear in fluence. This is illustrated in figure 2.2 below which plots the ratio of the ion and excited state populations to the initial ground state population, N_i/N_0 and N_1/N_0, against the incident photon flux Φ.

This approach can be extended to any number of intermediate levels, amd more realistic laser parameters such as a Gaussian beam profile, and spectral profile can be included, (Ackerhalt et al 1976, Singhal et al 1988c). Population rate equations have also been applied to molecular systems, (Zakheim 1980).

2.2 SEMICLASSICAL ATOMIC TRANSITIONS

INTRODUCTION

In order to see how induced absorption and emission cross-sections can be calculated for particular atoms a semi-classical model of the two level atom can be used. Under the influence of a weak EM field the transition can be viewed as a small perturbation of the stationary states of the atom, and first order perturbation theory can be applied. An expression for the induced absorption cross section of the atom can then be derived which is related to well defined physical constants and to the wave functions describing the two electronic states of the atom. These wavefunctions give an exact description of the hydrogen atom and approximate descriptions of multielectron atoms.
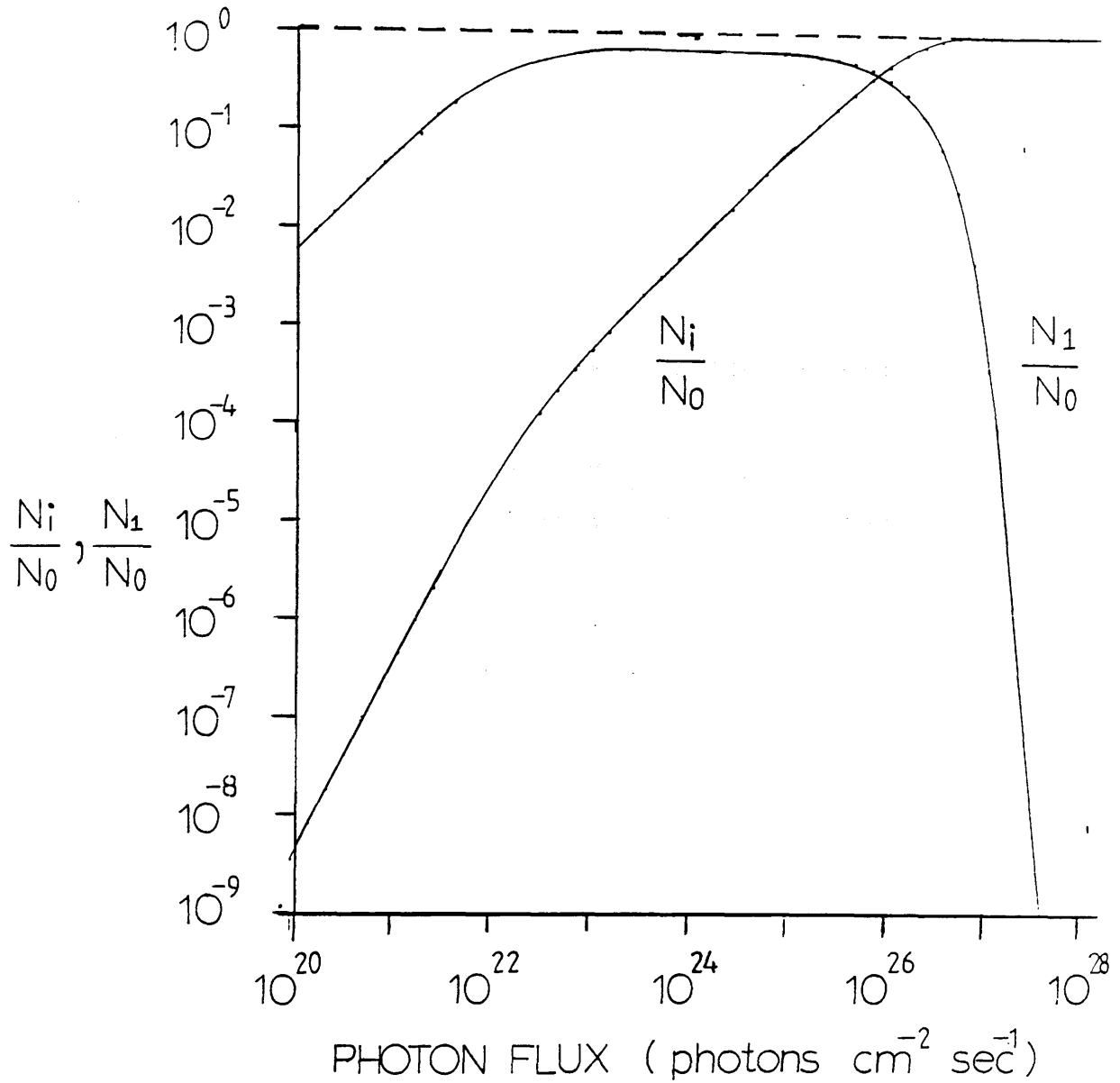
Fig 2.2   Dependence of ion and excited state populations on the incident photon flux from the population rate equation model.

The interaction between light and an atom introduces a time dependent element into the field free stationary electronic wave functions which can be viewed as a small perturbation. The Hamiltonian expressing the total energy of the atom in the field, H, can then be split up into a time independent part of the field-free atom, H_0, and the time dependent part of the atom-field interaction, H_i

$$H = H_0 + H_i \qquad (2 \cdot 17)$$

This Hamiltonian will be a solution to Schrodingers time dependent wave equation

$$H \Psi = i\hbar \, d(\Psi)/dt \qquad (2 \cdot 18)$$

The time dependent wave function Ψ can be built up from the stationary states of the unperturbed atom

$$\Psi(r,t) = \Sigma \, c_n(t) \, \psi_n(r) \, \exp[-iE_n t] \qquad (2 \cdot 19)$$

where $\psi_n(r)$ is an eigenfunction of the atom satisfying the time independent Schrodinger equation,

$$H_0 \, \psi_n(r) = E_n \, \psi_n(r) \qquad (2 \cdot 20)$$

and E_n is the eigenvalue for this eigenfunction. The exponential term is a time dependent phase factor. The coefficients $c_n(t)$ are time dependent and are related to the probability of finding the atom in any of the states $\psi_n(r)$. In a two level atom with stationary states $\Psi_1(r)$ and $\Psi_2(r)$, the time dependent wave function is,

$$\Psi(r,t) = c_1(t) \Psi_1(r) + c_2(t) \Psi_2(r) \qquad (2 \cdot 21)$$

and, if the wavefunction of the atom is normalised in a box of volume V,

$$|\Psi(r,t)|^2 = |c_1(t)|^2 + |c_2(t)|^2 = 1 \qquad (2 \cdot 22)$$

The values of $|c_1(t)|^2$ and $|c_2(t)|^2$ are the probabilities of finding the atom in states $\Psi_1(r)$ and $\Psi_2(r)$ respectively. These coefficients will evolve with time and can be used to calculate the rates of transition between the states.

Using the classical picture of light interacting with a quantum mechanical atom gives exactly the same expression for the rate of transition as the full quantum mechanical treatment for the interaction. However, the spontaneous decay of a level, which proceeds

naturally from the quantisation of the field, must be added on to the semi-classical model in an ad-hoc fashion.

The electric and magnetic fields of an electromagnetic wave can be described in terms of the vector and scalar potentials $\underline{A}$ and ϕ respectively.

$$\underline{E} = -\nabla\phi - \frac{d}{dt}(\underline{A}) \qquad (2\cdot23)$$

$$\underline{B} = \text{curl } \underline{A} \qquad (2\cdot24)$$

In the Coulomb gauge these potentials can have further constraints applied

$$\underline{\nabla} \cdot \underline{A} = 0 \qquad (2\cdot25)$$

In this gauge a monochromatic plane wave of frequency ω satisfying Maxwells wave equations will have solutions of the form:

$$\underline{A}(\underline{r}, \omega t) = \underline{A}_0(\omega)[e^{i(\omega t - \underline{k}\cdot\underline{r})} + e^{-i(\omega t + \underline{k}\cdot\underline{r})}] \qquad (2\cdot26)$$

where $\underline{k}$ is a propagation vector satisfying $\omega = kc$, and $\underline{A}_0(\omega)$ is a vector describing the amplitude of the wave and its polarisation. The electric and magnetic fields associated with the wave will have expressions using equations 2.23 and 2.24,

$$\underline{E} = 2\omega \underline{A}_0(\omega)\sin(\omega t - \underline{k}\cdot\underline{r}) \qquad (2\cdot27)$$

$$\underline{B} = 2(\underline{k} \cdot \underline{A}_0(\omega))\sin(\omega t - \underline{k}\cdot\underline{r}) \qquad (2\cdot28)$$

The energy density of this wave per unit angular frequency averaged over one cycle is

$$\rho(\omega) = 2\varepsilon_0\omega^2 \underline{A}_0^2(\omega) \qquad (2\cdot29)$$

The Hamiltonian describing the energy of an electron in an atom of charge Ze interacting with an EM wave is

$$\frac{1}{2m}[\underline{P} + e\underline{A}^2] + e\phi - \frac{Ze^2}{4\pi\varepsilon_0|\underline{r}|} \qquad (2\cdot30)$$

where the spin of the electron and the interaction between the nucleus and the field has been ignored and there are no reduced mass effects. The Schrodinger time dependent wave equation is therefore,

$$i\hbar\frac{d}{dt}[\Psi(\underline{r},t)] = [\frac{P^2}{2m} + \frac{e^2A^2}{2m} + \frac{\underline{P}\cdot e\underline{A}}{2m} + \frac{e\underline{A}\cdot\underline{P}}{2m} - \frac{Ze^2}{4\pi\varepsilon_0 r}]\Psi(\underline{r},t) \qquad (2\cdot31)$$

P is the momentum of the electron of mass m and the nucleus has charge Ze. In the Coulomb gauge $\phi = 0$.

Using the gauge condition (equation 2.25) div $\underline{A} = 0$ this may be rewritten,

$$i\hbar\frac{d}{dt}[\Psi(\underline{r},t)] = [\ H_o + H_i\ ]\ \Psi(\underline{r},t) \qquad (2\cdot32)$$

$$H_o = \frac{P^2}{2m} - \frac{Ze^2}{4\pi\varepsilon_o r} \qquad (2\cdot33)$$

$$H_i = \frac{e\underline{A}\cdot\underline{P}}{m} \qquad (2\cdot34)$$

This can be seen as a splitting up of the Hamiltonian into a time independent part H_0 and a time dependent part H_i. The term quadratic in A has been ignored since the applied field is assumed to be weak and only single photon processes are to be considered.

Putting the expressions for the time dependent wave function (equation 2.19) into Schrodingers wave equation (equation 2.32) gives,

$$i\hbar\frac{d}{dt}[\ \sum_n c_n(t)\ \psi_n(\underline{r})\ \exp\{\frac{-iE_n t}{\hbar}\}\ ] = [\ H_0 + \lambda H_i]\Psi_n(\underline{r},t) \qquad (2\cdot35)$$

If the perturbation is weak the coefficients can be expanded in powers of λ

$$c_n(t) = c_n^{(0)}(t) + \lambda c_n^{(1)}(t) + \lambda^2 c_n^{(2)}(t) + \ldots\ldots \qquad (2\cdot36)$$

The rate equation (2.35) can then be split up into terms corresponding to these expansions by equating equal powers of λ. Multiplying (2.35) from the left by $\psi_b^*(r)\exp(iE_b t/\hbar)$, integrating over all space, and using

$$\int_{vol} \psi_n^*(\underline{r})\ \psi_m(\underline{r})\ dv\ \begin{array}{l} = 0 \quad, n \neq m \\ = 1 \quad, n = m \end{array} \qquad (2\cdot37)$$

the first two terms of the rate equation (2.35) are,

$$i\hbar\frac{d}{dt}[c_b^{(0)}(t)] = 0 \qquad (2\cdot38)$$

$$i\hbar\frac{d}{dt}[c_b^{(1)}(t)] = \sum_n c_n^{(0)}(t)\exp[\frac{i(E_b - E_n)t}{\hbar}]\int_{vol}\psi_b^*(\underline{r})H_i\psi_n(\underline{r})d\underline{r} \qquad (2\cdot39)$$

The zeroth term states that the initial coefficents $c_n^{(0)}(t)$ are time independent.

If at time t=0 the atom was initially in state $\psi_a(r)$ with energy E_a, then $c_a^{(0)}(t) = 1$ and the first order rate equation is,

$$i\hbar\frac{d}{dt}[c_b^{(1)}(t)] = e^{i\omega_0 t} \langle b| H_i | a\rangle \qquad (2\cdot40)$$

where $\hbar\omega_0 = E_b - E_a$ and $\int_{vol}\psi_b^*(r)H_i\psi_a(r)\,dr = \langle b|H_i|a\rangle$

$$(2\cdot41),(2\cdot42)$$

If the interaction term H_i is now introduced (2.34),

$$i\hbar\frac{d}{dt}[c_b^{(1)}(t)] = e^{i\omega_0 t} \langle b| \frac{e}{m} \underline{A}.\underline{P} | a\rangle \qquad (2\cdot43)$$

then with plane polarised light and the vector $\underline{A}$ replaced by the polarization vector $\underline{\hat{e}}A$,

$$i\hbar\frac{d}{dt}[c_b^{(1)}(t)] = A_0 e^{i(\omega_0+\omega)t}\langle b| \frac{e}{m}\underline{\hat{e}}.\underline{P}\, e^{-i\underline{k}\cdot\underline{r}} |a\rangle$$

$$+ A_0 e^{i(\omega_0-\omega)t}\langle b| \frac{e}{m}\underline{\hat{e}}.\underline{P}\, e^{i\underline{k}\cdot\underline{r}} |a\rangle \qquad (2\cdot44)$$

This gives a solution for $c_b^{(1)}(t)$,

$$c_b^{(1)}(t) = A_0\left[\frac{1-e^{i(\omega_0+\omega)t}}{\hbar(\omega_0+\omega)}\right]\langle b|\frac{e}{m}\underline{\hat{e}}.\underline{P}\, e^{-i\underline{k}\cdot\underline{r}}|a\rangle$$

$$+ A_0\left[\frac{1-e^{i(\omega_0-\omega)t}}{\hbar(\omega_0-\omega)}\right]\langle b|\frac{e}{m}\underline{\hat{e}}.\underline{P}\, e^{i\underline{k}\cdot\underline{r}}|a\rangle$$

$$(2\cdot45)$$

In the rotating wave approximation only one of the terms on the right hand side of equation 2.45 will contribute significantly to either absorption or emission. If $E_b > E_a$ then, for absorption from level a to b the second term will be much larger than the first, whilst for emission from level b to a, the first term will be much larger than the second.

Therefore, the transition probability for absorption a to b to first order is, using the cycle averaged energy density of the radiation (equation 2.29),

$$P_{ba}(t) = |c_b^{(1)}(t)|^2 = \frac{2\rho(\omega)}{\hbar^2\varepsilon_0\omega^2}\left[\frac{\sin^2\{\frac{1}{2}(\omega_0-\omega)t\}}{(\omega_0-\omega)^2}\right]|\langle b|\frac{e}{m}\underline{\hat{e}}.\underline{P}\, e^{i\underline{k}\cdot\underline{r}}|a\rangle|^2$$

$$(2\cdot46)$$

If the plane wave is not monochromatic but an incoherent superposition of plane waves

with a range of frequencies $\Delta\omega$ centred around ω_0, then this expression for the probability density must be integrated over these frequencies.

$$P_{ba}(t) = \int_{\omega_0-\Delta\omega}^{\omega_0+\Delta\omega} d\omega \ \frac{2\rho(\omega)}{\hbar^2\varepsilon_0^2\omega^2}\left[\frac{\sin^2\{\frac{1}{2}(\omega_0-\omega)t\}}{(\omega_0-\omega)^2}\right]|\langle b|\frac{e}{m}\hat{\underline{e}}.\underline{P}\,e^{i\underline{k}\cdot\underline{r}}|a\rangle|^2 \qquad (2\cdot47)$$

In the limit $t\,\Delta\omega \gg 1$

$$\int d\omega = \frac{\rho(\omega_0)}{\omega_0^2}\frac{\pi t}{2} \qquad (2\cdot48)$$

and the single photon absorption rate from level a to b, W_{ba} is,

$$W_{ba} = \frac{P_{ba}(t)}{t} = \frac{\pi}{\varepsilon_0\hbar^2}\frac{\rho(\omega_0)}{\omega_0^2}|\langle b|\frac{e}{m}\hat{\underline{e}}.\underline{P}\,e^{i\underline{k}\cdot\underline{r}}|a\rangle|^2 \qquad (2\cdot49)$$

This expression assumes that the width of the atomic lines are infinitely sharp, and therefore that spontaneous decay from the level b is negligible over the interaction time t. As previously stated, first order pertubation theory also assumes that the initial population of level a does not change much with time, $|c_b(t)|^2 \ll 1$. Therefore this expression for the rate is only valid in weak fields.

ELECTRIC DIPOLE APPROXIMATION

In the optical region the value $\underline{k}\,.\,\underline{r}$ will be very small and the exponential $e^{i\underline{k}\cdot\underline{r}}$ can be replaced by 1. This effectively neglects retardation across the atom since the electric field is assumed constant across the atom. The expression for the rate can then be simplified,

$$W_{ba} = \frac{\pi\,e^2}{\varepsilon_0\hbar^2}\rho(\omega_0)\,|\,\hat{\underline{e}}\,.\,\langle b|\underline{r}|a\rangle|^2 \qquad (2\cdot50)$$

where $\underline{r}$ is the coordinate of the electron and $\langle b|\underline{P}|a\rangle = im\omega_0\langle b|\underline{r}|a\rangle$

For unpolarised radiation the polarisation vector $\hat{\underline{e}}$ will be in a random direction in space.

$$W_{ba} = \frac{\pi\,e^2}{3\varepsilon_0\hbar^2}\rho(\omega_0)\,|\langle b|\underline{r}|a\rangle|^2 \qquad (2\cdot51)$$

20

The incident energy flux, (Joules per cm^2 per second), is related to the energy density, $\rho(\omega_0)$

$$I(\omega) = \rho(\omega_0) c \qquad (2 \cdot 52)$$

where c is the velocity of light. The transition rate from level a to b is therefore,

$$W_{ba} = \frac{\pi e^2}{3 c \varepsilon_0 \hbar^2} I(\omega) |\langle b|\underline{r}|a\rangle|^2 \qquad (2 \cdot 53)$$

DIPOLE MATRIX ELEMENT

The parameter governing the rate of all single photon electric dipole transitions is the electric dipole matrix element describing the perturbation coupling the two states, $\langle b|\underline{r}|a\rangle$. Evaluation of this matrix requires a knowledge of the electronic wavefunctions describing both states. For non-hydrogenic atoms these can only be calculated approximately, and it can be an involved process. However Bates and Damgaard (1949) derived a general analytical expression for the transition integral, from which it is possible to obtain useful estimates of the cross-sections of a large number of single photon transitions in many different atoms. From this expression and their published tables, estimates of the oscillator strength of the transition a to b, f_{ba}, and of the spontaneous decay rate can be made. The oscillator strength is a dimensionless quantity and is defined for the transition a to b as,

$$|f_{ba}| = |\langle b|\underline{r}|a\rangle|^2 \, 2m\omega_{ba}/3\hbar \qquad (2 \cdot 54)$$

For degenerate states g_a and g_b

$$f_{ba} = -(g_b/g_a) f_{ab} \qquad (2 \cdot 55)$$

where, by convention, the oscillator strength for absorption is positive and the oscillator strength for emission is negative.

Transitions are often expressed as cross-sections in units of area. A definition of the absorption transition cross-section σ_{ba} from level a to b is the rate of absorption of energy per atom per unit time divided by the incident energy flux.

$$\sigma_{ba} = \frac{\hbar\omega}{I(\omega)} W_{ba} \qquad (2 \cdot 56)$$

In general for lasers with a bandwidth Δv_L much greater than the broadened width of a transition, the average cross-section for absorption a to b can be approximated (Hurst 1979a),

$$\sigma_{ba} = \frac{g_b}{g_a} \frac{\lambda^2}{8\pi} \frac{\Gamma_{ab}}{\Delta v_L} \qquad (2 \cdot 57)$$

where Γ_{ab} is the spontaneous decay rate b to a, and g_a and g_b are the statistical weights of levels a and b.

For example the spontaneous decay rate of the $7p_{3/2}\text{-}6s_{1/2}$ in caesium at 455.5 nm is 1.9×10^6 sec^{-1}, (Weiss and Martin 1980). With a laser of energy flux $10\ \mu J\ mm^{-2}\ sec^{-1}$ per 10 nsec pulse, and with a line width Δv_L of 8×10^{10} sec^{-1}, the average absorption cross-section is $\sim 4 \times 10^{-15}$ cm^2, and the transition rate W_{ba} is 8×10^{10} sec^{-1}, which is much greater than the spontaneous decay rate Γ_{ab} from b to a.

INTERACTION WITH STRONG FIELDS

When the incident radiation is strong the population of the upper level may approach the population of the lower level contrary to the assumption taken above in the weak field model.

In a two level atom with levels ψ_a and ψ_b,

$$H_0 \Psi_a = E_a \Psi_a \qquad (2 \cdot 58)$$

$$H_0 \Psi_b = E_b \Psi_b \qquad (2 \cdot 59)$$

If the applied electric field of the incident radiation is $\underline{E} = \underline{E}_0 \cos\omega t$, then the interaction Hamiltonian H_i will arise mainly from the potential energy of the atomic dipole in the electric field.

$$H_i = e\underline{r} \cdot \underline{E}_0 \cos\omega t \qquad (2 \cdot 60)$$

The rate equations to first order for the two levels ψ_a and ψ_b are then, in analogy with equation 2.29,

$$ih \frac{d}{dt}[c_a(t)] = e^{i\omega_0 t} \langle a| H_i |b\rangle \qquad (2\cdot61)$$

$$ih \frac{d}{dt}[c_b(t)] = e^{-i\omega_0 t} \langle b| H_i |a\rangle \qquad (2\cdot62)$$

$$\text{with} \quad \langle a| H_i |a\rangle = \langle b| H_i |b\rangle = 0 \qquad (2\cdot63)$$

Expanding the cosine term in the interaction Hamiltonian, and once again using the rotating wave approximation which neglects the high frequency terms,

$$i \frac{d}{dt}[c_a(t)] = c_b(t) R_{ab} e^{-i(\omega_0 - \omega)t} \qquad (2\cdot64)$$

$$i \frac{d}{dt}[c_b(t)] = c_a(t) R_{ab} e^{i(\omega_0 - \omega)t} \qquad (2\cdot65)$$

$$\text{where} \quad R_{ab} = \langle a| \underline{r} |b\rangle \frac{eE_0}{2\hbar} \qquad (2\cdot66)$$

$$\text{and} \quad \langle a| \underline{r} |b\rangle = \langle b| \underline{r} |a\rangle \qquad (2\cdot67)$$

With the initial condition that all the atoms are in state a at time $t = 0$, ($c_a(0) = 1$ and $c_b(0) = 0$) these equations may be solved to give the probability of the atom being in state b after time t.

$$P_{ba} = |c_{ba}(t)|^2 = \frac{4R_{ab}^2}{\Omega^2} \sin^2 \frac{1}{2}\Omega t \qquad (2\cdot68)$$

$$\text{where} \quad \Omega^2 = (\omega_0 - \omega)^2 + 4R_{ab}^2 \qquad (2\cdot69)$$

RABI OSCILLATIONS

On resonance P_{ba} varies as $\sin^2(R_{ab}t)$ and the system oscillates between the energy levels E_a and E_b with frequency R_{ab}. This is the Rabi flopping frequency and is illustrated in figure 2.3 which plots $|C_b(t)|^2$ against time. It is dependent on the dipole matrix element between the states $|a\rangle$ and $|b\rangle$, and on the amplitude of the electric field E_0. Off resonance this flopping frequency is also dependent on the degree of de-tuning of
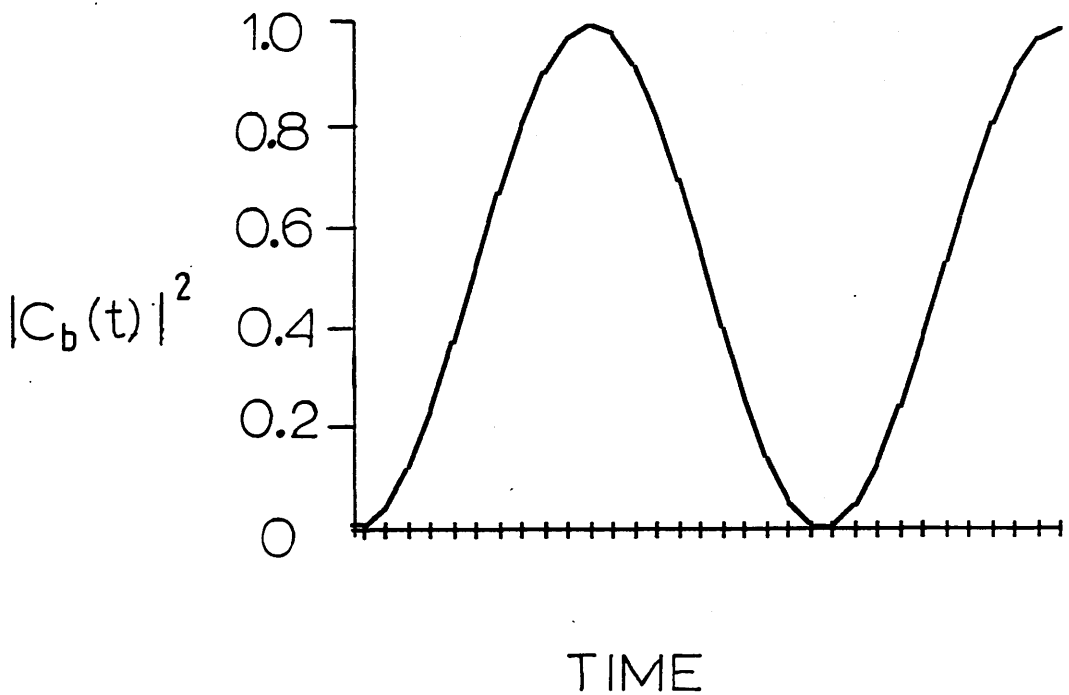
Fig 2.3   Population cycling on resonance between two levels, with intense incident light. The probability, $|C_b(t)|^2$, of the atom being in the excited level, ψ_b, cycles between 0 and 1 at the Rabi frequency.

the laser from the transition frequency, $(\omega_0 - \omega)$.

The factor $4R^2_{ab}/\Omega^2$ has a width at half maximum intensity of $4R_{ab}$ which leads to a broadening of the transition as the applied electric field is increased. This is commonly referred to as power broadening.

Inclusion of the spontaneous decay rate γ from the state $|b>$ to $|a>$ would further broaden the transition by a factor γ, and would tend to dampen the oscillatory behaviour of the probability.

The importance of the Rabi frequency is that it provides a limiting value to the intensity of radiation that can be applied to the system for rate equations to be valid. If the bandwidth of the laser is large compared to the Rabi frequency rate equations will apply, (Hurst 1979a). Since the bandwidth of the laser is essentially fixed while the Rabi frequency increases with the square root of the laser intensity, for population rate equations to be valid low light intensities should be used.

The energy flux I of the laser (J m^{-2} sec^{-1}) is related to the electric field strength of the laser E_0,

$$ I = \varepsilon_0 E_0^2 \, c/2 \qquad (2\cdot70) $$

For a laser of 10 uJ mm^{-2} per 10 nsec pulse, E_0 is of the order 10^6 Volts m^{-1}. Using equation x, which relates the oscillator strength to the dipole matrix element, for the $6s_{1/2}$-$7p_{3/2}$ transition in caesium, which has an oscillator strength $f_{ba} = 0.01$, the Rabi frequency, R_{ab}, is $\sim 1.5 \times 10^{10}$ sec^{-1}. The FWHM power broadening is thus $\sim 6 \times 10^{10}$ sec^{-1}, which is much less than the laser bandwidth $\Delta\omega_L = 4.5 \times 10^{11}$ sec^{-1}. The use of rate equations to model this resonant transition in caesium is valid. Rate equations can also be used if the collision or doppler broadened width is of the order of the Rabi frequency, (Ackerhalt et al 1977). In a proportional counter, at 760 torr buffer gas pressure, the collision rate is of the order 10^{10} sec^{-1} which would also validate the use of rate equations.

Two main assumptions where made in the derivation of the above transition rates. Firstly the non-linear component, $e^2 A^2/2m$, was ignored. To first order this term corresponds to transitions involving the creation or destruction of two photons. Secondly the transitions were restricted to electric dipole interactions only and to first order these involve single photon transitions between states of the same parity. Electric quadrupole, magnetic dipole and all other multipole transitions were ignored since these would only be important if electric dipole transitions were not allowed. For a transition between two states of the same parity the electric dipole matrix element between the states is zero to first order but may be non-zero to second order. If second order electric dipole terms are significant all higher order multipole terms can be neglected. (Loudon 1973)

If higher order multipole terms are ignored the total energy Hamiltonian of the coupled atom+field system is then,

$$\hat{H} = \hat{H}_0 + \hat{H}_i \qquad (2 \cdot 71)$$
$$= \hat{H}_0 + \hat{H}_{ED} + \hat{H}_{NL}$$

where ED is electric dipole and NL is non-linear

To second order in perturbation theory the transition rate $1/\tau$ between the atom+field states a and b with interaction H_i can be shown to be equal to, (Loudon 1973)

$$\frac{1}{\tau} = \frac{2\pi}{\hbar^2} \sum_b \left| <b|\hat{H}_i|a> + \frac{1}{\hbar} \sum_l \frac{<b|\hat{H}_i|l><l|\hat{H}_i|a>}{\omega_a - \omega_l} \right|^2 \delta(\omega_a - \omega_b)$$

$$(2 \cdot 72)$$

The first term $<b|H_i|a>$ represents transitions where the system changes directly from state a to state b, and the interaction Hamiltonian H_i in this term corresponds to the non-linear part of the total Hamiltonian, H_{NL}. The contribution of the non-linear term to the total transition rate can be shown to be negligible, as with the single photon transition rate.

The rate can therefore be approximated to the second term with the H_i replaced by the electric dipole operator, H_{ED}, (Loudon 1973),

$$\frac{1}{\tau} = \frac{2\pi}{\hbar^2} \sum_f \left| \sum_l \frac{<b|\hat{H}_{ED}|l><l|\hat{H}_{ED}|a>}{\hbar(\omega_a - \omega_l)} \right|^2 \delta(\omega_a - \omega_b)$$

$$(2 \cdot 73)$$

Where transitions occur between states involving N photons the time dependent perturbation theory must be calculated to the N th order.

VIRTUAL STATES

The states l are called virtual intermediate states for the transition a to b and the summation over l includes all states accessible to one photon transitions from a. Energy conservation requires that $\hbar\omega_a = \hbar\omega_b$ but the intermediate states do not in general have the same energy as the initial state. There is no need for energy to be conserved in transitions to these states since no real transitions are made into them. For each intermediate state there is an energy denominator $\hbar(\omega_a - \omega_l)$ which diminishes the contribution to the matrix element for those virtual states whose energy $\hbar\omega_l$ is greatly different from the initial state. These virtual states obey the usual selection rules for one photon transitions.

In general this transition rate is difficult to solve rigorously because, in the electric dipole approximation, the rate of two photon absorption depends on the statistical properties of the light, both temporal and spatial, over the pulse length. These statistical fluctuations in the laser pulses will not be reproducible from shot to shot. In particular the degree of second order coherence (which is related to the magnitude of the fluctuations in the instantaneous beam intensity) will influence the rate of absorption, (Kliger 1983). In a two photon process chaotic light will be absorbed at twice the rate of completely coherent light. In general for an N photon process chaotic light is absorbed at N! times that of coherent light, (Chin and Lambropoulus 1984).

2.3 SELECTION RULES FOR ELECTRIC DIPOLE TRANSITIONS

SINGLE PHOTON TRANSITIONS

One of the major advantages of multiphoton spectroscopy is that excited states of atoms and molecules can be reached, with a high degree of selectivity, which are normally forbidden by electric dipole selection rules. The single photon transition rules are well known.

$\Delta L = +/-1$ (change of parity)

$\Delta S = 0$

$\Delta J = 0, +/-1$ where $\underline{J} = \underline{L} + \underline{S}$

Normally laser light is polarised either linearly or circularly. This places extra constraints on the transitions.

$\Delta m_j = 0$ linearly polarised light

$\Delta m_j = +/-1$ circularly polarised light

MULTIPHOTON TRANSITIONS

For N photon excitation the selection rules (for the transition) are equivalent to applying the single photon rules N times, (Letokhov and Chebotayev 1977). For example two photon excitation from the ground state of caesium, $6 S_{1/2}$, will proceed via a virtual P state to either a D state or another S state. For two photon transitions using a single laser the selection rules are,

$\Delta L = 0, +/-2$

$\Delta J = 0, +/-1, +/-2$

$\Delta m_j = 0$ linear polarisation

$\Delta m_j = +/-2$ circular polarisation

CONCLUSION

Population rate equations provide a convenient method of makng quick calculations related to resonant ionisation, provided the laser is well behaved and the various transition cross-sections are known. Many single photon atomic cross-sections are

known but in general multiphoton cross-sections are not. In order to evaluate these for an N photon process a semiclassical approach can be taken and perturbation theory applied to the Nth order.

2.4 PHOTOIONISATION

If the energy of an incident photon is greater than the binding energy of an electron in an atom the electron may be ejected from the atom. The final continuum state will therefore be of an unbound electron moving in the field of the ion. If the energy of the incident photon is only slightly greater than the binding energy of the electron in the atom, the full coulombic wave functions must be obtained, as the ion will exert a considerable influence on the motion of the electron. However if the energy of the ejected electron is much larger than the binding energy (but small enough for relativistic effects to be negligible), the potential of the ion can be ignored and the wave function of the ejected electron approximated to a plane wave.

$$\text{Ejected electron wave function } = \frac{1}{\sqrt{V}} e^{i\underline{k}_f \cdot \underline{r}} \qquad (2\cdot74)$$

normalised in a box of volume V,

where the momentum of the electron is $\underline{P}_f = \hbar \underline{k}_f$

The expression for the cross-section for the transition to the continuum is then similar to that for the absorption cross section between two bound states.

$$\sigma_{ion} = 4\pi^2 \, \alpha \, \omega_0 \rho_b \int_{\text{ejection angles}} \left| \left< \psi_f | \, r \, | \psi_i \right> \right|^2 \, d\Omega \qquad (2\cdot75)$$

α = fine structure constant
ψ_f = ejected electron wave function
ψ_i = initial state wave function

where the integral is over all angles of ejection of the electron and ρ_b is the density of the final continuum states.

$$\rho_b = \left[\frac{1}{2\pi} \right]^{-3} Vm \frac{k_f}{\hbar} \qquad (2\cdot76)$$

The calculation of photoionisation cross-sections from excited states in atoms, using full coulombic wavefunctions for the initial and final states, is a formidable task. Burgess and Seaton (1960) and Peach (1967) have derived general formulas from which cross-sections for many atoms involving a wide range of electron ejection energies, can

be readily obtained. The method used is that of Bates and Damgaard (1949), the principle being that atomic absorption cross-sections should vary continuously across the ionisation threshold, and that an extrapolation of the cross-section into the continuum can be made, (Sobelman 1979)

2.5 AUTOIONISATION

Photoionisation is an inefficient process in that the photoionisation cross-section is very small in comparison to bound-bound cross-sections. The laser power required to saturate photoionisation is much greater than that required to saturate the photoexcitation steps.

Furthermore, whilst the excitation cross-section to highly excited states decreases at the rate $(1/n)^3$, where n is the quantum number of the excited state, photoionisation cross-sections from this state decrease even faster at a rate $(1/n)^5$. The more highly excited the intermediate state the more difficult it is to photoionise.

This problem can be partially addressed through autoionisation, which effectively increases the photoionisation cross-section. Autoionisation arises due to there being excited electronic configurations in atoms (and molecules), involving two or more electrons, the energy of which are greater than the ionic state of the atom. If the atom is excited to such a configuration, mixing of the electronic states will occur and the atom may decay non-radiatively, due to energy exchange between the electrons, ejecting one electron in the process. This is illustrated in figure 2.4.

Autoionisation states appear as resonances in the continuum and have cross=sections of around 10^{-16} cm^{-2}, a factor of 10-100 greater than photoionisation cross-sections. Use of this technique would also increase the selectivity of the ionisation step.

Alkali metals have only one valence electron orbiting closed shells and autoionisation is not feasible. Autoionisation states have been investigated in many atoms, examples being samarium (Dobryshin et al 1983) and beryllium (Clark et al 1985).
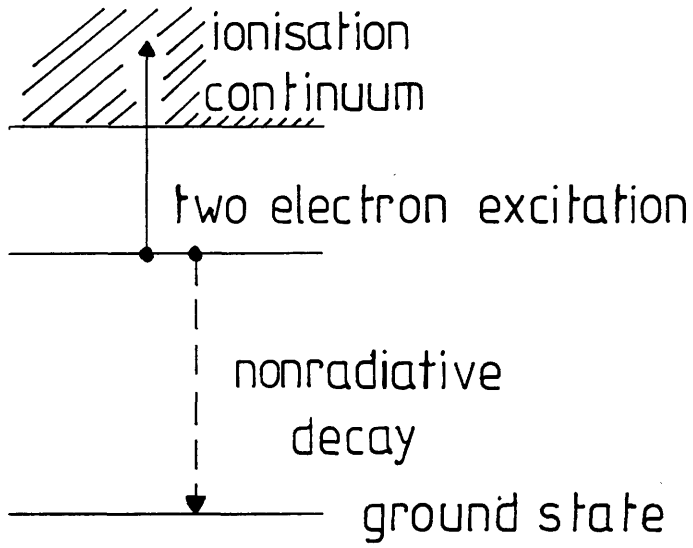
Fig 2.4   Autoionisation

2.6 TRANSITION LINE WIDTHS

The observed widths of the laser induced transitions in a proportional counter will depend on the natural linewidth of the transition, the pressure of the buffer gas, the vapour pressure and temprature of the atomic species, the linewidth and intensity of the laser, and the strength of external electric and magnetic fields. In mass spectrometers there will be no contribution from the buffer gas. Some simple calculations are sufficient to highlight the laser as the most important single contributor to the observed linewidth in these experiments.

NATURAL LINEWIDTH

An atom in an excited state b will eventually decay with the emission of radiation to some lower level a. This will occur spontaneously with a definite lifetime τ. By the uncertainty principle the energy of level b cannot be precisely determined but must be uncertain by an amount of order

$$\Delta E = \frac{\hbar}{\tau} \qquad\qquad (2 \cdot 77)$$

If the level a is also an excited state with a definite lifetime this will also add to the uncertainty of the transition energy. Therefore there will be a range of frequencies of radiation from such a transition around the value ω_0 of width $\Delta\omega$

$$\omega_o = \frac{E_b - E_a}{\hbar} \quad , \quad \Delta\omega = \frac{1}{\tau_a} + \frac{1}{\tau_b} \qquad (2 \cdot 78 a, b)$$

If the state a is the ground state then its energy is precisely determined and the line-width is termed the natural width of level b.

The $7p_{3/2}$-$6s_{1/2}$ transition in caesium has a spontaneous lifetime of 150 nsecs, (Hurst 1979a). Its natural linewidth is thus ~3×10^{-4} cm^{-1}.

DOPPLER BROADENING

The transition wavelengths of a radiating atom will depend on the atoms velocity. For non-relativistic atom velocities and with the observer along the x axis, the observed wavelength λ is,

$$\lambda = \lambda_0 \left[1 \pm \frac{v_x}{c} \right] \qquad (2 \cdot 79)$$

where λ_0 is the wavelength at zero velocity

v_x is the component of velocity along the x axis

$+/-$ atom travelling away from / towards the observer

If the atoms have a Maxwellian distribution of velocities then the intensity of the light in the frequency range v to $v + dv$ is,

$$I(v) = I_0(v_0) \exp \left[\frac{mc^2}{2kT} \left(\frac{v - v_0}{v_0} \right)^2 \right] \qquad (2 \cdot 80)$$

This has a Gaussian profile of width $\Delta v = 2(v_0 - v_1)$ where v_1 is the frequency at which the intensity has fallen by 1/2.

$$\Delta v = \frac{2v_0}{c} \left[\frac{2kT \log_e 2}{m} \right]^{\frac{1}{2}} \qquad (2 \cdot 81)$$

In the visible region at room temprature the doppler width exceeds the natural line-width by about two orders of magnitude. For caesium at room temprature the doppler width of the transitions from the $6s_{1/2}$ ground state to highlying p states will be of the order of 0.03 cm^{-1}. At 400 K the equivalent transitions in rubidium will be doppler broadened by around 0.05 cm^{-1}.

PRESSURE BROADENING

Inelastic collisions

An atom in an excited state may undergo radiationless de-excitation through a collision with another atom or molecule. This de-excitation is another decay channel which will tend to decrease the lifetime of the excited state and thereby increase the uncertainty of the transition energy.

31

If the number of collisions per second removing atoms from the excited state is W_c then the observed width of the line Γ would be:

$$\Gamma = \hbar \, (W_c + 1/\tau_b\,) \qquad \text{where } \tau_b \text{ is the natural lifetime of state b.}$$

$$(2\cdot82)$$

The collisional rate is proportional to the pressure of the collision partners and to the collision cross-section between the two atoms. At room temperature and atmospheric pressure a gas molecule will collide with surrounding atoms or molecules at a rate of the order of 10^{10} per second. If each collision changes the state of the atom the average lifetime of the state will be $\sim 10^{-10}$ sec. In proportional counters the buffer gas will collide with the excited states of the excited sample atom and decrease their effective lifetime, increasing the transition line-width. For rubidium atoms at 15° C in argon gas at 30 torr the $5s_{1/2}$-$6p_{3/2}$ transition has a collisional width of ~ 0.1 cm^{-1}, (Dermtroder 1982)

Elastic collisions

Collisions will also affect the energy levels of the colliding partners. The shift in the energy levels will depend on the distance apart of the partners which will depend in turn on the temperature and pressure of the atoms. If a transition occurs between the energy levels of one of the atoms during the collision, it will be shifted from its unperturbed position and be broadened by the fluctuation of the distance between the two atoms.

LASER INTENSITY BROADENING

If the intensity of the laser is such that the population between states is altered substantially then the induced transition rates may dominate over the spontaneous relaxation rate between the two levels. The population then oscillates between the two levels at the Rabi flopping frequency ω_R . In such a situation the lifetime of both states is shortened and the line width increases. Hurst (1979a) estimated the Rabi frequency to be of the order $\omega_R = 10^8(I)^{1/2}$, where I is the intensity of the laser in Watts cm^{-2}, and ω_R is in radians sec^{-1}. Typical unfocussed laser powers used for atomic excitation are of the order of 10^5 Watts cm^{-2}. The Rabi frequency would thus be of the order of 3×10^{10} sec^{-1}, which at a wavelength of 500 nm would correspond to a linewidth of

$4\omega_R = 0.25$ cm^{-1}, (Woodgate 1983).

All absorption transitions will perturb the two states connected by the transition to a degree depending on the intensity of the absorption. This perturbation can manifest itself as a shift of the energy levels of the two states. The intensity of the laser will be spatially and temporally dependent in general and hence the atoms will experience varying degrees of resonance depending on whether it is pulled into or out of resonance with the laser. The width of the observed line will therefore change. (Morrellec et al 1976, Pindzola et al 1984b, Otis et al 1981). Crance (1980) derived values of 0.043 cm^{-1}(GW cm^{-2})$^{-1}$ for the broadening of the four photon resonant ionisation of caesium via the three photon 6s-6f transition. For powers of ~10^5 W cm^{-2} this broadening would be negligible.

LASER LINE WIDTH

An experimental resolution of about 2.5 cm^{-1} was observed, measured by the ability to resolve doublet states in caesium and rubidium of known separation. The dye laser linewidth was of the order 3 cm^{-1} and was assumed to be the dominant contributor to this observed width. All other broadening mechanisms would seem to be less important.

CHAPTER 3

APPARATUS

INTRODUCTION

The application of lasers to the detection of atoms and molecules can be based on a number of different processes of which resonant ionisation is one. Two other prominent and well known methods are the measurement of the spectral absorption characteristics, and determining the spontaneous emission, or fluorescence, of laser excited atoms and molecules. The detection of fluorescence can be extremely sensitive (Fairbank et al 1975). However absorption studies with small numbers of atoms are difficult in that a comparison has to be made between two signals of comparable magnitude, the reference and the attenuated laser beams. The detection of charged particles can also be extremely sensitive with the ability to detect 100% of charged particles, and this technique has the additional advantage in that it can be readily combined with mass selection.

The early experiments at Glasgow were concerned with the resonant ionisation of organic molecules with low ionisation potentials, such as phenol and toluene, (Towrie et al 1986, Drysdale et al 1986). These were carried out using proportional counters with an excimer pumped dye laser. This basic system was also the starting point for work with caesium and rubidium vapours, work which progressed to resonant ionisation in a quadrupole mass-spectrometer and culminated in the construction of a time of flight resonant ionisation mass spectrometer, (RIMS-TOF). This chapter describes these three detection systems, beginning with the laser systems used, and including other apparatus such as the data collection systems.

The reasoning behind the decision to work with caesium and rubidium vapours was linked to the initial use of proportional counters as detectors and is explained at the end of the chapter.

Figures 3.1 and 3.2 are schematic diagrams illustrating the layout of the apparatus used with the proportional counter and the quadrupole mass spectrometer. Each of the major components is described beginning with the laser systems and other optical apparatus, then the ionisation detectors (proportional counter and quadrupole mass spectrometer), and finally the electronics for data acquisition. The arrangement of the apparatus for work with the time of flight instrument is similar, apart from the data acquisition which is described separately.

3.1 LASER SYSTEMS

The ability to ionise atoms of only one element is the basis of resonant ionisation mass spectrometry and, in order to do this efficiently ie. with a high probability, large laser fluxes are required over a wide range of wavelengths. The bandwidth of the laser is also important in that elemental selectivity may be reduced if the bandwidth is too large while, if the bandwidth is too narrow, isotopic selectivity will occur. Isotope selective ionisation may not be desirable in trace element detection with mass spectrometers. In principle, for trace analysis, the wavelengths of the exciting/ionising lasers are fixed so as to give the largest resonant ionisation signal, with the laser bandwidth large enough so as to ionise all the isotopes of a particular element with equal probability, (Beekman et al 1980). The mass spectrometer is then used to discriminate between different isotope masses. In this situation laser induced isotope separation would not be an advantage. Gross (1974) has estimated the isotope shift in atomic spectra, for atoms with atomic numbers between 10 and 200, to be less than the doppler line widths at temperatures where the vapour pressure is about 1 torr. For ^{133}Caesium the doppler width of the 6s - 7p transition at this temperature (600 K) is ~0.03 cm^{-1}, and for ^{85}Rubidium (700 K) the width is ~0.05 cm^{-1} for the 5s - 6p transition.

These three main requirements can be met with tunable, pulsed dye lasers. They are capable of delivering of the order of a milli-joule per 10 nsec pulse, from the near UV to the infrared, with a bandwidth around 1 cm^{-1}. These lasers are thus used extensively in resonant ionisation mass spectrometry.

At Glasgow there are currently two laser systems, an excimer laser pumping a single
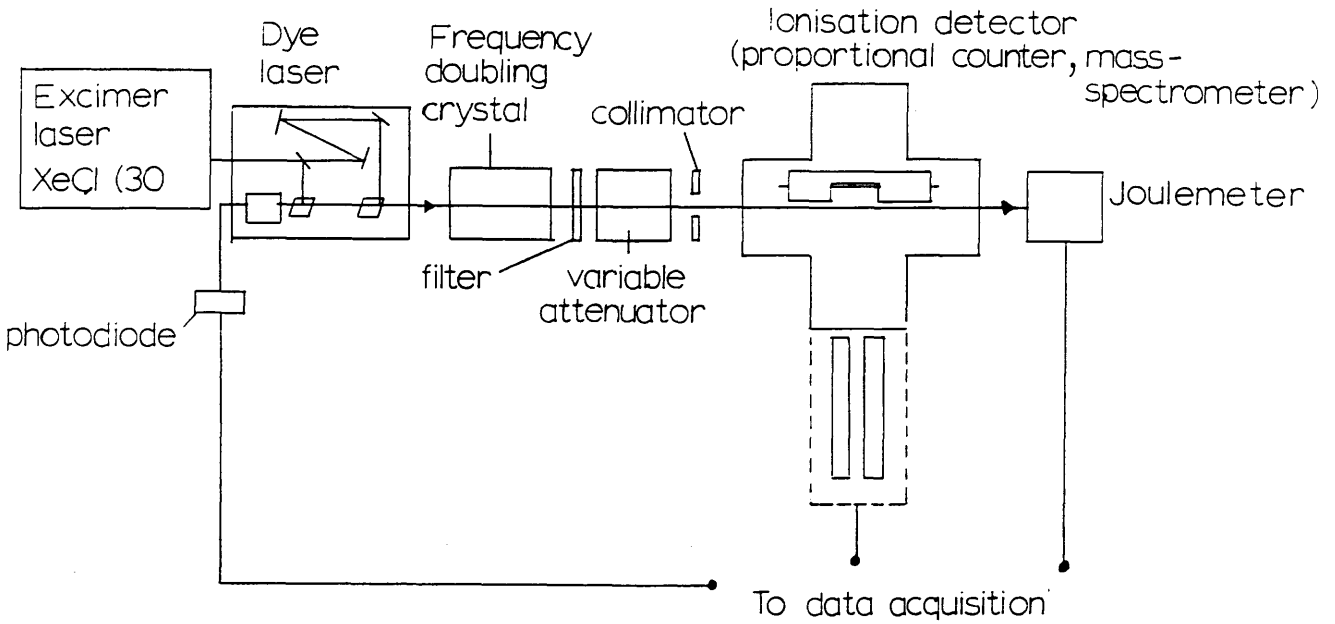
Fig 3.1   Apparatus used with proportional counter and quadrupole mass
spectrometer.
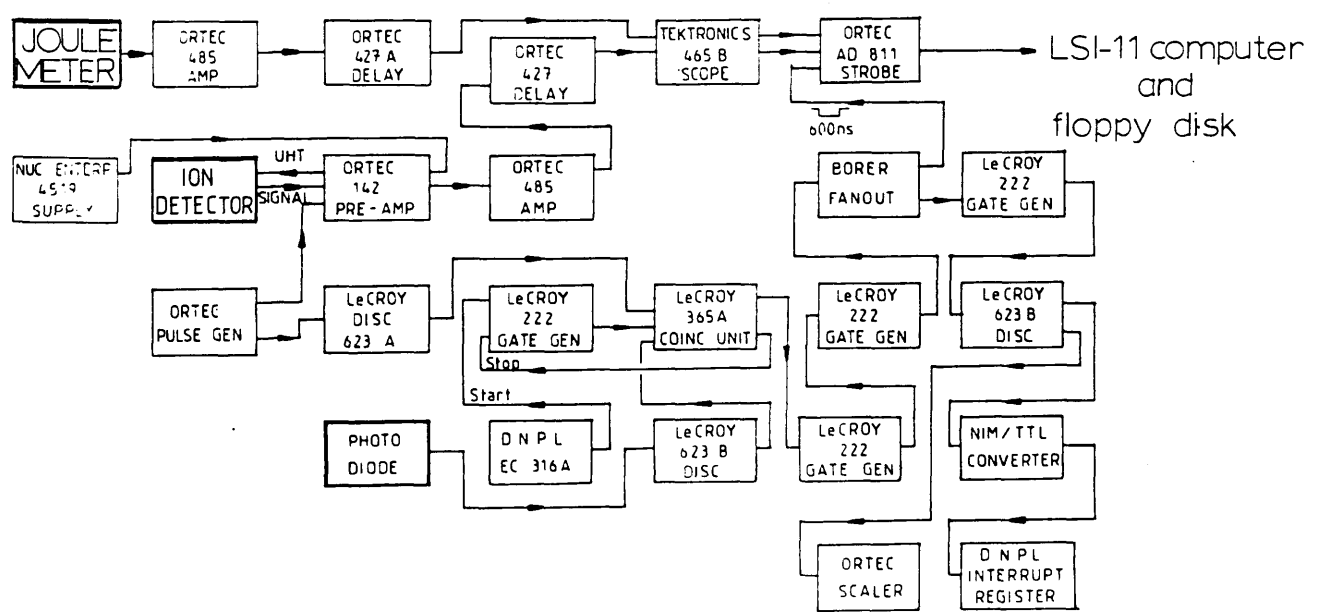
Fig 3.2   Electronic arrangement for generating timing signals for acquisition of
data from the proportional counter and quadrupole mass spectrometer.

dye laser and a Nd:YAG laser pumping two dye lasers. All the work carried out on caesium and rubidium vapours, in the proportional counter and the quadrupole mass spectrometer, used the single excimer pumped dye laser for the resonant photoionisation, whilst the twin dye laser system is currently used with the time of flight mass spectrometer.

Ideally, for analytical work, lasers should be viewed and used as black box sources of light. However some knowledge of the lasing mechanisms, and of wavelength selection and tuning, is useful for an understanding of the limitations that the laser imposes on the experiment. It is also useful when the lasers break down. Brief descriptions of the excimer, Nd:YAG and dye lasers are therefore given, and the manufacturures specifications for each laser are listed in tables 3.1 and 3.2.

EXCIMER LASER

Excimer lasers are high powered UV lasers delivering tens of millijoules per pulse. They are ideal pumps for dye lasers.

The lasing action hinges on the ability of certain molecules, such as inert gas halides, to form bound states of lifetime ~10 nsec when excited, and to dissociate in ~10^{-12} sec when in the ground state. An excited molecule is formed by, for example, an electrical discharge, and a population inversion then automatically exists between the two lasing levels, figure 3.3. For pumping the dye laser in this experiment XeCl was used which provided light of 308 nm wavelength. The cavity had stable optics installed producing 80mJ per pulse and with a pulse length of between 8 ns and 12 ns. Stable optics imply that the light is passed through the lasing medium many times before being emmitted. The laser beam produced from stable optics is slightly diverging which is suitable for pumping a dye laser.

Nd:YAG LASER

The active medium in Neodynium : YAG lasers is a crystal made of yittrium, aluminium and garnet, (YAG). Neodynium^{3+} ions are doped into the crystal structure and are the centres of the lasing action. The surrounding crystal atoms serve to split the low lying energy levels of the Nd^{3+} ion. The ion has broad absorption bands from the ground to high lying excited states which undergo non-radiative transitions to lower lying levels

formation

$Xe^+ + Cl^-$

$Xe^* + Cl$

$(XeCl)^*$

lasing transition

308 nm

Energy

dissociation
Xe + Cl

Inter Nuclear Separation
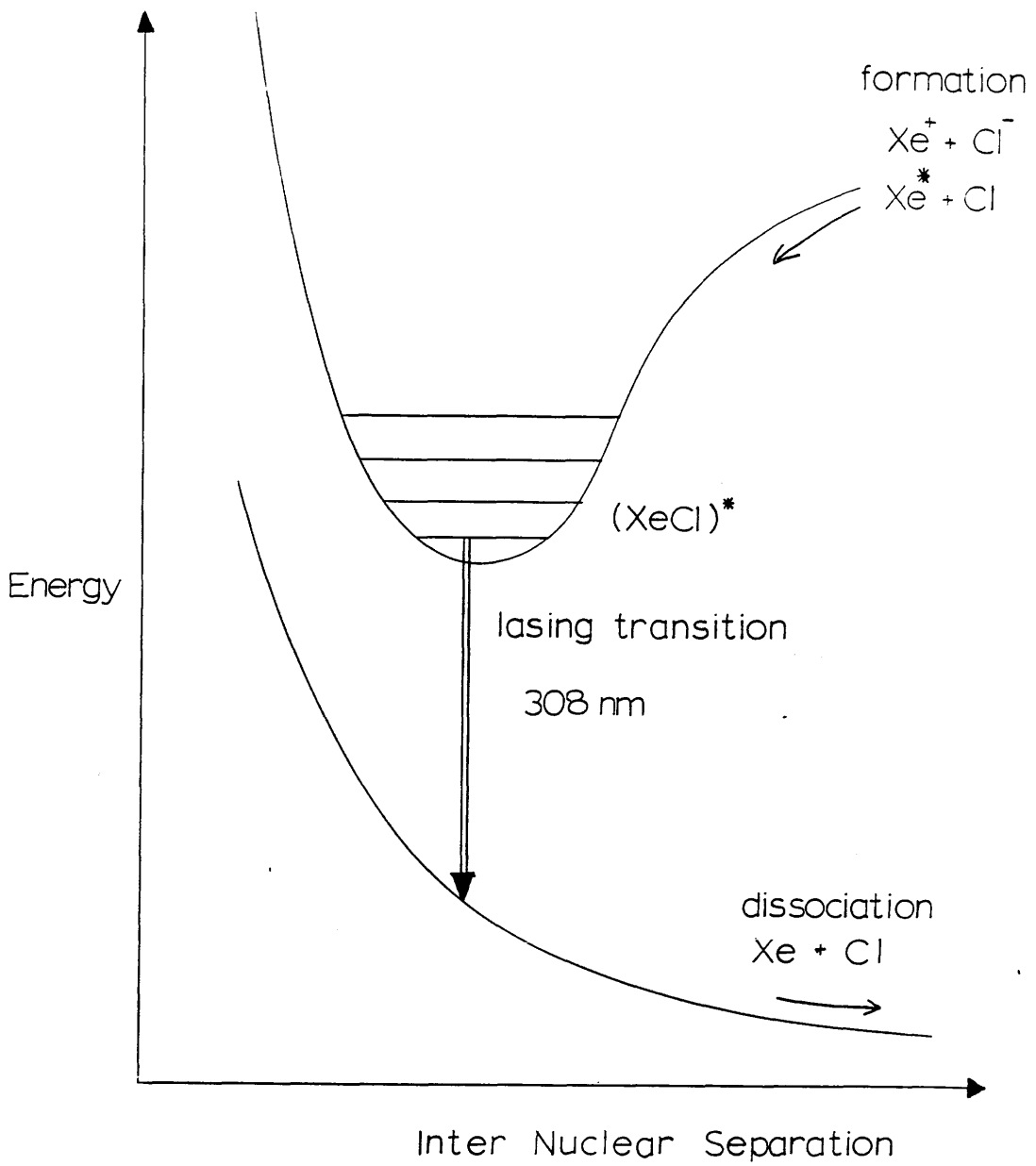
Fig 3.3   Schematic energy level diagram of the excimer molecule $(XeCl)^*$

fast decay

metastable

broadband
pump

lasing transition

fast decay
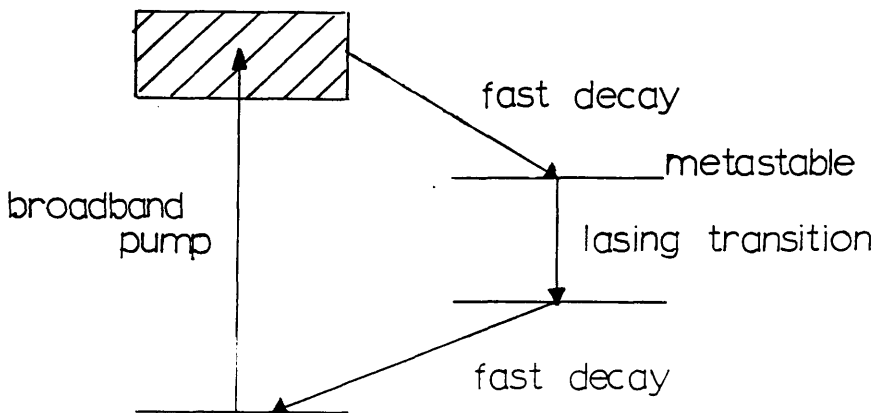
Fig 3.4   Energy levels of the Nd^{3+} ion used in the four level Nd:YAG laser

as illustrated in figure 3.4. Lasing occurs predominantly at 1064 nm between two of these lower levels. Pumping of the ion to the excited levels is by high-powered flashlamps whose spectral output overlaps the absorption band of the Nd^{3+} ion.

In order to act as a pumping laser for the two tunable dye lasers, the 1064 nm output from the Nd:YAG can be frequency doubled (532 nm), tripled (355 nm) and quadrupled (266 nm), ensuring an efficient pumping wavelength for the particular dyes. The pulse length of the Nd:YAG is ~16 nsec.

EXCIMER PUMPED DYE LASER

The lasing medium in dye lasers is a liquid solvent in which is dissolved an organic dye. The energy level scheme of a typical dye is shown schematically in figure 3.5. It consists of a ground state, S_0, together with a series of excited singlet states, $S_1, S_2,..$, and a series of excited triplet states, $T_1, T_2,..,$. Each of these electronic states include a range of energies determined by the vibrational and rotational states of the molecule. Rapid relaxation processes, due to collisional and electrostatic interactions with surrounding solvent molecules, smear out the rotational and vibrational levels, and this accounts for the broad continuous absorption and emission profiles of organic dye molecules.

Radiation from the pumping source, which lies in the absorption band of the dye molecules, excites the molecule from the low-lying vibrational-rotational levels of the S_0 state to higher lying vibrational-rotational levels of the electronically excited S_1 state. The molecule may then either spontaneously decay back to the ground level, or may be non-radiatively de-excited by collisions to the lower vibrational levels of the excited state. The lasing action is the fluorescence that occurs between the lower vibrational levels of the excited state and the high lying vibrational levels of the ground electronic state. Further collisional de-excitation quickly transfers molecules back to the lower vibrational level of the ground state.

Lasing is possible over almost the entire fluoresence band.

The laser oscillator cell and amplifier cell were pumped transversely. Wavelength selection is by a fixed grazing-incidence grating with 2400 lines/mm, as illustrated

singlet excited
state

collisional
de-excitation

collisional
de-excitation

inter system
crossing

S_1

triplet
state

T_1

pump
absorption — fluorescence

phosphorescence

singlet
ground
state

S_0
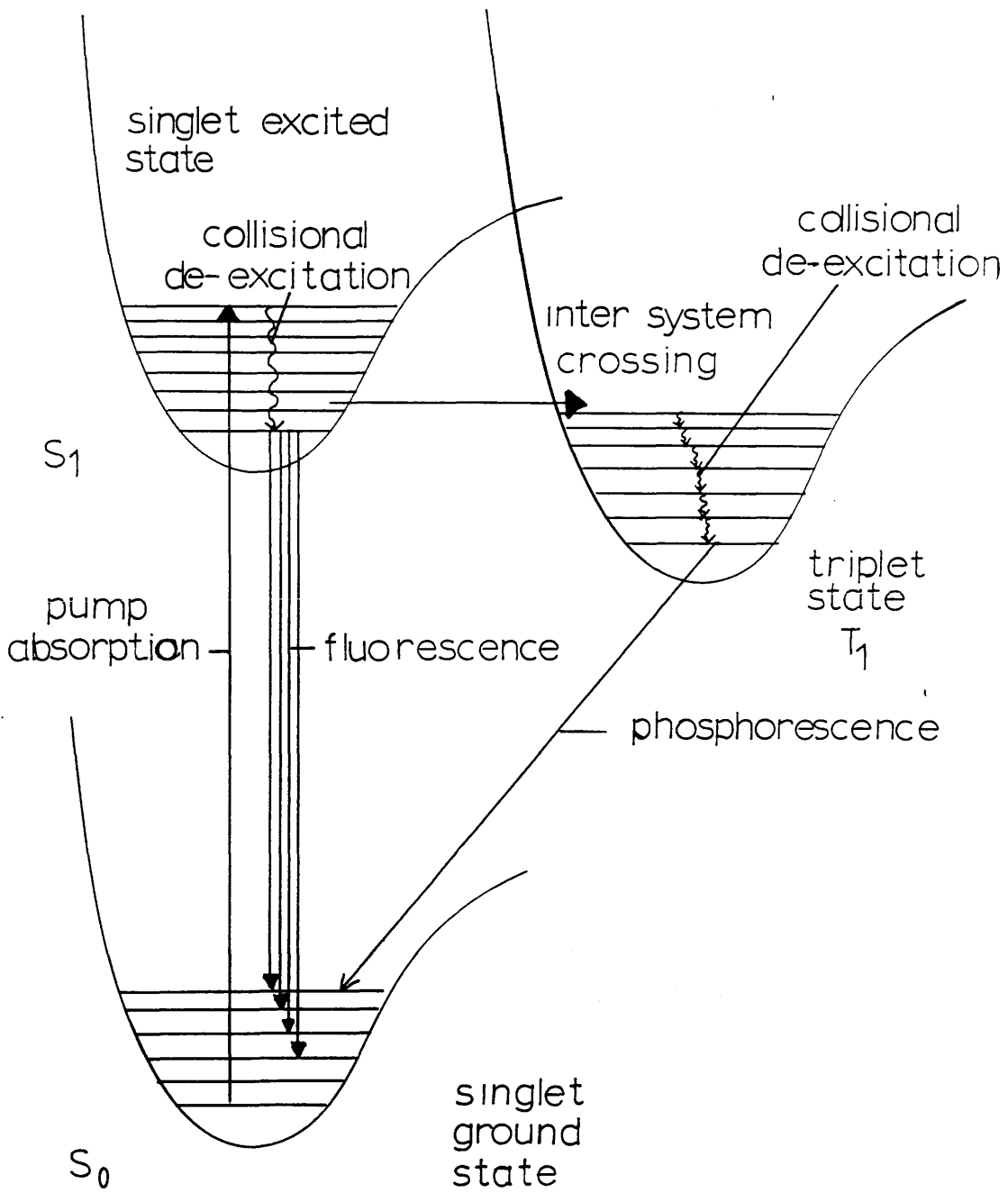
Fig 3.5   Schematic energy level diagram of typical dye molecule dissolved in a
solvent.

in figure 3.6. This results in an almost constant laser linewidth of about 0.05 nm over the entire lasing spectrum (350 nm – 700 nm). By using a beam expander to illuminate more grooves on the grating the linewidth could be reduced to 0.003 nm. The wavelength tuned laser beam then passes through an amplifier cell. The pulse length of the laser is less than that of the pump laser and when using the XeCl excimer laser was of the order of 10 ns. The dyes used in the experiments and the wavelengths covered with them are given below in table 3.3.

The absolute wavelength of the dye laser could be determined to within 1 nm using a simple monochromator. A more accurate method involved using known atomic transitions in caesium and rubidium which provided fixed points to which the dye laser wavelength, as stated on the electronic controller, was aligned. However when tuned away from these transitions, the dye laser wavelength became inaccurate by an amount proportional to the spectral distance from the "fixed point". This linear displacement could be adjusted for in the subsequent data analysis, figure 3.7.

Nd : YAG PUMPED DYE LASERS

Resonant ionisation in the TOF mass spectrometer is with two pulsed dye lasers pumped simultaneously by the Nd:YAG laser. The use of two independently tunable dye lasers allows the resonant ionisation of atoms with ionisation potentials up to around 10 eV, and increases the selectivity of the process.

The design and mode of operation of the two Nd:YAG pumped dye lasers are similar to that of the excimer pumped dye laser descibed above. The oscillator and amplifier cells are transversely pumped and wavelength selection is by a grazing incidence holographic grating. One dye laser operates in the range 540 nm to 700 nm with a power of 20 mJ per pulse, the other from 400 nm to 700 nm with a power of 1 mJ per pulse . Both have a line width of ~0.1 cm^{-1} when operated with beam expanders, and pulse lengths of approximately 10 nsec.

External wavelength calibration is by a uranium hollow cathode, the absorption and emmision spectra of which has numerous, well documented, frequencies from the UV to the infra-red, figure 3.8, (Palmer et al 1980). This will be provide on-line calibration of the dye lasers, the spectra from the hollow cathode being recorded alongside the ionisation and laser power signals from the mass-spectrometer.

38
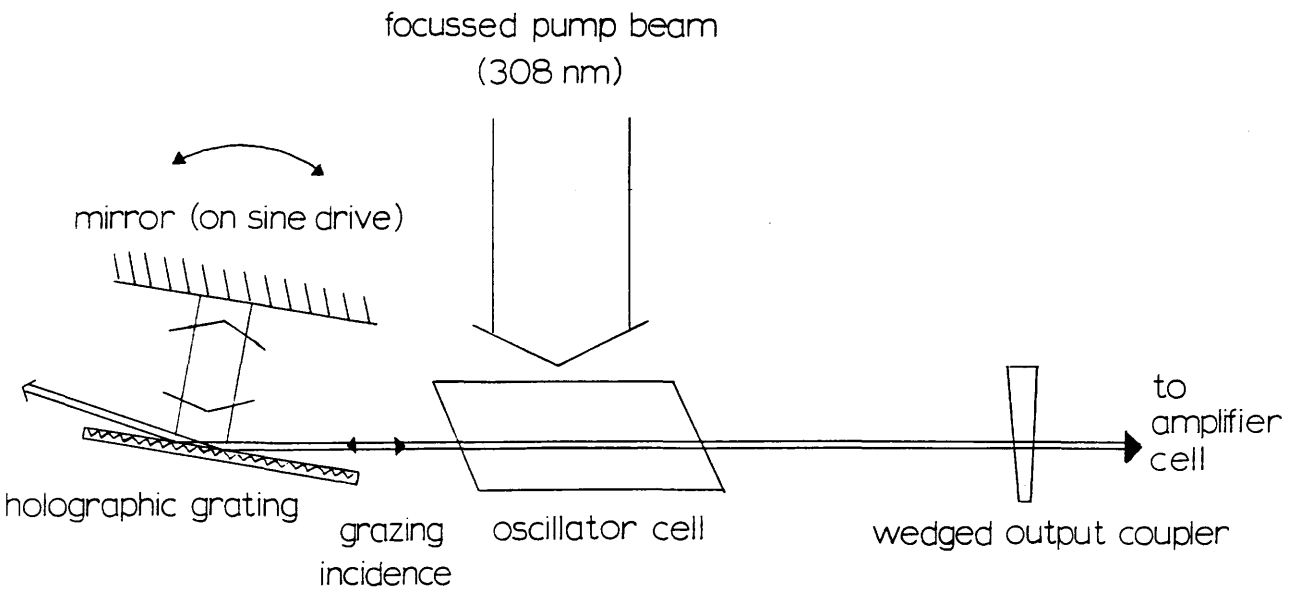
Fig 3.6   Wavelength selection and tuning in the transversely pumped dye lasers
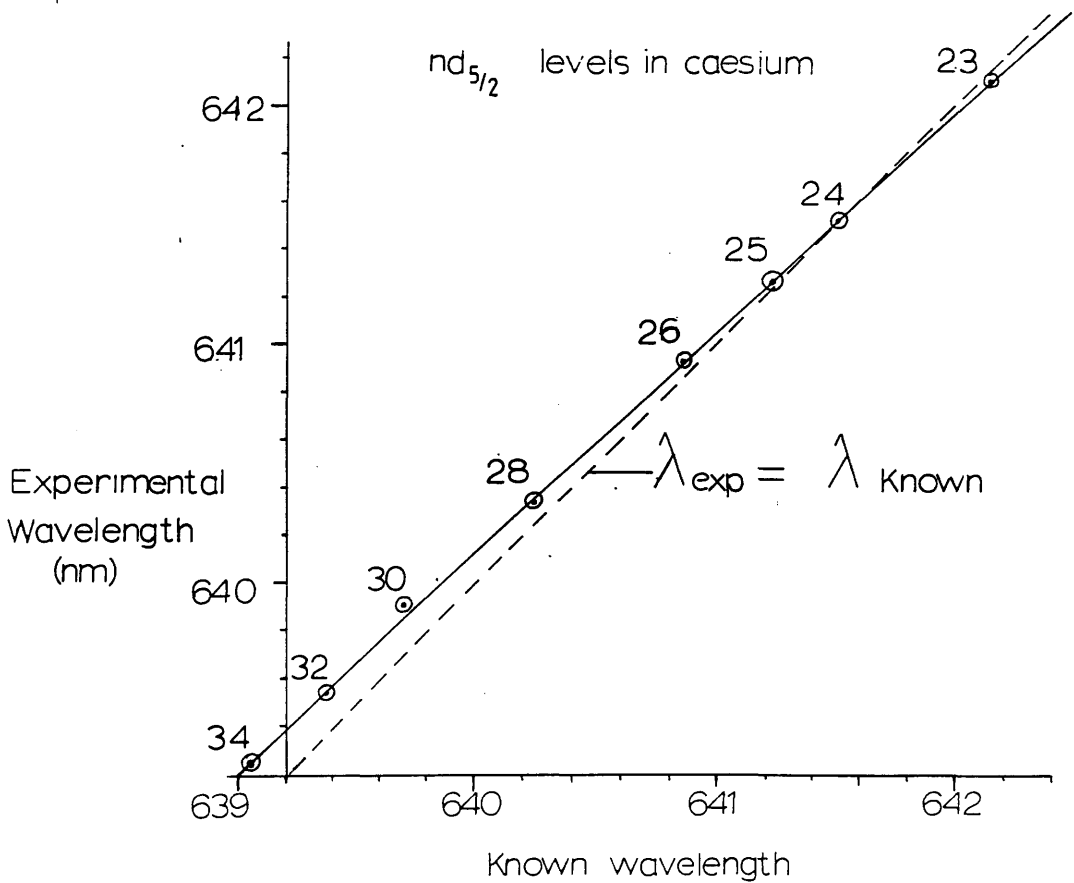
Fig 3.7   Wavelength calibration of the dye laser. Known wavelengths from Weber and Sansonetti (1987).
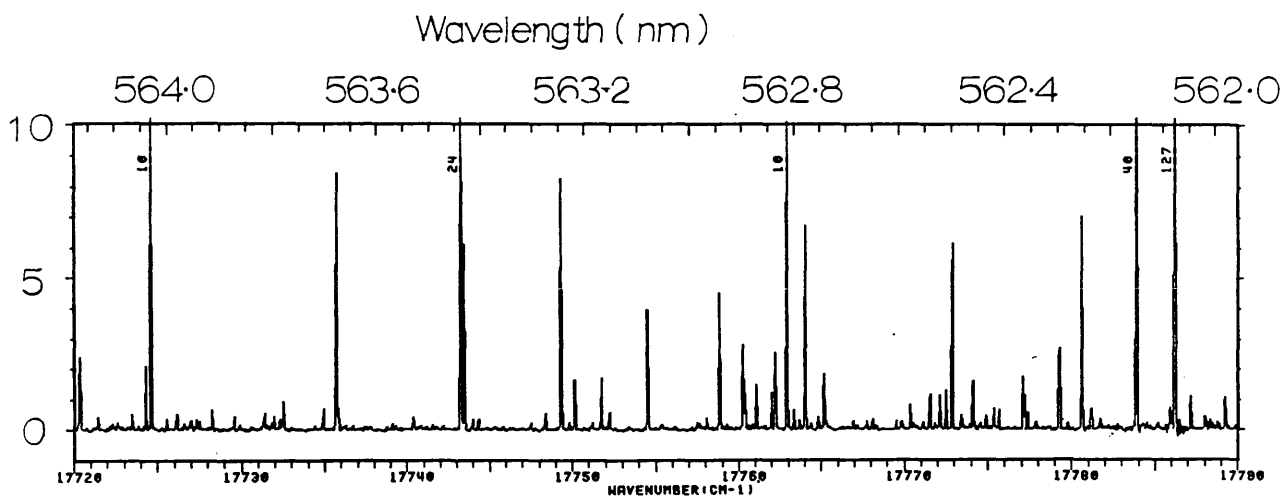
Fig 3.8   Part of the spectrum from an uranium hollow cathode which is used to calibrate the Nd:YAG pumped dye lasers.

TABLE 3.1   EXCIMER PUMPED DYE LASER SYSTEM

Type	XeCl Excimer	Excimer pumped dye laser
Manufacturer	Lumonics	Lumonics
	TE 860-3	EPD 330
Wavelength (nm)	308	tunable 320 - 950
Pulse energy (mJ)	80	~10% pump energy
Pulse length (nsecs)	12	8
Line width (cm^{-1})	-	(with beam expander) 0 .15
		(without beam expander) 2.5
Average power (W)	5	~ 1
Max repetition rate (sec^{-1})	80	80
Pulse to pulse variation (%)	3	3

TABLE 3.2.   Nd:YAG PUMPED DYE LASER SYSTEM

Type	Nd:YAG	Nd:YAG pumped dye lasers	
Manufacturer	Spectron Laser Systems	Spectron Laser Systems	
	HL-21	Spectrolase 4000	
Wavelength (nm)	1064 fundamental	-	
	532 frequency doubled	540-760	
	355 frequency tripled		400-760
	266 frequency quadrupled	-	
Pulse energy (mJ)	850 fundamental	-	
	310 doubled	20	
	90 tripled		1
	50 quadrupled	-	
Repetition rate (sec^{-1})	10	10	10
Pulse length (nsec)	16	12	12
Pulse to pulse variation (%)	5	5	5
Line width (cm^{-1})	- (with beam expander)	0.12	0.08

TABLE 3.3

Dye name	Tuning range (nm)		Transitions covered
	Fundamental	Frequency doubled	
DCM	602-686	301-343	1. Cs: one and two photon transitions from 6s ground state to s,p and d Rydberg states
			2. Rb: two photon transitions from 5s ground state to intermediate lying s and d states
			3. Two photon ionisation of organic impurites in proportional counters
Coumarin 153	521-594	260-297	Two photon ionisation of organic impurities in proportional counters
Rhodamine-6-G	569-608	284-304	1. Rb: one and two photon transitions from 5s ground state to s,p and d Rydberg states
			2. Two photon ionisation of organic impurities in proportional counters
Stilbene 3	410-454	-----	Rb: one photon transition 5s-7p

FREQUENCY DOUBLING OF THE DYE LASERS.

Frequency doubling crystals are used to extend the wavelength of the dye lasers below the pumping laser wavelength, into the near UV.

Under intense radiation the polarisation P of the atoms in a crystal may not be linearly dependent on the electric field E of the radiation field, but may be expressed as a series of terms dependent on higher powers of E.

$$P = a_1E + a_2E^2 + a_3E^3 + ...$$

where $a_1 = N\alpha$, (α is the polarisability of the atom, and N is the density of active electrons). For radiation of frequency ω, and $E = E_0 \sin\omega t$ this can be expanded to give,

$$P = a_1 E_0 \sin \omega t + (a_2/2)E_0^2(1 - \cos2\omega t) + (a_3/4)E_0^3(3\sin\omega t - \sin3\omega t) + ...$$

In frequency doubling the fundamental frequency sets up a polarisation wave, in second order, of wavelength $\lambda_1 = c/2\nu n_1$, where n_1 is the refractive index of the crystal at the fundamental frequency ν. The polarisation wave induces the generation of light at frequency 2ν with wavelength $\lambda_2 = c/2\nu n_2$, where n_2 is the refractive index of the crystal at the frequency 2ν. In general λ_1 is not equal to λ_2 because n_1 is not equal to n_2. Hence λ_1 and λ_2 propagate out of phase. For propagation along the direction of the secondary beam the intensity of the second harmonic beam is, (Hecht and Zajac 1974),

$$I(2\omega) \propto \frac{\sin^2(\frac{2\pi\Delta n l}{\lambda})}{(\frac{2\pi\Delta n}{\lambda})^2}$$

where $\Delta n = n_1 - n_2$, l is the distance along the beam, and λ is the wavelength of the fundamental in vacuo. For normal crystals the distance l over which the intensity $I(2\omega)$ is significant is of the order of 10's μm. In order to get the coherence length l large Δn must be small and $n_1 = n_2$.

The effective method of providing equal phase velocities for the fundamental and second harmonic wave in the nonlinear medium, utilises the fact that in some anisotropic

crystals normal dispersion is smaller than birefringence. Under such conditions the spherical surface $n_{1o}(x,y,z)$ representing the index of refraction for ordinary waves at one frequency, will intersect the surface n_{2e} (x,y,z) of the extraordinary refractive index at the second frequency, (fig 3.9). When $n_{1o}=n_{2e}$, at angle θ, ϕ, I can become quite large (~cm), and the frequency doubling efficiencies can reach ~20% when the incident power density of the fundametal is of the order 100 MWatts cm^{-2}.

Potassium dihydrogen phosphate (KDP) doubling crystals were used to give light from 260 nm to 330 nm. The main difficulty encountered in using the crystals was in maintaining their correct orientation with respect to the incident beam. As the wavelength changes the angle of incidence necessary to ensure efficient frequency doubling also changes. This can be done manually, using a power meter to gauge the efficiency of the frequency doubling at every wavelength. All of the experimental work on determining the spectral dependence of the ionisation of background impurities in proportional counters was carried out by manually changing the orientation. Only discreet ionisation spectra can be obtained in this manner unless the wavelength steps are made smaller than the resolution of the dye laser, (~0.05nm).

A much more efficient and costly approach is to use a dedicated piece of hardware to orientate the crystals. The one used was the INRAD Model 5-12 Autotraking System. By sampling a small percentage of the UV output from the crystals, and focussing this onto two photodiodes, the orientation of the crystal could be continuously adjusted using a servo controlled motor, figure 3.10. This maximises the doubling efficiency of the crystal as the wavelength of the fundamental dye laser is changed. By these two methods of control, manual and electronic, wavelengths in the range 262-330 nm could be reached with a lasing power of around 10% of the power from the dye laser.

CRYSTAL RANGE (nm)	FUNDAMENTAL WAVELENGTH (nm)	FREQUENCY DOUBLING
KDP'B1'	525-565	262-283
KDP'R6G"	565-660	282-330

40
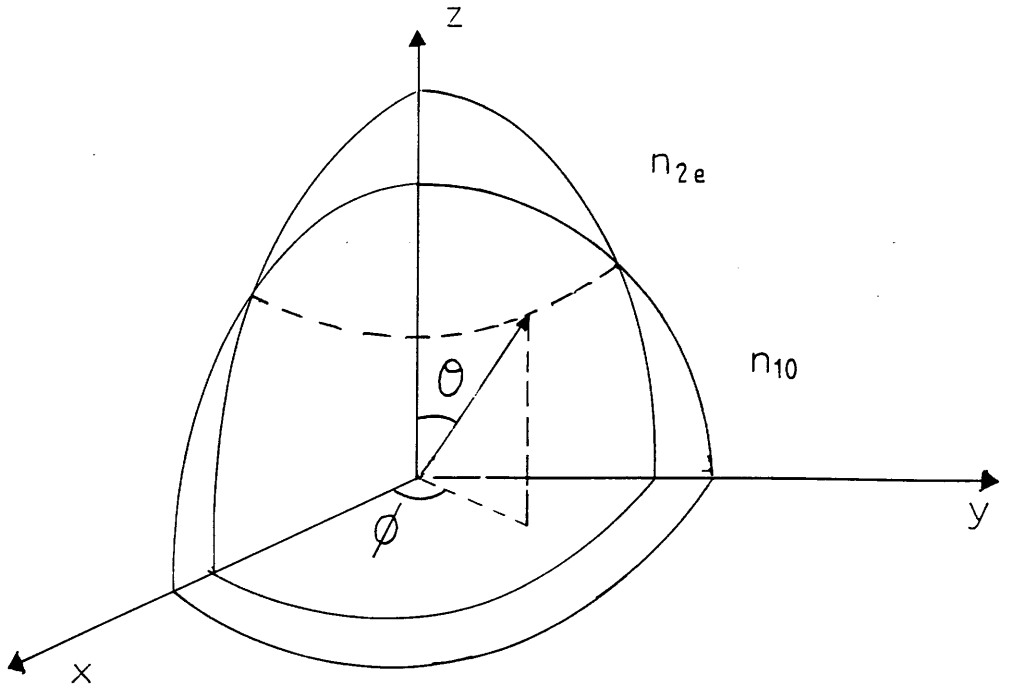
Fig 3.9   Matching of the ordinary n_{1o} and extraordinary n_{2e} refractive indices
           in KDP crystal for frequency doubling of incident light.
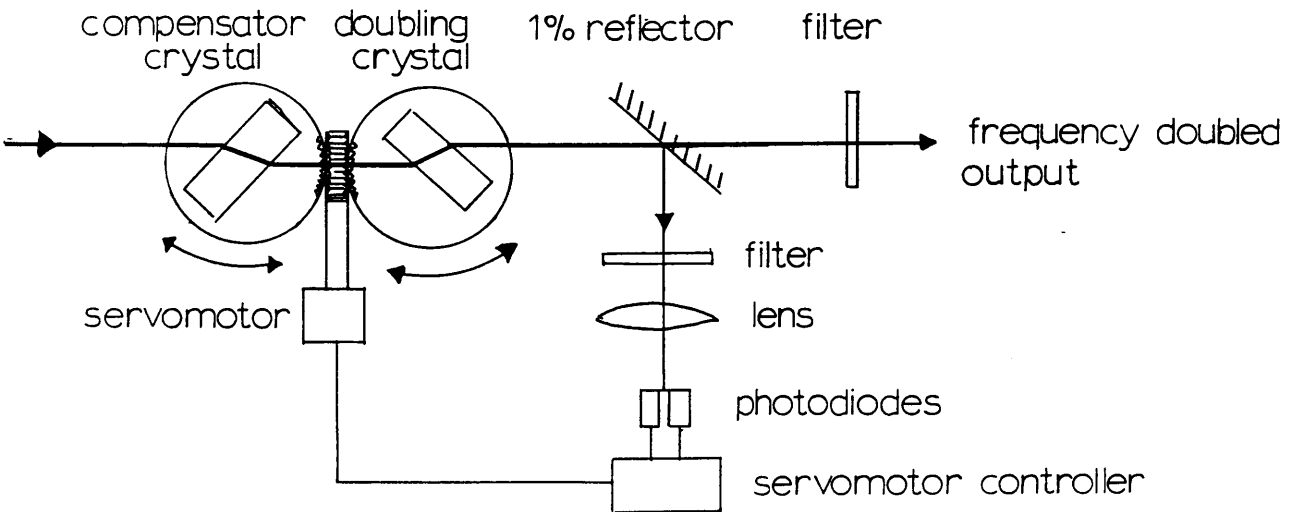
Fig 3.10   Electronic control of angle of incident light on KDP doubling crystal.

VARIABLE ATTENUATOR

The varible attenuator provided a means of manually regulating the laser power, without (in theory) either distorting the beam profile or changing the position of the beam line.

The variable attenuator was made from four quartz plates arranged in two pairs providing eight planes at which the laser light was both transmitted and reflected. The two pairs of plates could be rotated with respect to each other, changing the angle of incidence and the attenuation of the laser beam, figure 3.11. The attenuation was continuously variable between the minimum 80% transmittance and the maximum 0% transmittance.

In practice, when operated near the maximum 100% attenuation, the beam line shifted appreciably. This caused problems in that the level of ionisation recorded by the proportional counter and quadrupole mass spectrometer was always dependent, to some extent, on the position of the laser beam through the ionisation region. In some instances this shift resulted in the ionisation increasing as the laser power decreased. Therefore caution should be exercised in interpreting the dependence of the ionisation at low laser power (near maximum attenuation) in the log/log plots of ionisation against laser flux.

LASER POWER METER

Pyroelectric joulemeters (Molectron J3-05 and J3-02), with a constant fast response from 200 nm to 4000 nm, determined the laser pulse power. The joulemeter integrates each pulse outputting a linearly rising voltage, the peak amplitude of which is proportional to the total energy in the laser pulse. The signals from these meters (J3-05; 2.68 volts per mJ laser power: J3-02; 0.87 volts per mJ) were amplified, delayed to coincide with the signal from either the proportional counter or quadrupole, and then digitised pulse by pulse and stored on floppy disks.

OPTICAL ATTENUATOR

counter-rotating wedged optical plates
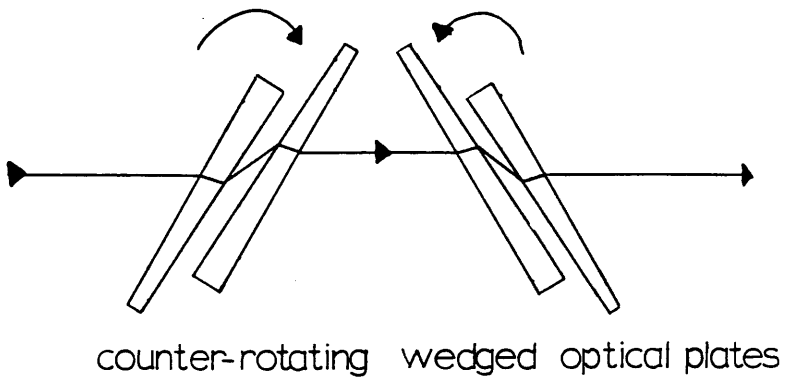
Fig 3.11   Optical attenuator.

3.2 PROPORTIONAL COUNTER

As an introduction to resonant ionisation proportional counters have three main advantages. They are easy and cheap to build, simple to operate and can be very efficient, detecting down to single electrons, (Hurst et al 1975)

OPERATION

In a proportional counter a thin detector wire (diameter ~0.002") is held at a high positive potential (~1000 Volts), and is surrounded by a cylindrical (earthed) cathode. Electrons, formed from the resonant ionisation of atoms or molecules, accelerate towards the wire colliding with buffer gas (noble gas) atoms. If the collisions are energetic enough the buffer gas atoms will be ionised creating more electrons. All the electrons, initial and collisionally induced, then accelerate towards the wire and cause further ionisation. This avalanche effect amplifies the original signal. Finally the electrons impinge on the wire and are detected as a charge pulse with a fast amplifier. The buffer gas also has a certain percentage of quenching gas added to stop the avalanche process continuing too long. Standard P10 counter gas consists of 90% argon and 10% methane, the methane acting as the quenching gas.

IONISATION CHAMBER HOLDING THE PROPORTIONAL COUNTER

Figure 3.12 shows the main details of the chamber. The design of the chamber holding the proportional counter centred around the intense reactivity of the caesium metal. In order to hold caesium in its unreacted state for a period of weeks, a very clean counter was desired. This was achieved by using stainless steel high vacuum components which could be baked out under vacuum. The problem of the introduction of the caesium sample into the counter was solved by keeping it in a small glass ampoule, which could be broken and the caesium released, when the counter was "clean enough"; clean enough was defined as being when the background ionisation from impurities in the counter reached a level of around 0.5 ion pairs $mm^{-2} \mu J^{-1}$ at 308 nm wavelength. The sample holder was designed to collimate the caesium atoms but in the event the source of the caesium atoms was found to be the stainless steel probe that was used to break open the glass ampoule of caesium.

LINEAR MOTION DRIVE
(ALLOWS VERTICAL MOVEMENT
OF PROBE)

COPPER SEAL

EDGE WELDED BELLOWS

PROBE(TO RELEASE Cs FROM AMPOUL

SIGNAL OUT
(TO EXTERNAL ELECTRONICS
inc. LSI-11 MICROCOMPUTER
via. BNC CONNECTOR)

SIX-WAY CROSS PIECE
PROPORTIONAL COUNTER

LASER BEAM

QUARTZ WINDOW

LASER BEAM
COLLIMATOR

GLASS/METAL SEAL

Cs IN GLASS
AMPOULE

^{55}Fe RADIOACTIVE SOURCE
COLLIMATED X-RAY BEAM

FIG. 3·53: CAESIUM CHAMBER MARK 3 STAINLESS STEEL DESIGN

Fig 3.12   Stainless steel chamber to house the proportional counter used for
detection of caesium and rubidium.

CALIBRATION OF THE PROPORTIONAL COUNTER

An [55]Fe X ray source was mounted so that the collimated X rays would be emitted parallel to the laser beam, and would cause ionisation in approximately the same region as the laser. These 5.9 keV X rays produce approximately 227 ion pairs per photon in P10 counting gas, (Hubricht et al 1985).

IONISATION VOLUME

The proportional counter was designed so that the effective ionisation length was well defined. A window 2 cm long was cut in the earthed casing surrounding the counter wire. This window enabled the electric field from the wire to leak out into the ionisation region causing electrons formed there to drift towards the window and be amplified in the strong fields close to the wire. Any ions produced outside this window should not be detected.

The unfocussed laser was normally collimated to a 1mm x 1mm size, giving an ionisation volume of 2×10^{-2} cm^3. When focussed using a 25 cm lens the laser was not collimated. The diameter of the focussed laser beam at the focal point was measured to be 0.13 mm using a Spiricon diode array, and the ionisation volume was estimated at 1.7×10^{-4} cm^3.

OPERATING PRESSURE

The operating pressure of the counter was normally 30 torr. This relatively low pressure was chosen for two main reasons, to reduce the photoelectron background, and to reduce the number of organic impurities in the chamber.

Photoelectrons arise from stray or scattered light striking the inner surfaces of the counter and ionising caesium or rubidium atoms that have condensed there. It occurs at all wavelengths and contributes to the background ionisation. Some scattering is dependent on the pressure of the buffer gas and therefore lowering the pressure should reduce the photoelectron background.

Organic impurities are known to be responsible for laser induced background ionisation in proportional counters, (Hubricht et al 1985). They may also react with

caesium metal and reduce its active life in the chamber. Lowering the pressure of the gas would reduce their concentration in the chamber, and increase the lifetime of the caesium metal.

At a pressure of 30 torr, the amplification in the proportional counter is slightly unstable in that the electron avalanche is not adequately quenched. This was evidenced by a very rapid change of gain in the counter gas with voltage. In order to increase the stability a different gas mixture was used consisting of 70% argon and 30% methane. For work on rubidium however the P10 counter gas was successfully used at 30 torr pressure.

ETALONING IN THE QUARTZ WINDOWS

When the laser wavelength was scanned and the laser beam passed through the chamber at angles close to the normal, etaloning in the quartz windows became noticeable. The problem was most evident in the three photon ionisation of caesium using a focussed laser. Condensation of caesium on the inner surfaces of the quartz windows of the ionisation chamber acts as a mirror and increases the effect, fig 3.13. The cycling ionisation tends to hide real spectroscopic detail, figure 3.14.

The quartz windows are close to parallel and, when the thickness of the window, d, is equal to an integral number of half wavelengths, constructive interference occurs in the transmitted light. The peaks of succesive orders, which indicate high transmission, are separated by $(1/2nd)$ cm^{-1}, where d is the thickness of the window in cm and n is the refractive index of quartz (~1.5)

To reduce the problem the angle of incidence of the laser light through the chamber was increased although this tended to increase the background ionisation from scattered light. A more suitable solution would be to use wedge-shaped non-parallel windows.

DISADVANTAGES OF PROPORTIONAL COUNTERS

The main dis-advantage with proportional counters is the absence of mass discrimination. Electrons formed from the ionisation of different atoms can only be distinguished by their spectral dependence. Isotopic analysis therefore requires narrow band-width lasers and was not possible with the excimer pumped dye laser.
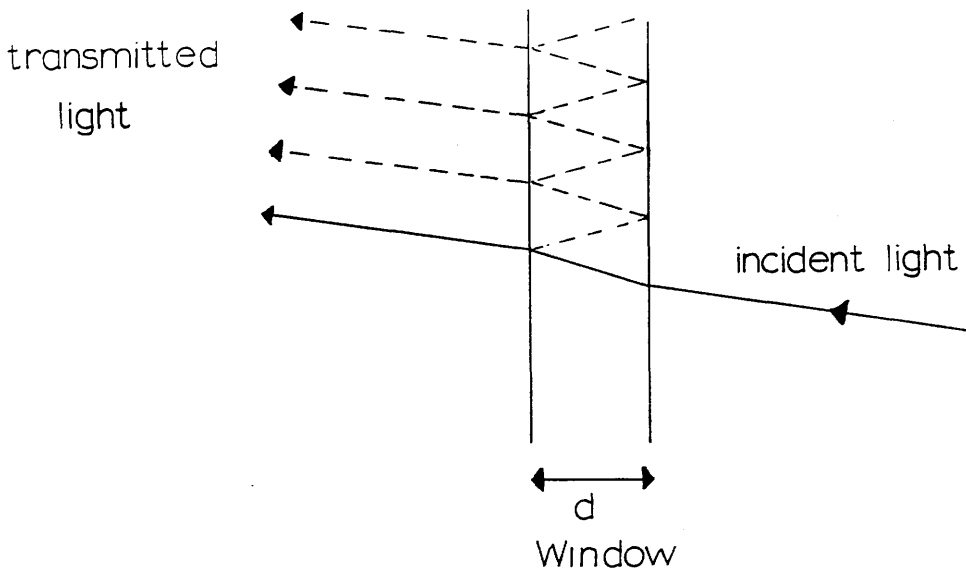
Fig 3.13   Quartz window acting as transmission etalon.
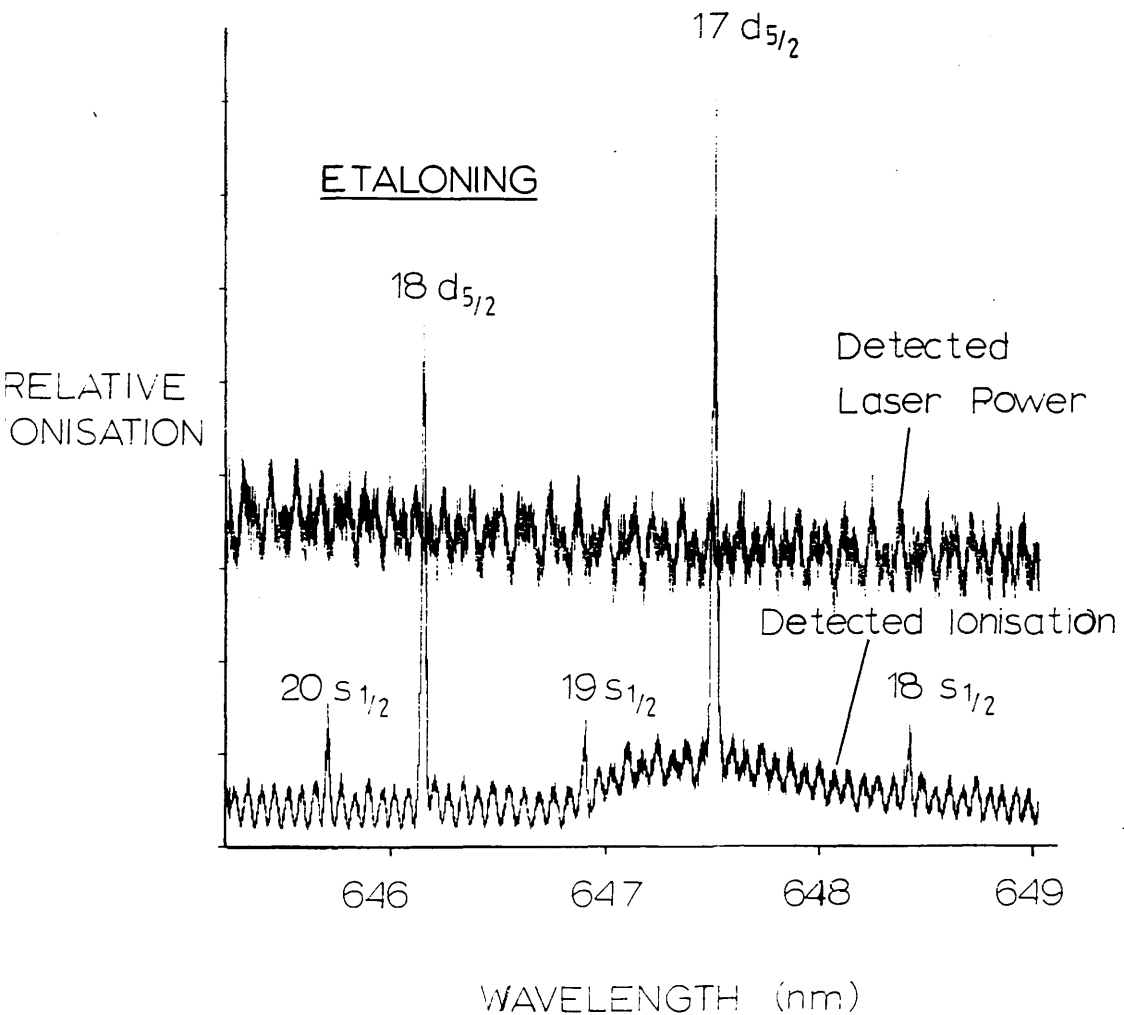
Fig 3.14   Effect of etaloning on ionisation in the proportional counter, and on the detected laser power.

The presence of the buffer gas collisionally broadens the spectral lines and further reduces isotopic selectivity.

Impurities in the buffer gas may also react with the sample shortening its useful lifetime, and may also contribute to the background ionisation which reduces the ability of the counter to detect small numbers of atoms. These impurities are known to outgas from the chamber walls, but were also reported as being an inherent impurity in P10 counter gas, (Boerner 1985)

Finally, the electric field from the counter wire will perturb the transition wavelengths, shifting and broadening them, and will also field ionise atomic levels close to the continuum.

3.3 MASS SPECTROMETERS

From detection using a proportional counter, with elemental selectivity, the next step was the inclusion of mass analysis. The most widely favoured mass spectrometers for resonance ionisation detection are quadrupole, time of flight and magnetic sector, of which quadrupole and time of flight instruments have been used at Glasgow. The quadrupole instrument was used to separate the ionisation signals of the two rubidium isotopes and to determine the strength of the ionisation of Rb_2 dimers relative to the atomic signal. Resonant ionisation of rubidium continued in the TOF instrument as a means of optimising its detection efficency. Samples, from the National Bureau of Standards (NBS), of coals with known impurities at levels down to parts per billion, will be used to determine the absolute detection efficiency of the instrument.

3.3 a) QUADROPOLE MASS SPECTROMETER

OPERATION

The mass separator consists of four metal bars (a quadrupole) running the length of the instrument, each bar set at the corner of a square. DC (direct current) and RF (radio frequency) fields of one potential are applied to an opposing pair of bars, whilst

quadrupoles

-ve(DC+RF)

+ve (DC+RF)
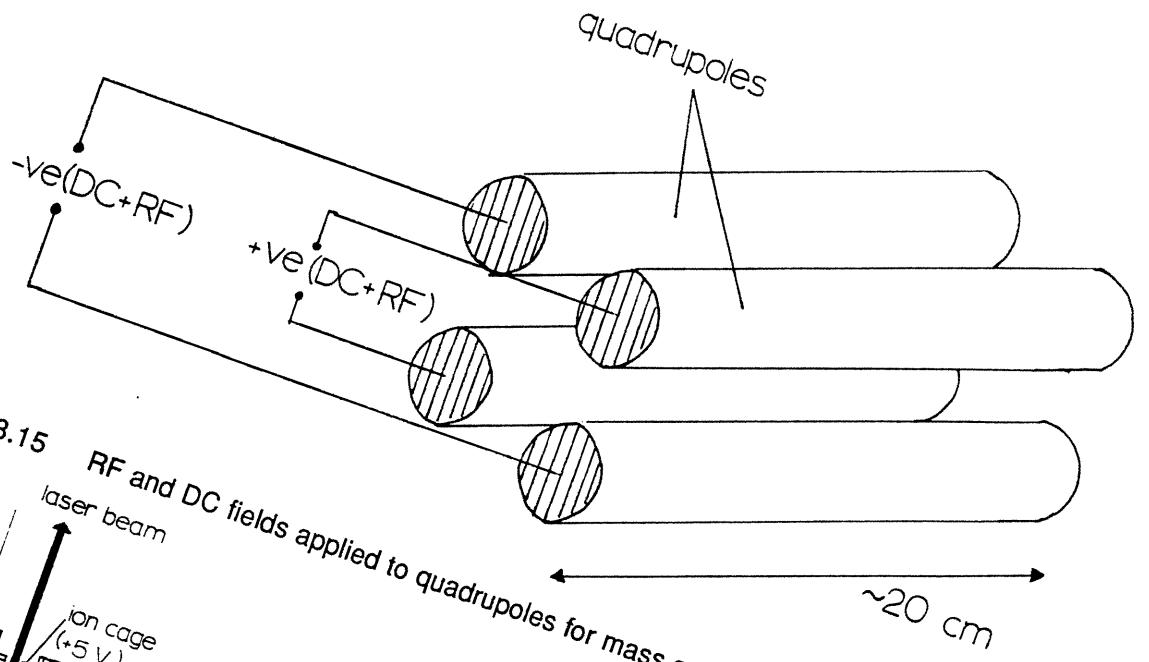
Fig 3.15   RF and DC fields applied to quadrupoles for mass selection.

~20 cm

grid

laser beam

proportional
counter

ion cage
(+5 V)

quadrupole

extension piece (earthed)

faraday cup

channeltron
(off axis)

ion cage

proportional counter

gas inlet
and
pressure
guages

laser

extension piece

turbo molecular
pump

quadrupole

caesium / rubidium
holder

ion detect
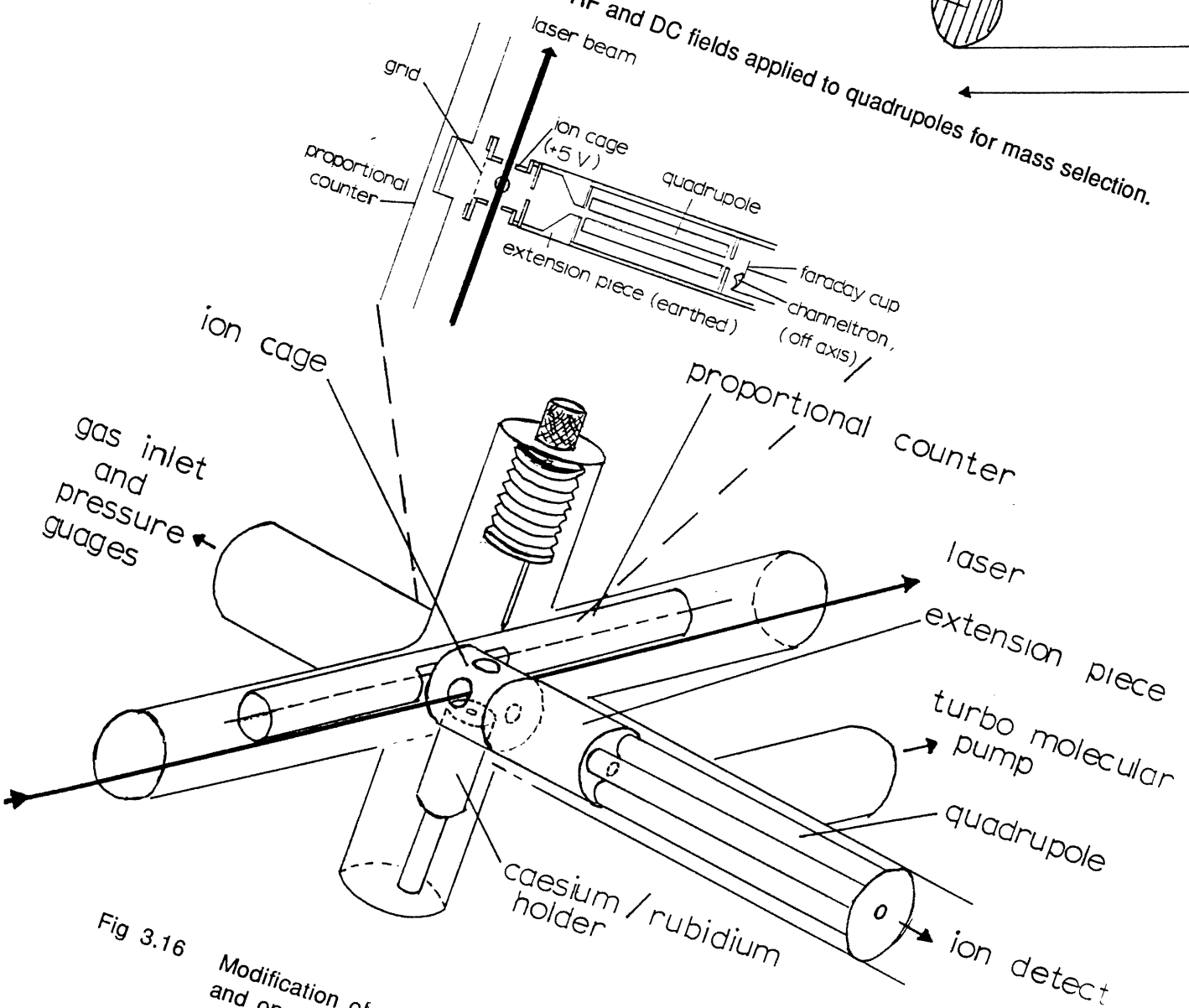
Fig 3.16   Modification of quadrupole mass spectrometer for resonant ionisation
and operation with proportional counter.

similar fields of the reverse potential are fed onto the other pair of bars. This is illustrated in figure 3.15. Ions entering the quadrupole oscillate in particular trajectories dependent on the RF/DC ratio and on the ions charge/mass ratio. These trajectories will be either stable, allowing the ions to pass through the quadrupole field, or unstable, in which case the ions impinge directly on the quadrupoles or the walls of the mass spectrometer and are lost. By varying the RF/DC ratio, different ion masses (or charge/mass ratios) are allowed to pass through the mass filter.

MODIFICATIONS FOR LASER IONISATION

The instrument used in these experiments was a VSW Mass Analyst with a mass range 0-200 amu. and a resolution of approximately 1000. Ions were normally formed by electron bombardment in a cylindrical ion grid cage. These were extracted, focussed and injected into the quadrupole by ion focussing elements.

To enable this instrument to be used with laser ionisation in conjunction with the six way cross holding the proportional counter, an extension piece approximatedly 3 cm long was bolted on to the mass spectrometer, effectively moving the ion cage further forward. This is illustrated in figures 3.16 and 3.17. The filaments used for electron impact ionisation were removed, and the ion cage was operated with a positive voltage of between 2 and 10 volts to encourage the ions to enter the quadrupole. The extension piece was kept earthed. The proportional counter remained in place, as illustrated in figure 3.10, and could be easily used by switching off the high voltage to the ion detector in the mass spectrometer and filling the entire instrument with counter gas. Use was made of this to determine the wavelength of atomic resonances before switching over to the mass spectrometer, to try to "tune up" the mass spectrometer.

The effect of this modification was to split masses into four components, figure 3.18 The mass resolution was also reduced. This phenomena is indicative of defects in the ion optics, (Austin 1976).

The arm of the six way cross holding the sample could be heated so as to increase the vapour pressure of the sample, although rubidium atoms were easily detected when at room temperature, at a pressure of around 10^{-7} torr.
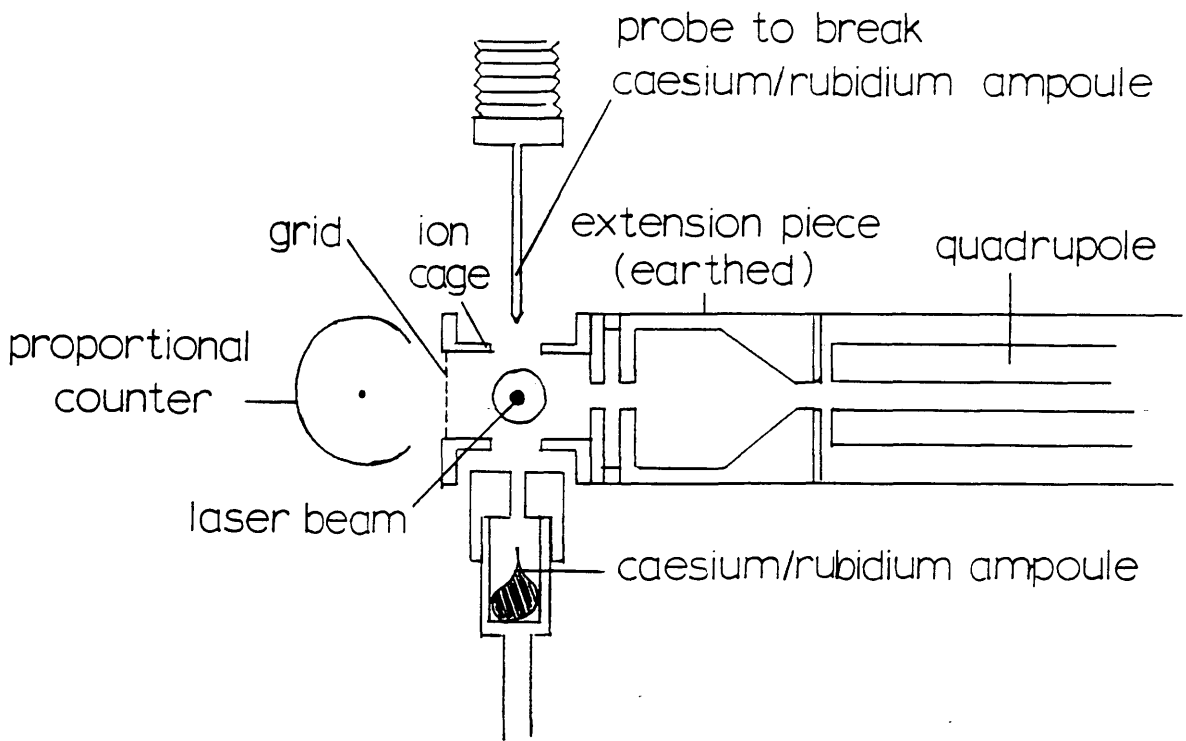
Fig 3.17   Modification of quadrupole mass spectrometer for resonant ionisation
and operation with proportional counter.
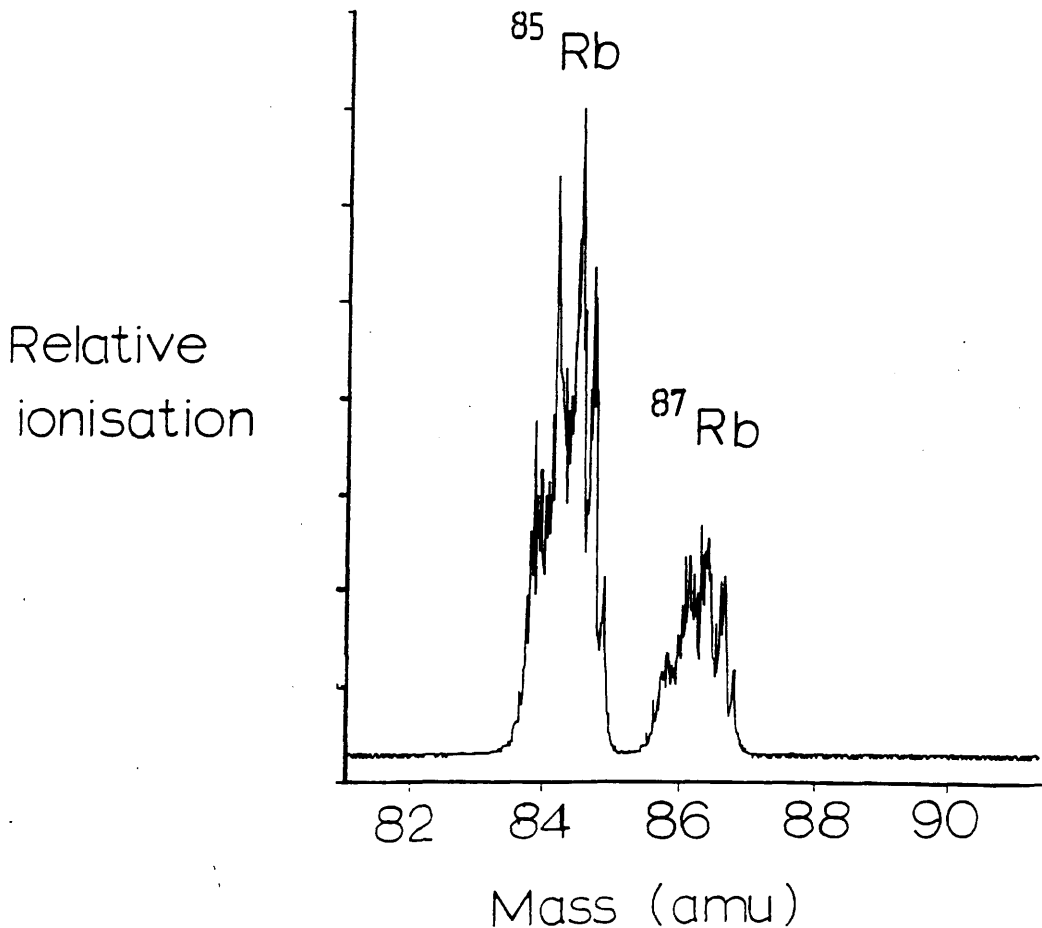
Fig 3.18   Typical mass spectra from modified quadrupole mass spectrometer
showing splitting of each mass peak.

One definition for the overall detection efficiency is the product of the ion injection efficiency into the quadrupole, the transmission efficiency through the quadrupole and the detection efficiency of the ion detector. It can be determined from the ratio of the number of ions detected, at one particular mass, to the number of laser induced ions of that mass formed in the ionisation volume. It was difficult to determine an accurate value for this efficiency due to the modifications made to the quadrupole, but by comparing the ionisation signals detected in the quadrupole with known ionisation signals in the proportional counter taken at similar laser powers, and at the same resonant transition, the detection efficency as defined above, relative to the proportional counter, was estimated to be 10^{-2}. A major assumption in this rough calculation was that collisional ionisation of the photoexcited state in the proportional counter was negligible. Ionisation was via the 5s - 8d two photon transition in atomic rubidium which lies about 0.3 eV below the ionisation continuum. The efficiency was determined at unit mass resolution at mass 85, ($m/\Delta m = 85$), ie. at a much lower mass resolution than the quoted specification for the instrument when operated in electron bombardment mode, ($m/\Delta m \sim 1000$). With higher mass resolution the efficiency would drop lower.

Most of the ion loss was thought to be due to a low ion injection efficiency into the quadrupole field. Only those ions which are injected nearly parallel to the quadrupole axis are transmitted, all others impinge on the poles and are lost. Since the laser induced ions are formed along an axis at right angles to the poles, most will enter the fields at large angles and will not be transmitted. The transmission effeciency of ions through the quadrupole was stated, by the manufacturures, as ~15% at mass resolution 1000 ie. of those ions injected into the quadrupole along the pole axis only ~15%, at any mass, reach the detector. At the lower resolution of around 100, (at which the work on rubidium was carried out), the transmission should approach unity, assuming the transmission efficiency to be inversely proportional to the square of the mass resolution, (Brunnee 1987).

ION DETECTOR

The detector used was a Gallileo 4771 dynode electron multiplier (channeltron) with a maximum gain of about 10^5. This was mounted off axis, to reduce signals from

neutrals and stray photons. The detection efficiency of the channeltron was ~50%.

The pressure in the mass spectrometer was normally 9×10^{-6} torr and was maintained using a turbo molecular pump backed by a rotary pump.

DISADVANTAGES OF QUADRUPOLE MASS-SPECTROMETERS

The main disadvantage of the quadrupole mass spectrometer when used with pulsed laser ionisation is that only one mass is detected per laser pulse. Therefore in order to build up a complete ion mass picture (0-200 amu), many laser pulses are needed. The pulse to pulse variation in the laser power is then a problem when comparing ionisation signals at two different masses. This can be solved by averaging the ionisation signal at one mass over a number of laser pulses, which increases the time taken to build up a complete mass scan.

Other major drawbacks with this particular quadrupole, and which may not be generally true, were the low detection efficiency, and poor mass resolution.

3.2 b) TIME OF FLIGHT MASS SPECTROMETER

The construction of a purpose built resonant ionisation TOF mass-spectrometer was the immediate aim of the Laser Ionisation Studies group at Glasgow. Its design and gradual construction began in 1986 and the first results from the instrument were recorded early in 1988. Figure 3.19   illustrates the main features of this instrument.

OPERATION

The principle behind time-of-flight mass separation is quite simple, figure 3.20. Ions are accelerated in an electric field, gain kinetic energy and then drift a set distance in a field-free region before hitting an ion detector. The flight time, t, of an ion in the drift region is related to its mass, m, and charge, q, by

$$t = [md^2/2qV]^{1/2}$$

4 8

X,Y,Z,θ MANIPULATOR

SAMPLE TRANSFER PROBE

SAMPLE

GATE VALVE

ROUGHING PUMP

ION OPTICS

Ar/Kr ION GUN

GAS INLET

DIFFERENTIAL TURBO PUMP

DIFFUSION PUMP

SUBLIMATION PUMP

PUMP

ELECTRIC CONNECTIONS

CHANNEL PLATE DETECTOR

15 METRE REFLECTRON
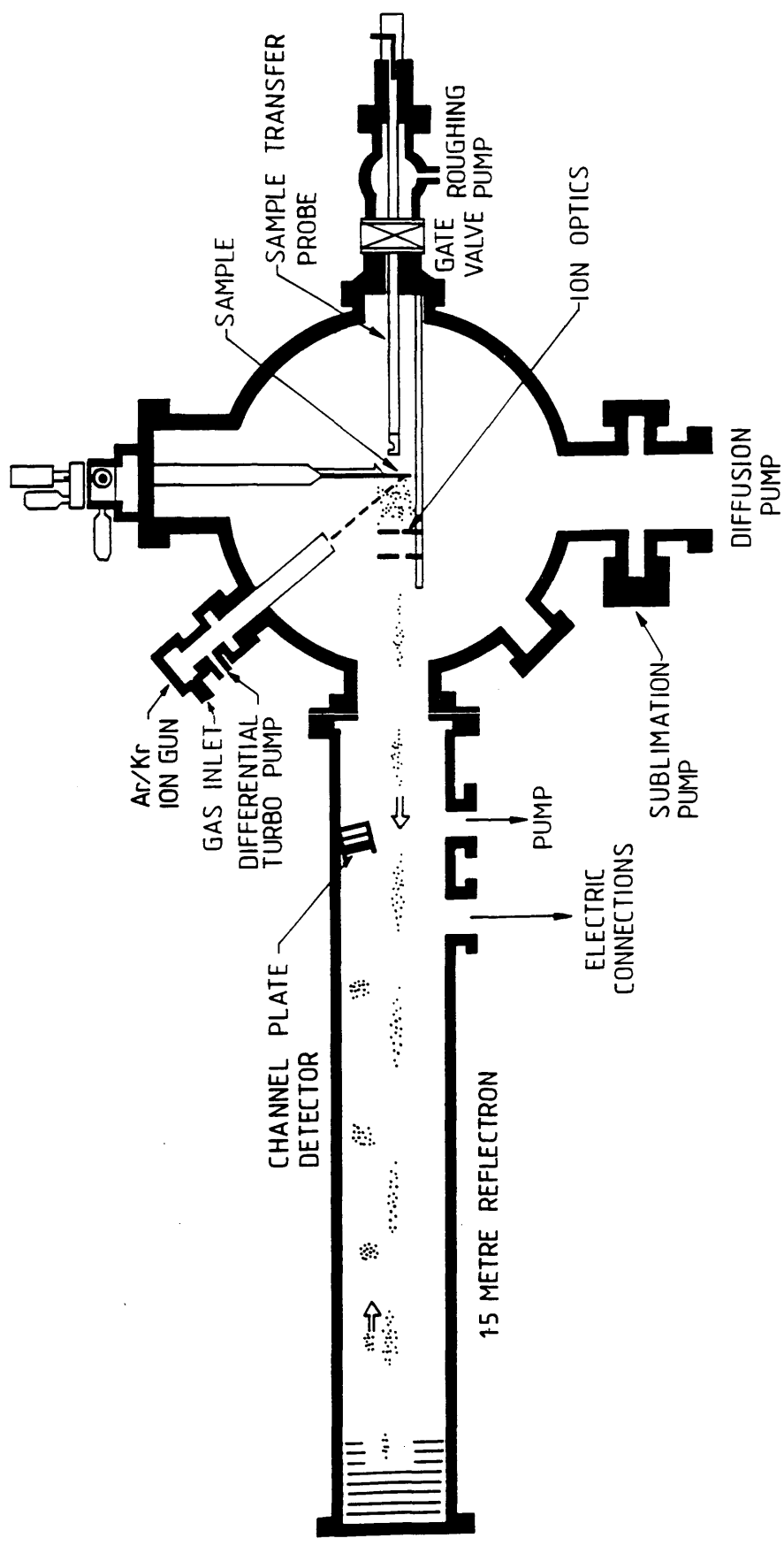
Fig 3.19   Main features of the resonant ionisation time of flight mass spectrometer with ion ablation.
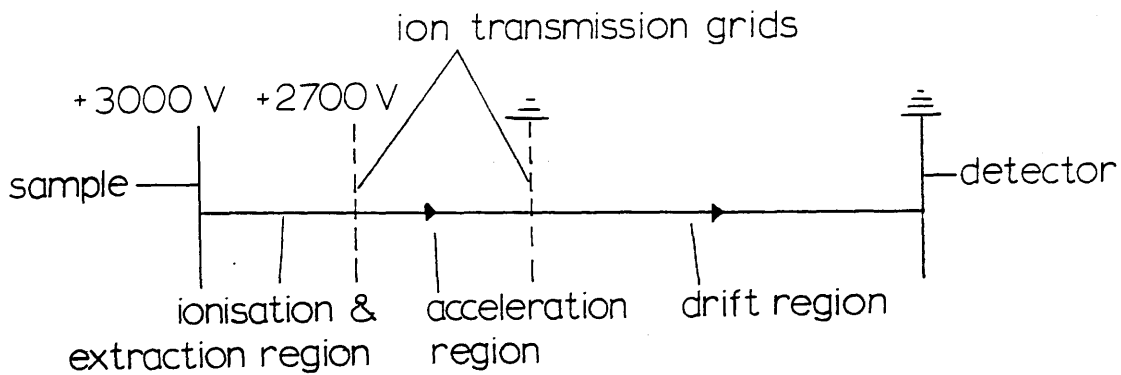
Fig 3.20   Principle of operation of time of flight mass spectrometer.
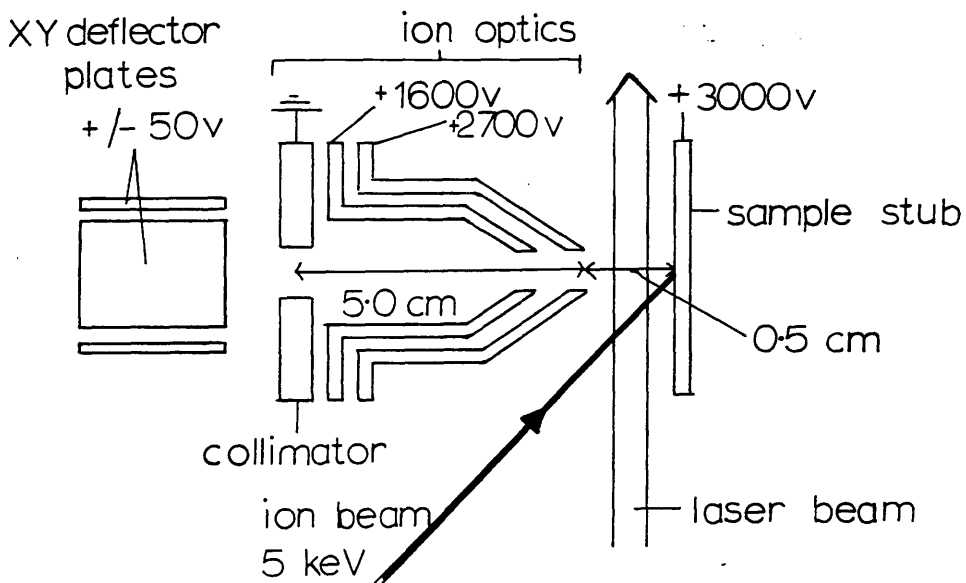
Fig 3.21   Ion optics used for time of flight mass spectrometer.

where V is the accelerating voltage and d is the drift length. The mass resolution can be expressed,

$$m/\Delta m = t/2\Delta t$$

The mass resolution is defined as the mass at which the FWHM of the time spread is equal to 1 mass unit. It increases with the square root of the mass, and can be of the order of 2500, for a laser pulse width of 10 nsec and ion flight time of 50 μsec, assuming that the laser is the sole contributor to the spread of the time packet.

SAMPLE VAPOURISATION

The sample may be vapourised by bombarding the surface of the sample with high energy ions (sputtering), or by ablating the surface with a laser. An argon ion gun is currently used and is set at 55 degrees to the normal of the sample surface. It produces a 30 μA beam current with ion energies up to 5 kV. The gun has been adapted for both continuous and pulsed operation, the pulses being variable between 0.2 μsec and 10 μsec long. Pulsed mode utilises the sample more efficiently in that with a laser repetition rate of 20 Hz, sputtering is timed to coincide with the laser pulse. Continuous sputtering is wasteful of the sample and also results in a large background ionisation signal of secondary ions formed during the sputtering process itself. Laser ablation may be carried out by focussing through a quartz window, at an angle of either 45° or 55° to the sample normal.

Sputtered ions and laser induced ions are extracted towards the ion optics by a 200-300 V potential between the sample stud and optics, figure 3.21. The ions are then accelerated over a ~2700 V potential and are then focussed into the field free region where they drift towards the ion mirror, using an electrostatic guide wire to increase transmission. After reflection the ions drift back down the flight tube, with a total round flight path of about 2.5 metres, and impinge on the ion detector.

REFLECTRON ION MIRROR

The reflectron ensures that all singly charged ions of the same mass have the same flight time from the ion optics to the detector. Mamyrin et al (1973) originally described the principle of operation, and demonstated it experimentally. By setting up electrostatic fields through which the ions are transmitted, those ions which are

Electrostatic Ion Reflector
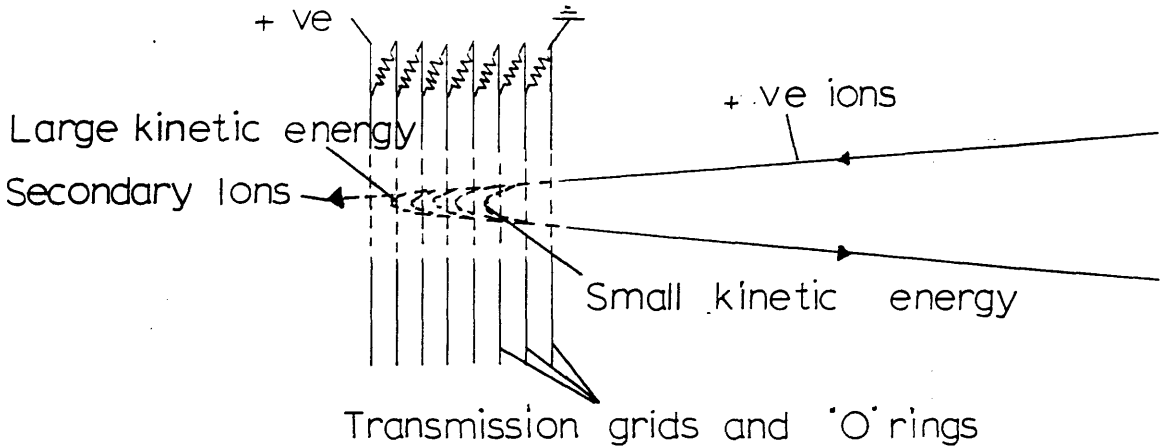
Fig 3.22 Principle of operation of electrostatic ion reflector. With the correct fields, secondary ions sputtered from the sample surface pass through the reflector and are not detected.
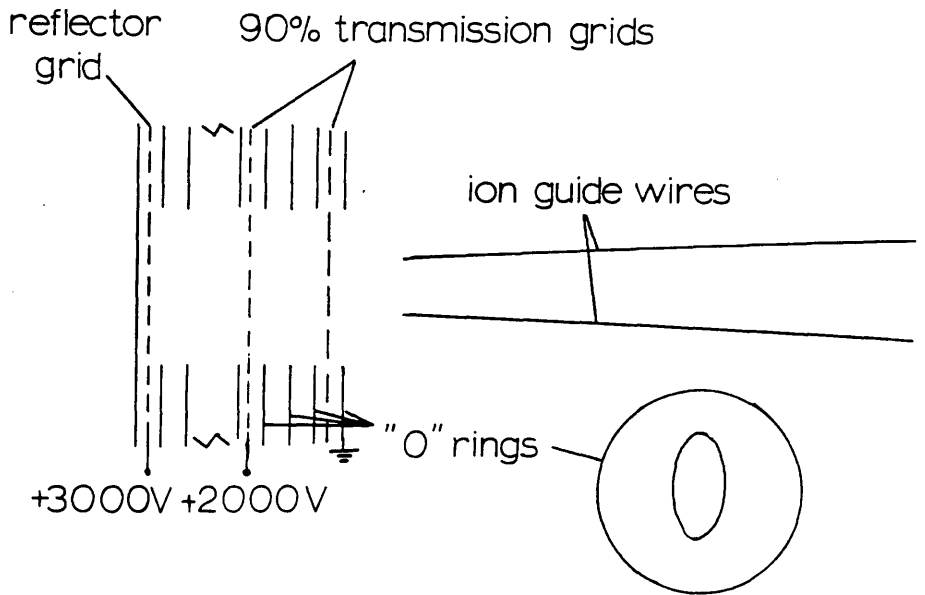
Fig 3.23 Ion relector used in Glasgow TOF system. The electric fields are set up by ~20 "O" rings and two transmission grids. Thin wires held at a small negative potential (-ve ~30 V) act as guide wires for the incoming and outgoing ions.

travelling faster (with more kinetic energy) probe deeper into the electric fields and take a longer time to be reflected. The slower moving ions (with less kinetic energy) penetrate less deeply and spend less time in the reflector. As a result all ions of the same mass should have the same "drift" flight time, figures 3.22 and 3.23.

However the reflectron cannot compensate for the initial time spread of ions when they enter the drift region, produced in the ionisation/extraction region. This time spread has three main causes, (Singhal 1988b),

1. The spatial orientation of the atoms resulting from the finite width of the laser beam, fig 3.15. Those ions formed closer to the sample stub receive more energy in the extraction field than those formed further away from the stub. Reducing the spatial cross-section of the laser beam reduces this time spread.

2. The initial velocity distribution of the atoms. Ions moving toward the stub must be slowed down, turned around and accelerated towards the extraction optics. Increasing the voltage potential in the initial extraction region would reduce this effect.

3. Finite pulse length of the laser. Ions are created throughout the 10 nsec pulse of the lasers. Increasing the extraction voltage over the period of the laser pulse would compensate for this by giving the ions formed at the end of the laser pulse more energy.

One other purpose of the reflectron is to reduce the background ion signal from secondary ions formed during the sputtering of the sample by either the ion gun or laser. These "secondary ions" are produced in a different region of the acceleration field from the laser induced ions, and subsequently have more energy. By a judicious selection of voltages on the reflectron grids these secondary ions pass through the reflectron and are not detected.

ION DETECTOR

The detector is a double micro channel plate detector with a gain of about 10^7 and is illustrated in figure 3.24. A micro channel plate is an array of 10^4-10^7 miniature electron multipliers orientated parallel to one another. Each channel is around 10-100 um wide and is set at an angle of 10^0 to the normal. The channel matrix is
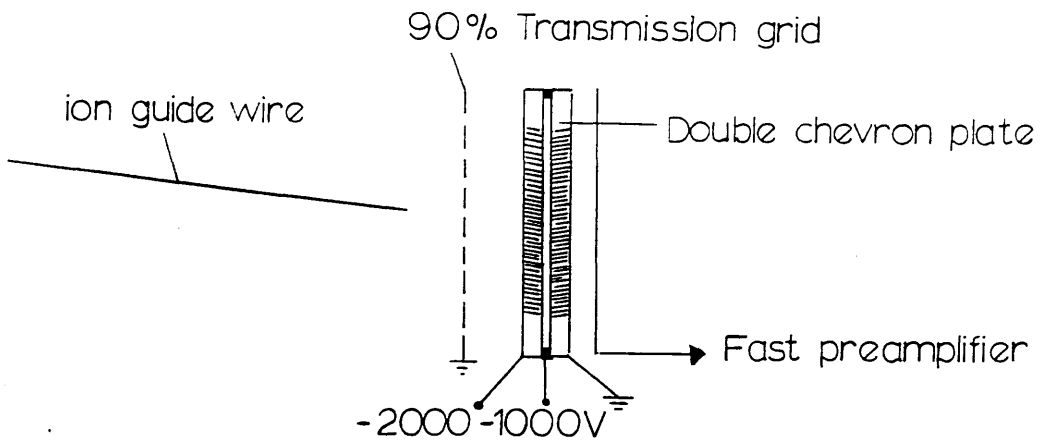
Fig 3.24 Double microchannel plate ion detector used in TOF system.
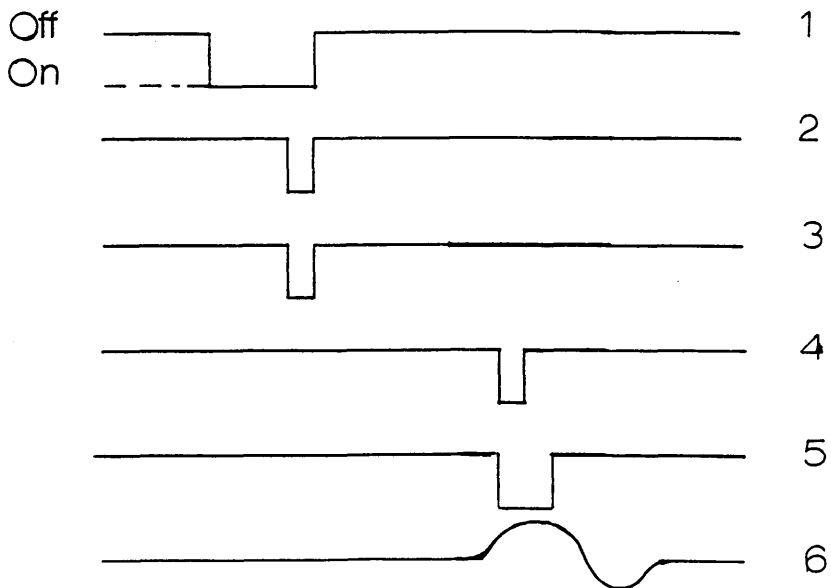
Fig 3.25 Timing signals for data acquisition.

fabricated from lead doped glass making the channel walls semiconducting. By applying a voltage potential of around 1000 V between the front and rear surfaces of the plate, each channel acts as an electron multiplier with a gain of about 10^4. To obtain a higher gain two plates separated by 150 μm may be used as shown in figure 3.18. Electrons finally hit a metal anode situated behind the two plates and a charge pulse is detected. This is commonly called a Chevron configuration. Chevrons detect incident positive ions with high efficiency (60-85%) in the energy range 2-50 keV and at a lower efficiency of 5%-85% for lower energies 0.5-2 keV. The rise time of the charge pulse is less than 500 psecs and the pulses are less than 1nsec wide. This fast response time is the major advantage of the MCP over electron multipliers such as the channeltron in the quadrupole, since the rise time and pulse width will limit the separation of adjacent masses and hence the mass resolution.

DATA ACQUISITION FOR TIME OF FLIGHT MASS SPECTROMETER

The ions are distinguished by their arrival times at the ion detector. The spread in times will be of the order of 100 μsecs for a mass spread of 1000, and must be split up into a large number of smaller "time bins".

A Le Croy 2261 transient recorder provides up to 1280 channels each of 5 nsec width giving a total detectable time spread of 6.4 μsec. Masses over a range of 40 amu are therefore detected for each laser shot, but this is dependent on the particular voltages used on the ion extraction and acceleration optics. The width of each time bin can also be increased which decreases the mass resolution but increases the mass range. Data from each laser pulse is digitised, stored in these bins and transferred from the transient recorder to an IBM PC for a permanent record of the spectra. Analysis and plotting of the data is carried out using an IBM PC. The maximum laser repetition rate at which the data acquistion system can record data is 10 Hz.

ADVANTAGES AND DISADVANTAGES OF TOF MASS SPECTROMETERS

TOF mass spectrometers operate in pulsed mode and are thus ideally suited to pulsed laser ionisation.

1. Each laser shot will produce a complete mass scan and the repetition rate is only limited in theory by the flight time of the slowest ions. The pulse to pulse variation in

laser power is therefore immaterial.

2. In trace element analysis the pulsed mode combined with pulsed sample ablation and complete mass scans increases the efficiency of sample utilisation.

3. The resolution of the instrument is not dependent on accurate construction of the flight tube, but is much more dependent on the speed of the electronic data acquisition system, and on optimising the electric fields of the ion optics.

4. Transmission of the ions from the accelerating region to the detector can be made very efficient, up to 50%.

5. The maximum detectable mass is not theoretically limited.

Disadvantages include a low mass resolution, which makes the instrument unsuitable for measuring for example large isotope ratios, and the large electric field strengths in the ionisation region which, if applied continuously, will perturb atomic states and tend to lower the resonant ionisation yield.

3.4 DATA ACQUISITION SYSTEM FOR PROPORTIONAL COUNTER AND QUADRUPOLE MASS SPECTROMETER

The arrangement of the electronic apparatus used to amplify and record the data is shown in figure 3.2. The high voltage supply to the proproptional counter wire (Ortec 456) was fed through a pre-amplifier (Ortec 142). The charge pulses from the proportional counter wire were passed through the preamplifier, a main amplifier (Ortec 485) and a delay amplifier (Ortec 427). Signals from the laser power meters were also amplified (Ortec 485) and delayed (Ortec 427) to coincide with the ionisation signal.

The now coincident signals were fed into two channels of a peak sensing seven channel analogue/digital convertor (ORTEC AD 811) which had a resolution of 11 bits (2048) and could digitise signals between 0 and 2 volts. The conversion time was 80 μS. The data was stored event by event on floppy discs and was displayed on line. The data

acquisition and storage was controlled using a LSI-11 computer running a BASIC language. A photodiode picked up light from the dye laser and provided the timing signal for the computer.

ELECTRONIC TIMING SIGNALS FOR DATA ACQUISITION   (figure 3.25)

1) The computer signifies its readiness to accept data by switching on the gate generator.

2) The photodiode pulse after passing through a octal discriminator.

3) If 1 and 2 are coincident a NIM pulse is generated. This stops the gate generator (1).

4) The NIM pulse is delayed to coincide with the incoming ionisation and laser power signals.

5) The NIM pulse is widened from 10ns to 600ns, the gate width for the ADC.

6) Incoming ionisation or laser power signals.

The electronic controls and data acquisition supplied with the quadrupole mass spectrometer were associated with electron bombardment ionisation and were not suited to pulsed laser ionisation operation. The ionisation signals were amplified in a Nuclear Enterprise 4603 amplifier, to shape the pulse, and then fed into the data acquisition system normally used for ionisation in the proportional counter, as described above.

DATA ANALYSIS

The ionisation signal and the laser pulse power were recorded shot by shot on to floppy disks. The data was then transfered to an IBM mainframe computer for analysis and plotting.

For plots of the spectral dependence of the ionisation, all the data points were plotted separately with the exception of those points for which the recorded laser power was zero.

Normalisation of the ionisation with respect to the laser power was possible but not usually justifiable for three main reasons.

1. The resonant ionisation was generally of a different dependence to the nonresonant ionisation.

2. In some spectra the laser power varied so much over a single scan that the dependence of the resonant and/or nonresonant ionisation clearly changed.

3. When using UV dyes it was found that, towards the limits of the dyes, the recorded laser power would sometimes increase, even with there being no lasing action at the recorded wavelength. This fluorescence, (or amplified spontaneous emission), is broadband and centred at the maximum of the dye gain efficiency profile.

Thus, short of recording the dependence of ionisation with flux at every point, normalisation of the data was considered inadvisable. Instead attempts were made to keep the laser power constant throughout the scan by using the variable attenuator. In all the spectra illustrated in chapter 5, the spectral power dependence of the laser is shown as a dotted line. The given value of the laser flux refers to the maximum flux recorded during the spectrum.

For the log/log plots of the ionisation against laser power at particular wavelengths, the laser power signal, which was made to vary between 0 and 2 volts, was divided into 200 bins each 10 mV wide, and an average value taken of the ionisation signals in each bin. However this does not indicate the weight of each point, those averaged from just one value having the same weight as those averaged from ten values. Some log/log graphs have therefore been drawn in which all the data is plotted. As mentioned previously the variable attenuator, when used near maximum attenuation, was liable to distort the ionisation produced in both the proportional counter and quadrupole mass spectrometer, with the result that an unambiguous interpretation of the log/log plots is difficult at low power.

The alkali metals were deemed the most suitable elements with which to investigate resonant ionisation in proportional counters. The choice of caesium for the initial experiments was for the following reasons.

1. The gross atomic structure of the alkalis is simple and similar to hydrogen.

2. All the alkalis have low atomic ionisation potentials (4 - 5 eV) enabling two photon resonant ionisation with a single dye laser.

3. Caesium has a melting point of 301.6 K and a pressure of about 1×10^{-6} torr at room temperature, which would make its detection at room temperature (or slightly above) feasible.

4. Comparison of the results on the saturation conditions for caesium could be made with other authors.

Rubidium was chosen for further studies for broadly similar reasons, but its detection was considered slightly more involved in that it has two naturally occuring isotopes, ^{85}Rb and ^{87}Rb. With a rather broadband laser a mass spectrometer must be used in order to discriminate between these two isotopes. Use could then be made of these isotopes as an indicator of the mass resolution of the instrument. Also previous work on the resonant ionisation of caesium vapour had indicated the presence of a substantial molecular ionisation signal. The limited mass range of the spectrometer (0-200 amu) ruled out the detection of these caesium dimers, but allowed the detection of rubidium dimers. It was hoped that the importance of this dimer signal with respect to trace element detection would be determined. The detection of rubidium in the quadrupole mass-spectrometer was also thought important since it had been decided to detect rubidium at low levels in the time of flight instrument in order to test its sensitivity. Comparison of the results from the two different mass spectrometers would be useful.

Rubidium was thus studied in the proportional counter and the quadrupole and time of flight mass spectrometers. Some of the relevant physical properties of caesium and rubidium are listed in table 3.4.

The main disadvantage with using alkali metals, and especially caesium and rubidium, is their intense reactivity and toxicity. Caesum and rubidium ignite spontaneously in air and react violently with water. They also react with many other substances, such as plastics and organic solvents, and are thus stored in an inert atmosphere in glass ampoules.

TABLE 4

	RUBIDIUM	CAESIUM
Average atomic weight	85.47	132.91
Z	37	55
Naturally Occuring Isotopes	^{85}Rb, ^{87}Rb	^{133}Cs
Melting Point (^{o}C) [1]	38.89	28.40
Boiling Point (^{o}C) [1]	688	669.3
Vapour pressure at 300 K (torr)[2]	10^{-7}	10^{-6}
Atomic ionisation potential (eV)	4.176	3.893

1. Handbook of Chemistry and Physics 1973

2. Samson 1966

CHAPTER 4

ELECTRONIC STRUCTURE OF ALKALI METALS

The alkali metals have been used extensively in laser induced spectroscopy for two main reasons, their low ionisation potentials (4 - 5 eV), and simple hydrogen-like spectral structure, which makes a theoretical analysis and interpretation of experimental results tractable.

4.1 HISTORICAL BACKGROUND OF LASER INDUCED IONISATION OF ALKALI METALS

Earlier work was reported on the nonresonant ionisation of caesium and potassium atoms using a focussed Nd:Glass laser, (Held et al 1971). This was extended to a study of resonant ionisation at the focal point of a laser, (Held et al 1973, Bjorkholm et al 1974, Morellec et al 1976, Gontier et al 1978, 1979, 1980). Absolute values of the nonresonant two and four photon ionisation cross sections of caesium atoms were also determined by this group, (Normand et al 1980). Spectroscopic studies of caesium atoms, (Collins et al 1974), and rubidium atoms, (Collins et al 1976), have also been carried out with a sensitive thermionic diode detector capable of detecting ion signals of a few per second.

PHOTOELECTRON ANGULAR DISTRIBUTIONS

Studies on the angular distribution of photoelectrons arising from the multiphoton resonant ionisation of alkali atoms have also been reported. Photoelectron angular distributions of caesium (Compton et al 1984a, Pindzola et al 1984b, 1985), and rubidium and sodium (Dodhy et al 1987) have been investigated.

RYDBERG LEVELS

The study of the highly excited of Rydberg states of alkali atoms also attracted considerable attention, although this had to await the arrival of narrow bandwidth dye lasers capable of resolving these levels. Gallagher et al (1975) studied the Rydberg states of sodium and in particular reported on the lengthening of the lifetime of these states due to collisions with rare gas buffer atoms.

Field ionisation of Rydberg states of sodium was also demonstrated using a pulsed electric field (Ducas et al 1975) whilst the DC Stark effect was investigated in Rydberg levels of rubidium (Liberman et al 1979, Luc-Koenig et al 1979) and caesium (Klots et al 1985). Collision induced ionisation of Rydberg state atoms with rare gas buffer atoms was also demonstrated, (Whitaker et al 1981, Neimax 1983), and the ionisation of highly excited rubidium and potassium atoms through collisions with ground state atoms, (Thompson et al 1987). Theoretical work on the ionisation of alkali Rydberg atoms has been conducted by Kaulakys et al (1987a,1987b), Mihajlov (1981), Duman et al (1980), Weiner et al (1986).

ALKALI MOLECULES

Although much of the attention was focussed on alkali atoms, the ionisation of alkali dimer molecules was known to be a signficant component of the total ion yield especially at low laser powers. Held et al (1972) pointed out the importance of this molecular component when investigating the resonant ionisation of caesium vapour with a fixed frequency Nd:Glass laser. Collins et al (1973) using a tunable pulsed dye laser reported on the two photon ionisation spectrum of caesium molecules in a thermionic diode detector. Absorption spectra in the visible and near-visible of Cs_2 and Rb_2 molecules were also invesigated by Gupta et al (1978). Drummond et al (1976) examined the absorption and flouresence spectra of Rb_2 in the infrared. Two photon ionisation cross-sections of Cs_2 and Rb_2 were determined by Granneman et al (1976), and the kinetics of the photo-dissociation and ionisation of Cs_2 molecules was investigated by Collins (1981a, 1981b).

The gross electronic structure of alkali metals atoms is comparable to the hydrogen atom. Alkali metals have closed inner shells and a single electron in the outer shells. For example the electronic terms of rubidium and caesium are,

$$\text{Rb}.. \quad (1s)^2(2s)^2(2p)^6(3s)^2(3p)^6(3d)^{10}(4s)^2(4p)^6(4d)^{10} \, 5s$$

$$\text{Cs} .. \quad (1s)^2(2s)^2(2p)^6(3s)^2(3p)^6(3d)^{10}(4s)^2(4p)^6(4d)^{10}(5s)^2(5p)^6 \, 6s$$
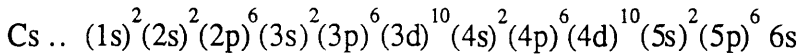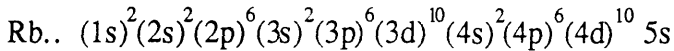
Because of the spherical symmetry of the closed shells, the central field approximation is a very good description of the field surrounding the nucleus in which the single valence electron moves. The energy levels of the atom should qualitatively resemble those of hydrogen. In order to establish some of the principle features of the alkali metal atomic energy levels a comparison with the energy levels of hydrogenic atoms, that is atoms having only one electron, will be drawn.

HYDROGENIC ATOMIC STRUCTURE

An hydrogenic atom consists of an atomic nucleus of charge +Ze and an electron of charge -e interacting by means of the Coulombic potential, $V(\underline{r})$,

$$V(\underline{r}) = -\frac{Ze^2}{4\pi\varepsilon_o \underline{r}}$$

where $\underline{r}$ is the distance between the nucleus and the electron. The wavefunction, $\psi(\underline{r}, t)$, describing the motion of the electron of mass m moving in this potential, must satisfy Schrodingers time dependent equation,

$$\left[-\frac{\hbar^2}{2m}\nabla^2 - \frac{Ze^2}{4\pi\varepsilon_o \underline{r}} \right] \psi(\underline{r}, t) = i\hbar \frac{d}{dt}\left[\psi(\underline{r}, t) \right]$$

This equation contains the kinetic and potential energies of the constituent particles of the atom. It can be shown that Schrodingers time-dependent equation has solutions of the form, (Woodgate 1983)

$$\psi(\underline{r}, t) = \psi(\underline{r}) \, e^{-iEt/\hbar}$$

where $\psi(\underline{r}, t)$ is a solution of the time-independent energy eigenvalue equation,

$$H_o \, \psi(\underline{r}) = E \, \psi(\underline{r})$$

The constant E is the total energy of the state $\psi(\underline{r})$.

Because of the spherical symmetry of the Coulomb potential, V(r), the wave equation may be split into two independent equations, in spherical symmetric coordinates, describing the radial and angular parts of the motion of the particles of the atom. The wavefunction describing the atom may also be separated into a product of two functions, one a function of the radial coordinate and the other a function of the angular coordinates.

$$\psi(r) = R(r)\ Y(\theta,\ \phi)$$

The energy of the system is determined by the radial part of the wavefunction, R(r). However solutions of the radial equation, are only found for certain values of the energy E, and for certain values of the constant l, the angular momentum quantum number, which are determined by solving the angular equation, $Y(\theta, \phi)$. It is found that there are bound state solutions which remain finite only if the total energy E has a value, (Woodgate 1983),

$$E_n = -\frac{\mu Z^2 e^4}{(4\pi\varepsilon_o)^2 2\hbar^2 n^2}$$

where n = l+1, l+2, l+3,......, and μ is the reduced mass of the electron-nucleus system. These energies can be presented on an energy level diagram, with the letters s, p, d, f,...., representing the allowed values of l = 0, 1, 2, 3,.......

ENERGY LEVELS OF ALKALI METALS

The gross electronic structure of alkali metals atoms is comparable to the hydrogen atom and Grotrian energy level diagrams of caesium and rubidium are illustrated in figures 4.1 and 4.2 respectively. The main differences between hydrogen and the alkalis in the gross electronic structure are:

1. The energy levels for a given n are at lower energy than the hydrogen atom and these energy levels are nondegenerate in l, in contrast with hydrogen. For small l the valence electron has highly elliptical classical orbits and penetrates the inner core of closed subshells. The electron experiences a greater Coulombic attraction and its energy is therefore lower than the corresponding level in hydrogen. For larger l, the orbits are more circular, little or no penetration occurs and the energy levels more closely correspond to hydrogen. Also for high values of n (at all levels of l) the energy levels
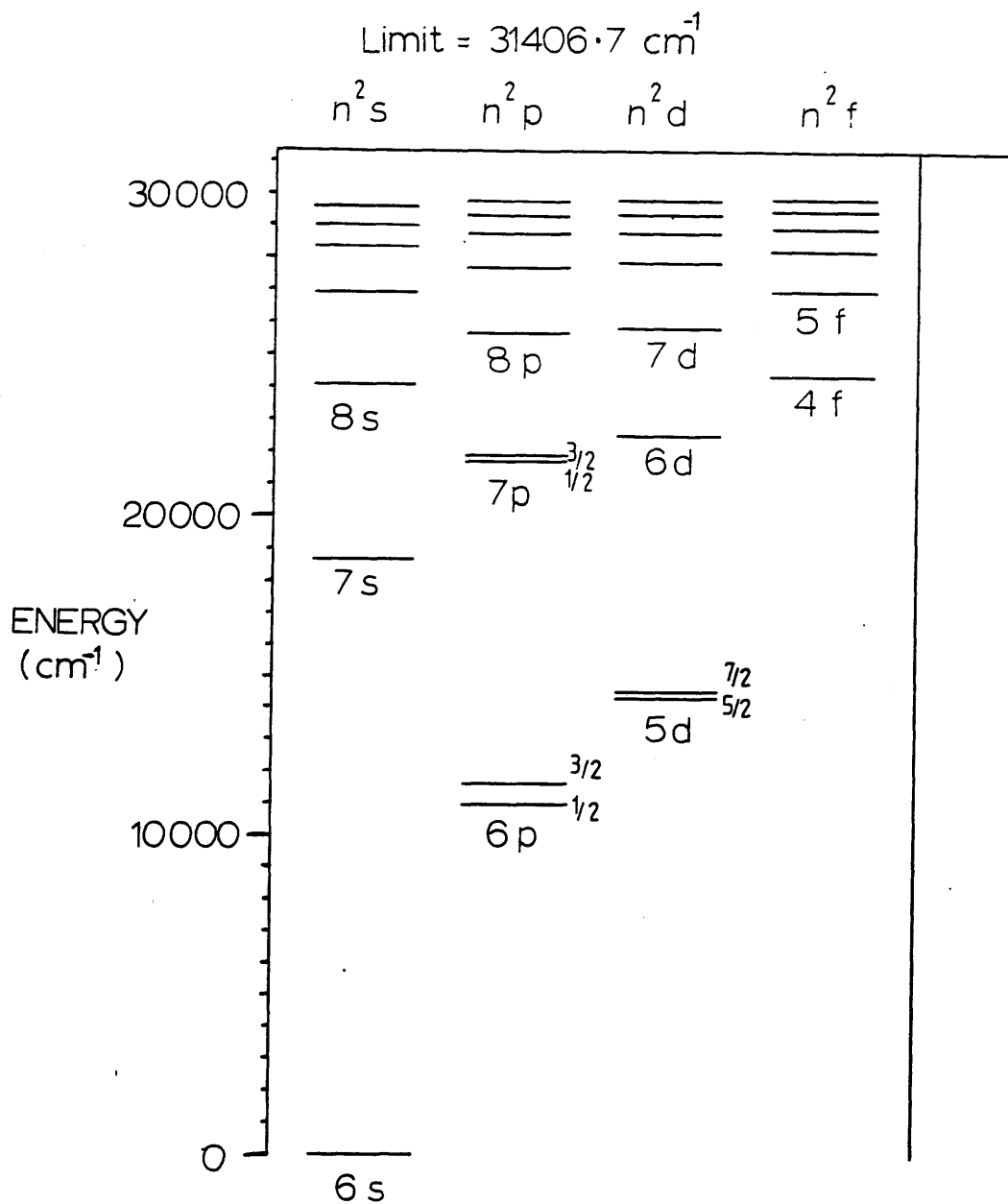
Fig 4.1   Energy level diagram of atomic caesium. All levels with l >= 1 are doublets

Fig 4.2 Energy level diagram of atomic rubidium. All levels with l >= 1 are doublets.

correspond to hydrogen and there is near degeneracy in l.

2. All the ionisation potentials of the alkalis are of similar size (4 - 5 eV) and they are all much less than hydrogen (~13.6 eV).

	Lithium	Sodium	Potassium	Rubidium	Caesium
Atomic ionisation potential (eV)	5.39	5.14	4.34	4.18	3.89

3. In the optical region all transitions will involve only the single valence electron, since inner core electrons are strongly bound (second ionisation potential ~20 eV).

4. The energy levels of the alkali metals are found to fit the empirical Rydberg formula, originally devised for hydrogen, if a modification in the value of n is taken into account. The use of an effective principle quantum number n^* enables the energy of the level to be smoothly dependent on n.

$$E_{nl} = \frac{-hcR_H}{n^{*2}}$$

where $n^* = n-\delta(l)$ is the effective quantum number. The quantum defect $\delta(l) = n-n^*$ is, to a good approximation, independent of n for a given l, (Filipovicz et al 1985), and expresses the difference of the state from hydrogenic behaviour. The f levels, and those with higher angular momentum, have small quantum defects and are therefore almost hydrogen-like.

Approximate quantum defects for rubidium and caesium

	s	p	d	f
l =	0	1	2	3
Rb	3.13	2.66	1.34	0.01
Cs	4.06	3.59	2.46	0.02

All the energy levels of the valence electron of the alkalis (with the exception of those with $l = 0$) are split into two, corresponding to the two j values, $l+1/2$, $l-1/2$. The interaction causing this fine structure splitting is almost entirely due to the spin-orbit effect. The relativistic corrections, which in hydrogen are of comparable magnitude to the spin-orbit correction, are negligible (Sobelman 1979). The spin-orbit interaction arises from the interaction of the electron with the nucleus. This is due to the existence of a magnetic moment, μ, of the electron connected with its spin.

$$\underline{\mu} = -\frac{e\hbar}{mc}\,\underline{s}$$

where m is the mass and $\underline{s}$ the spin of the electron. This couples with the magnetic field $\underline{H}$, associated with the electron moving in an electric field $\underline{E}$ due to the nucleus. The energy splitting to first order is , (Sobelman 1979),

$$\Delta E = \frac{\hbar^2}{2}[j(j+1) - l(l+1) - s(s+1)]\,\frac{1}{2m^2c^2}\,\frac{Ze^2}{4\pi\varepsilon_o}\left<\frac{1}{r^3}\right>_{nljm_j}$$

$$\Delta E = \alpha^2\,\frac{j(j+1) - l(l+1) - s(s+1)}{2l(l+1)(l+\frac{1}{2})}\,\frac{Z^4}{n^3}\,R_y$$

α = fine structure constant

$$R_y = \frac{1}{2}\alpha^2mc^2$$

For s levels, $l = 0$ and the splitting is zero. In alkali atoms, those orbitals having a high degree of penetration will see an effective nuclear charge, Z_{eff}, which will not be 1 (the value of Z + core electrons). Therefore for those orbitals with large quantum defects the splitting of the states will not be proportional to n^{-3} but can be approximated by a series of odd powers of $1/n$ (Harvey et al 1977). The effective nuclear charge is a function of n and l and will differ between alkali metals. For a given alkali atom with high angular momentum the splitting should vary approximately as n^{-3} and decrease with increasing l.

RYDBERG STATES OF ALKALI ATOMS

A recent review of experimental work on Rydberg atoms has been compiled by Gallas et al (1985).

If the valence electron of an alkali atom (or any atom or molecule) is excited to an orbit with high principle quantum number and therefore to an orbit far from the ionic core, the energy levels are hydrogen-like and can be described by the Rydberg formula. The energy difference between adjacent n states will therefore vary as $(n^*)^{-3}$.

The radius of a Rydberg atom r_n scales as

$$r_n \sim n^{*2} a_0$$

where a_0 is the Bohr radius.

SPONTANEOUS DECAY LIFETIME

Although the atoms of high n are very large their spontaneous decay life-times are very large due to the small overlap of their radial wavefunctions with lower states. The rate of spontaneous emission A_{fi} from state i_n to state $f_{n'}$ is given by (Gallas et al 1985),

$$A_{fi} \propto \omega_{fi}^3 \; |<f_{n'}|r|i_n>|^2$$

If $n' \gg n$ the matrix element is small and $A_{fi} \propto n^{*-3}$ for small l, and $A_{fi} \propto n^{*-5}$ for large l, (Filipovicz et al 1985). If $n' \approx n$ the matrix element scales as n^{*4}, but the transition frequency term ω_{fi}^3, which scales as n^{*-9}, dominates and $A_{fi} \propto n^{*-5}$.

INDUCED TRANSITIONS

However induced transitions will have high probabilities. The induced transition rate B_{fi} is proportional to

$$B_{fi} \propto \Phi(\omega) \; |<f_{n'}|r|i_n>|^2$$

where $\Phi(\omega)$ is the incident energy flux. In the Rayleigh-Jeans limit of low frequency, $\Phi(\omega)$ scales as ω^2, and the overall induced transition rate B_{fi} between states of high principal quantum number ($n' \approx n$) is proportional to n^{*2}. Therefore at high n^* the

induced transition probability ($\propto n^{*-2}$) will be larger than the spontaeous decay rate ($\propto n^{*-5}$). This will also occur at room temperature with the result that high n states will be rapidly mixed, l->l+1, l->l-1, (Filipovicz et al 1985)

FINE STRUCTURE

In hydrogen the fine structure interval shows an n^{-3} dependence. In alkali metals however there is a large degree of penetration of the core for low l states, and the dependence on n of the fine structure interval for those l states at low n shows some departure from the hydrogenic behaviour. For high n states and those with small quantum defects (l>2) the dependence should more closely resemble the hydrogen atom. (Edelstein et al 1978, Tursunov et al 1985)

EXTERNAL ELECTRIC FIELDS

Rydberg atoms will be very sensitive to external fields since they have large dipole moments which scale as the orbital radius n^{*2}. For quite modest DC electric fields of 10 - 50 V cm^{-1} the interaction of the field with the atom may be stronger than the Coulomb interaction with the core. This produces a Stark mixing of l states of different parity which may appear as forbidden electric dipole transitions, (Stebbings et al 1975). A shift in energy levels is also produced in weak electric fields, (Liberman et al 1979)

For somewhat larger field strengths 500 V cm^{-1} - 10 kV cm^{-1} the electric field may ionise the Rydberg atom (Bayfield and Koch 1974). This is due to the highly excited electron tunnelling through the potential hill resulting from the external field combining with the Coulombic field. The electric field effectively decreases the life-time of all of the states in the atom (including the ground state), and in particular those states close to the saddle point, by providing another decay channel to the continuum. Field ionisation can be very efficient and highly selective in that different n states for a given l can be distinguished. (Gallagher et al 1977)

PHOTOIONISATION

The cross section for photoionization of Rydberg atoms is very small and decreases, for states with small quantum defects, as n^{*5}, (Sobelman 1979). Thus the photoionization

cross-sections of highly excited states is small.

COLLISIONAL EFFECTS

Rydberg atoms will be highly susceptible to collision-induced effects due to their large geometric size, large polarisability, small binding energy and long life times. Elastic collisions with rare gas atoms will mix the angular momentum states of the same n^* value. This manifests itself as an increase in the lifetime of the initially excited n^* state, (Gallagher et al 1975)

Highly excited atoms, A^{**}, may also collide with ground state atoms of the same, or different, species and be de-excited, or may be ionised through collisions.

$$A^{**} + B \longrightarrow A^+ + B^-$$
$$A^{**} + B \longrightarrow A^+ + B + e^- \quad \text{Penning ionisation}$$
$$A^{**} + B \longrightarrow AB^+ + e^- \qquad \text{Associative ionisation}$$
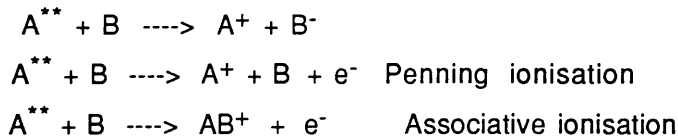
Associative ionisation rate constants for highly excited sodium atoms have been determined theoretically by Weiner et al (1986).

DEPENDENCE OF ATOMIC PROPERTIES ON THE EFFECTIVE QUANTUM NUMBER

Binding energy	n^{*-2}
Energy between adjacent n states	n^{*-3}
Orbital radius	n^{*2}
Geometric cross-section	n^{*4}
Dipole moment $\langle n_1 d \lvert r \rvert n_2 f \rangle$, $n_1 \approx n_2$	n^{*2}
Polarisability	n^{*7}
Radiative life-time	n^{*3} (large quantum defect)
	n^{*5} (small quantum defect)
Fine structure interval	n^{*-3}

4.3 ELECTRONIC STRUCTURE OF ALKALI MOLECULAR DIMERS

INTRODUCTION

The excitation and ionisation of alkali dimer molecules has been shown to be a significant component of the total laser induced ionisation in alkali metal vapours, (Held et al 1972, Grannemann et al 1976). The photodissociation of excited alkali molecules has also been shown to contribute to the spectral structure of the resonant ionisation of alkali metal vapours, (Collins et al 1976). In order to describe these processes a qualitative model of the diatomic molecule is useful.

Molecules are bound systems of electrons with more than one nucleus. The most simple molecule is the hydrogen ion molecule H_2^+, which has one electron bound to two protons. The structure of diatomic molecules can be approached in two different ways. By assuming that the electronic structure of the individual atoms is largely preserved, the covalent bonding can be shown to arise from an "electron exchange" force between the two neutral atoms, (Heitler 1954). This leads to the idea of valence electrons in atoms, which are those electrons in the outermost, unfilled shells mainly responsible for the binding energy of molecules. The second model starts out from the motion of the individual electrons in the field of the two nucleii and other electrons, and builds orbitals that extend around both nucleii, in analogy with atomic electronic orbitals. This is the molecular orbital approach which, in the limiting case of molecular Rydberg levels, becomes a united atom model. Qualitatively the two models provide similar answers to the question: Why do neutral atoms combine to form stable molecules? In general, except for the hydrogen molecule, the MO approximation is the more accurate, (Bransden and Joachaim 1983)

The time independent Schrodinger equation for a diatomic homopolar molecule, (two nucleii of equal charge), with N electrons, and with internuclear coordinate R, (figure 4.3), can be written,

$$(\hat{T}_N + \hat{T}_E + \hat{V}) \, \psi(R \, ; \, \underline{r}_1, \underline{r}_2, \dots \underline{r}_N) = E \, \psi(R \, ; \, \underline{r}_1, \underline{r}_2 \dots \underline{r}_N)$$

$\hat{T}_N$ is the kinetic energy operator for the nucleii,

$\hat{T}_E$ is the kinetic energy operator of the electrons,

$\hat{V}$ is the total potential energy of the system.

$\psi(\underline{R} \, ; \, \underline{r})$ is the total wavefunction of the system

E   is the total energy of the system

The potential energy $\hat{V}$ will include the repulsive terms between the two nuclei and between the pairs of electrons, and the attractive terms between the individual electrons and the two nuclei.

The energies associated with the rotational and vibrational motions of the nucleii and the electronic motion can be differentiated because of the great difference in mass between the electrons and the nucleii. The periods of vibration of the nucleii are much lower than the electronic vibrations, with the result that the energy of electronic states can be determined for nucleii at a fixed distance. The parameter which then determines the energy of a particular electronic state is the internuclear seperation, $\underline{R}$. The motion of the nucleii can be treated seperately from the electronic motion, and the total wavefunction of the molecule is then a product of the electronic wavefunction and the nuclear vibrational and rotational wavefunctions.

THE ELECTRONIC STRUCTURE OF THE HYDROGEN MOLECULE

The structure of alkali dimers will resemble that of the hydrogen molecule. The general electronic structure of diatomic homopolar molecules can be obtained from a linear combination of molecular ion electronic wavefunctions. For instance molecular hydrogen wavefunctions can be obtained from hydrogen ion H_2^+ wavefunctions. In turn the molecular ion is constructed from a linear combination of atomic electronic wavefunctions.
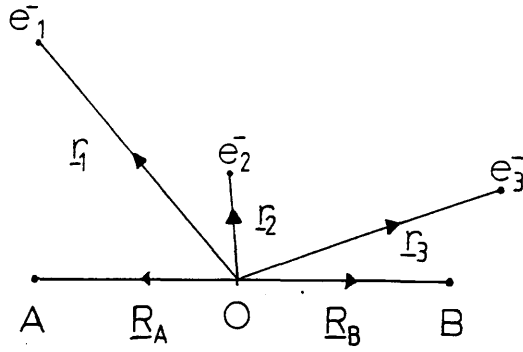
Fig 4.3 Three electron diatomic molecule with nuclei A and B of equal charge an internuclear separation $\underline{R} = \underline{R}_A - \underline{R}_B$.
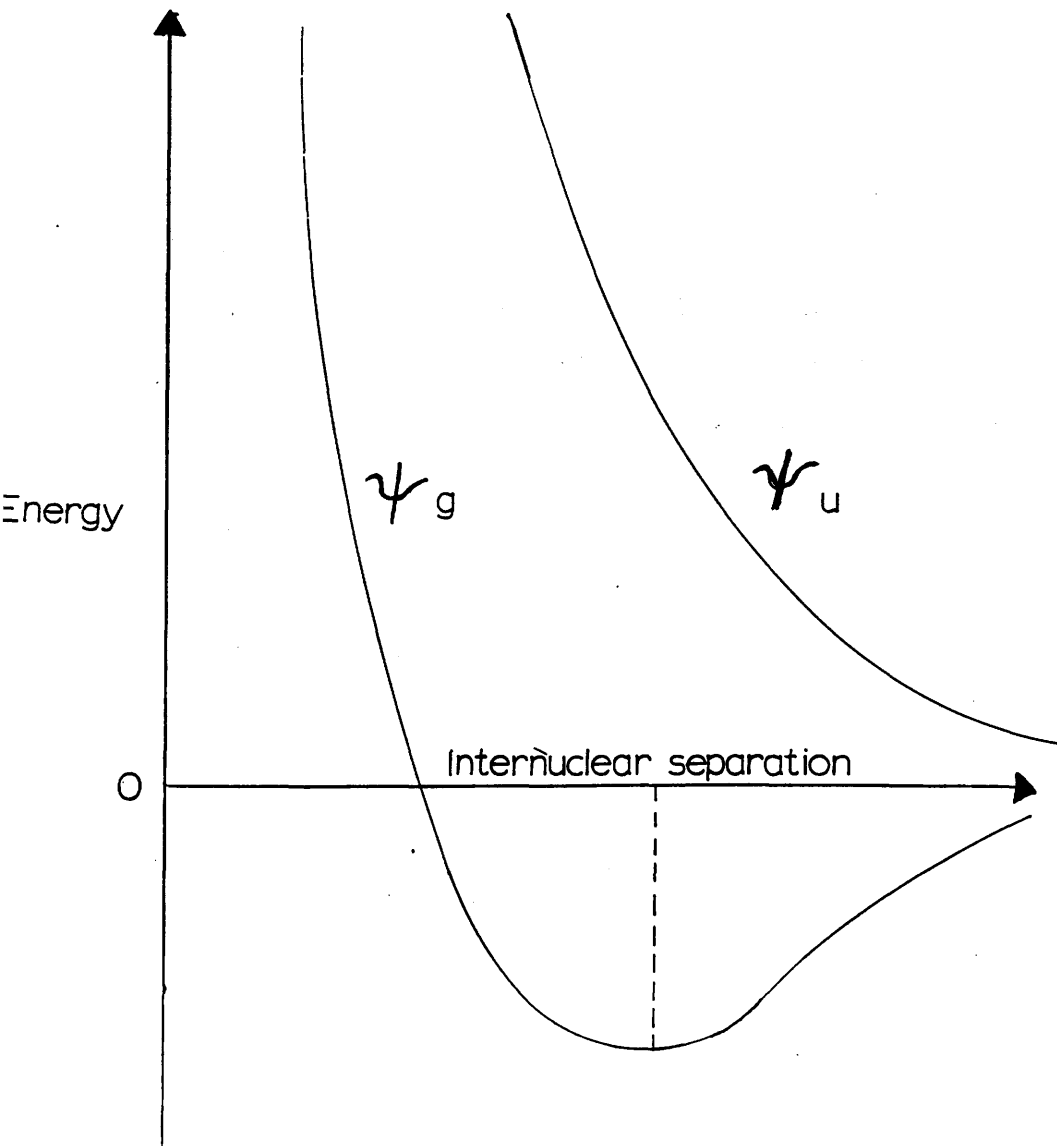
Fig 4.4 Potential energies of the gerade and ungerade wavefunctions of the hydrogen molecular ion H_2^+. Only the gerade wavefunction has a potential well and is stable.

If $\psi(r_A)$ and $\psi(r_B)$ are the seperated atom wave functions corresponding to the single electron being in the ground state of either atom A or B then, as the atoms approach each other, the combined molecular ion wavefunction will be of the form

$$\psi_g(R;r) = \psi(r_A) + \psi(r_B)$$

$$\psi_u(R;r) = \psi(r_A) - \psi(r_B)$$

where g labels a wavefunction (gerade) which does not change sign under inversion through O the centre of coordinates, and u labels a wavefunction (ungerade) which changes sign under inversion through O.

The energies of these states will be a function of R, the internuclear seperation. A plot of the energies of these two wavefunctions as a function of the internuclear separation shows that only the gerade function provides the potential well necessary for a stable molecule, whilst the ungerade function leads to a dissociative state of the molecule at all internuclear distances, figure 4.4

The hydrogen molecule H_2 can be considered as a linear combination of the even (gerade) and odd (ungerade) wavefunctions of the the molecular H_2^+ orbitals, combined with either antisymmetric singlet χ_{oo} or symmetric triplet $\chi_{1,ms}$ ($m_s=0,+/-1$) spin wave functions. There are therefore six combinations, three with the singlet spin wavefunctions,

$$\Phi_A = [\psi_g(1)\ \psi_g(2)]\ \chi_{oo}$$

$$\Phi_B = [\psi_u(1)\ \psi_u(2)]\ \chi_{oo}$$

$$\Phi_C = [\psi_g(1)\ \psi_u(2) + \psi_u(1)\ \psi_g(2)]\ \chi_{oo}$$

and three with the triplet wavefunctions,

$$\Phi_{D,E,F} = [\psi_g(1)\ \psi_u(2) - \psi_u(1)\ \psi_g(2)]\ \chi_{1,ms} \qquad m_s = 0, +/-1$$

For example the wave function Φ_A implies that the two electrons of opposite spin are both in gerade binding orbitals. Since the ground state wave function is generally the most symmetric, Φ_A would be expected to be the ground state. A calculation of the energy of Φ_A as a function of R, the internuclear seperation, leads to a potential well of depth 2.68 eV at an equilibrium seperation R = 0.8 A . The experimental values for the hydrogen molecule are R = 0.74 A and D = 4.75 eV. Therefore the use of Φ_A as the ground state of H_2 must be seen as an approximation.

The different types of electronic states arising from the joining together of two neutral atoms have been tabulated by Herzberg (1957).

When two atoms of orbital angular momentum l_1 and l_2, and spin angular momentum s_1 and s_2, are brought together, the internuclear axis (z-axis) picks out a preferred direction in space, and l_1 and l_2 are quantised with reference to this direction with components m_{l1} and m_{l2}. M_l is therefore the only good orbital momentum quantum number. The resultant orbital angular momentum about the line joining the two nucleii AB is,

$$\Lambda = |\, m_l + m_l \,|$$

By combining all the the possible m_l states of the individual atoms all the Λ values are obtained and, in analogy with atomic notation, the different values of Λ are assigned code letters.

Value of Λ	0	1	2	3	....
Code letter	Σ	Π	Δ	Φ	....

The resultant spin s of the molecule is found from s_1 and s_2 ,

$$s = (s_1 + s_2),\ (s_1 + s_2 - 1),\ .\ .\ ,\ |s_1 - s_2|$$

In general the different orientations of l_1 and l_2, and thus the different Λ values, correspond to different energies in the electric field arising from the bringing together of the atoms. Thus for a given combination of atomic states there will be molecular states differing in their energy according to their values of m_{l1} and m_{l2} . All the states except $\Lambda = 0$ will be two-fold degenerate in that for the same value of Λ , m_l can be either positive or negative. The Σ states have a special symmetry, in that, upon reflection in any plane through the inter-nuclear axis, the wavefunction corresponding to Σ can either change sign Σ^-, or be unchanged Σ^+. These are two different states with two different energies. All closed shells are Σ^+. For a homopolar molecule, that is one having nucleii of the same charge, the parity, gerade or ungerade, will depend on the parity of the atoms and on their l values l_1 and l_2. Herzberg (1957) has tabulated many useful combinations.

Using these rules it is possible to establish the term configurations for the molecule from the individual atomic terms. For example the H_2 ground state wavefunctions can be designated,

$$\Phi_A = {}^{1}\Sigma_g^{+} \qquad \Phi_C = {}^{1}\Sigma_u^{+}$$

$$\Phi_B = {}^{1}\Sigma_g^{+} \qquad \Phi_{D,E,F} = {}^{3}\Sigma_u^{+}$$

A better approximation to the experimentally obtained energy of the ground state of H_2 is obtained if a linear combination of the wavefunctions Φ_A and Φ_B is used for the ground state, instead of just Φ_A. The triplet state ${}^{3}\Sigma_u^{+}$ is a dissociative state of H_2.

The diatomic molecules of rubidium and caesium will have similar low energy electronic terms to molecular hydrogen, and the potential curves for some of the bound and unbound states of molecular caesium and rubidium are illustrated in figures 4.5 and 4.6. The curves for Cs_2 have been taken from Collins et al (1981b), Granneman et al 1976), and the curves for Rb_2 have been taken from Drummond et al (1976), Collins et al (1976), Gupta et al (1978) and Wagner et al (1985).

SINGLE PHOTON TRANSITIONS IN MOLECULES

The total wavefunction of a molecule is approximately a product of the electronic, vibrational and rotational wavefunctions which are assumed to be independent of each other. The transition amplitude between two states A and B is proportional to the matrix element of the dipole operator between them.

Since rotational and vibrational motions preserve the parity of a molecular state the matrix elements will vanish unless the electronic state changes. Using the Franck-Condon principle which states that the nucleii are essentially fixed during the time of an electronic transition, and that the dipole operator is therefore independent of R, the transition probability can be shown to be proportional to the Franck-Condon factor, $f_{v,v}$, (Bransden and Joachin 1983)

$$f_{v',v} = \int_{vol} \phi_{v'}^{*} \phi_{v} \, dR$$

70
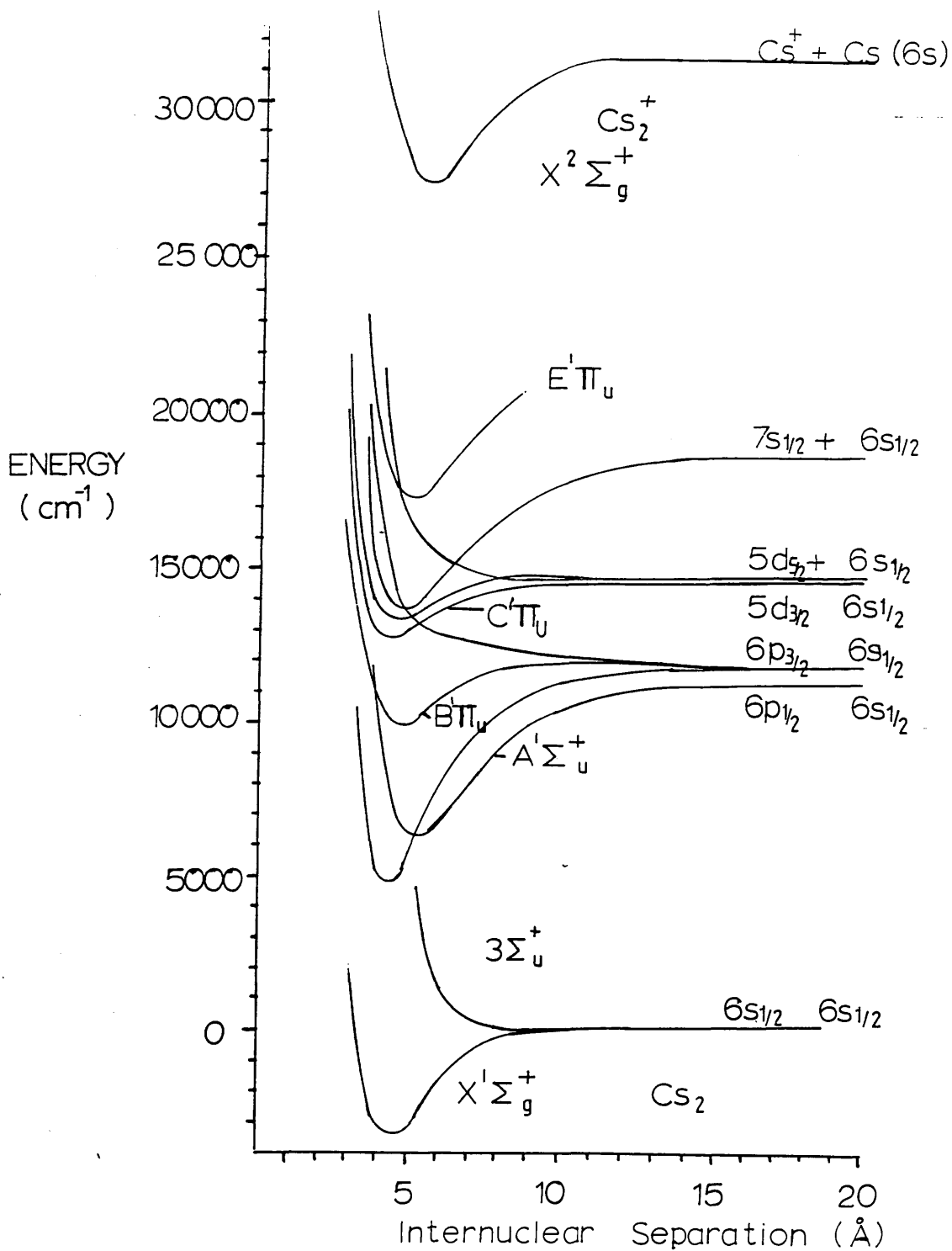
Fig 4.5 Some of the energy levels of the Cs$_2$ molecule.
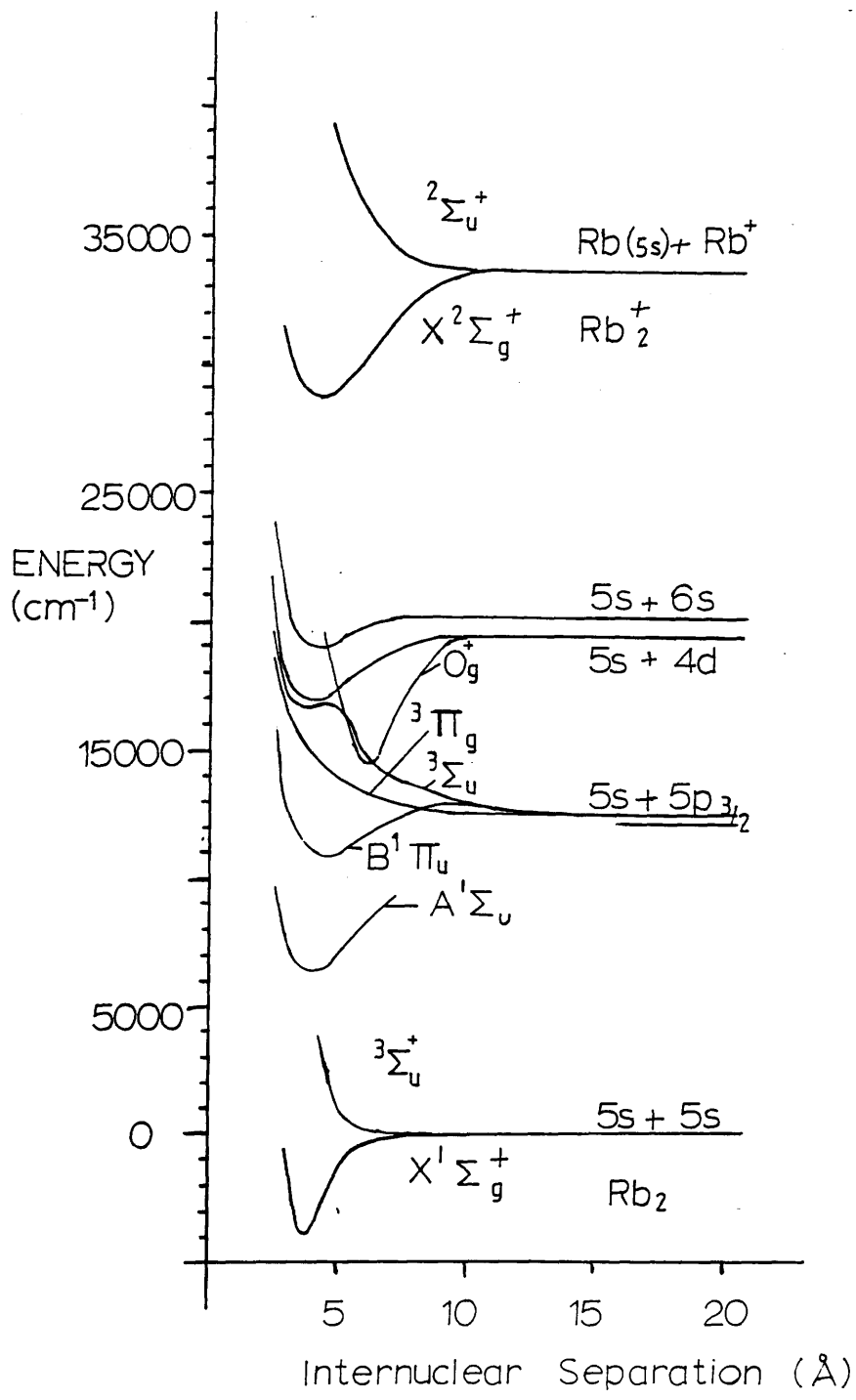
Fig 4.6   Some of the energy levels of the Rb_2 molecule.

Electric dipole transitions will therefore occur between two molecular states if the overlap integal between vibrational wavefunctions ϕ_v from two different electronic states is non-zero.

SELECTION RULES

For electric dipole transitions the general considerations for transitions in molecules are similar to those for atomic transitions. The total angular momentum J must change, and the parity must change

$$\Delta J = 0, +/-1 \qquad J = 0 <-/-> J=0$$

$$+ <---> - \qquad + <-/-> + \qquad - <-/-> -$$

$$g <---> u \qquad g <-/-> g \qquad u <-/-> u$$

In addition to these very general rules, there are others that can be applied which depend on the molecule itself, and in particular on the degree of coupling between the various angular momenta of the molecule. There are five general cases in which these more specialised rules can be applied, known as Hunds cases (a),(b),(c),(d) and (e). Transitions in caesium and rubidium molecules correspond approximately to case (a), (Collins 1981a). In case (a) the orbital and spin angular momenta, l and s , are coupled strongly to the internuclear axis, and Λ is a good quantum number. In this case,

$$\Delta\Lambda = 0, +/-1$$

$$\Sigma^+ <---> \Sigma^+ \qquad \Sigma^- <---> \Sigma^- \qquad , \qquad \Sigma^+ <-/-> \Sigma^-$$

$\Delta S = 0$ where S is the resultant spin vector.

$\Delta\Sigma = 0$ where Σ is the component of S along the internuclear axis.

Singlet to triplet transitions are forbidden in this case.

However this rule is only approximate and is increasingly violated as the spin-orbit interaction increases with increasing molecular weight. This leads to case (c) where the coupling between l and s may be stronger than the coupling with the internuclear axis. In this case Λ and Σ are no longer good quantum numbers. If Ω is the component of the total electronic angular momentum J along the internuclear axis, $\Omega = |\Lambda + \Sigma|$, then

$$\Delta\Omega = 0, +/-1$$

If Ω is the only good quantum number for a molecular state the state is classified by the value of Ω.

GENERAL FEATURES OF SINGLE PHOTON ELECTRONIC TRANSITIONS

Generally, when labelling transitions, the higher excited state is written first and the lower second with an arrow indicating emission or absorption if necessary. The ground state is usually denoted by an X whilst excited bound levels of the same multiplicity are labelled A,B,C,....., and those of different multiplicity a,b,c,..... For example $C^1\Pi_u$ <-- $X^1\Sigma_g^+$ denotes absorption from the ground state to an excited C state.

The Franck-Condon principle assumes that electronic transitions take place instantaneously without the internuclear separation changing during the transition. Transitions are therefore represented by vertical lines connecting the electronic states. Transitions from the lowest vibrational level will occur from R_0, the centre of the potential well, since it is at the centre that the probability density for an electron is greatest. For higher vibrational levels the probability density is greatest at the classical turning points of the vibration where the velocity is equal to zero, and transitions to and from these higher levels will occur at the ends of the lines as illustrated in figure 4.7 and figure 4.8.

ENERGY

excited electronic level

absorption

emmission

lower vibrational levels

ground electronic level

INTERNUCLEAR   SEPARATION
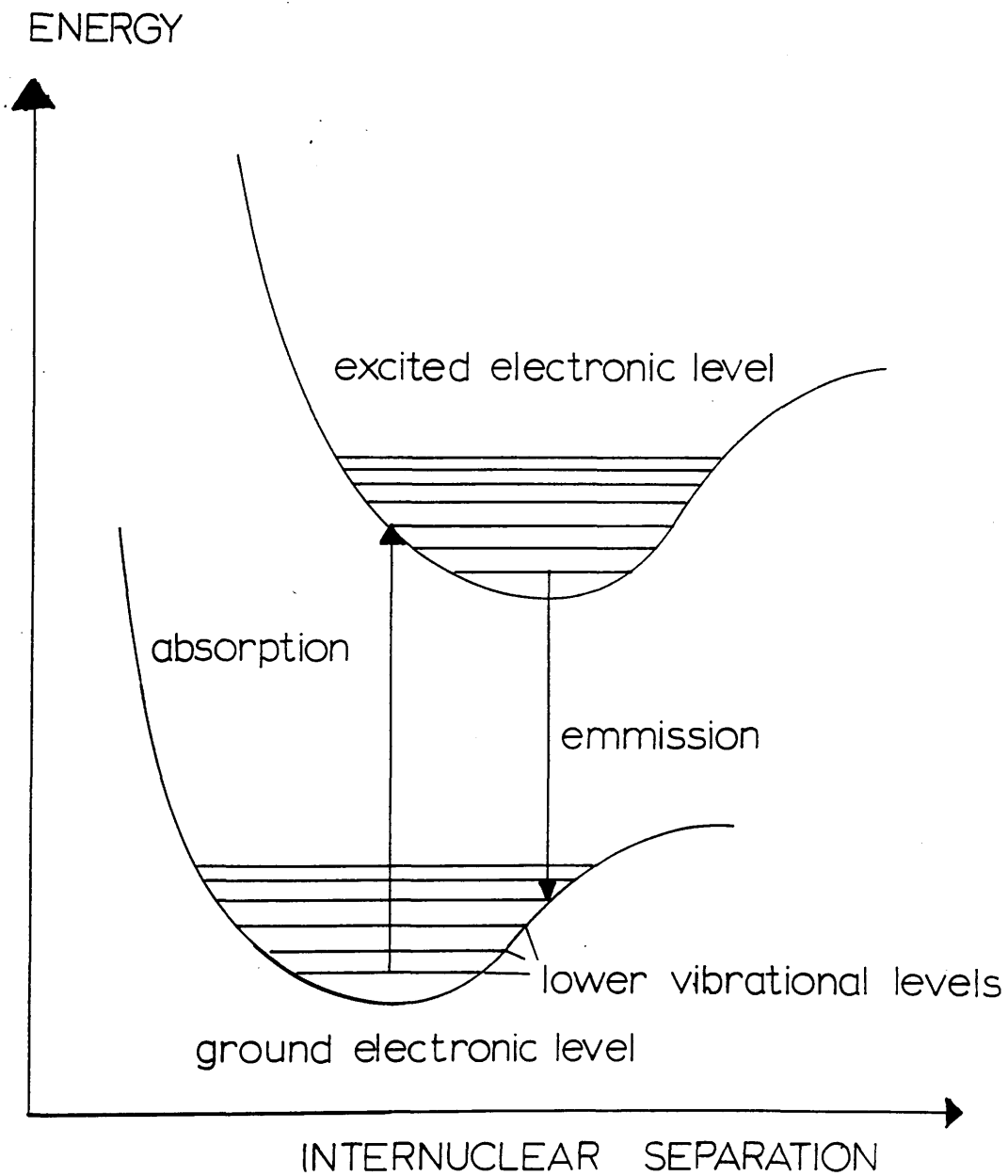
Fig 4.7   Franck-Condon principle in single photon transitions in molecules.

ENERGY

bound excited state

two photon
transition
(via real intermediate
state)

dissociative excited state

photo-
dissociation

radiationless transition

fluorescence

predissociation

vibrational levels

bound electronic ground state

Internuclear separation
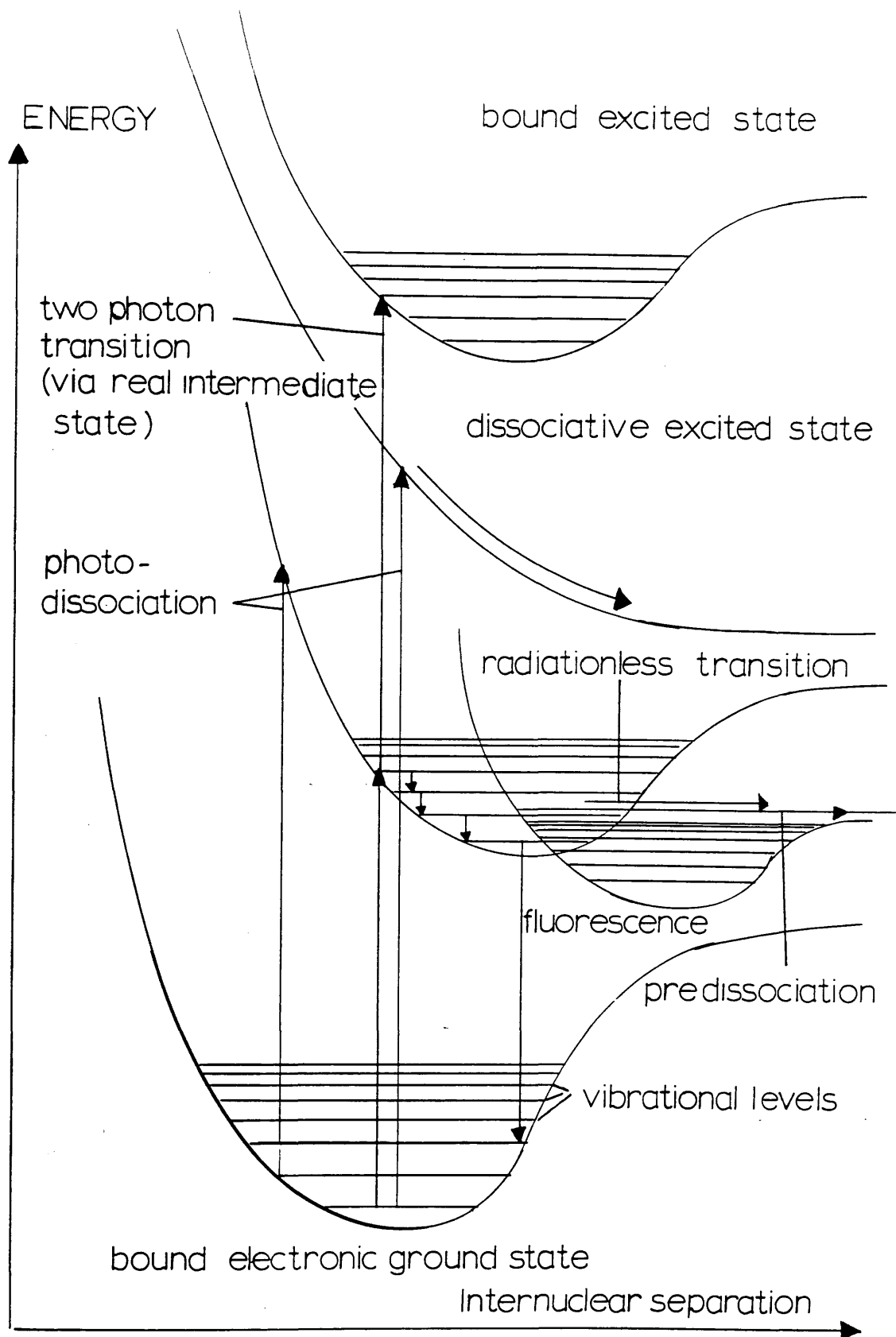
Fig 4.8   Molecular electronic transitions illustrating;
a) Photodissociation
b) Pre-dissociation
c) Fluorescence
d) Two photon transition via real intermediate state.

CHAPTER 5

LASER INDUCED IONISATION OF IMPURITIES IN PROPORTIONAL COUNTERS

5.1 INTRODUCTION

A laser will induce ionisation in a proportional counter filled only with commercial grade P10 counter gas, (Hubricht et al 1985). Early laser ionisation work at Glasgow concentrated on determining the cause of this ionisation. Further studies, complementary to this work, were aimed at finding a chemical which could be added to proportional counter gas and ionised with lasers, in a controlled and reproducible way, in order to calibrate large multiwire proportional counters currently being built at CERN. It was thought that if the impurities responsible for the laser induced ionisation in a clean proportional counter could be identified, then adding more of the impurity, at a known pressure, could provide the ideal solution to this calibration problem.

Thus a considerable effort was expended in identifying the impurities responsible for the backgrond ionisation. The results obtained are thought to be of general interest in that they bring to light a number of factors which may limit the sensitivity of RIMS. The results are also of importance if proportional counters are used for analytical measurements involving low concentrations of elements, or for spectroscopic studies of atoms and molecules which have low vapour pressures. Clearly the ideal proportional counter would have no ionisable impurities in it which might complicate the spectroscopic analysis of the molecular or atomic species of interest. The next best situation would be to have only known impurities, with their associated resonant ionisation spectra. This chapter deals with the attempts at Glasgow to identify some of the more prominent impurities found in proportional counters, which are also likely to be found in other ionisation spectrometers.

There were in all four designs (types 1 to 4) of proportional counters used for these experiments. The design of each counter, and the materials of which it was constructed, were generally modified in an attempt to make a cleaner counter, that is one with a lower level of background ionisation. Other factors which influenced the designs were

safety and the ease of dismantling and reassembly. Diagrams outlining the main features of types 1, 2 and 3 counters are shown in figures 5.1, 5.2 and 5.3 respectively, while the type 4 counter is more fully described in Chapter 3.

5.2 BACKGROUND IONISATION IN TYPE 1 COUNTER

The first experiments attempted to define the spectral dependence of the ionisation over a wide range of wavelengths from 266 nm to 1064 nm. The constructional details for the type 1 proportional counter are more fully described by Raine et al (1983). The normal operating pressure was 760 torr of commercial grade P10 counter gas. Calibration was achieved by using an external X ray sources (^{55}Fe (5.9 keV)and Tb (44.2 keV)) which provide known numbers of ion pairs per X ray in P10 gas. The results are tabulated below (Table 5.1). The lasers used were a nitrogen laser (PRA IN 100), an excimer laser (Lambda Physik EMG 201) and an Nd:YAG laser (JK Systems 2000).

There is a large drop in the ion yield of about 800 fold as the photon energy decreases from 4.98 eV to 1.17 eV. If account is taken of the large increase in the laser power as the wavelength increases then the drop in ionisation expressed per unit laser power becomes even more pronounced. The difference in ionisation could be accounted for by a wavelength dependent ionisation cross-section for the impurities, or simply by a greater number of ionisable molecules at the shorter wavelengths. The power dependency figures suggested that there were at least two different components to the ionisation, one with an ionisation potential between 4 eV and 10 eV, the other with an ionisation potential around 11.7 eV. At a single wavelength, 337 nm, the background ionisation was shown to be independent of the pressure of the buffer gas when it was varied between 228.0 torr and 1520 torr. This suggested that the contaminants were not from the buffer gas itself or coming from the gas bottle.

Fig 5.1   Type 1 proportional counter

Labels within the figure:

MOLECTRON JOULEMETER

ORTEC 121 PRE-AMP.

LENS

LASER BEAM

THIN ALUMINIUM WINDOW

QUARTZ WINDOW

OPTICAL ATTENUATOR

BEAM COLLIMATOR SPLITTER

LENS FIELD TUBES

PERSPEX

50μ WIRE

ALUMINIUM

260mm

Quartz Window.

Thin Aluminium Window.

0.05mm. Anode Wire.

Laser Beam.

Quartz Window.

Ceramic Insulators.

Glass Insulators.

Field Tubes.

Earth Tubes.

Scale:- 0 10 20 30 mm.
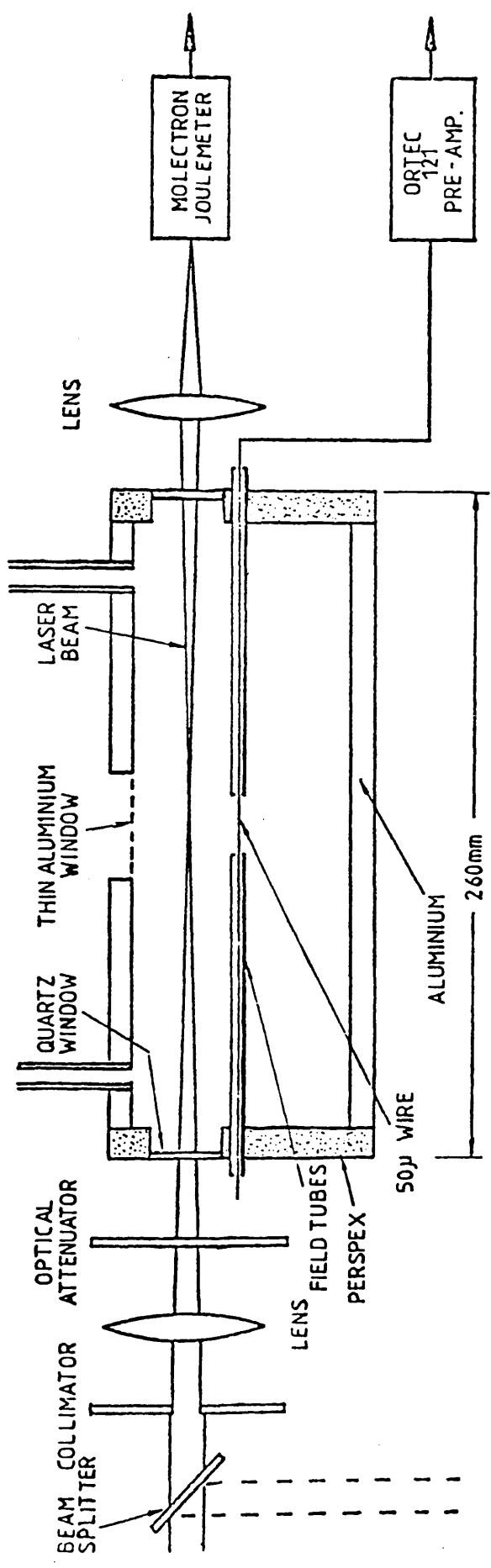
Fig 5.2   Type 2 proportional counter

VALVE

GAS OUT

VALVE

GAS IN

TO PREAMP & POSITIVE H.T.

NEGATIVE H.T.

INSULATING SPACERS

LASER BEAM

TEFLON INSULATORS

55 Fe SOURCE

STAINLESS STEELWIRE 0·05 m.m. φ

QUARTZ WINDOWS

LASER BEAM

CENTRAL WIRE

0   10   20   30
m.m.
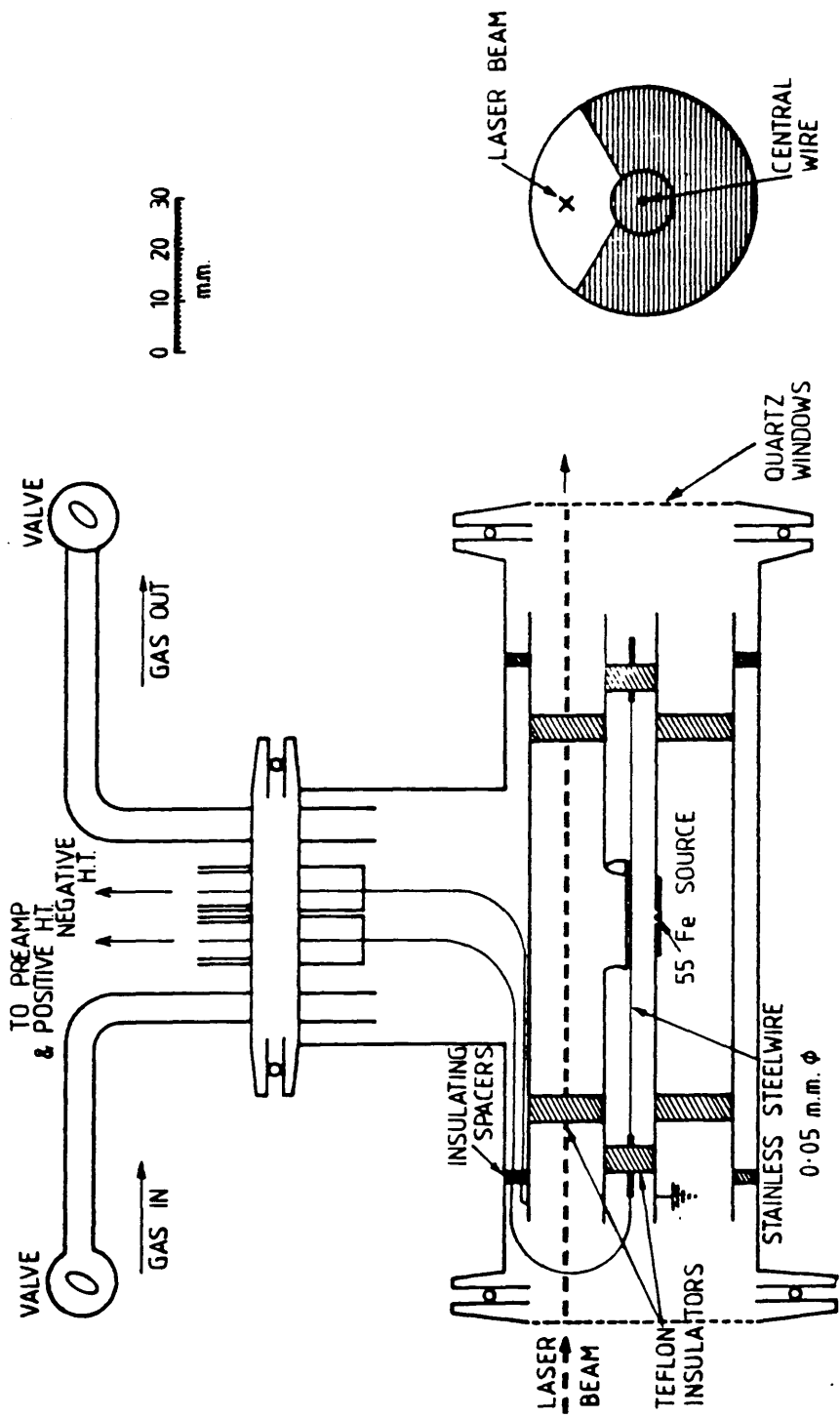
Fig 5.3   Type 3 proportional counter

TABLE 5.1

Laser	Wavelength (nm)/ photon energy (eV)	Pulse length (ns)	Power (mm^{-2})	Ion Yield (pairs cm^{-1})	Dependence of ionisation on flux
Excimer (KrF filling)	249 / 4.98	16	50 µJ	8.5×10^5	quadratic
Nd:YAG (quadrupuled)	265 / 4.68	25	50 µJ	1.2×10^5	quadratic
Nitrogen	337 / 3.68	0.3	140 µJ	5×10^3	quadratic
Excimer (XeF filling)	351 / 3.53	14	20 µJ	6.5×10^5	quadratic
Nd:YAG (tripled)	354 / 3.50	25	20 mJ	3×10^4	quadratic
Nd:YAG (doubled)	530 / 2.34	25	150 mJ	1.5×10^4	~5
Nd:YAG (fundamental)	1060 / 1.17	25	7.5 J	1.1×10^3	> 10

5.3 BACKGROUND IONISATION IN TYPE 2 COUNTER AND THE IDENTIFICATION OF PHENOL AS AN IMPURITY

The different lasers used, with differing mode structures, could account for some of the differences in the levels of background ionisation described above, but it was felt that a closer look at the spectral dependence of the ionisation around 300 nm was needed. This was achieved using a frequency doubled pulsed dye laser which had a continuous wavelength range from 260 nm to 335 nm. The excimer pumped dye laser and doubling crystals are described in chapter 4. A new proportional counter, type 2, was also constructed with the aims of safety and cleanliness in mind. The materials used in this counter were considered to be less likely to outgas contaminants into the counter gas than those used previously in the earlier type 1 counter, and an intrinsically cleaner counter was expected. Details of its construction are found in Towrie et al (1986). The counter was filled to 760 torr with P10 gas and calibration was again achieved using an external ^{55}Fe X-ray source.

The spectral dependence of the ionisation between 260 nm and 325 nm is shown in figure 5.4. The laser wavelength was changed in 0.5 nm and 1nm increments and the ionisation at each setting was averaged over the number of laser pulses at that setting. Between 260 nm and 325 nm the ionisation drops by about four orders of magnitude, the greatest fall coming between 275 nm and 300 nm. At all wavelengths the ionisation was shown to be quadratically dependent on laser power, indicative of a two photon ionisation process. An example of this quadratic behaviour is shown in figure 5.5 which was taken at 275 nm.

The laser power was kept below the saturation level for the two-photon process over the wavelength range, and the ionisation, (expressed as the number of ion pairs per cm of sensitive counter wire), was then normalised quadratically to 1μJ mm^{-2} for ease of comparison with the work of other groups. As indicated, three different dyes were frequency doubled in order to cover the range of wavelengths from 260 nm to 325 nm, Coumarin 153, Rhodamine-6-G and DCM. The ionisation from each dye can be distinguished. Even though the level of ionisation was normalised to 1 μJ mm^{-2} some differences were seen in the ionisation from the different dyes where the wavelengths from each dye overlapped. This may be due to differences in the spatial and temporal profiles of the laser pulses for the different dyes, and also drops in the efficiency of the dyes near the limits of their lasing action. Amplified spontaneous emission (ASE) begins
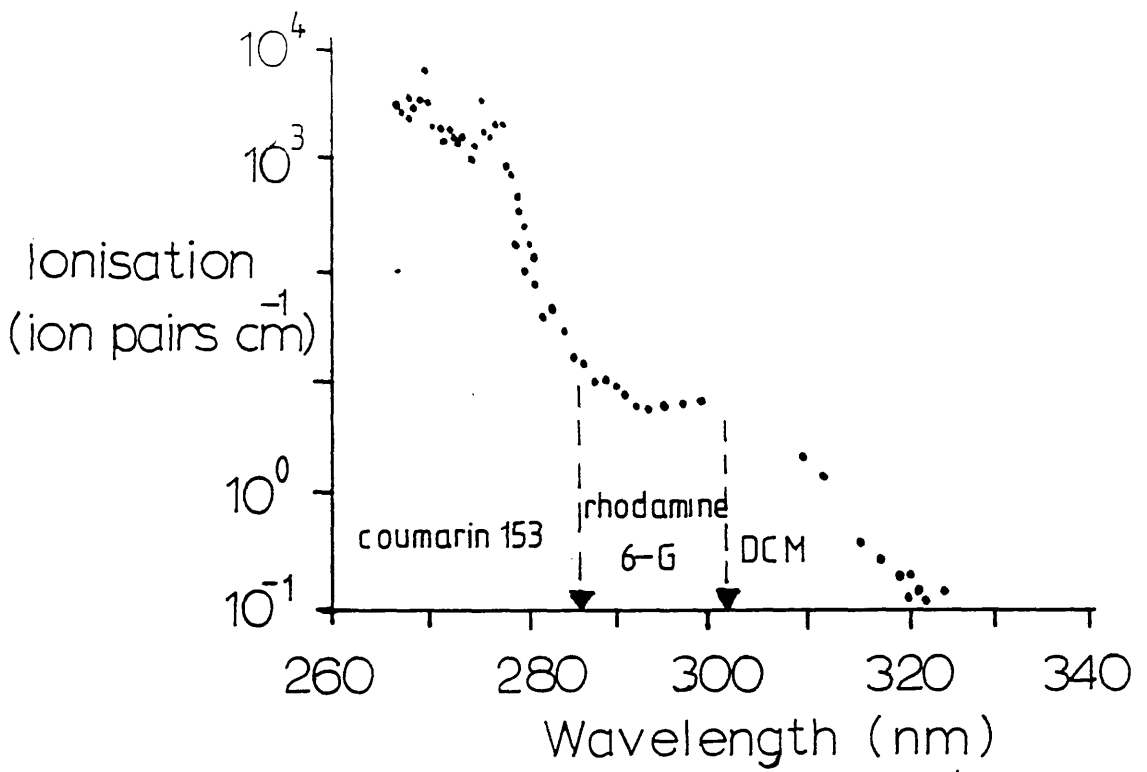
Fig 5.4   Background ionisation in type 2 counter showing structure around 274 nm. The three dyes used and their approximate spectral range are indicated.
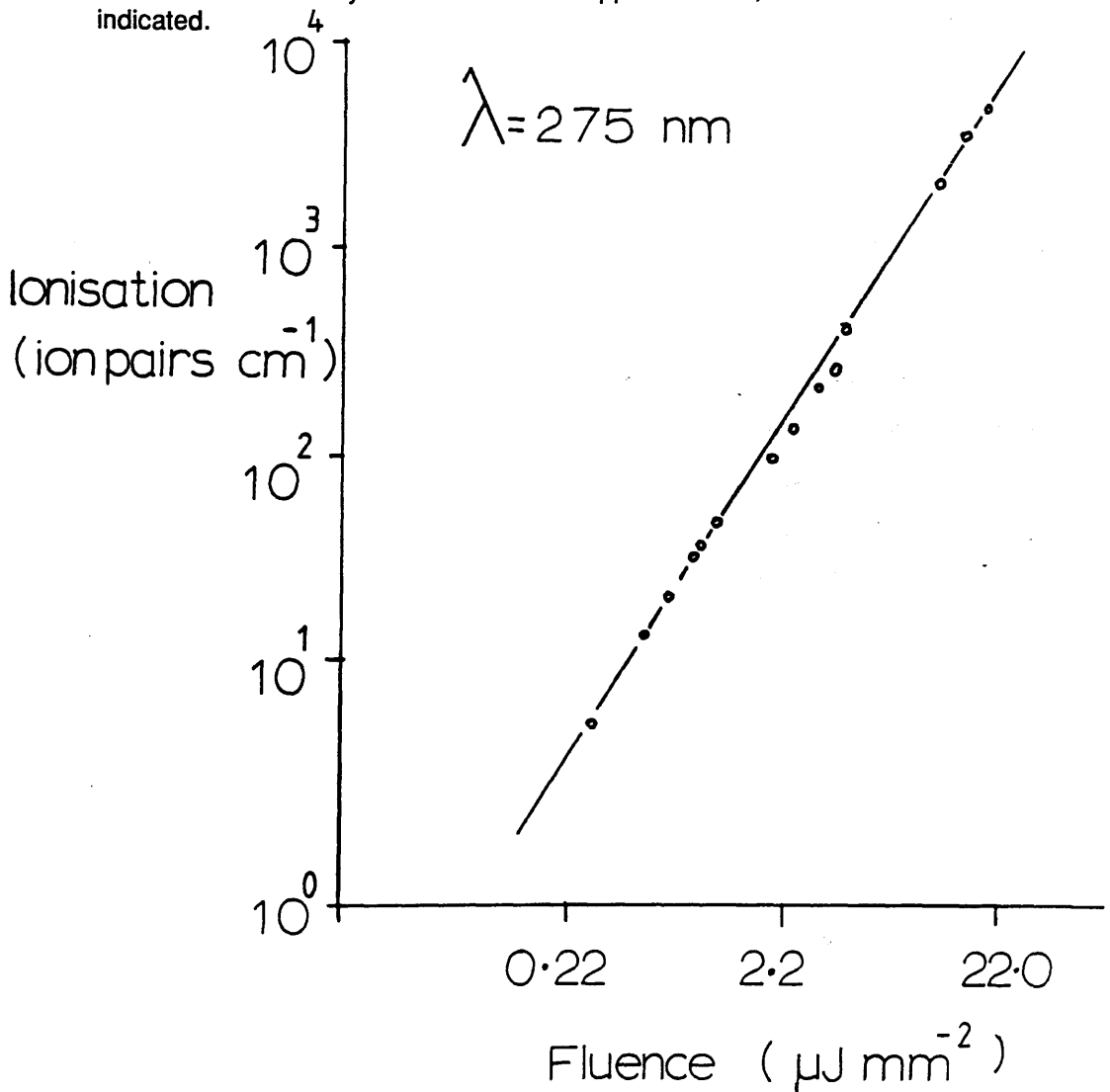
Fig 5.5   Dependence of ionisation on laser fluence in type 2 counter at 275 nm.

to dominate the output from the dye laser when operating near the limit of the dye range, and normalisation with respect to the laser power then becomes difficult.

The apparent structure in the spectrum around 270 nm was examined with greater resolution, the wavelength being stepped in 0.025 nm increments. An ionisation spectrum taken between 266 nm and 278 nm is shown in figure 5.6a (1). From the complexity of the structure and its spectral position in the UV, it was surmised that organic molecules were probably responsible for this ionisation rather than atoms or simple inorganic molecules. The vapour phase two photon ionisation spectrum of a molecule should be similar to its vapour phase single photon electronic absorption spectrum. This is because the first excitation step in both processes is the same, while the second step in the two-photon ionisation process usually shows only a small dependence on wavelength, (Brophy and Rettner 1979). Thus use would be made of the many documented UV absorption spectra (eg, UV Atlas of Organic Compounds, 1966) to identify the impurities. Many compounds were found to have electronic absorption structure in the 266-278 nm range, in particular benzene and some of its derivatives which had spectral strucure (when dissolved in methanol solution) quite similar to figure 5.3. These compounds were also known to have ionisation potentials around 9 eV, compatible with two photon ionisation in the 260-280 nm wavelength region. In order to compare the spectra more fully, single photon absorption spectra of a number of simple benzene derivatives and other compounds (benzene, zylene, P-clorotoluene, phenol, 2-acetylfuran, Di-methyl analine, trimethyl amine, triethyl amine, naphthalene) were taken in the vapour phase at room temperature, in a Beckman spectrophotometer (UV 5270), which has a resolution comparable with the dye laser (0.05nm), (Towrie et al 1987). The best match to the unknown background resonant two-photon ionisation (R2PI) spectrum of figure 4 was obtained with phenol (hydroxybenzene), and this comparison is illustrated in figure 5.6a.

5.4 BACKGROUND IONISATION IN A TYPE 3 COUNTER AND THE IDENTIFICATION OF TOLUENE AS AN IMPURITY

In order to investigate the two photon ionisation spectrum of phenol in a proportional counter, a new counter, the type 3, was constructed, which could be rapidly dismantled, cleaned and reasssembled (Ledingham et al 1985). The counter was again normally operated when filled with 760 torr of P10 gas, (the static mode), although gas feedthroughs allowed the counter gas to flow through the counter while in operation,
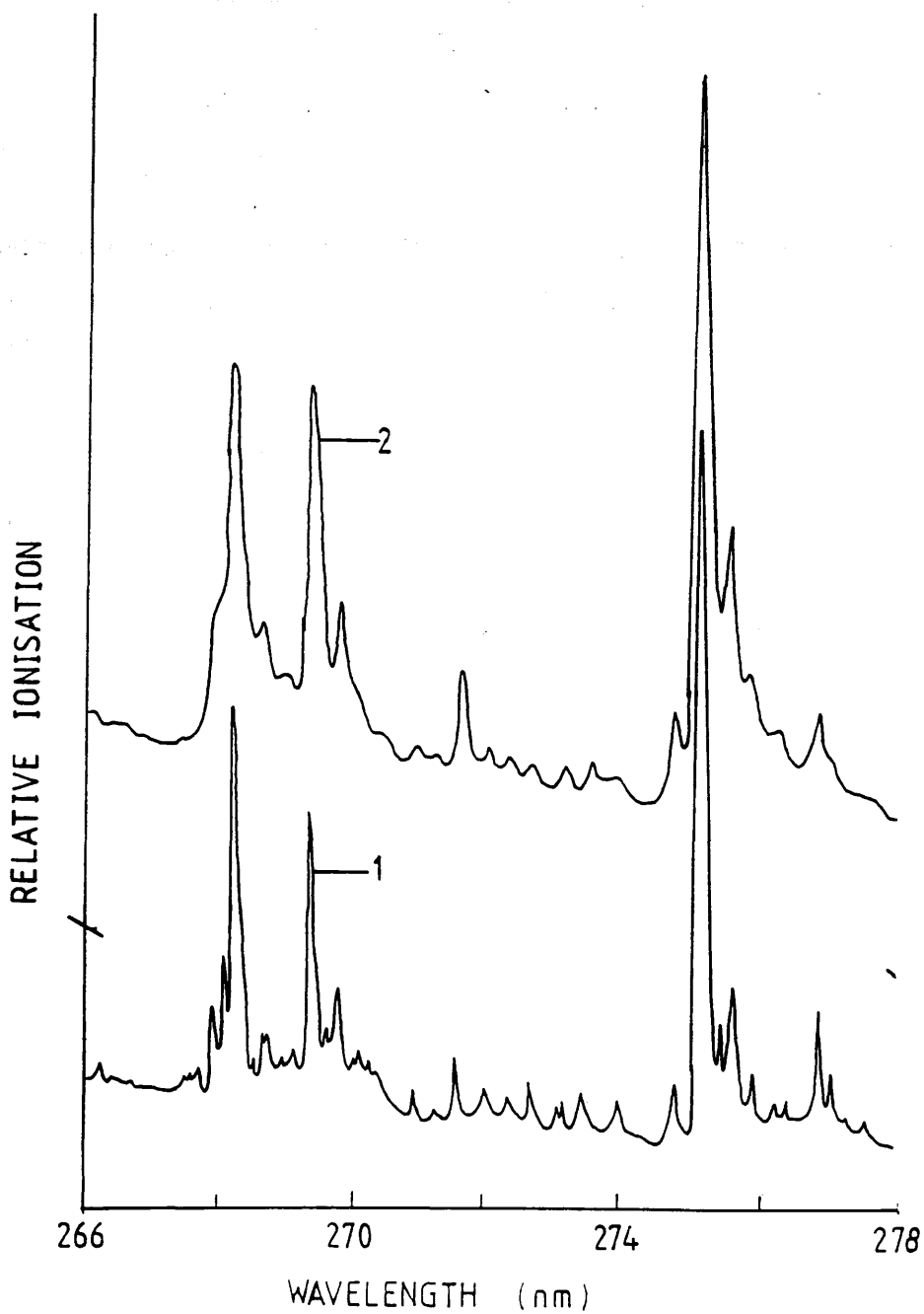
Fig 5.6a   Comparison of the background ionisation in type 2 counter (1) with the
single photon absorption spectrum of phenol (2)

figures 5.6b.

This counter was deliberately contaminated with phenol by flowing the counter gas over a small solid sample of phenol held at -10° C. The resonant two photon ionisation spectrum for this contaminated counter in the 265-278 nm range was shown to be identical to the single photon absorption spectrum of phenol and also to the two photon resonant ionisation spectrum of the background, illustrated in figure 5.6a. Evidence for phenol being a major component of the impurities in the proportional counter also came from a single photon absorption spectrum of a sample of counter gas in which the impurities had been concentrated in a liquid nitrogen cold trap. The single photon absorption spectrum of the concentrated counter gas showed similar structure to the resonant two photon ionisation (R2PI) spectrum of the counter gas.

Thus phenol was judged to be responsible for at least part of the background ionisation shown in figure 5.4. By comparing the two photon ionisation spectrum of phenol taken at its (known) saturated vapour pressure at room temperature, with the R2PI background ionisation spectrum of phenol in the "clean" counter, the background concentration of phenol in these counters was estimated to be of the order of 1 part per million.

The source of the phenol was traced to reinforced plastic tubing used to flow gas from the bottle to the proportional counter. This was disconnected and flexible stainless steel tubing used instead. Once in a counter, phenol proved difficult to remove, either by pumping out, baking out or flushing out with clean gas. Instead the counter had to be dismantled and the individual parts cleaned separately.

DETECTION OF TOLUENE

Once phenol was identified as an impurity in the counters, and its source identified, new impurities became evident. A spectrum taken between 260 nm and 330 nm in a "clean" type 3 counter is shown in figure 5.7. There is no evidence of any phenol structure between 270 nm and 280 nm, but there is other structure at a slightly lower wavelength around 268 nm which is resolved in figure 5.8c. This indicated the presence of another impurity which was identified as toluene by a similar technique to that used to identify phenol, that is by comparison of the background R2P1 spectrum with both the single photon absorption spectrum of toluene taken in a Beckman

Static mode
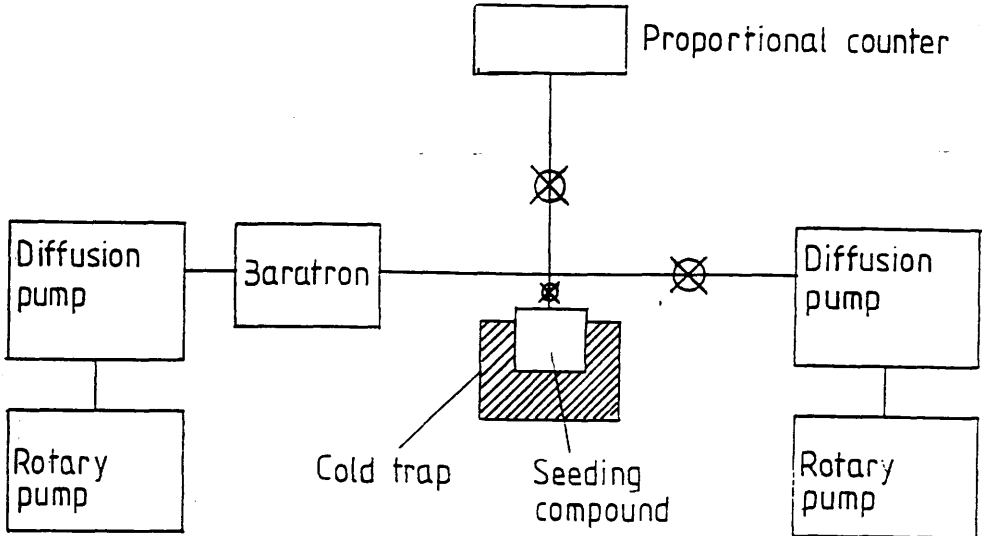
Flowing mode
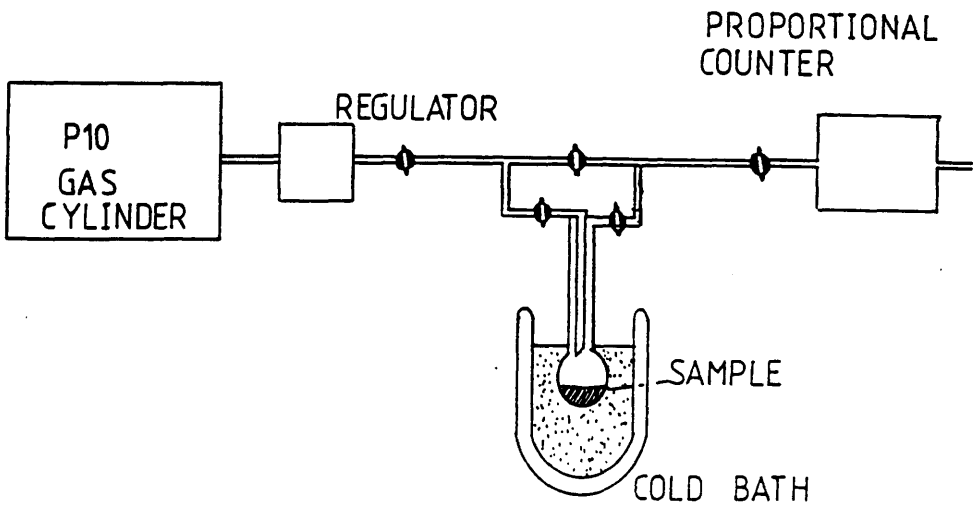
Fig 5.6b   Apparatus used to introduce samples into the type 3 counter in flowing
and static modes.
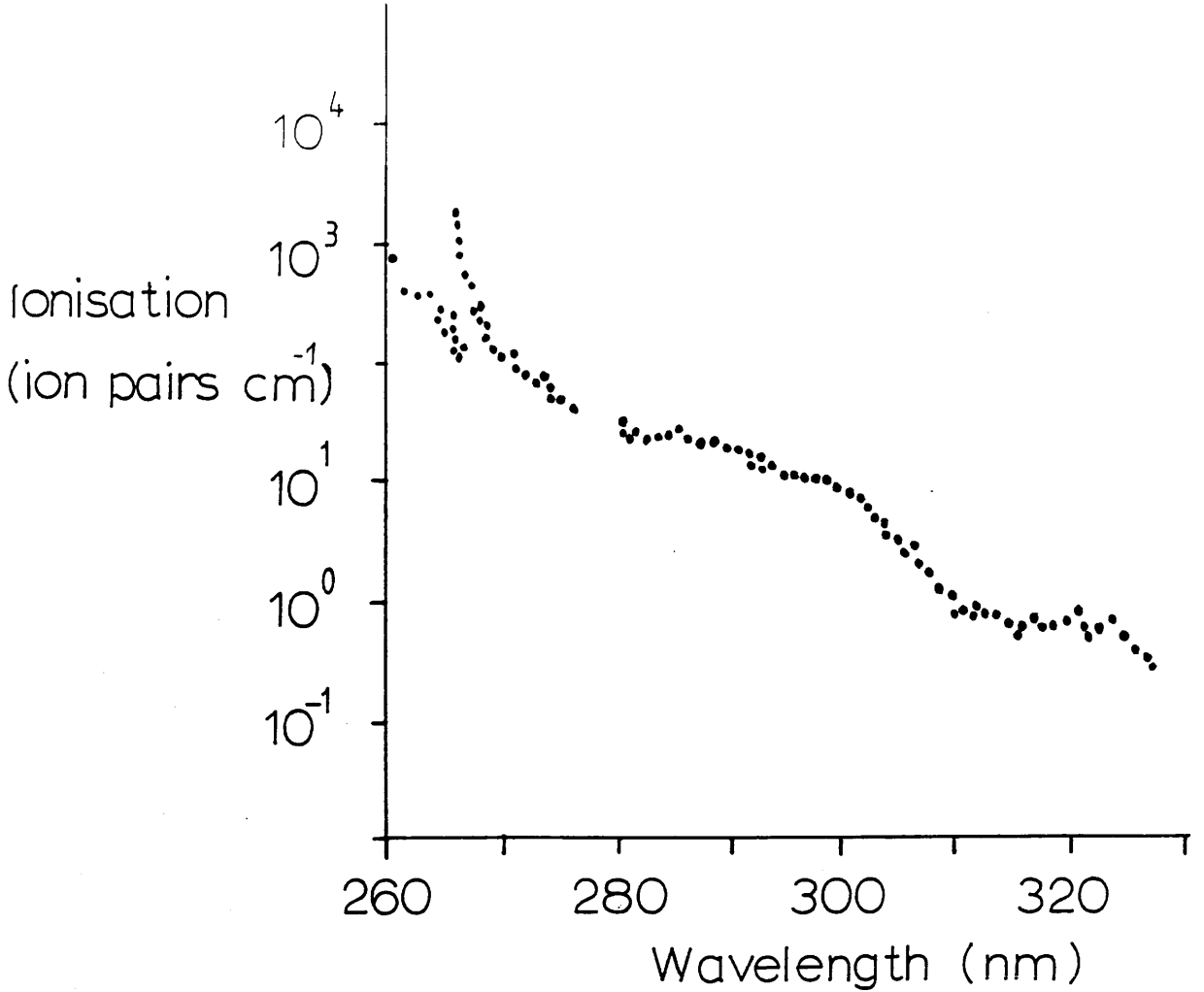
Fig 5.7   Background ionisation in type 3 counter showing structure around 268 nm.
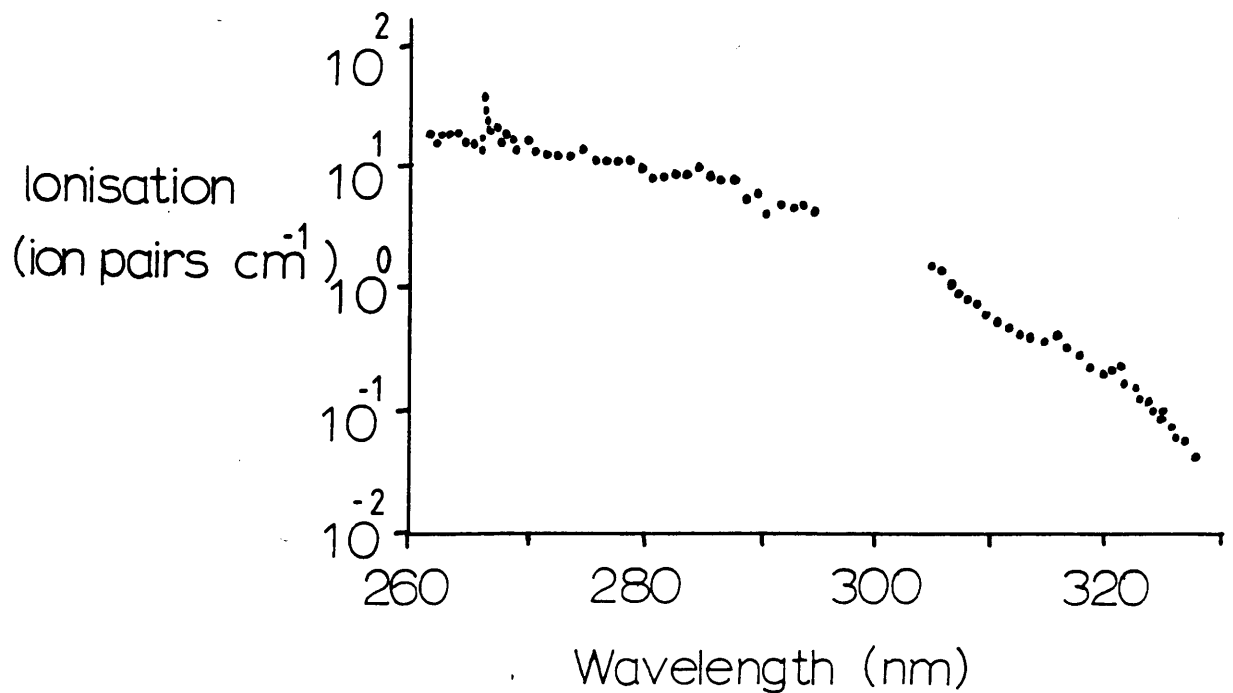
Fig 5.9   Background ionisation in type 4 counter. The structure at 268 nm is attributed to toluene at a level of ~1 part per billion. The overall level of ionisation is around two orders of magnitude less than in the type 3 counter.

spectrophotometer, and also with the two photon resonant ionisation spectrum of toluene taken in the proportional counter, figure 5.8. Further, by comparing an R2PI spectrum of toluene taken at a known vapour pressure (5×10^{-3} torr at -80° C) with the background spectrum of a clean type 3 counter, figure 5.7, the concentration of toluene in the clean counter was estimated at approximately 50 ppb, (Drysdale et al 1986)

5.5 BACKGROUND IONISATION IN A TYPE 4 COUNTER

When a fourth type of proportional counter was constructed, (the one in which work with caesium and rubidium was done), some effort was expended in ensuring the counter was kept clean during and after assembly. A background spectrum taken over the region 266 nm to 330 nm is shown in figure 5.9. The overall level of background ionisation has been lowered when compared with the earlier "clean" counter of figure 5.7, but the structure around 268 nm which is attributed to toluene is still present, at a concentration of around 1 part per billion.

Toluene would seem to be a persistant contaminant therefore and its source has not been discovered yet. It is suggested that it may be a trace impurity in the solvents (methanol and ethanol) which are used to clean the counter components prior to baking and assemblying them. The toluene would then outgas from the counter walls into the P10 gas. Evidence for this came from three experiments. The first showed that the level of ionisation decreased as counter gas was flowed through the counter (figure 5.10a), the second showed a 6 fold increase in the level of background ionisation when the temperature of a part of the counter was increased to around 100° C (figure 5.10b), and the third showed that the background ionisation increased over a period of 10 hours with a static gas fill in the counter, (figure 5.10c). However Boerner (1985) produced evidence that toluene was also an inherent impurity in the P10 counter gas.

Relative ionisation

Wavelength (nm)

262   264   266   268

a
b
c
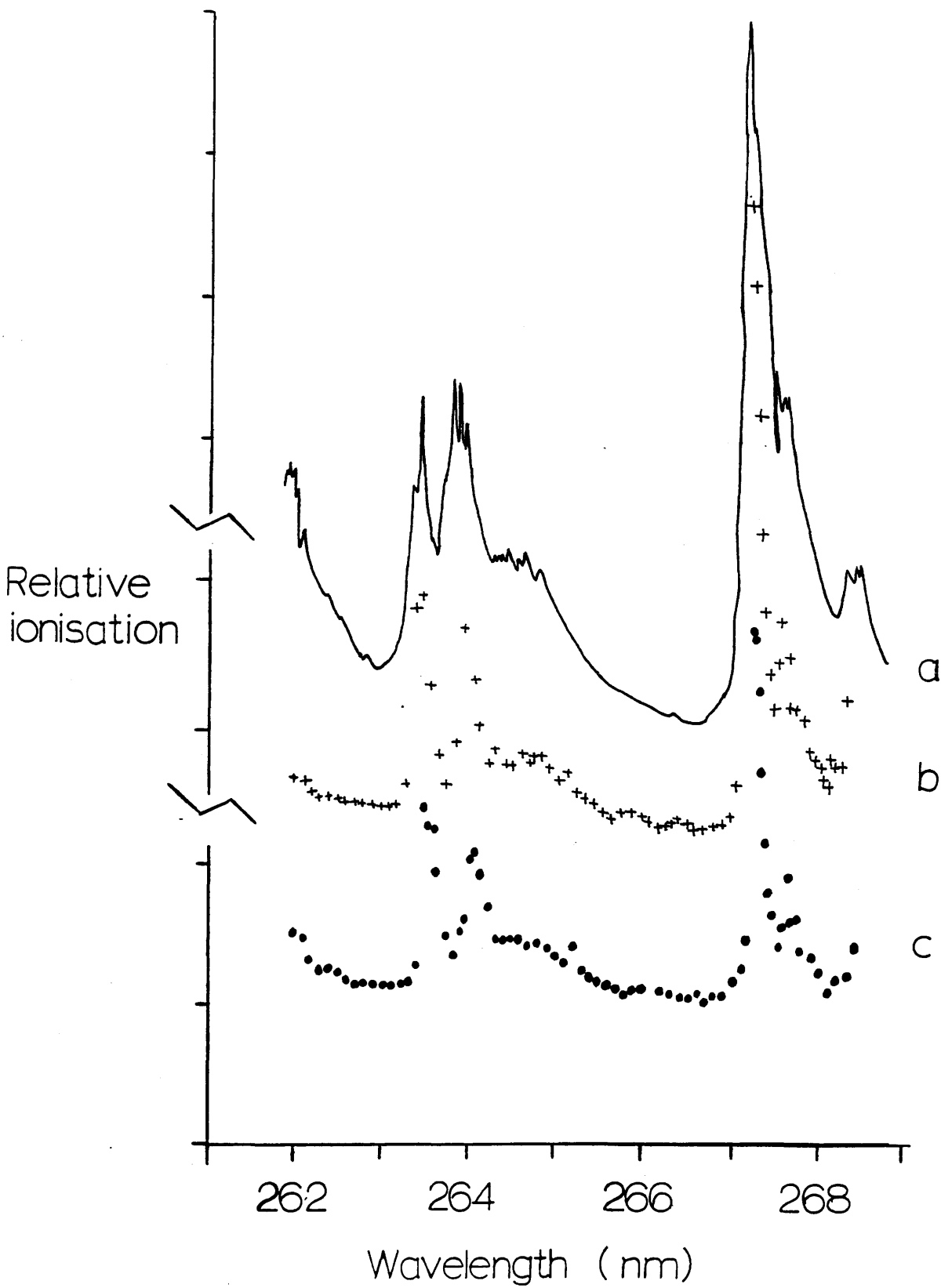
Fig 5.8   a) Single photon absorption spectrum of toluene
b) Two photon resonant ionisation spectrum of toluene
c) Background ionisation in type 3 counter.
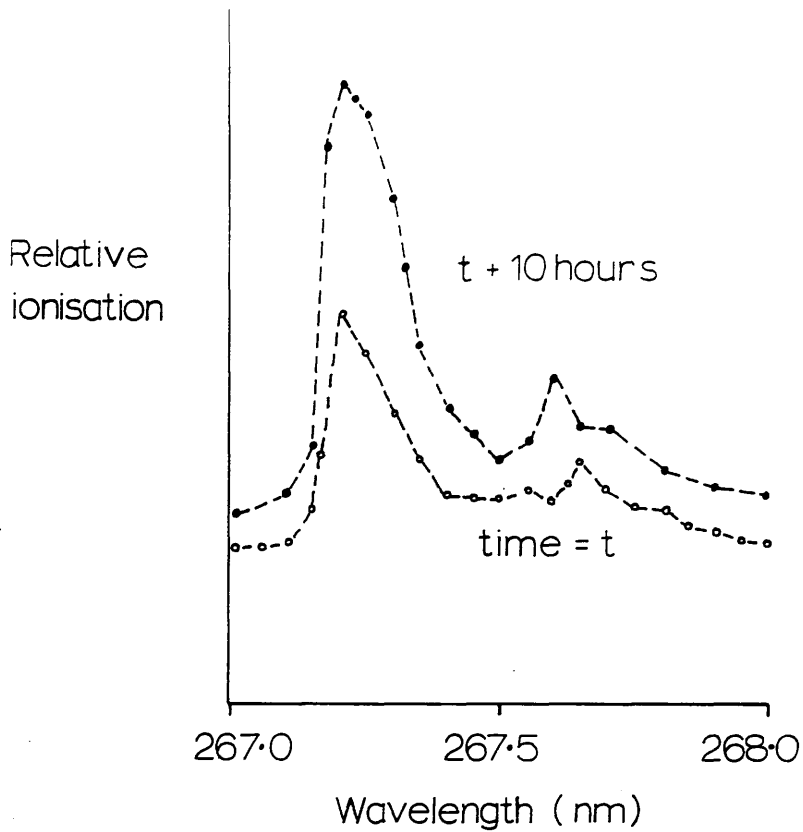
Fig 5.10 **a) Increase in ionisation in type 3 counter over period of 10 hours with a static gas fill**
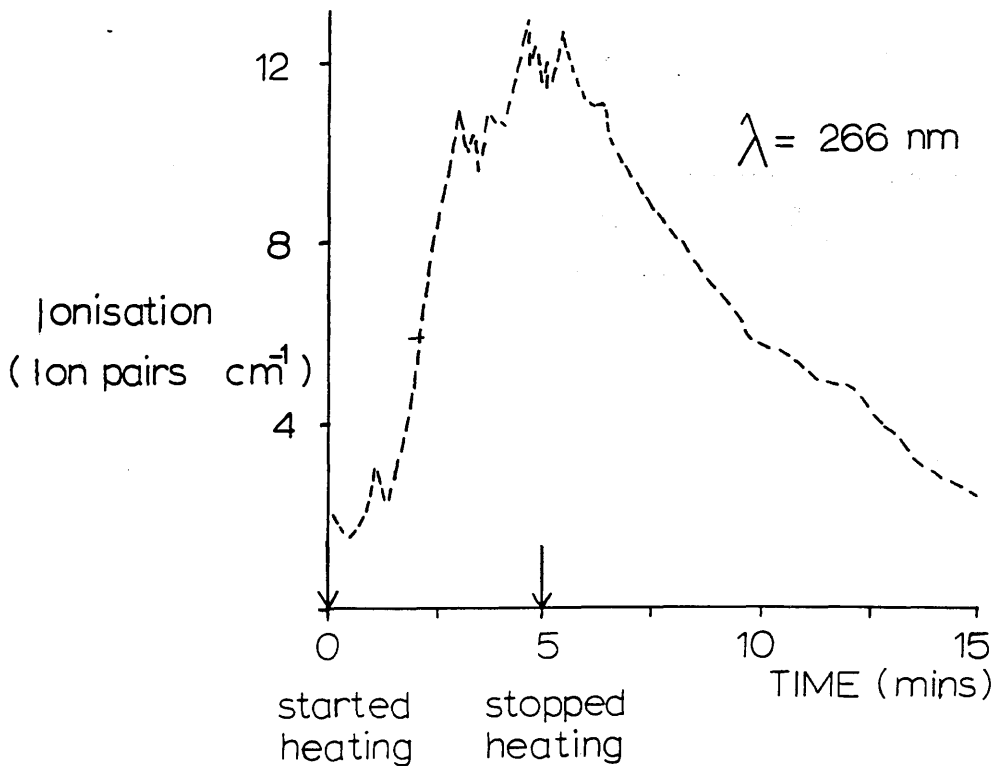
b) Increase in ionisation with increasing temperature in type 3 counter.
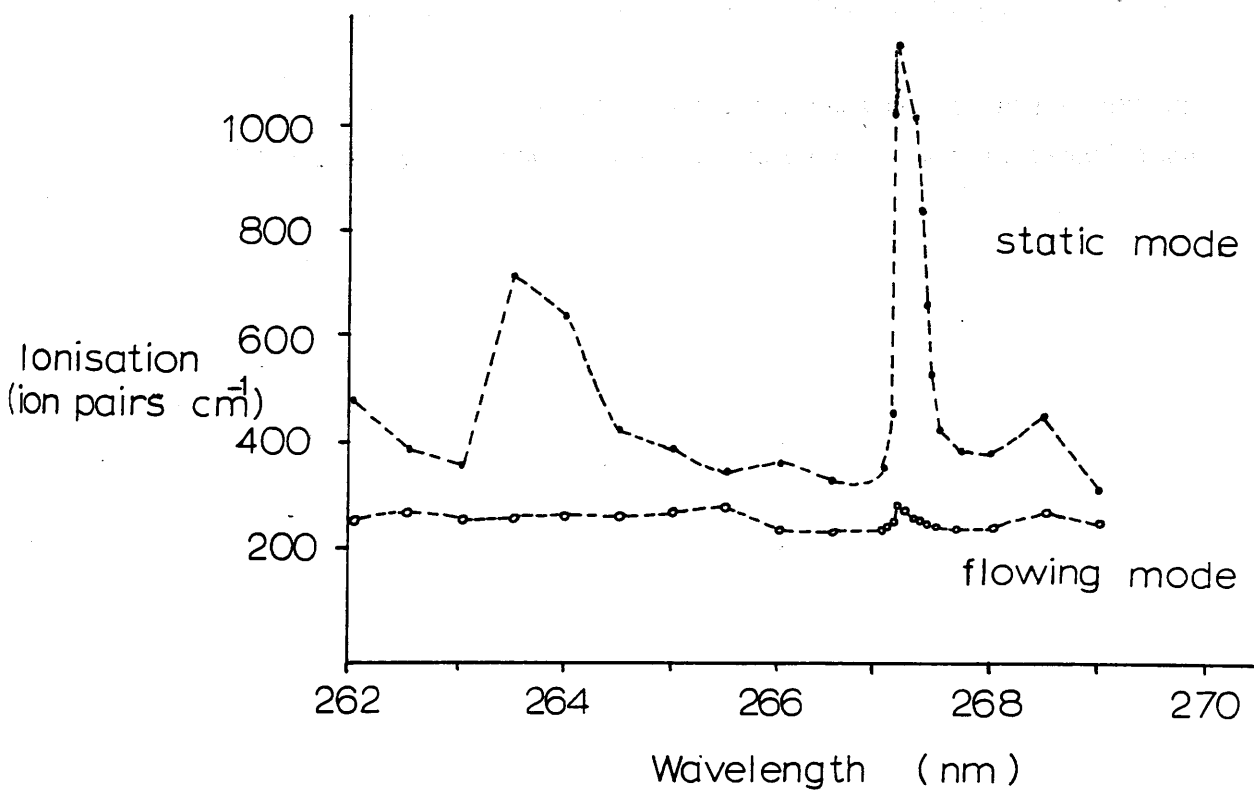
c) Decrease in ionisation as buffer gas is flowed through the type 3 counter.

5.6 LASER IONISATION OF PHENOL AND TOLUENE IN A QUADRUPOLE MASS SPECTROMETER

Other impurities apart from toluene are thought to be responsible for the background ionisation in this "very clean" type 4 counter. Lack of observable structure in other parts of the spectrum restricts identification of these impurities using the techniqes described above. Instead an attempt was made to mass analyse the impurities in the counter gas using a quadrupole mass spectometer. The mass spectromter was modified to enable a laser beam to pass through the ionisation cage. Ionisation of a gaseous sample by the laser and also by electron bombardment could both be used for mass analysis.

However the level of concentration of the impurities in a clean proportional counter (~0.02 ppm in type 3 counters) was found to be well below the detection limit of the mass spectrometer. No background impurity was detected at this concentration in the mass spectrometer using either laser ionisation or electron bombardment ionisation. Cold trapping the impurities to concentrate them in a sample of P10 gas before introducing them into the mass spectrometer also failed to produce any ions at any mass. This limit is imposed by the maximum operating pressure of the instrument, which at a pressure of 5×10^{-6} torr gives a limit of 2 ppm to the concentration of phenol that can be detected.

Nevertheless it was felt that in more sensitive mass spectrometers the ionisation of impurities, such as toluene, outgassing from the components of the instrument, might be more noticeable, and possibly detrimental to the sensitivity of the instrument. Resonant ionisation mass spectra of phenol and toluene were therefore recorded at differing laser powers.

In order to observe toluene and phenol ions in the quadropole mass spectrometer, samples of each were vapourised in a stream of counter gas which was then injected through a needle valve into the ionisation cage of the mass-spectrometer. This procedure allows a much higher local pressure of sample to be analysed whilst keeping the ambient pressure of the mass spectrometer below 10^{-6} torr. Resonant two photon ionisation mass spectra of phenol and toluene were then produced. Figures 5.11a and 5.11b show two examples of these obtained at two different laser powers. In both cases the laser was focused and at a wavelength of 266 nm. Considerable fragmentation of the
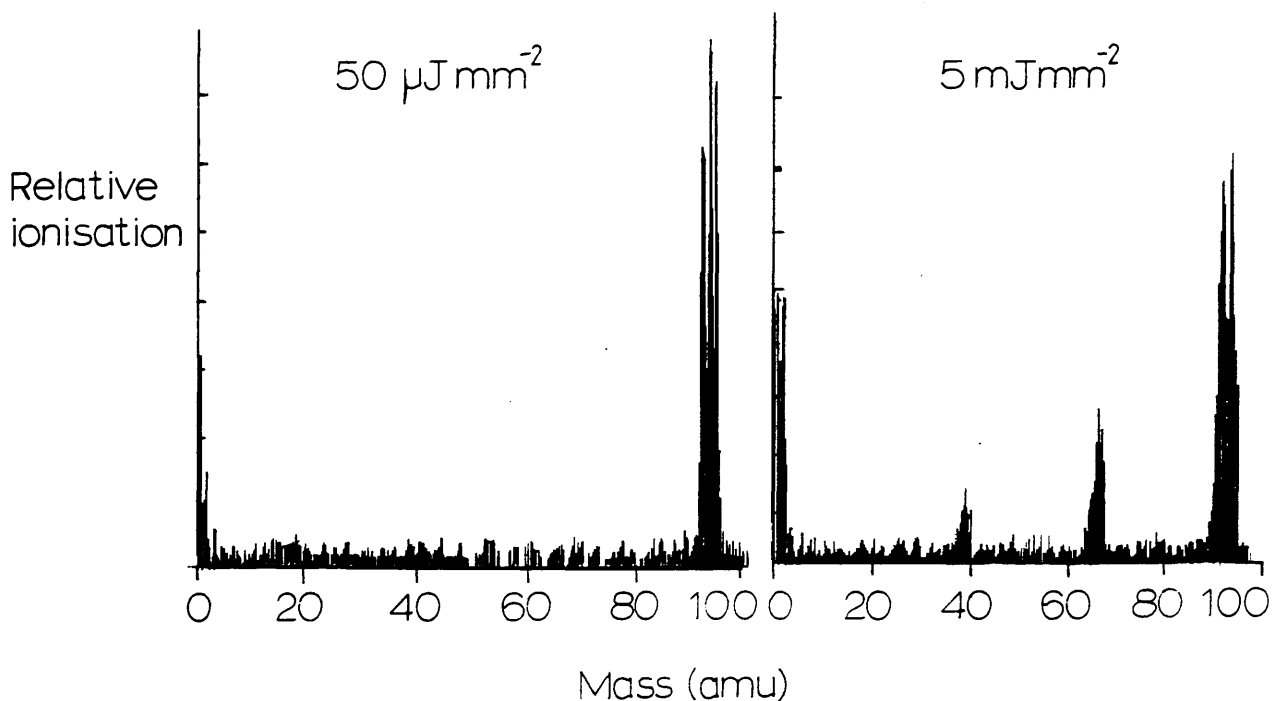
Fig 5.11a Mass spectra of phenol showing increasing fragmentation with increasing laser power. (C_6H_5OH, molecular weight = 94.11)
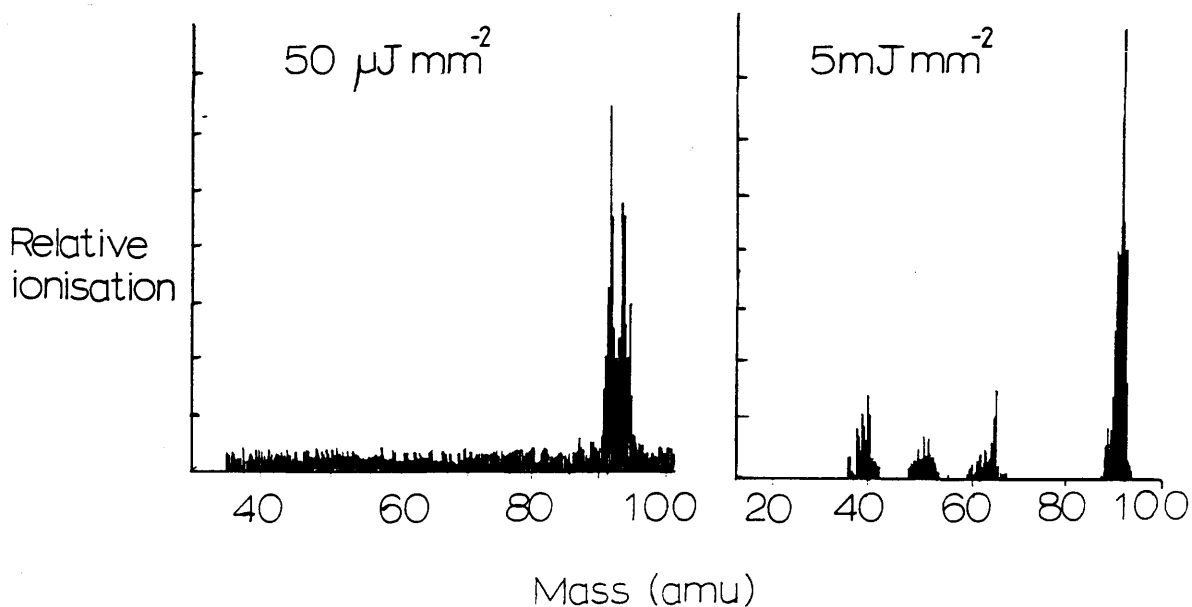
Fig 5.11b Mass spectra of toluene showing increasing fragmentation with increasing laser power. (($C_6H_5CH_3$, molecular weight = 92.13)

parent molecule is apparent at the higher laser power, and it is this aspect of the ionisation process of these molecules which may present problems when real samples are analysed in sensitive mass-spectrometers. The fragmentation of impurities may cause isobaric interferences over a range of masses. Allied to this is the broad photoexcitation resonances of many organic molecules which tends to reduce the elemental selectivity normally associated with laser induced resonant ionisation.

Therefore in order to reduce the likelihood of ionising low ionisation potential molecules which may be contaminants in the system, the lasers should have wavelengths greater than ~330 nm to reduce ionisation, and be operated at low power to avoid fragmentation.

CHAPTER 6

LASER IONISATION OF CAESIUM AND RUBIDIUM IN A PROPORTIONAL COUNTER AND QUADRUPOLE MASS SPECTROMETER

6.1 INTRODUCTION

The study of the resonant ionisation of caesium vapour was carried out entirely using a proportional counter. The initial work centred on designing a relatively clean chamber that would hold the pure caesium metal in its unreacted state for a sufficient length of time to enable spectra to be recorded. A chamber was eventually built that would hold caesium for a number of weeks. The same chamber was used successfully for proportional counter work on rubidium, and was then bolted on to a modified quadrupole mass spectrometer, where it served both as a proportional counter and as an ion source for the mass spectrometer.

The initial work on caesium was done with the aim of determining the laser flux conditions necessary to ensure saturation of the two-photon ionisation of caesium atoms from the 6s ground state to low lying 7p, 8p and 9p levels, (Houston et al 1988). Further studies on caesium dealt with transitions from the ground state to highly excited Rydberg levels. Both one photon s-p transitions and two photon s-s and s-d transitions were investigated.

Work on rubidium metal began using the same proportional counter, and the one photon s-p transitions and two photon s-s and s-d transitions from the 5s ground level to Rydberg levels were studied. A modified mass spectrometer was then used in conjunction with the proportional counter to study the effect of the buffer gas on the three photon ionisation process in rubidium vapour. These were via two photon transitions from the ground state to low lying s and d levels. Eventually the proportional counter was removed and the two photon ionisation of atomic rubidium via the 5s-6p single photon transition at 421 nm was investigated. This enabled the two naturally occurring isotopes of atomic rubidium to be resolved and also separated out the molecular Rb_2^+ component of the ionisation.

6.2 VAPOUR PRESSURE OF CAESIUM AND RUBIDIUM

CAESIUM

The vapour pressure of caesium at room temperature is sufficient for the ionisation of the vapour to be easily detected in a proportional counter. In an effort to reduce the level of impurities in the counter high purity gas was substituted for the commercial grade P10 gas, and the operating pressure was reduced to 30 torr. In order to try to stabilise the gain of the counter at this lower pressure the gas mixture was also changed to 70% argon + 30% methane.

At 300 K the saturated vapour pressure of caesium is approximately 2×10^{-6} torr and the pressure of molecular caesium dimers, Cs_2, is approximately 4×10^{-11} torr, (Samson 1966, Morellec et al 1976). The ratio of molecular caesium to atomic caesium at 300 K is around 2×10^{-5}. The number density of caesium atoms is 6×10^{10} cm^{-3} and of caesium molecules, 1×10^6 cm^{-3}. In an unfocussed laser beam of dimensions 1mm x 1mm x 20mm the number of caesium atoms is therefore 1×10^9 and that of caesium dimers is 2×10^4, and in a focussed beam of dimensions 0.13mm x 0.13mm x 10mm there are 1×10^7 atoms and about 200 molecules.

RUBIDIUM

It was found necessary to raise the temperature of the rubidium vapour to around 350 K in order to see any spectral structure in the ionisation using the proportional counter, and to around 410 K to obtain reproducible spectra. This was achieved initially by heating the arm of the chamber that contained the rubidium ampoule. The positioning of the laser beam with respect to the rubidium "oven" was in this case quite critical, small changes in beam position (<<1mm) causing large variations in the ionisation signal. Furthermore, as the experiment progressed over a few weeks, the rubidium condensed more and more heavily on the windows, causing the laser light to scatter more profusely. This scattered light was able to eject photoelectrons from the rubidium that had condensed on the surface of the proportional counter, giving a background level of ionisation that increased linearly with laser power, but which never saturated. Heating up the entire chamber to 410 K, including the windows, prolonged the life-time of the counter but did not altogether cure the problem of condensation.

At a temperature of 410 K the pressure of Rb atoms is about 4×10^{-4} torr and that of Rb$_2$ dimers is 1.6×10^{-7} torr, (Samson 1966). These pressures correspond to number densities for rubidium atoms of 1.4×10^{13} cm^{-3} and for Rb$_2$ 5.6×10^9 cm^{-3}. In an unfocussed laser beam of dimensions 1mm x1mm x20 mm there are 2.8×10^{11} atoms and 1×10^8 molecules, and in a focussed beam of dimensions 0.13 mm x 0.13 mm x 10 mm there are 2.4×10^9 atoms and 1×10^6 molecules.

However Houston (1986) has shown that the saturated vapour pressure of caesium in proportional counters can be reduced by up to two orders of magnitude due to reactions of the metal with inpurities, which are either in the counter gas, or are outgassed from the chamber surfaces. This became apparent if the caesium sample was left untouched for a few days. The level of resonant atomic ionisation dropped markedly and could only be restored by heating the sample to liquify it, dipping the probe into the now liquid caesium reservoir and then withdrawing the probe to its original position. A reduction of the same magnitude in the vapour pressure of rubidium in a proportional counter was noticed by Whitaker et al (1981). The above values for caesium and rubidium should therefore be viewed as the maximum numbers of atoms and molecules that may be detected in the focussed and unfocussed laser beam volumes.

6.3 TWO PHOTON IONISATION OF CAESIUM VAPOUR

By frequency doubling the laser, two photon resonant ionisation spectra of caesium vapour were recorded. Figure 6.1 illustrates the spectral dependence of the ionisation from 317.5 to 330 nm. The laser was not focussed and in the ionisation volume of 1mm x 1mm x 20mm the flux was 2×10^{22} photons cm^{-2} sec^{-1}.

ATOMIC IONISATION

The resonances are the single photon transitions from the 6s ground state,

$$6\,s_{1/2} + h\nu \quad ----> \quad n\,p_{3/2} \quad n > 13$$
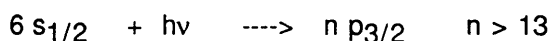
This series terminates at the single photon ionisation edge which in field free conditions lies at 318.4066 nm.

The doublet structure of the lower p states was not seen in this spectrum due to the relatively small oscillator strength of the $6s_{1/2}$-$np_{1/2}$ transitions compared with the $6s_{1/2}$-$np_{3/2}$ transitions. Pichler (1976) attributed this to a strong spin-orbit effect in the caesium atom. He measured the ratio of the oscillator strengths of the 13p levels to be 62 +/- 23, and also showed that the ratio increased with increasing p levels at a rate $(1/n^*)^3$. Part of a spectrum, taken at a much larger flux $(3 \times 10^{25}$ photons cm^{-2} $sec^{-1})$ obtained by focussing the laser, is illustrated in figure 6.2, which indicates the relative sizes of the ionisation yields from the ground state to the lower resolved $p_{3/2,1/2}$ states. In this spectrum the ratio of the $p_{3/2}/p_{1/2}$ ionisation (greater than 10:1) is understated due to saturation of the $6s_{1/2}$-$np_{3/2}$ transitions. At the low flux level of figure 6.1 therefore the $6s_{1/2}$-$np_{1/2}$ transitions are not observed.

Figure 6.3 records the dependence of the ionisation yield at 319.6 nm, resonant with the $6s_{1/2}$-$27p_{3/2}$ transition. At the flux used in figure 6.1 $(2 \times 10^{22}$ photons cm^{-2} $sec^{-1})$ the resonant ionisation is linearly dependent on the laser flux. At this flux however the excitation step for this transition should not be saturated. An estimate can be made of the photon flux necessary to saturate the $6s_{1/2}$-$27p_{3/2}$ transition from the known value of the spontaeous decay rate of the $27p_{3/2}$ level, (Weise and Martin 1980). Assuming a laser line width $\Delta\nu_L$ of $\sim 10^{11}$ Hz the
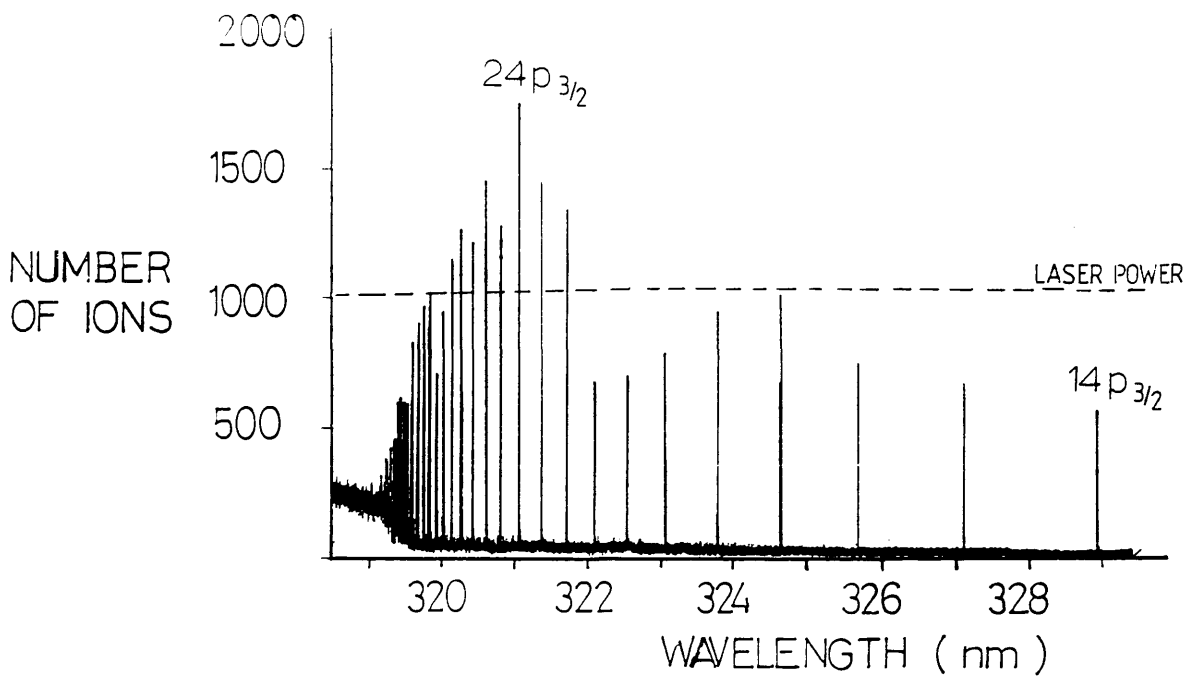
Fig 6.1   Two photon ionisation spectrum of caesium vapour. The resonances are the single photon $6s_{1/2}$-$np_{3/2}$ transitions.
(not focussed, flux = 2×10^{22} photons cm^{-2} sec^{-1})
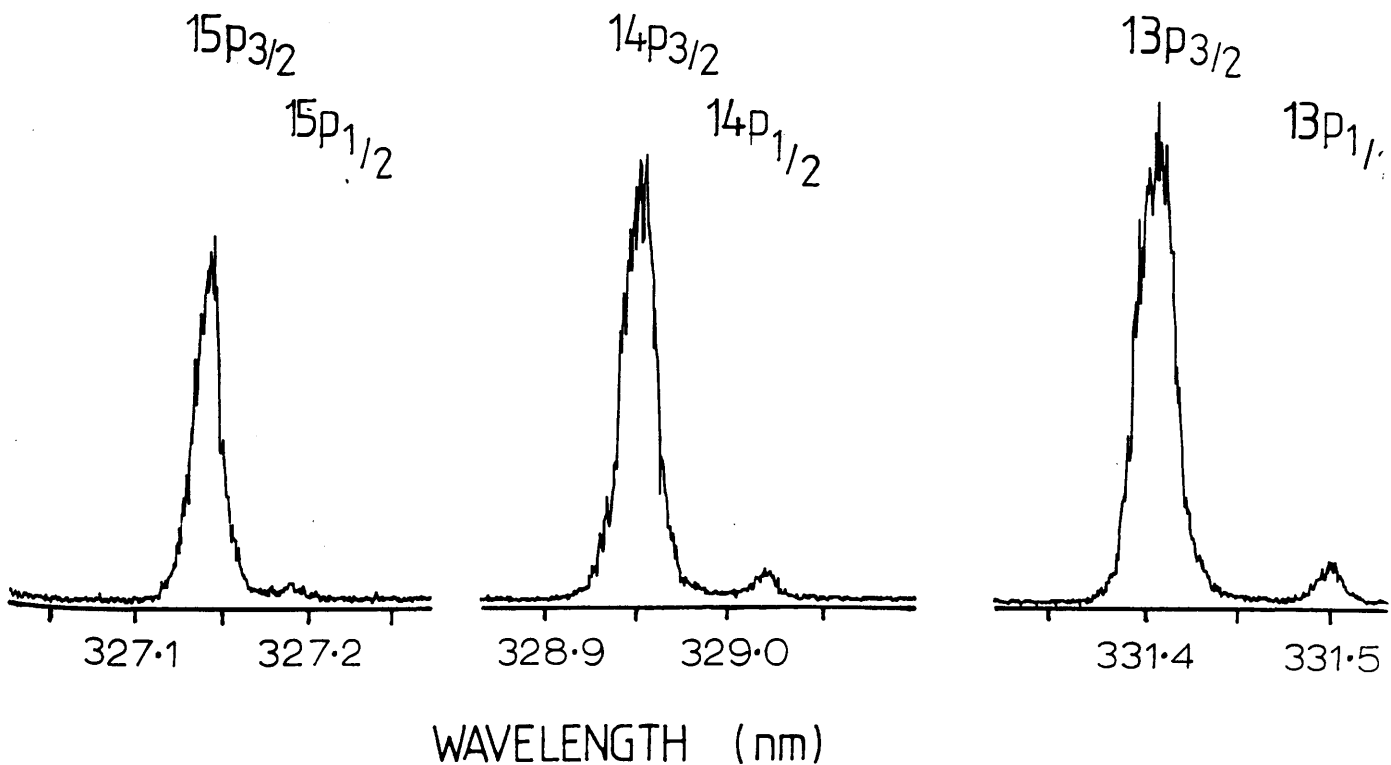
Fig 6.2   Doublet structure of the lower p levels in atomic caesium showing the large $p_{3/2}/p_{1/2}$ ionisation ratio
(focussed laser, flux= 3×10^{25} photons cm^{-2} sec^{-1})
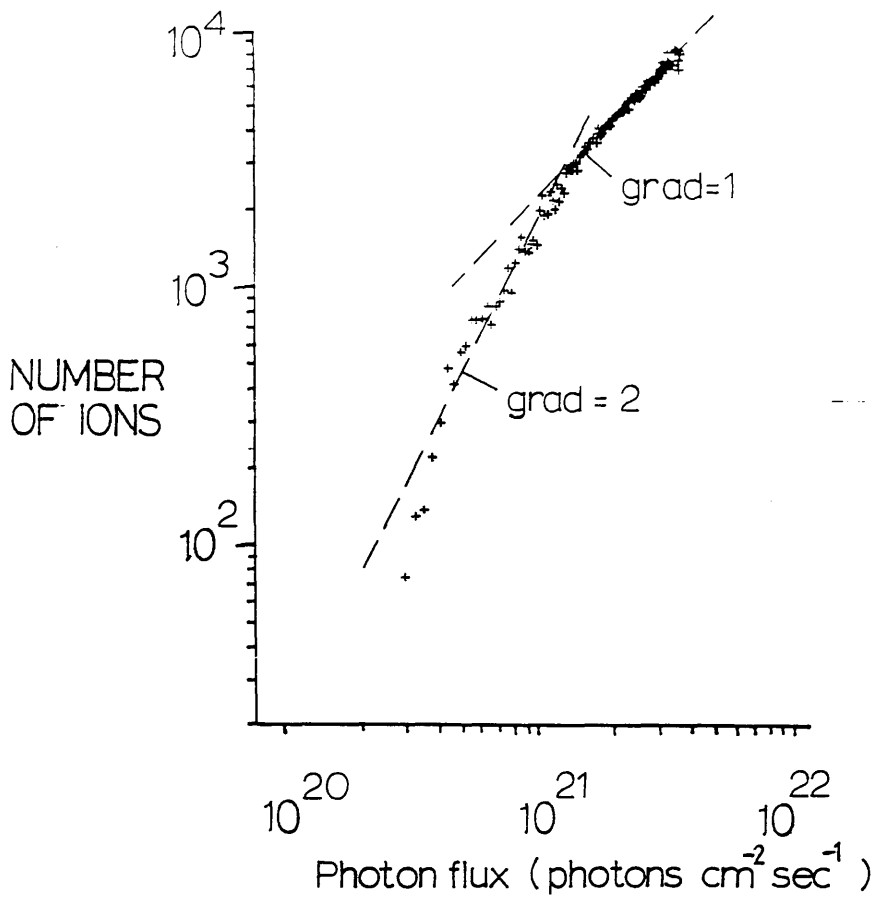
Fig 6.3 Dependence of the resonant ionisation in caesium vapour on photon flux
(λ = 319.6 nm, $6s_{1/2}$ - $27p_{3/2}$)
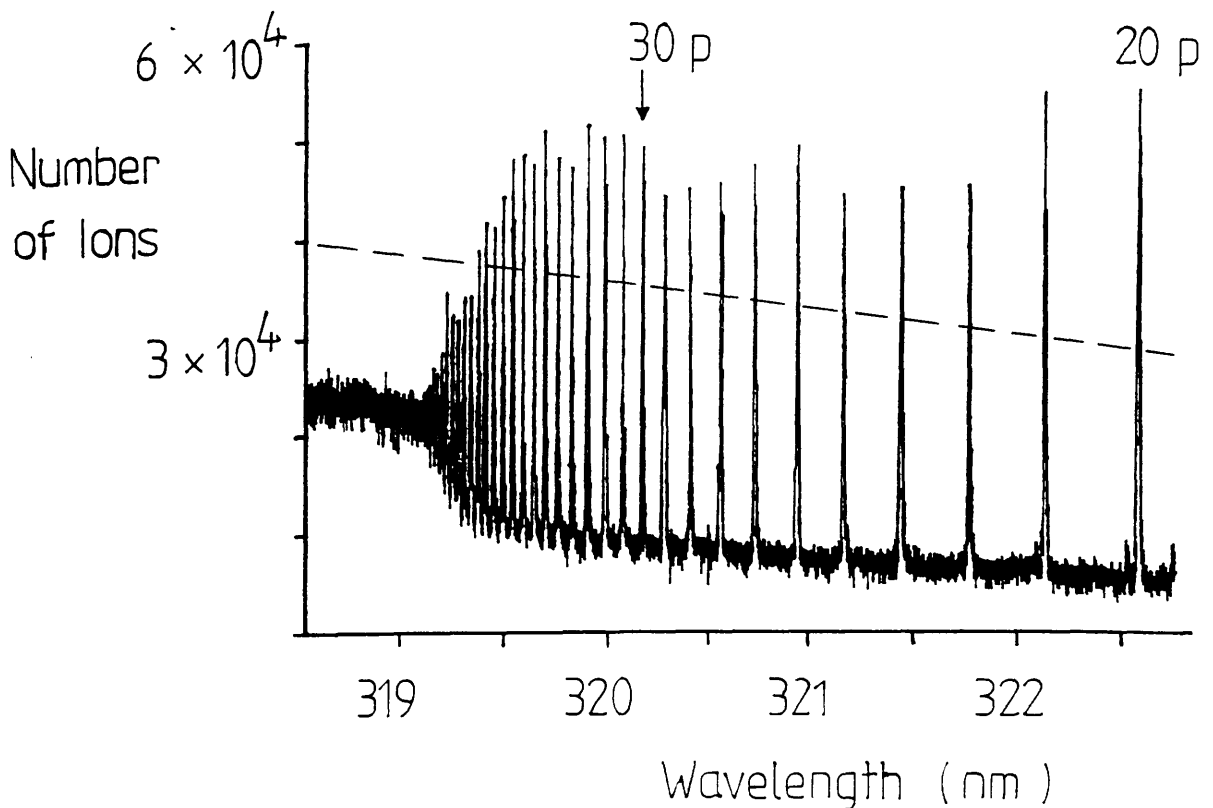
Fig 6.4 Two photon ionisation spectrum of caesium vapour with a focussed laser. The ionisation is saturated up to ~36p.
(focussed, flux = 10^{26} photons cm^{-2} sec^{-1})

cross-section for the excitation transition from level 1 to 2, σ_{exc}, can be estimated from (Tursunov et al 1985, Hurst et al 1979a),

$$\sigma_{exc} = (g_2/g_1)(\lambda^2 \, A_{12}/8\pi \, \Delta v_L)$$

where g_1 and g_2 are the statistical weights of levels 1 and 2, and A_{12} is the spontaneous decay rate from level 2 to 1. This gives a value for σ_{exc} of 5×10^{-19} cm^{-2}, which would require a flux of approximately $(2\tau\sigma_{exc})^{-1} = 10^{26}$ photons cm^{-2} sec^{-1} to saturate, where τ is the laser pulse length of 10^{-8} sec. Therefore it is assumed that the linear dependence of ionisation on flux shown in figure 6.33 is not due to the excitation step being saturated but the ionisation step. This may be through collisions with the buffer gas atoms, or by some other mechanism not dependent on the laser, such as associative ionisation with ground state atoms.

When the laser is focussed as shown in figure 6.4 the level of ionisation from the p states is almost constant between n = 20 and n = 36 which suggests that saturation of both the excitation and ionisation steps is occuring. However at this higher flux the nonresonant background ionisation of Cs_2 dimers has increased reducing the resonant/nonresonant ionisation ratio. This reduction was even more marked in the two photon ionisation of rubidium vapour.

Figure 6.5 records the dependence of the ionisation at 317 nm, at a wavelength shorter than the single photon ionisation edge. The linear dependence is interpreted as single photon ionisation of caesium atoms.

MOLECULAR IONISATION

Figure 6.6 records the dependence of the non-resonant ionisation at 322.6 nm, (3.84 eV). This is quadratic at all the laser powers shown. This is surprising in that the ionisation potential of Cs_2 molecules is 3.71 eV (Kappes et al 1985), and that the non-resonant background ionisation in caesium vapour is expected to be dominated by the ionisation of caesium dimers (Held et al 1972, Granneman et al 1976), which should show up as a linear, single photon process. However it has been shown that caesium molecules (and rubidium molecules) after being ionised, may absorb one or more photons from the same laser pulse, and be further excited into high lying states of the ionic molecule, before dissociating into an excited neutral atom and an ionised atom, (Wagner and Isenor 1985). A similar situation may apply here, involving a two photon
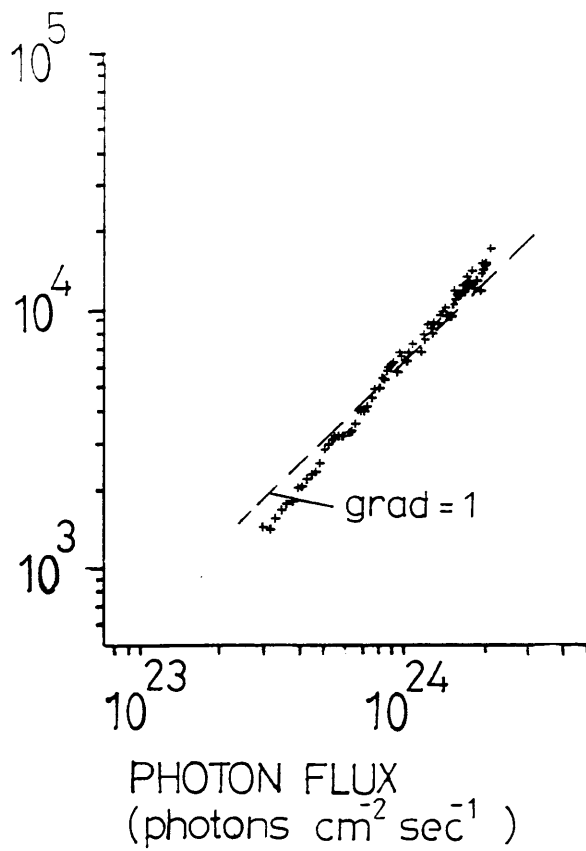
Fig 6.5 Dependence of the ionisation on photon flux in caesium vapour
(λ = 317 nm)
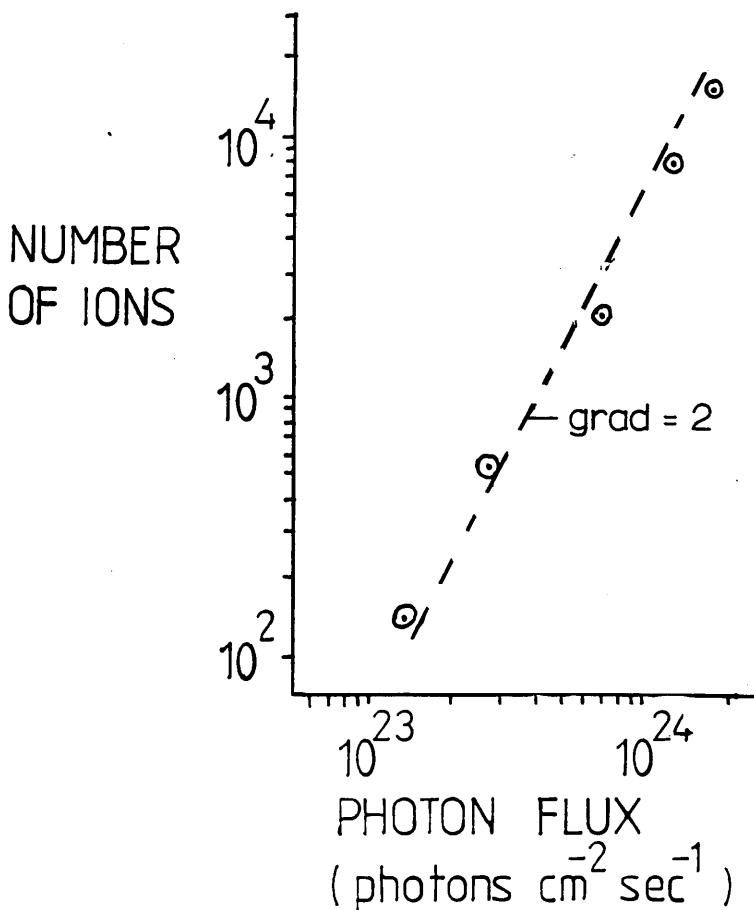
Fig 6.6 Dependence of the nonresonant ionisation on photon flux in caesium
vapour
(λ = 322.6 nm)

absorption process from the ground state molecule to an excited state of the molecular ion.

Another cause of the background ionisation in the proportional counter gas, would be from the ionisation of organic impurities, such as toluene, which are known to be quadratically dependent on laser flux. From the recorded levels of the background ionisation in this type 4 counter (figure 5.9), the ionisation of organic impurities is expected to be approximately 0.3 ion pairs μJ^{-1} mm^{-2}, which is very similar to the level of ionisation of figure 6.6, 0.5 ion pairs μJ^{-1} mm^{-2}. Organic impurities may therefore be responsible.

FIELD IONISATION OF RYDBERG LEVELS

One of the problems of using proportional counters as detectors is illustrated in figure 6.7, which is a finer resolution scan of the two photon ionisation of caesium vapour over the single photon continuum edge, with two different voltages on the proportional counter wire.

The external electric field from the proportional counter wire field-ionises the higher lying excited states and causes the continuum edge to appear to shift from the field free position at 318.403 nm towards longer wavelengths.

A plot of the effective quantum number, n^*, of the maximum $p_{3/2}$ level which can be resolved against the voltage applied to the wire is shown in figure 6.8, and a line of gradient -4 is drawn through the points. This $(1/n^*)4$ dependence is in agreement with the critical field strength dependence on n^* required to field ionize a particular Rydberg level. An estimate of the electric field strength in the ionisation volume of the proportional counter (around 27 mm from the counter wire), yielded a value of 20 V cm^{-1} when 540 volts were applied to the wire, and 5 V cm^{-1} when 120 volts were applied. The critical field strength of any atomic level can be estimated from the semi-empirical formula, (Letokhov 1987)

$$E_{crit}\ [\,V\ cm^{-1}] \ =\ 5 \times 10^9 \ / \ 16\ (n^*)^4$$

This gives a value of 116 V cm^{-1} for the field strength needed to ionise the 44p level and 23 V cm^{-1} for the 64p level, which are a factor of 4 greater than the estimated
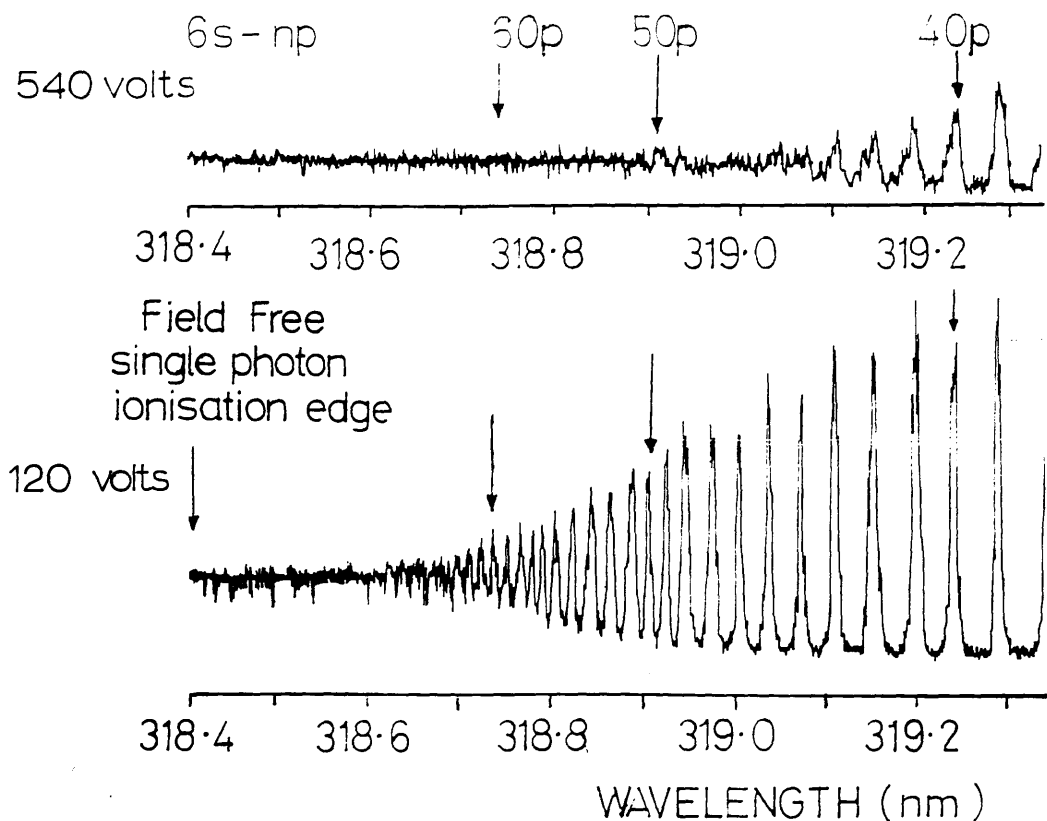
Fig 6.7   Field ionisation of highlying atomic caesium p states. As the voltage on
the proportional counter wire is increased the ionisation continuum
appears to shift towards the longer wavelengths.
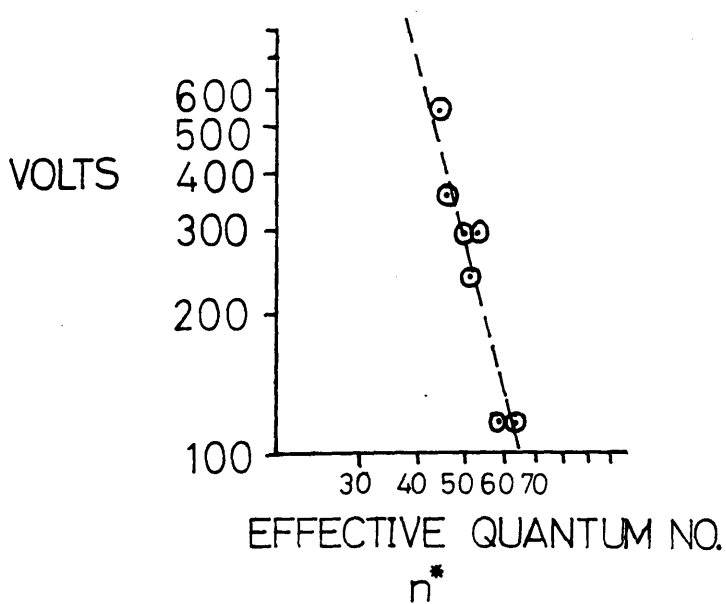
Fig 6.8   Dependence of the highest resolvable p state on the applied voltage to the
proportional counter wire.

fields produced by the counter wire. Field ionisation must therefore be only partly responsible for the ionisation of these levels.

Electric fields will also shift energy levels. Liberman et al (1979) measured a shift of ~0.6 cm^{-1} for the 33p level of rubidium in a field of 50 V cm^{-1}. The absolute wavelength of the resonant transitions could only be measured to within 5 cm^{-1} using a simple monochromator. Any shift of a magnitude much smaller than this would not be detected therefore.

There is also some evidence that the transitions are broader in the stronger electric field and this may be due to the presence of parity forbidden single photon s-s and s-d transitions, induced by the electric field. These would not be fully resolved, due to the 0.05 nm laser line-width, but their appearance would tend to broaden the s-p transitions. These parity forbidden transitions were much more evident in the two and three photon ionisation spectra of rubidium vapour.

6.4 TWO PHOTON IONISATION OF RUBIDIUM VAPOUR

By frequency doubling the Rhodamine-6-G dye, photons with wavelengths between 290 nm and 300 nm were obtained and transitions from the ground state of rubidium to Rydberg p levels were resolved. Figure 6.9 is an ionisation spectrum showing these transitions.

$$5 \, s_{1/2} \; + \; h\nu \; \longrightarrow \; n \, p_{3/2, 1/2} \qquad n > 21$$

The laser was unfocussed and in the focal volume of 1mm x 1mm x 20mm the flux was 6×10^{22} photons cm^{-2} sec^{-1}. The fine structure of these transitions was not resolved.

ATOMIC IONISATION

On the $5s_{1/2}$-$21p_{3/2}$ resonance at 299.4 nm the ionisation was found to be linear with photon flux, with some saturation taking place at the higher flux levels, figure 6.10. This linear dependence was interpreted, as in the case with caesium, as implying the saturation of the ionisation of the highly excited p levels of rubidium through collisions with the buffer gas. The linear increase in ionisation reflects the linear increase in the single photon excitation with laser flux.
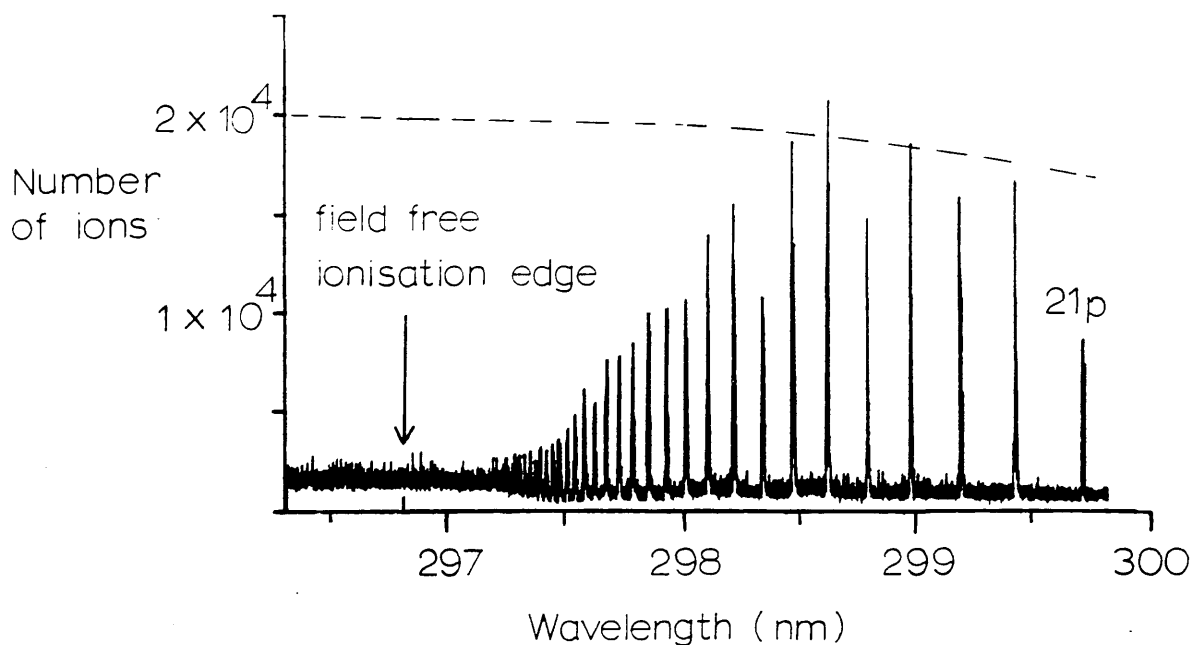
Fig 6.9 Two photon ionisation spectrum of rubidium vapour. The resonances are the single photon $5s_{1/2}$-$np_{3/2}$ transitions.
(not focussed, flux = 6×10^{22} photons cm^{-2} sec^{-1})
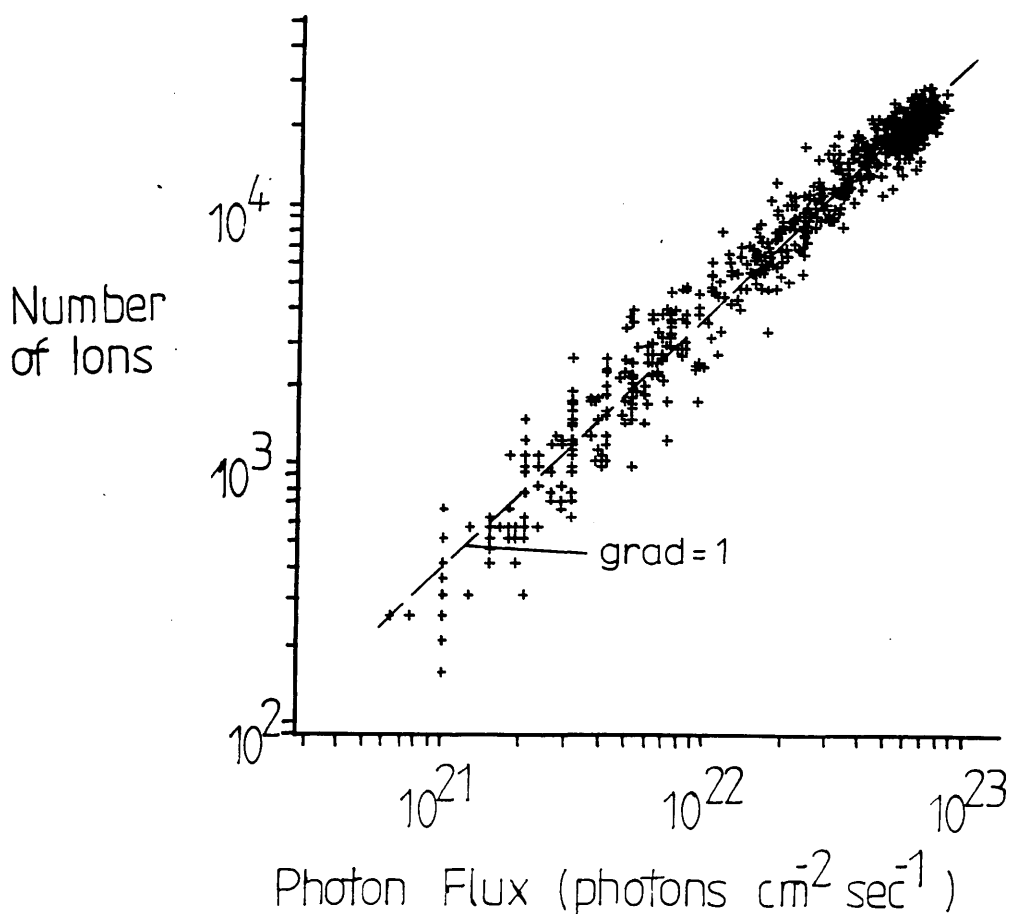
Fig 6.10 Dependence of the resonant ionisation on photon flux in rubidium vapour
(λ = 299.4 nm, $65s_{1/2}$ - $21p_{3/2}$)

Above the ionisation limit at 296 nm the ionisation is linear with photon flux and is attributed to the single photon ionisation of rubidium atoms, figure 6.11.

MOLECULAR IONISATION

The nonresonant ionisation at wavelengths longer than 296 nm, the position of the single photon ionisation edge, is expected to be dominated by the ionisation of molecular Rb_2 dimers. Off resonance at 299 nm the ionisation was found to be quadratic with flux, figure 6.12. This is a similar situation to that found in caesium vapour. The ionisation potential of Rb_2 dimers is 3.9 eV (Kappes et al 1985) and the photoionisation of these should show up as a single photon linear process. However, as with caesium, the quadratic dependence of the ionisation with laser flux can be explained by the two photon ionisation/dissociation of Rb_2 molecules, (Wagner and Isenor 1985).

The level of ionisation in figure 6.12 is approximately 30 ion pairs μJ^{-1} mm^{-2}, which is a factor of 10 greater than the background ionisation at room temperature due to impurities, as shown in figure 5.9. However, because the proportional counter was heated to 410 K in order to increase the vapour pressure of rubidium, the background ionisation from organic impurities would tend to increase as shown in figure 5.10b.

Increasing the photon flux, by focussing the laser, dramatically altered the ratio of the atomic resonant ionisation to background ionisation. This is illustrated in figure 6.13 which shows the spectral dependence of the ionisation at a flux of 4.5×10^{24} photons cm^{-2} sec^{-1}. The ionisation of organic impurities being the cause of this increase in background ionisation in the counter can be discounted by comparing figure 6.13 with an ionisation spectrum over the same wavelengths with no rubidium in the counter, figure 6.14. The ionisation spectrum due to the organic impurities rises smoothly, by a factor of 2, as the wavelength decreases, in agreement with figure 5.9. The fall in ionisation at 298 nm shown in figure 6.13 would tend to rule out organic impurities as being responsible.

The atomic transitions can just be resolved but the signal to noise ratio has decreased to around 2:1. The molecular component of the ionisation is most easily seen at wavelengths greater than 296 nm and this is shown in figure 6.15 which plots the dependence of the ionisation against the focussed photon flux at 295.5 nm. The ionisation
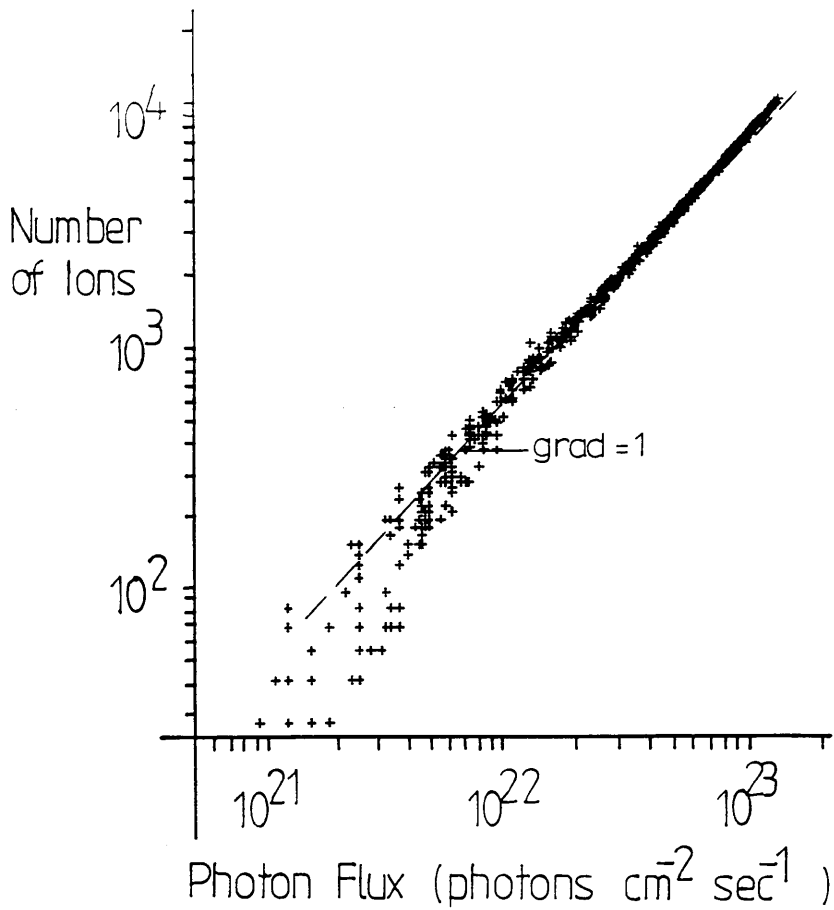
Fig 6.11 Dependence of the ionisation on photon flux in rubidium vapour
($\lambda = 296$ nm, single photon ionisation of atomic rubidium)
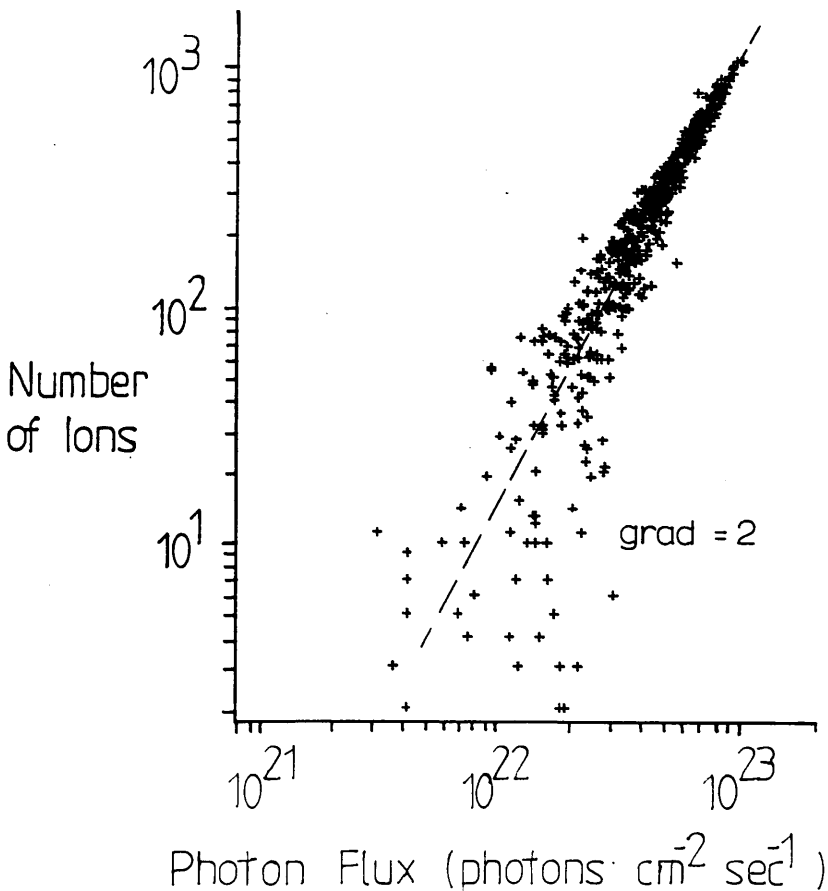
Fig 6.12 Dependence of the nonresonant ionisation on photon flux in rubidium vapour
($\lambda = 299$ nm, two photon ionisation of Rb_2)
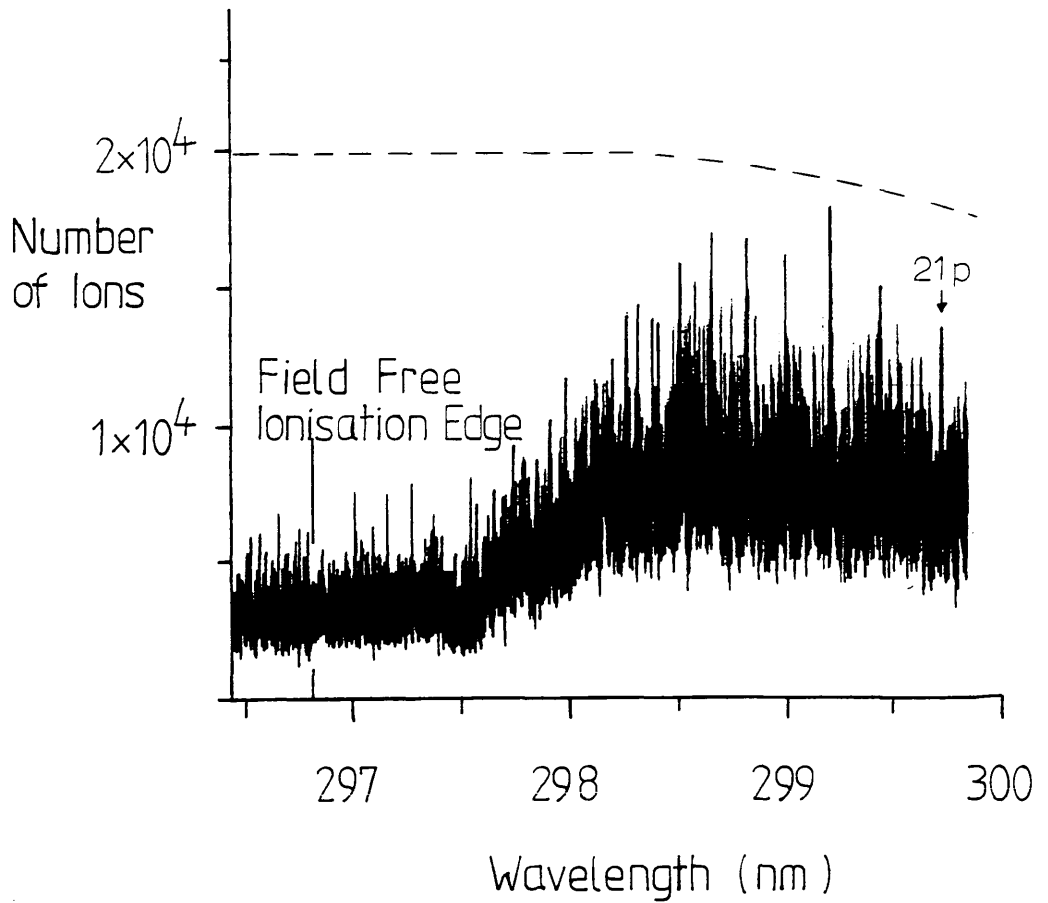
Fig 6.13 Ionisation spectrum of rubidium vapour with a focussed laser.
(focussed, flux = 4.5 x 10^{24} photons cm^{-2} sec^{-1})
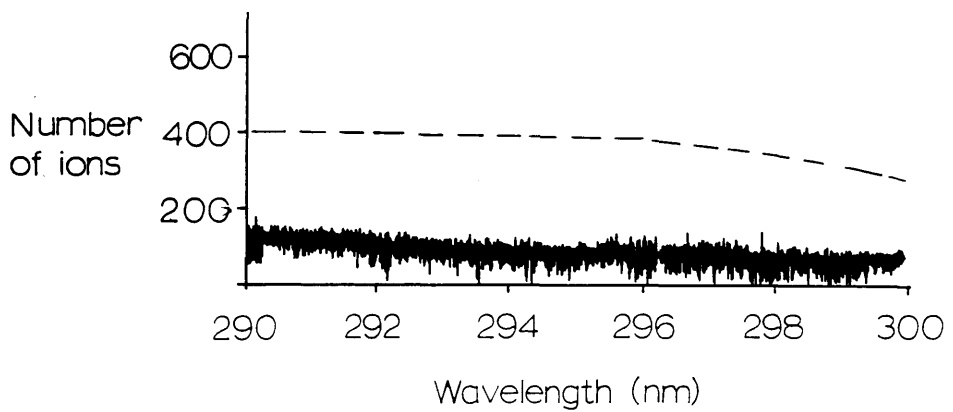
Fig 6.14 Background ionisation with no rubidium in the ionisation chamber.
(not focussed, flux = 6 x 10^{22} photons cm^{-2} sec^{-1})
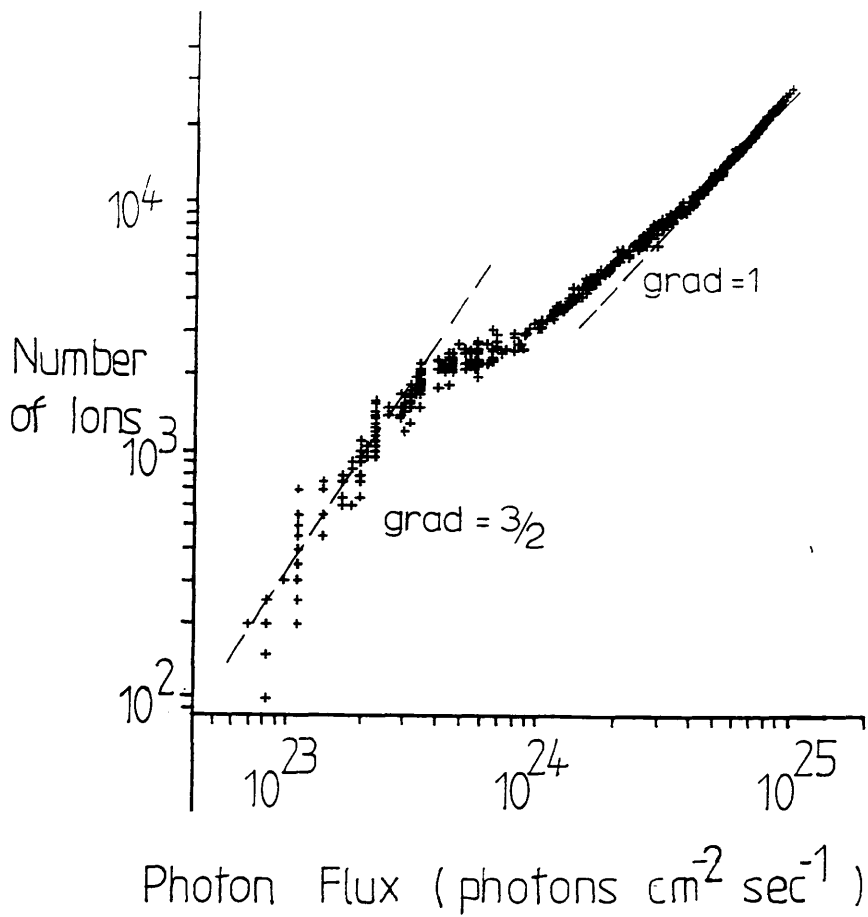
Fig 6.15 Dependence of the ionisation on focussed photon flux in rubidium vapour
(λ = 295.5 nm)
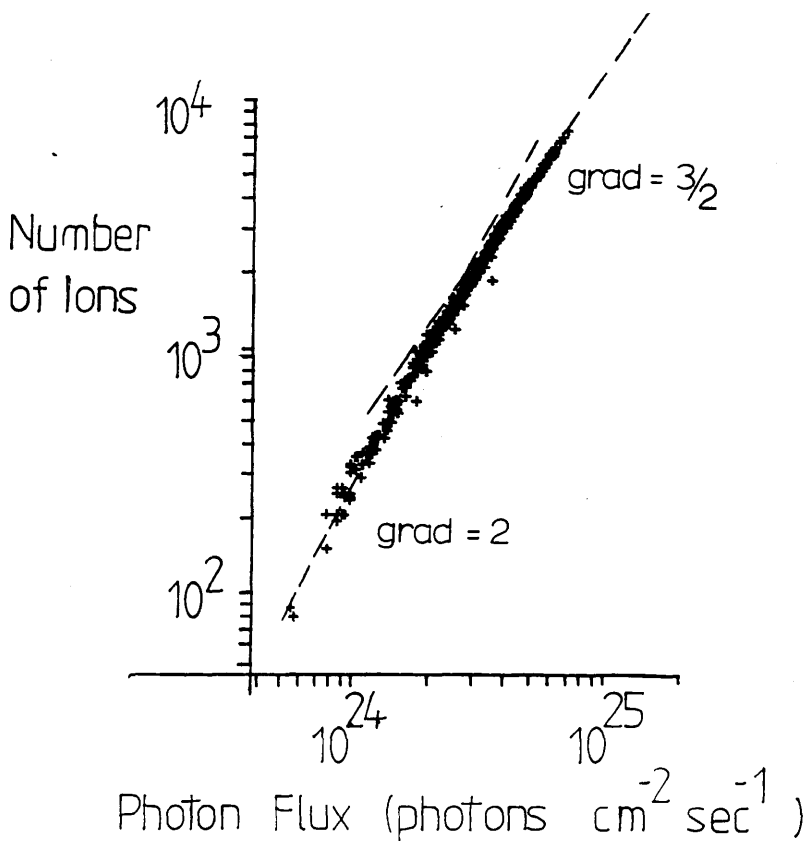
Fig 6.16 Dependence of the nonresonant ionisation on focussed photon flux in
rubidium vapour
(λ = 299 nm)

is from three sources, the resonant two photon ionisation of organic impurities, the two photon ionisation/dissociation of Rb_2 dimers and the single photon ionisation of rubidium atoms. The molecular component dominates at low flux but saturates, allowing the atomic ionisation to become dominant at high flux. The power dependence of the the molecular ionisation at 299 nm is shown in figure 6.16 the 3/2 dependence indicating saturation of the molecular ionisation.

There is some difference therefore between the two photon ionisation yields of caesium and rubidium vapour at high photon flux which could be attributed to differences in the dimer/atom ratio of the two vapours, and to the much higher density of rubidium dimers at 400 K compared to the caesium dimers at room temperature. The dimer/atom ratio for caesium vapour at room temperature is 2×10^{-5} and for rubibium vapour at 410 K $\sim 4 \times 10^{-4}$, whilst the pressure of rubidium dimers is ~6000 times greater than that of caesium dimers.

6.5 THREE PHOTON IONISATION OF CAESIUM AND RUBIDIUM VAPOUR

INTRODUCTION

The main advantages in using just one laser to multiphoton excite atoms are;

1. Straight-forward to set up. In general to observe two photon excitation the laser must simply be focussed.

2. The energy separating the two transition levels is doubled, and more states may become accessible for excitation.

3. States can be excited that are normally forbidden by electric dipole selection rules. Multiphoton excitation is thus complementary to the single photon technique and, by frequency-doubling the laser light, one can switch quickly between both processes.

4. The longer wavelengths used may also be advantageous in that the background ionisation of organic impurities, with ionisation potentials around 9 eV, becomes less likely.

The disadvantage is singular;

1. The process has a small cross-section. Typical two photon transition cross-sections, σ_T, are of the order 10^{-50} cm^4 sec^1, (Johnson and Otis 1981).

In order to observe two-photon transitions at a significant rate ($W = \sigma_T \Phi^2$), the laser photon flux Φ must be large and of the order of 10^{26} photons cm^{-2} sec^{-1}, for a laser of 10 nsec pulse length. This can normally be achieved by focussing pulsed dye lasers. However experimental complications associated with focussed lasers, such as power broadening (Hurst et al 1979a) and resonance shifts (Morellec et al 1976, Gontier et al 1978), are the inevitable results in using this technique. Its use in analytical measurements, such as trace element detection, may be limited, since large laser beam volumes are normally desired in such instruments.

THREE PHOTON IONISATION OF CAESIUM VAPOUR

ATOMIC IONISATION

Figures 6.17, 6.19 and 6.20 record the spectral dependence of ionisation from 635 nm to 660 nm. The laser was focussed with a 25 cm lens and, for figures 6.17 and 6.19, at the focal point the flux was 1.2×10^{27} photons cm^{-2} sec^{-1}, and for figure 6.20 the flux was 6×10^{26} photons cm^{-2} sec^{-1}. The fine structure of the lower d levels could be resolved (figure 6.18) which aided the assigning of the rest of the transitions (Houston et al 1988). There are two major series of sharp resonances converging to the same limit, the two photon ionisation edge which in field free conditions lies at 636.807 nm. They are both two photon absorption transitions from the ground state of caesium,

$$6 s_{1/2} + 2 h\nu \quad \text{------>} \quad n d_{5/2, 3/2} \quad n > 12$$

$$6 s_{1/2} + 2 h\nu \quad \text{------>} \quad n s_{1/2} \quad n > 13$$
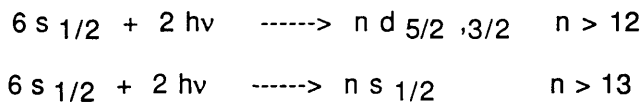
These can be resolved up to 39 s and 38 d, (figure 6.19).

The dependence of the ionisation on laser flux at the wavelength resonant with the $6s_{1/2}$-$13d_{5/2}$, is shown in figure 6.21. At the lower flux levels the ionisation is dominated by the two photon resonant ionisation of caesium dimers, which effectively masks the atomic signal, but as the laser flux increases the molecular signal saturates and the atomic ionisation increases cubically with laser flux. At the highest flux the ionisation of the atomic signal begins to saturate, and the ionisation increases with a 3/2 dependence on laser flux.

According to calculations by Pindzola (1984a) the weakness of the resonant ionisation via s states relative to the resonant ionisation via d states can be attributed in part to the difference between the photoionisation cross sections of the s and d levels. For instance he has calculated that the ratio of the ionisation cross-sections for the n=12 level (12s/12d) is equal to 0.008. Also according to calculations based on very general formula derived by Burgess and Seaton (1960) for determining photoionisation cross-sections, this ratio increases slightly with increasing quantum number, n, from 0.025 (12s/12d) to 0.031 (13s/13d) to 0.037 (14s/14d). In figures 6.17, 6.19 and 6.20 however the s/d ratios are seen to be significantly larger. For example the 15s/15d ratio is 0.25. The enhancement of the ionisation of the s levels can be
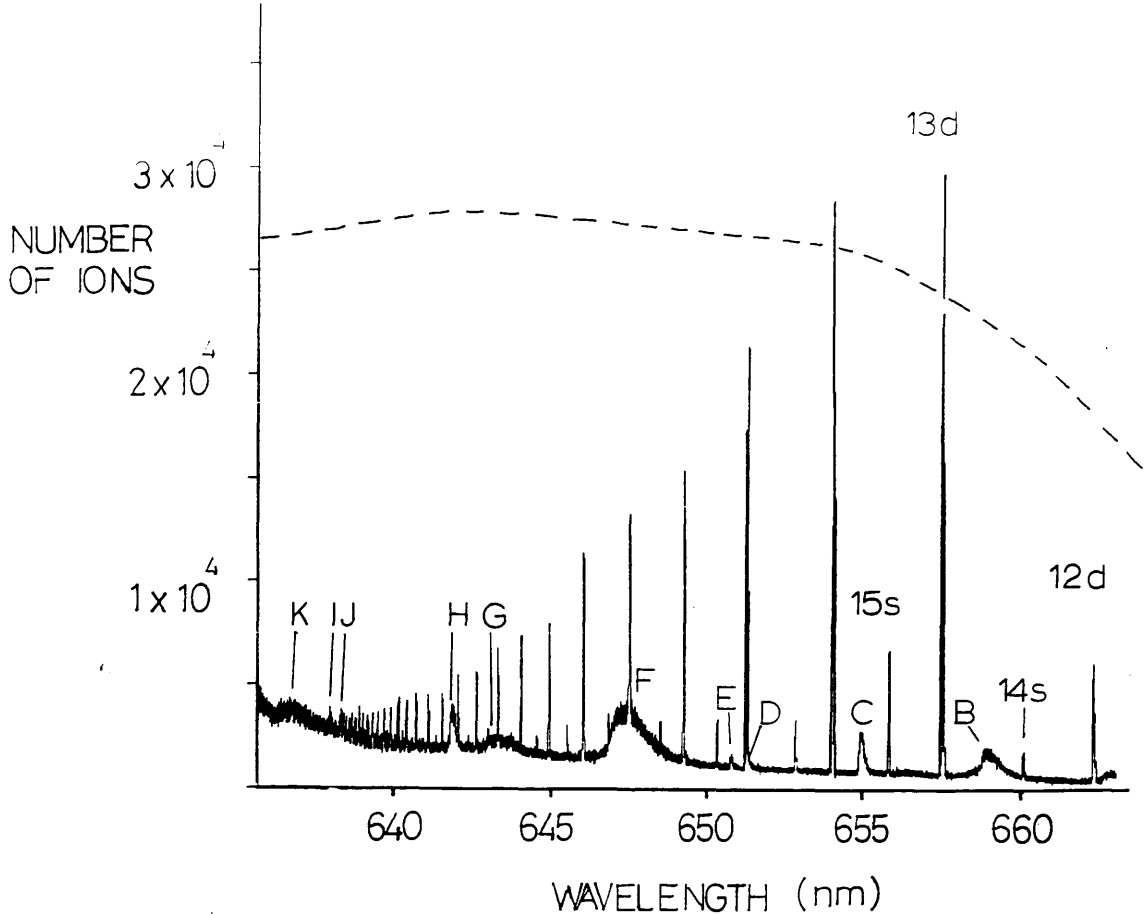
Fig 6.17 Three photon ionisation spectrum of caesium vapour. The resonances are the two photon $6s_{1/2}$-$ns_{1/2}$, $6s_{1/2}$-$nd_{5/2,3/2}$ transitions. (focussed, flux $= 6 \times 10^{26}$ photons cm^{-2} sec^{-1})
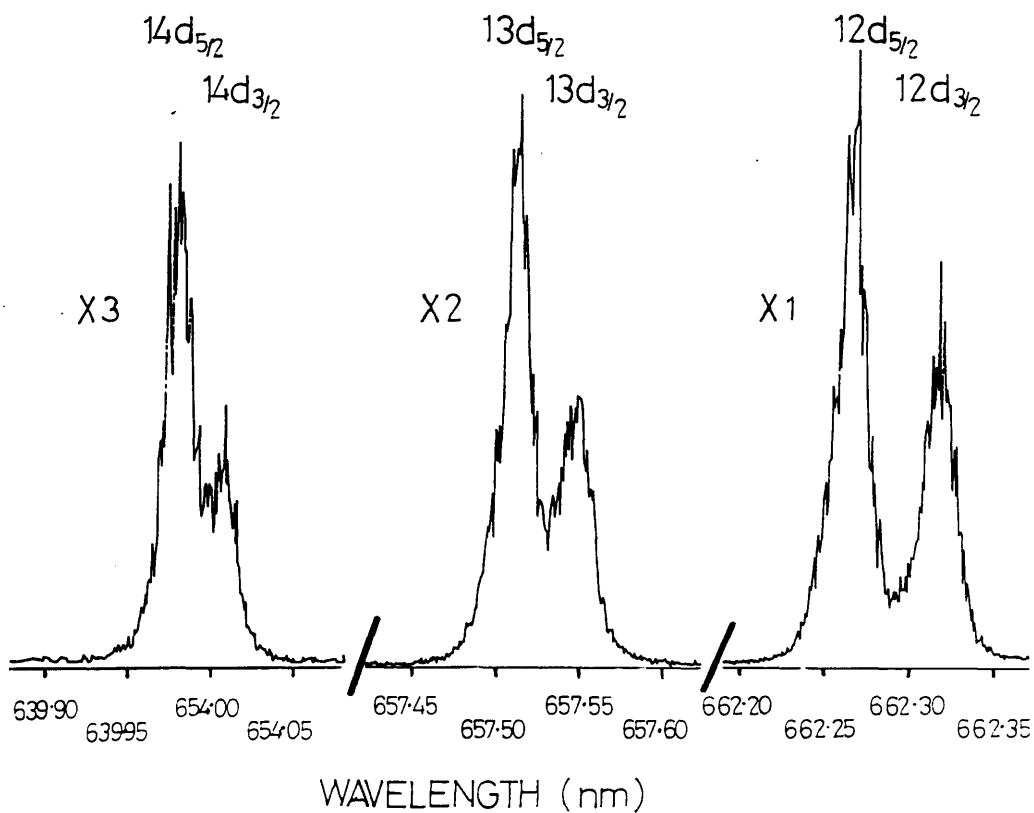
Fig 6.18 Fine structure of the lower d states in atomic caesium
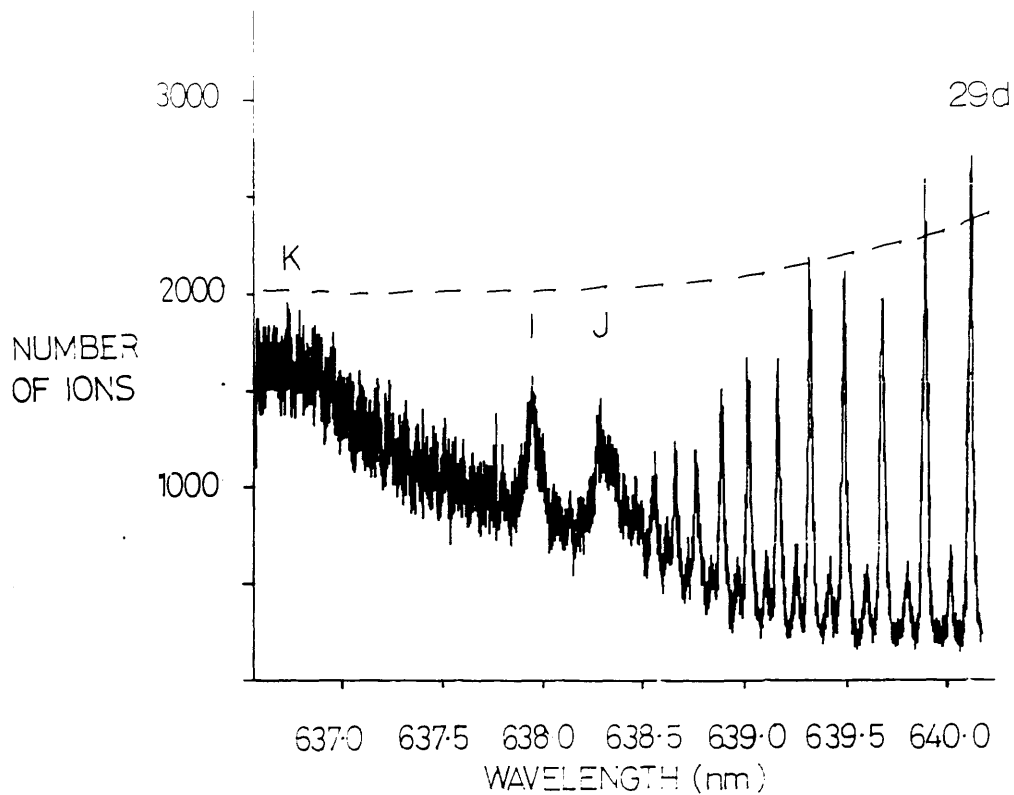
Fig 6.19 Three photon ionisation spectrum of caesium vapour over the two photon ionisation edge.
(focussed, flux = 5×10^{26} photons cm^{-2} sec^{-1})
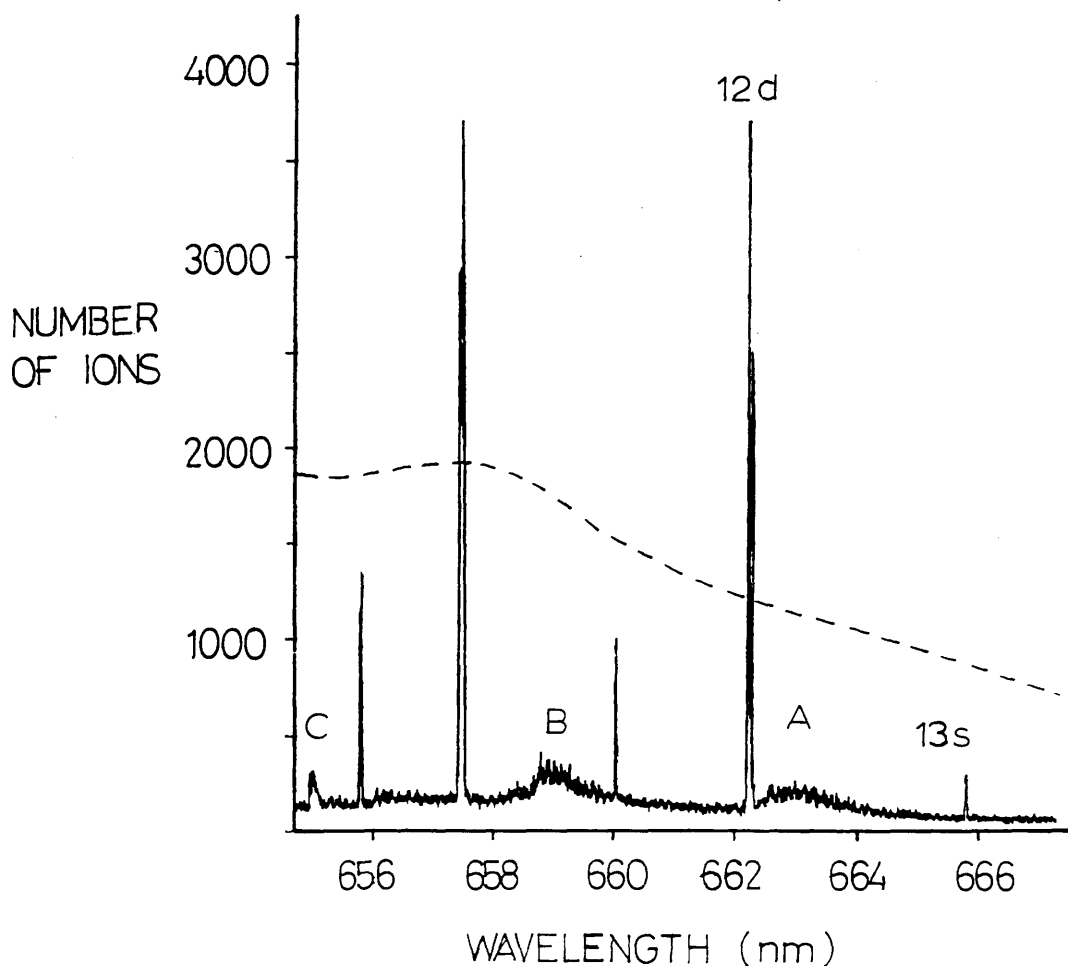
Fig 6.20 Three photon ionisation spectrum of caesium vapour.
(focussed, flux = 6×10^{26} photons cm^{-2} sec^{-1})
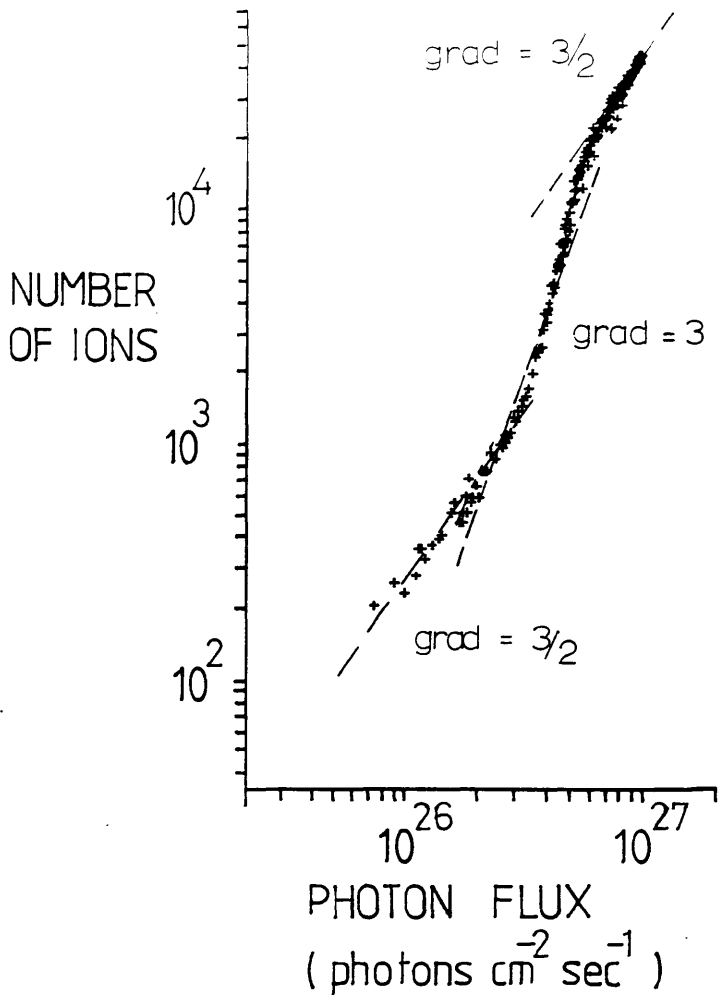
Fig 6.21   Dependence of the three photon resonant ionisation on focussed photon flux in caesium vapour
(λ = 656.7 nm, $6s_{1/2}$ - $13d_{5/2}$)
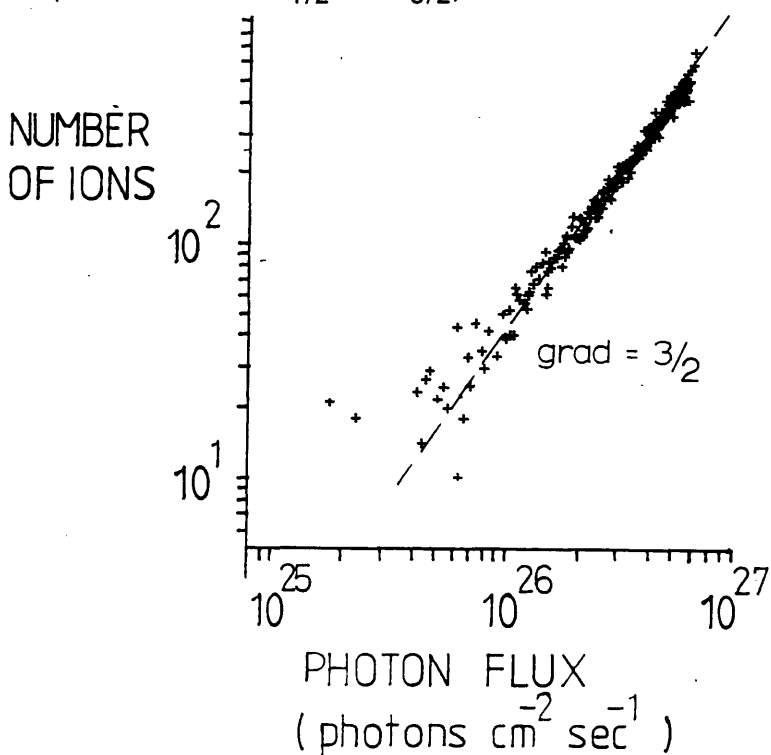
Fig 6.22   Dependence of the nonresonant ionisation on focussed photon flux in caesium vapour
(λ = 645.3 nm)

explained in terms of collisions between the excited caesium atoms and the argon atoms and methane molecules that make up the buffer gas. It is not thought that simple thermal collisions with buffer gas atoms at room temperature would directly ionise the excited state atoms, (Whitaker and Bushaw 1981). Instead these collisions are thought to transfer the caesium atoms in the excited s states (and d states) into other angular momentum states of similar energy such as np, n+1p and n-1p, which have values of photoionisation cross-sections similar to d levels. This angular momentum mixing has been observed in sodium vapour (Gallagher et al 1975) and magnesium vapour (Zhang 1986). The collisional angular mixing rate should be dependent on the pressure of the buffer gas and proportional to the geometric cross section of the excited atom. It would thus favour the most highly excited levels. A similar observation was made in the three-photon ionisation of rubidium vapour in a proportional counter. The final ionisation step would be through collisions with the buffer gas, associative ionisation through collisions between excited caesium atoms and ground state atoms, photoionisation, and field ionisation by the interaction of the excited atom with the electric field from the proportional counter wire.

MOLECULAR IONISATION

As was shown in figure 6.21 at low flux, the ionisation is dominated by the resonant ionisation of molecular dimers. This is indicated on the energy level diagram shown in figure 4.5, (Collins et al 1973).

$$X\ ^1\Sigma_g^+\ \ (Cs_2) + h\nu\ \ ---> \ C\ ^1\Pi_u\ \ (Cs_2^*)$$
$$C\ ^1\Pi_u\ \ (Cs_2^*) + h\nu\ \ ---> \ X\ ^2\Sigma_g^+\ \ (Cs_2^+)$$
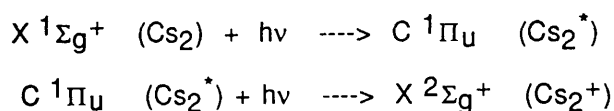
Cs_2^* represents an excited state of the molecule. The dependence of the background non-resonant ionisation at 645.3 nm is shown in figure 6.22, and a line of gradient 3/2 is drawn through the points. There should be three main contributors to this ionisation, the three photon non-resonant ionisation of atomic caesium, the two photon resonant ionisation of molecular caesium dimers, as indicated above, and photoelectrons from scattered light ionising caesium which has condensed on the surfaces in the counter. At these wavelengths the ionisation of organic impurities such as toluene would require at least 5 photons and would therefore not be important. It would be expected that at low laser flux the ionisation of the Rb_2 molecular component would dominate

93

(Morellec et al 1980). Thus the 3/2 dependence is interpreted as saturation of the two photon ionisation of molecular Cs_2, the ionisation increasing due to the increasing focal volume as the laser power increases.

QUASI-MOLECULAR STRUCTURE.

The two photon edge should resemble a step function, (Klots et al 1985), and be shifted to longer wavelengths due to the interaction of the electric field from the proportional counter wire with the caesium atoms. Oscillator strengths of absorption transitions from the ground state vary smoothly across the ionisation threshold, (Bethe and Jackiw 1986, Burgess and Seaton 1960), but an external DC electric field enables bound electrons to tunnel through the potential hill created by the interaction of the external and Coulombic fields, resulting in ionisation of the atom. External AC electric fields can mix together discreet and continuum states which may also result in ionisation, (Bayfield and Koch 1974).

However in figure 6.19 the edge is obscured by broad bands of resonant ionisation unconnected with the two main series of atomic transitions. These broad resonances, evident in all three spectra of figures 6.17, 6.19 and 6.20, were tentatively explained by Houston et al (1988) as arising from absorption and ionisation of molecular Cs_2 dimers. In fact they are atomic resonances and correspond in wavelength to single photon absorption transitions from the $5d_{5/2}$ and $5d_{3/2}$ levels to p and f levels of caesium. The excited atoms in the $5d_{5/2}$ and $5d_{3/2}$ levels arise from the photodissociation of molecular caesium as indicated in the energy level diagram, figure 6.23, (Collins et al 1981b). The Cs_2 molecule, either in a high lying vibrational level of the singlet state, $X\,^1\Sigma_g^+$, or in the shallow potential well of the dissociative triplet state, $^3\Sigma_u^+$, resonantly absorbs a single photon which excites it into either a more energetic dissociative state, $^1\Sigma_u^+$, or a highly excited bound state, $^1\Sigma_g^+$ or $C\,^1\Pi_u$.

$$Cs_2 \;+\; h\nu \;\; \text{----->} \;\; Cs_2^{**}$$
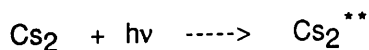
In either case the excited molecule dissociates into a ground state atom and an excited d state atom.

$$Cs_2^{**} \;\; \text{----->} \;\; Cs^*\,(5d_{5/2,3/2}) \;+\; Cs\,(6s_{1/2})$$

94

IP   314 06.71

n²S   n²P   n²D   n²F

Cs₂ — Cs_2

POTENTIAL ENERGY (cm⁻¹)

30000

25000

20000

15000

10000

5000

0

$^3\Sigma_u$

$^1\Sigma_u^+$

$5d_{5/2} + 6^2s_{1/2}$

$5^2d_{3/2} + 6\ s_{1/2}$

$6^2p_{3/2} + 6\ s_{1/2}$

$C^1\Pi_u$

$^3\Sigma_u^+$

Energetically allowed regions
for molecular transitions

$X^1\Sigma_g^+$

$^3\Sigma_u^+$

$6^2s_{1/2} + 6^2s_{1/2}$

6s

9s

8s

7s

10p
9p

8p

7p

6p

9d
8d

7d

6d

5d

6f
5f

4f

30000

25000

20000

15000

5   10   15   20

Internuclear separation (Å)
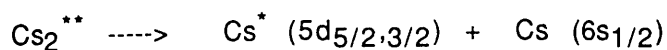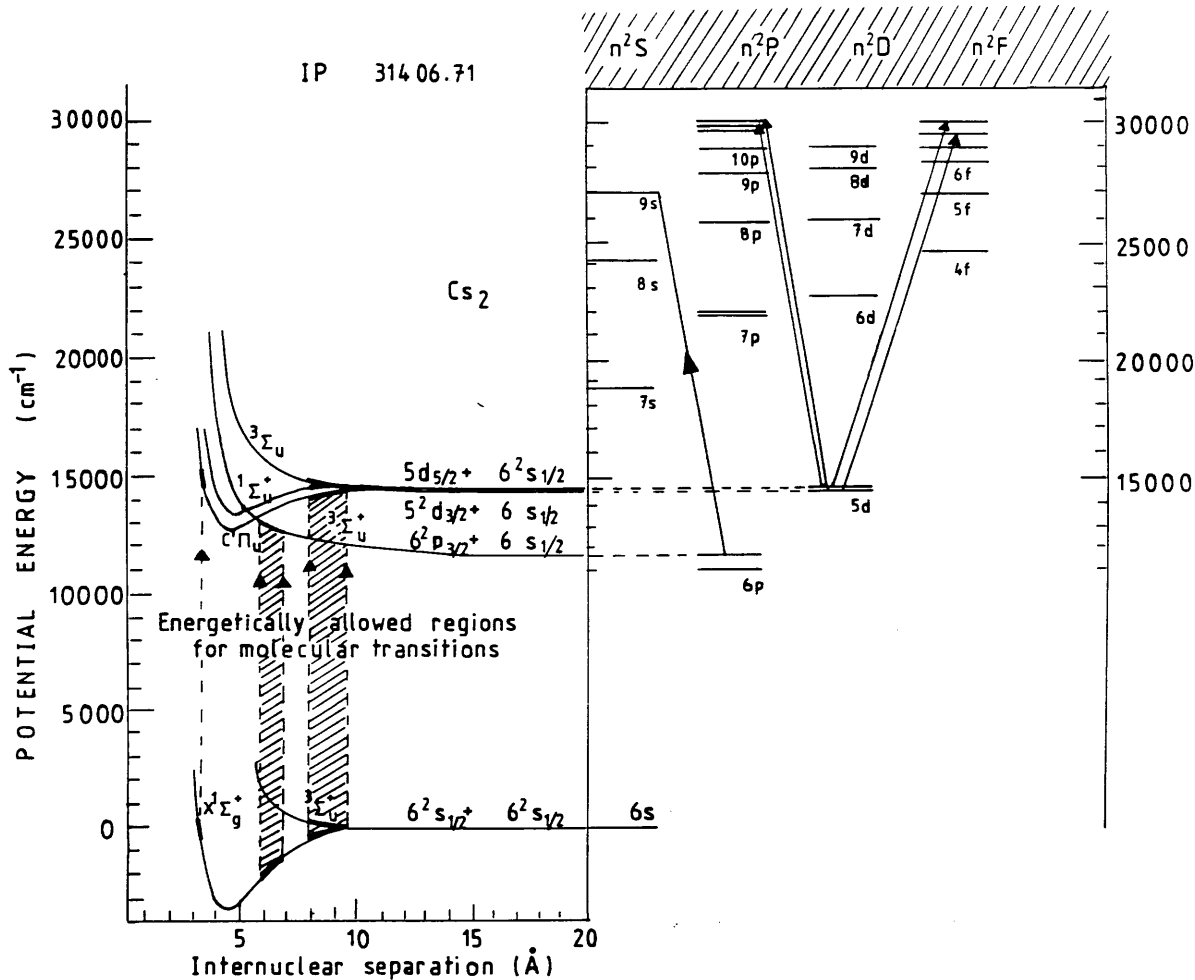
Fig 6.23   Single photon dissociation of Cs_2 molecules to $5d_{5/2}$, $5d_{3/2}$ and $6p_{1/2}$ excited state atoms at wavelengths from 630 nm to 660 nm.

The dissociation product (d state atom) then absorbs a second photon which is resonant with high lying atomic p and f levels.

$$Cs^* (5d_{5/2,3/2}) + h\nu \longrightarrow Cs^{**} (np, nf)$$
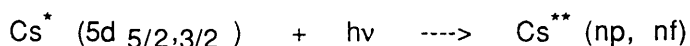
These levels are then ionised, either by photons or by some other means such as penning and associative ionisation with ground state atoms (Lee and Mahan 1965, Collins et al 1974, Mihajlov et al 1981, Duman et al 1980, Kaulakys et al 1987a,1987b), or by collisions with the buffer gas, (Whitaker and Bushaw 1981, Neimax 1983).

$$Cs^{**} (np, nf) + h\nu \longrightarrow Cs^+ + e^- \qquad \text{(photoionisation)}$$
$$Cs^{**} (np, nf) + Cs (6s) \longrightarrow Cs^+ + Cs + e^- \qquad \text{(penning ionisation)}$$
$$Cs^{**} (np, nf) + Cs (6s) \longrightarrow Cs_2^+ + e^- \qquad \text{(associative ionisation)}$$
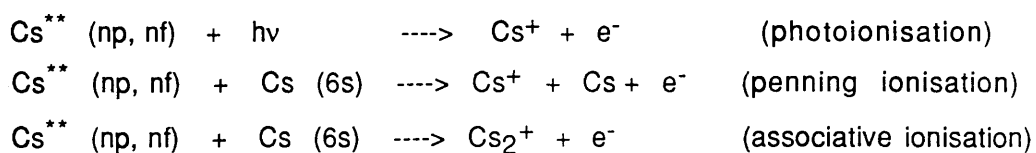
It is the resonant ionisation of the excited state atom via the intermediate p and f levels which is observed in figures 6.17, 6.19 and 6.20. This quasi-molecular ionisation effectively obscures the two photon ionisation edge at 636.866 nm, and in particular the resonant absorption transition $5d_{5/2}$ - $10f_{7/2,5/2}$ which occurs at a wavelength of 636.81nm. These transitions are labelled A to K in figures 6.17, 6.19 and 6.20, and the wavelengths of the transitions are listed in Table 6.1.

TABLE 6.1

| PEAK | TRANSITION | WAVELENGTH (nm) | | WIDTH (nm) |
		KNOWN	EXPERIMENTAL	FWHM
A	$5d_{5/2}$ - $8f_{5/2,7/2}$	663.04	663.0	1.2
B	$5d_{3/2}$ - $8f_{5/2}$	658.78	658.9	1.0
C	$5d_{5/2}$ - $12p_{3/2}$	655.00	655.0	0.2
D	$5d_{3/2}$ - $12p_{1/2}$	651.32	651.3	<0.05
E	$5d_{3/2}$ - $12p_{3/2}$	650.82	650.9	0.1
F	$5d_{5/2}$ - $9f_{5/2,7/2}$	647.44	647.4	0.6
G	$5d_{3/2}$ - $9f_{5/2}$	643.37	643.2	0.5
H	$5d_{5/2}$ - $13p_{3/2}$	641.95	642.1	0.2
I	$5d_{3/2}$ - $13p_{1/2}$	638.30	638.2	0.1
J	$5d_{3/2}$ - $13p_{3/2}$	637.96	637.9	0.1
K	$5d_{5/2}$ - $10f_{5/2,7/2}$	636.73	636.6	>1.0

The most surprising feature of these quasi-molecular broad transitions is their strength relative to the atomic signal given that the ratio of caesium molecules to atoms at room temperature is approximately 2×10^{-5}. We were not able to distinguish Cs^+ ions from Cs_2^+ ions and therefore the contribution of the ionisation of Cs_2 molecules could not be determined.

The widths of these quasi-molecular transitions (FWHM) vary from 0.1 nm ($5d_{3/2}$-$13p_{3/2}$) to 1.2 nm ($5d_{3/2}$-$8f_{5/2}$), while for comparison the purely atomic transitions have widths of around 0.02 nm, as shown in figure 6.18. Part of this increased width could be accounted for by a fast dissociation of the excited Cs_2 molecule which would tend to blur the energy levels of the excited 5d atom. However the width is dependent to a much greater extent on the particular atomic transition from the 5d level, transitions to f states being considerably broader than those to p states, (Table 6.1). One explanation of this phenomenon is that the f states and those with higher angular momenta are near degenerate and are mixed together either by the external electric field of the proportional counter wire or by collisions with buffer gas atoms. The energy difference between the $8f_{5/2}$ level and the $8g_{7/2}$ level is $\sim$10.4 cm^{-1}, and this is reduced to 5.5 cm^{-1} for the energy difference between the $10f_{5/2}$ and $10g_{7/2}$ levels, (Weber and Sansonetti 1985). However the purely atomic excitation and ionisation of the s and d levels can be resolved up to 39d and 34s. If the mixing of near degenerate states was causing the broadening of the quasimolecular transitions, it should also broaden the atomic transitions to high lying s and d levels, which are also separated by $\sim$10 cm^{-1}. No satisfactory explanation for this preferential broadening has been formulated yet.

Three photon ionisation spectra of rubidium vapour were also obtained in a proportional counter, and an example of this, at a flux of 2.5×10^{26} photons cm^{-2} sec^{-1}, is shown in figure 6.24.

ATOMIC IONISATION

As with the three photon ionisation spectrum of caesium there are two main series of atomic transitions which, in field free conditions, converge to the same limit, the two photon ionisation edge at 593.6 nm.

$$5\, s_{1/2} + 2\, h\nu \quad \text{---->} \quad n\, s_{1/2} \qquad n > 20$$

$$5\, s_{1/2} + 2\, h\nu \quad \text{---->} \quad n\, d_{5/2\,,\,3/2} \qquad n > 19$$
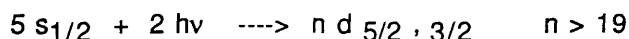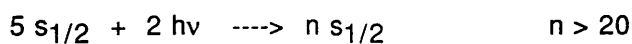
The fine structure of the lowest d levels could not be resolved.

The dependence on laser flux of the resonant ionisation for the transition $5s_{1/2}\text{-}20d_{5/2}$ is shown in figure 6.26 and that for the transition $5s_{1/2}\text{-}28s_{1/2}$ is shown in figure 6.25. The s-d transition shows a cubic dependence at low flux, changing to a quadratic dependence at higher flux as the ionisation step becomes saturated, through collisional enhancement with buffer gas atoms and/or ground state caesium atoms. The s-s transition shows a somewhat different dependence. At a low flux it is quadratically dependent but changes to a 3/2 dependence at a higher flux. Thus direct photoionisation, which should show up as a cubic dependence, does not seem to contribute significantly to the total ionisation yield for the s state at these flux levels, whilst for the d states only at the lowest fluxes is it significant.

In analogy with the s states of caesium, the s states of rubidium are thought to have small photoionization cross-sections relative to the d states. Therefore the relatively large s/d ratios of figure 6.24, which are of similar magnitude to those of caesium (figure 6.17), are also thought to arise from the collisional enhancement of the ionisation of the s states.

The power dependence of the ionisation above the two photon limit, at a wavelength of 591 nm, is shown in figure 6.27. The ionisation is quadratically dependent on laser
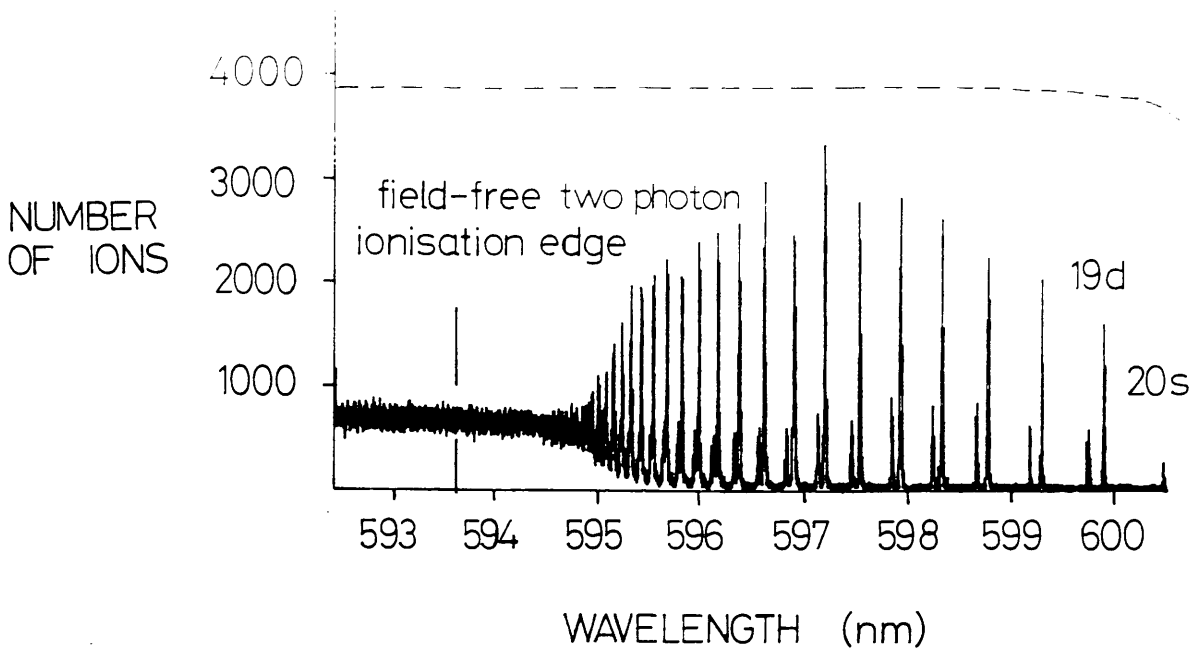
Fig 6.24 Three photon ionisation spectrum of rubidium vapour. The resonances are the two photon $5s_{1/2}-ns_{1/2}$, $5s_{1/2}-nd_{5/2,3/2}$ transitions. (focussed, flux = 2.5×10^{26} photons cm^{-2} sec^{-1})

PHOTON FLUX (photons cm^{-2} sec^{-1})
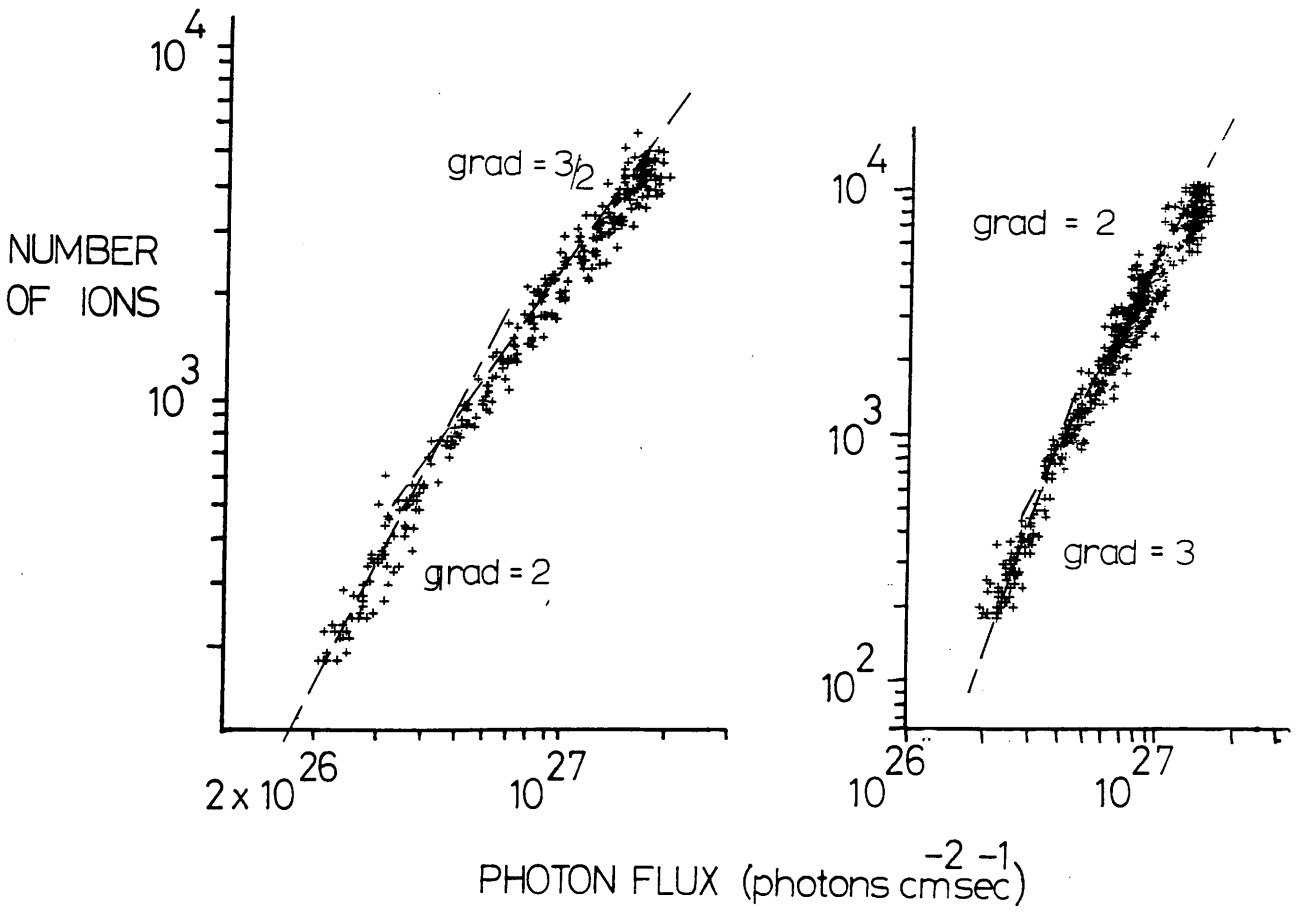
Fig 6.25 Dependence of the three photon resonant ionisation on focussed photon flux in rubidium vapour
(λ = 596.7 nm, $5s_{1/2}$ - $28s_{1/2}$)

Fig 6.26 Dependence of the three photon resonant ionisation on focussed photon flux in rubidium vapour
(λ = 599.4 nm, $5s_{1/2}$ - $20d_{5/2}$)
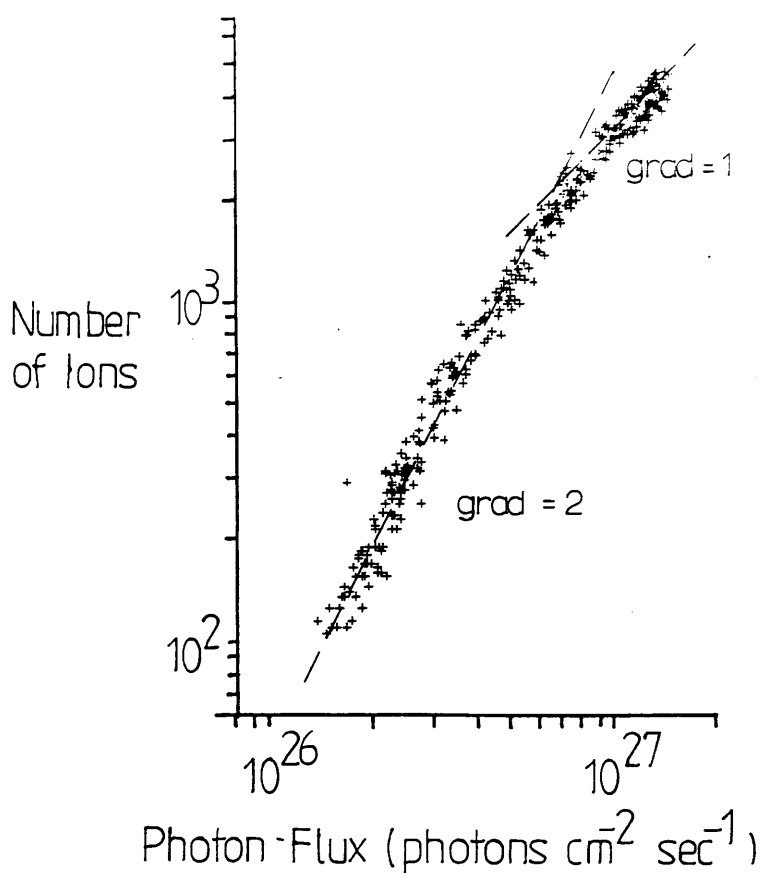
Fig 6.27 Dependence of the nonresonant ionisation on focussed photon flux in rubidium vapour
(λ = 591 nm, Two photon ionisation of atomic rubidium)
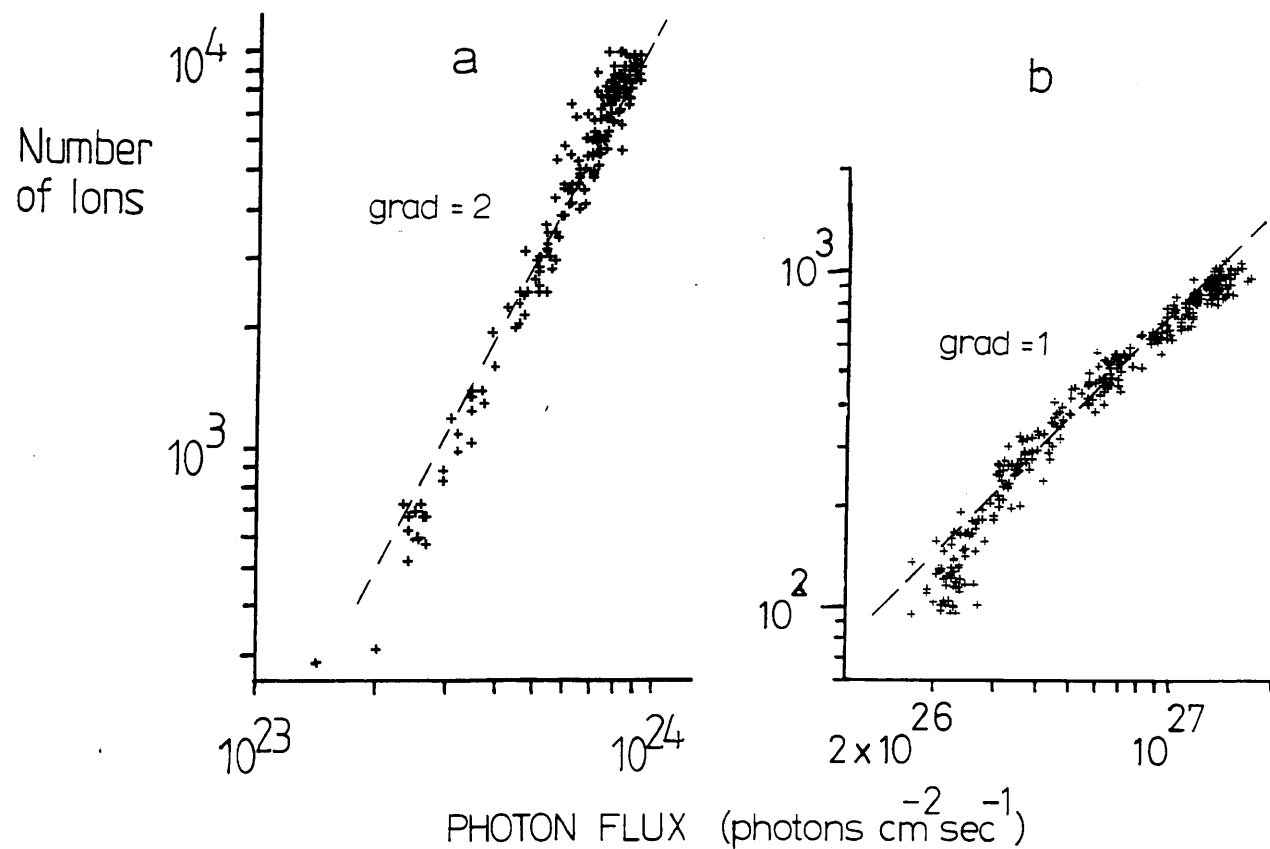
Fig 6.28 Dependence of the nonresonant ionisation on photon flux in rubidium vapour
a) not focussed
b) focussed
(λ = 599 nm, two photon ionisation of Rb_2 molecules)

flux at low powers and begins to saturate at high powers. This can be accounted for by the two photon nonresonant ionisation of Rb atoms, although at the lower flux the molecular ionisation would be a large component of the signal.

MOLECULAR IONISATION

The dependence of the nonresonant ionisation below the two photon ionisation limit with a focussed laser at 599 nm is shown in figure 6.28b. It changes from greater than linear at low flux to linear at high flux and is attributed to the saturation of molecular Rb_2 ionisation. Rubidium dimers have an absorption band centred around 690 nm resulting from transitions from ground state molecules to B state molecules, (Gupta et al 1978).

$$X \ {}^1\Sigma_g^+ \ + \ h\nu \ \longrightarrow \ B \ {}^1\Pi_u \ \ (Rb_2^*)$$
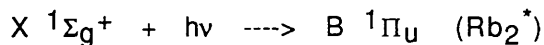
These excited molecules are then photoionised to the ground state of the molecular ion.

$$B \ {}^1\Pi_u \ + \ h\nu \ \longrightarrow \ X \ {}^2\Sigma_g^+ \ \ (Rb_2^+)$$
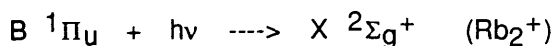
The photoionization of Rb_2 molecules would therefore be a resonant two photon process, and this can be seen in figure 6.28a, which plots the quadratic dependence of the nonresonant ionisation at a lower flux in an unfocussed beam.

QUASI-MOLECULAR IONISATION

There is no evidence for any quasi-molecular structure in this spectrum with the result that the two photon ionisation edge can be distinguished. At these wavelengths the dissociative ground state of the Rb_2 molecule, ${}^3\Sigma_u^+$, may absorb photons in the transition,

$$Rb_2 \ ({}^3\Sigma_u^+) \ + \ h\nu \ \longrightarrow \ Rb_2^{**} \ (O_g^+)$$
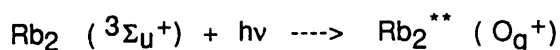
This state predissociates to give a ground state atom and an excited $5p_{3/2}$ atom, figure 6.29, (Collins et al 1976):

$$Rb_2^{**} \ (O_g^+) \ \longrightarrow \ Rb \ (5\ s_{1/2}) \ + \ Rb^* \ (5\ p_{3/2})$$
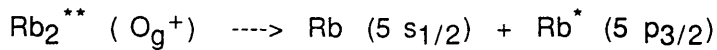
At the wavelengths in use in figure 6.24 (590 nm - 600 nm), there are no transitions from the $5p_{3/2}$ level that are resonant with s and d levels, with the result that no broad ionisation resonances equivalent to those in caesium are seen.

PARITY FORBIDDEN ELECTRIC DIPOLE TRANSITIONS

Also evident in figure 6.24 are parity forbidden two photon 5s - np transitions. They can just be resolved at n = 28 and, with increasing intensity, continue up to n = 48 (figure 6.30). These may be induced either by collisions with the buffer gas and/or by the external electric field from the proportional counter wire. The intensity of the s-p transitions compared to the s-s and s-d transitions increases rapidly with n^*, the effective quantum number. Compton et al (1984b) reported a $(n^*)^{10}$ dependence for the ratio between the ionisation probabilities (s-p/s-d) of atomic caesium, as the result of an applied external DC electric field.

Similar parity forbidden transitions were observed in the two photon ionisation of rubidium and were found to be dependent on the voltage applied to the proportional counter wire. When the voltage on the wire was reduced from 540 volts to 120 volts the single photon parity forbidden s-d transitions disappeared (figure 6.31).

This lends weight to the electric field also being the principle cause of the parity forbidden two photon s-p transitions shown in figure 8. The external electric field is thus mixing near degenerate levels together of different angular momenta. The normal parity selection rules then break down and s-s , s-p, s-d and s-f transitions should all be possible. As the levels become more degenerate, i.e. the higher the degree of excitation, the greater is the degree of mixing and the more pronounced the forbidden transitions.
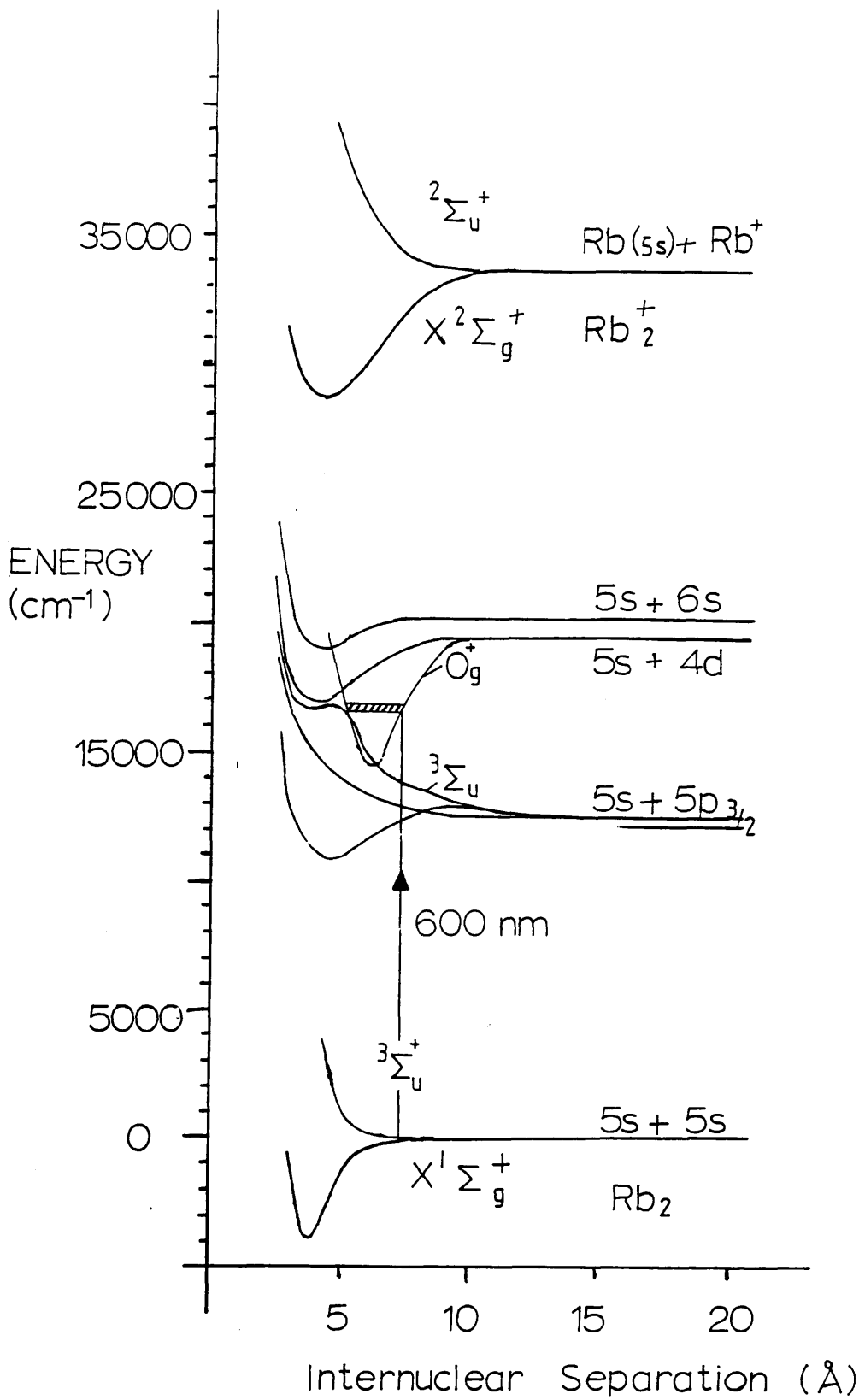
Fig 6.29 Pre-dissociation of Rb_2 molecules at wavelengths around 600 nm. The 0_g^+ state pre-dissociates to give a ground state atom and an excited $5p_{3/2}$ atom.

Fig 6.30   Three photon ionisation spectrum of rubidium vapour across the two photon ionisation edge. Parity forbidden two photon s-p transitions become increasingly evident at the shorter wavelengths, up to 5s-48p.

Fig 6.31   The dependence of the parity forbidden transitions in atomic rubidium on the external field from the voltage applied to the proportional counter wire. The one photon s-d transitions are evident up to 5s-47d. With a lower voltage applied to the wire the s-d transitions are not as evident.

6.7 DEPENDENCE OF THE IONISATION ON EFFECTIVE QUANTUM NUMBER IN PROPORTIONAL COUNTERS

It has been argued that resonant photoionisation via an intermediate state should fall with increasing effective quantum number of that state, n^*, at an approximate rate of $(1/n^*)^8$, this being the sum of the excitation dependence $(1/n^*)^3$ from the ground state to the intermediate state, and the photoionisation dependence $(1/n^*)^5$ from the intermediate state to the continuum. Compton et al (1984b) showed this dependence in the three photon ionisation of atomic caesium.

An attempt to study this dependence in the proportional counter was unsuccessful due to the small signal to noise ratio. The buffer gas was removed from the chamber and the residual pressure reduced to 2×10^{-5} torr to reduce collisional ionisation. At this pressure the detector operates as an ionisation chamber with no gas amplification. Figure 6.32 illustrates an ionisation spectrum, taken in this mode, of the two photon ionisation of rubidium atoms via the $5s_{1/2}$-np transitions, with a laser flux of 2.5×10^{22} photons cm^{-2} sec^{-1}. The resonant ionisation is only about twice the background level. An estimate of the expected resonant two photon ionisation yield via the $5s_{1/2}$-$21p_{3/2}$ transition can be made from the simple population rate equation model. The spontaneous decay rate A_{12} for the $21p_{3/2}$ level is 1.6×10^3 sec^{-1} (extrapolated with a $(n^*)^{-3}$ dependence from the known spontaneous transition rate for the $16p_{3/2}$ level (Weise and Martin 1980) and, assuming a laser bandwidth Δv_L of $\sim 10^{11}$ Hz, the cross-section for the $5s_{1/2}$-$21p_{3/2}$ transition, σ_{exc}, from equation 1 is equal to $\sim 1 \times 10^{-18}$ cm^2. The photoionisation cross-section, σ_{ion}, for the $21p_{3/2}$ level was estimated at 4×10^{-22} cm^2, by extrapolating with a $(n^*)^{-5}$ dependence (Sobelman 1979) from the calculated photoionisation cross-section of the $6p_{3/2}$ state (Ambartsumyan et al 1976). With a photon flux of 2.5×10^{22} photons cm^{-2} sec^{-1} the excitation step is not expected to be saturated and, with a pulse length τ much shorter than the spontaneous decay rate A_{12}, the ion yield N_i is equal to,

$$N_i = (N_0(0)\ \sigma_{exc}\ \sigma_{ion}\Phi^2\ \tau^2)/2$$

where $N_0(0) = 2.8 \times 10^{11}$ is the (maximum) number of ground state atoms in the unfocussed laser beam volume at time $t=0$, and Φ is the photon flux. The ion yield from these estimated figures is of the order 10, implying that the resonant photoionisation of

101
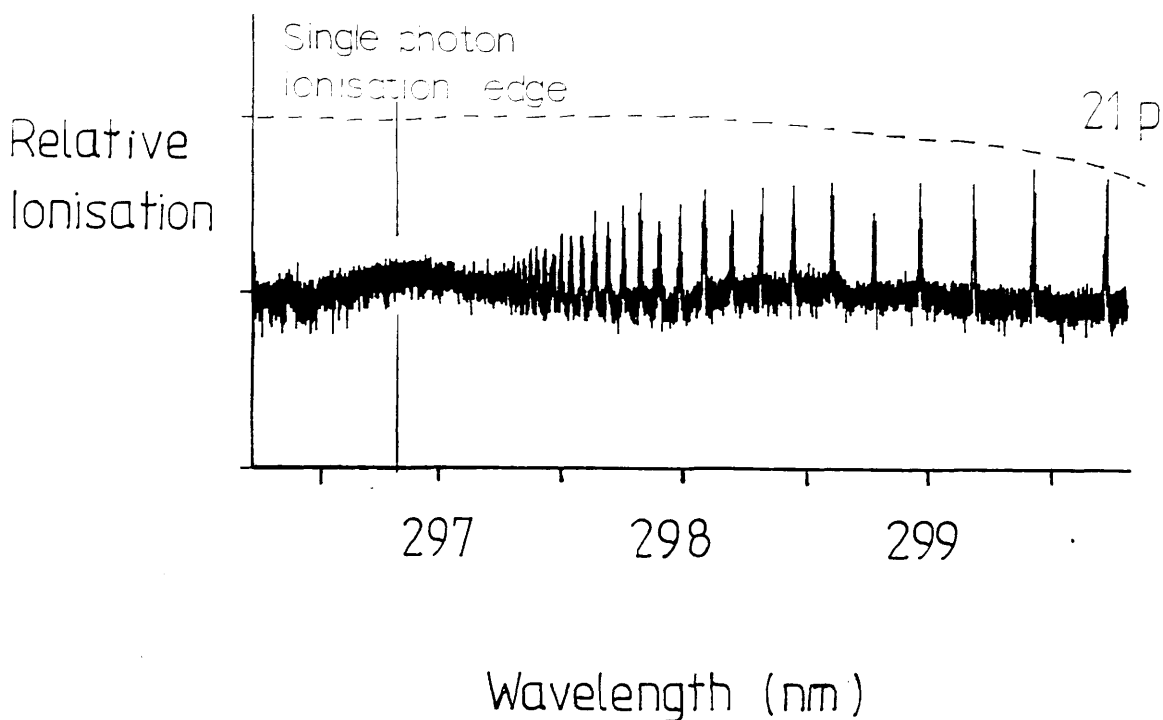
Fig 6.32 Two photon ionisation spectrum of rubidium vapour in proportional counter operated with no buffer gas. The resonances are the single photon $5s_{1/2}$-$np_{3/2}$ transitions.
(not focussed, flux = 2.5×10^{22} photons cm^{-2} sec^{-1})
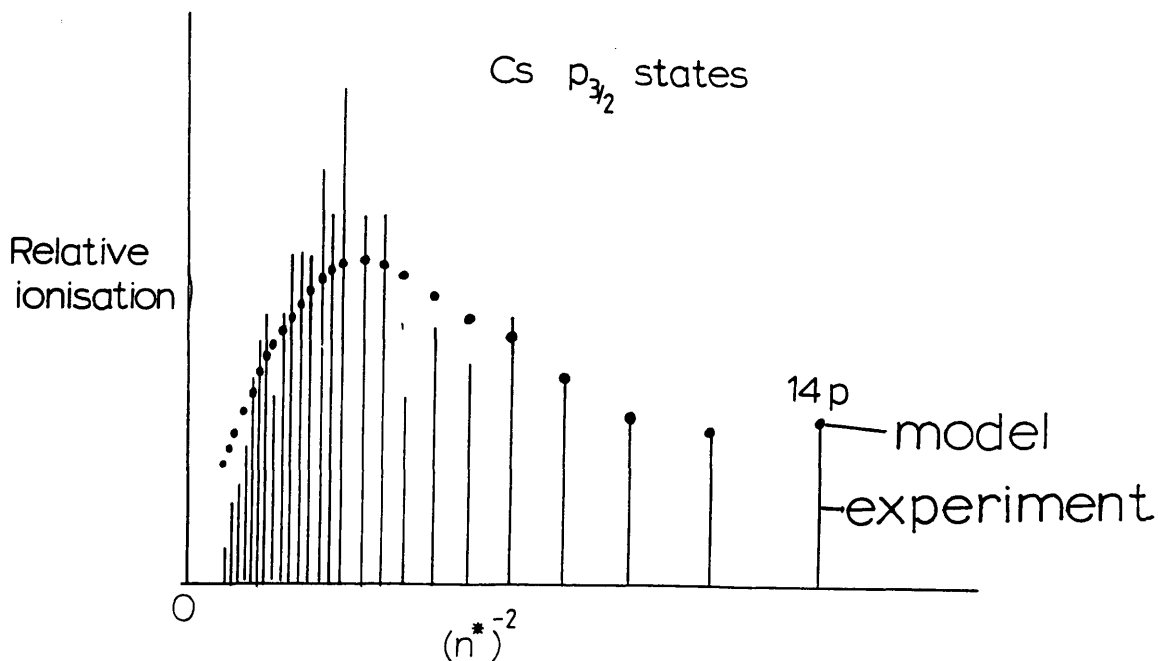
Fig 6.33 Modelling of the collisional enhancement of the two photon ionisation of atomic caesium in a proportional counter

$$I_n = \alpha/(n^*)^8 + \beta \ \exp\text{-}(\gamma/(n^*)^2)/(n^*)^3$$

$$\alpha = 2.5 \times 10^3, \ \beta = 3.4 \times 10^6, \ \gamma = 559$$

these states is small and would be difficult to detect in an ionisation counter. However from figure 1 an estimate of the number of resonant electrons detected can be made from simple electrostatic theory. With no buffer gas in the counter there is no amplification of the initial ionisation amplification. The detected signal is the initial resonant signal. Estimating the capacitance of the detector as ~100 pF, and with an amplified signal (x1500) of ~80 mV, the number of electrons incident on the wire is ~3 x 10^4. These calculations imply that photoionisation is not the main cause of the resonant ionisation in figure 6.32, and this is bourne out by the dependence of the ionisation on the effective quantum number, which does not fall at the expected $(n^*)^{-8}$ rate. The actual mechanism of the ionisation in this spectrum has not yet been determined.

COLLISIONAL IONISATION OF HIGHLY EXCITED LEVELS

Neimax (1983) has shown that highly excited rubidium atoms (n > 25) in a thermionic diode, operated with a rare gas buffer at a pressure of 12 torr, will be collisionally ionised with almost unit probability. In a proportional counter, operated at 30 torr pressure, collisional ionisation will also dominate the ionisation of highly excited atoms. A suitable model of this would require the ionisation I_n of the photoexcited level n to be the sum of photoionisation, which dominates at low values of n, and collisional ionisation, which dominates at high n. A simple model would be that collisions between buffer gas atoms travelling at thermal velocities and Rydberg atoms induces ionisation. A suitable function describing this is $\exp-(E_n/kT)$, where $E_n = R_H/(n^*)^2$ is the energy of the Rydberg level n, and R_H is the Rydberg energy. For $E_n \gg kT$ ie. for levels far from the continuum, the exponential tends to zero, and for $E_n < kT$ the exponential tends to unity. The ion yield I_n is then given by,

$$I_n = \alpha/(n^*)^8 + \beta \, \exp-(\gamma/(n^*)^2)/(n^*)^3$$

where α, β and γ are constants. The first term is proportional to the photoionisation probability ans the second term is proportional to the collisional ionisation probability. This function was fitted to the experimental data for the ionisation of caesium and rubidium in proportional counters, using a least squares fit routine that minimised the χ^2 function. This routine returned values of α, β and γ at the minimum. An example of the fitted function is illustrated in figure 6.33, along with values of α, β and γ. An

effective temperature of 280 +/- 15 K was obtained from $\gamma = R_H/kT$, as expected. The fitting was found to be fairly insensitive to the photoionisation term, $\alpha/(n^*)^8$, due to a lack of data at low n where photoionisation would tend to dominate.

In an effort to improve the fit at high values of n the function was altered slightly, allowing the ionisation to fall at high values of n as $(n^*)^\kappa$.

$$I_n = \alpha/(n^*)^8 + \beta \ \exp\text{-}(\gamma/(n^*)^2)/(n^*)^\kappa$$

Examples of fitted data are shown in figures 6.34a, 6.34b, 6.35 and 6.36. In all cases the effective temperature has dropped to around 150 K and the value of κ is around 5.5. These results are not as expected and are also at variance with those reported by Neimax (1983). The main difference lies in the rate at which the ionisation falls, at those levels where the collisional ionisation probability is expected to be unity. In this region the limiting factor should be the rate of excitation which falls at a rate $(n^*)^{-3}$. However all of the ionisation spectra of caesium or rubidium showed a fall in this region of approximately $(n^*)^{-5.5}$. The low effective temperature is a defect of the thermal model, as used here, which underestimates the degree of collisional ionisation. At n = 25 at 30 torr buffer gas pressure the collisional ionisation probability is unity, (Neimax 1983), whereas the thermal model suggests a probability of ~0.4.

COLLISIONAL ENHANCEMENT OF PHOTOIONISATION

It has been suggested that use could be made of collisional ionisation to enhance, by up to two orders of magnitude, the photoionisation yield from selected Rydberg levels, (Whitaker et al 1981). The photoionisation cross section of Rydberg levels is very small and deceases rapidly the closer the level lies to the continuum. To saturate the photoionisation requires a high flux, which is in general much larger than that required to saturate the excitation step to the Rydberg level. The collisional ionisation of Rydberg levels has been shown to be very efficient however, and may be used in place of photoionisation, lowering the flux needed to saturate the resonant ionisation process.

An estimate of the degree of enhancement possible can be made by comparing the ion yields from the n=14 and n=24 levels in the two photon ionisation spectrum of caesium shown in figure 6.1. Assuming the validity of the $(1/n^*)^8$ dependence for the photoionisation yield, it can be seen that the ionisation of the 24p state has been
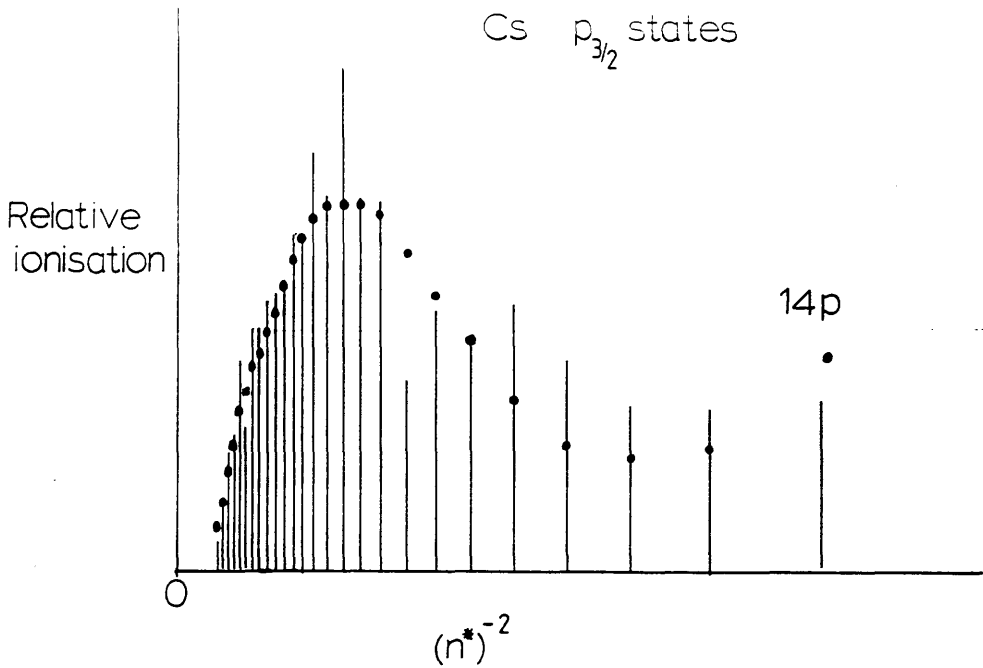
Fig 6.34a Modelling of the collisional enhancement of the two photon ionisation of atomic caesium in a proportional counter

$$I_n = \alpha/(n^*)^8 + \beta \; \exp{-(\gamma/(n^*)^2)}/(n^*)^\kappa$$

$$\alpha = 1.5 \; \times 10^7, \; \beta = 6.5 \; \times 10^6, \; \gamma = 1100, \; \kappa = 5.4$$
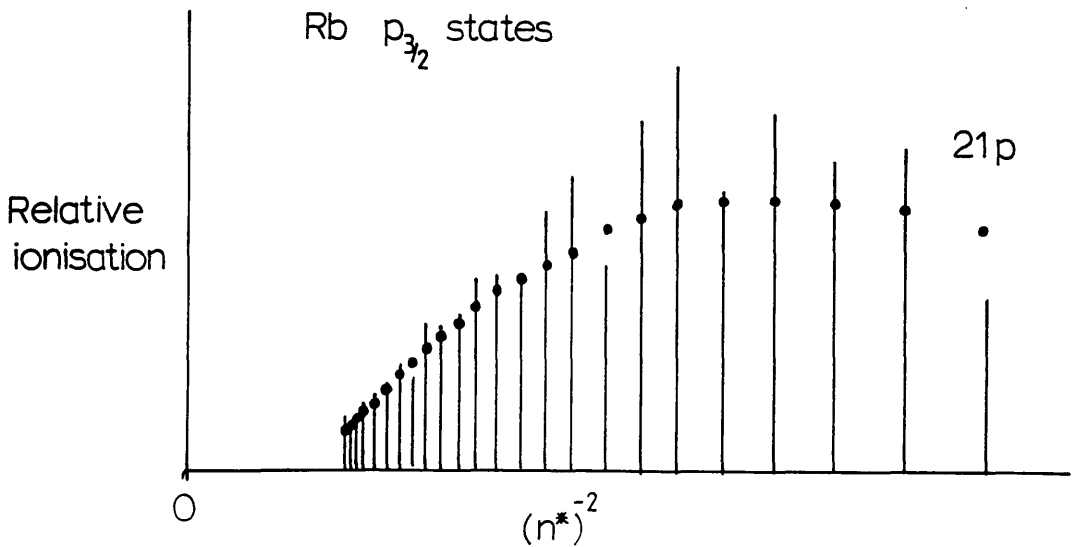
Fig 6.34b Modelling of the collisional enhancement of the two photon ionisation of atomic rubidium in a proportional counter

$$I_n = \alpha/(n^*)^8 + \beta \; \exp{-(\gamma/(n^*)^2)}/(n^*)^\kappa$$

$$\alpha = 1.5 \; \times 10^7, \; \beta = 6.9 \; \times 10^6, \; \gamma = 1200, \; \kappa = 5.5$$
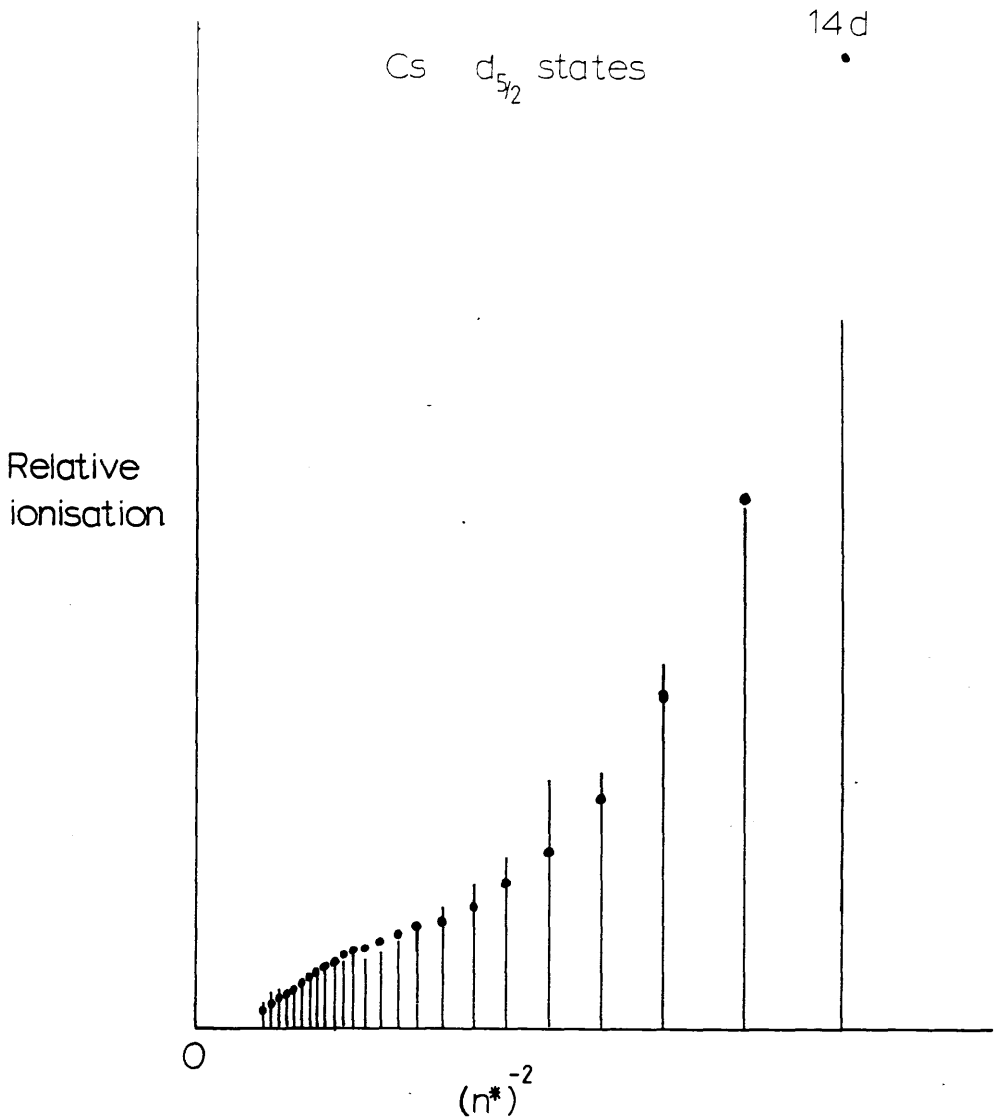
Fig 6.35 Modelling of the collisional enhancement of the three photon ionisation
of atomic caesium in a proportional counter

$I_n = \alpha/(n^*)^8 + \beta \ \exp\text{-}(\gamma/(n^*)^2)/(n^*)^\kappa$

$\alpha = 4.5 \ \times 10^6, \ \beta = 6.2 \ \times 10^7, \ \gamma = 1100, \ \kappa = 5.6$
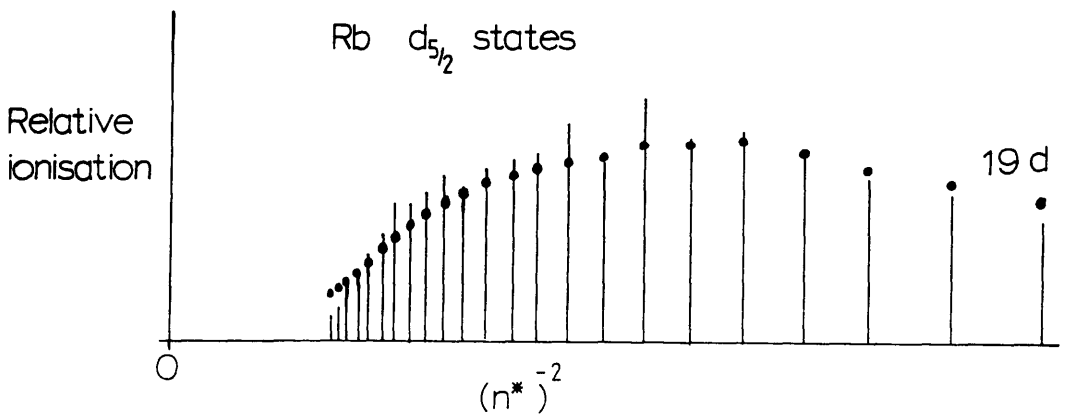
Fig 6.36 Modelling of the collisional enhancement of the three photon ionisation
of atomic rubidium in a proportional counter

$I_n = \alpha/(n^*)^8 + \beta \ \exp\text{-}(\gamma/(n^*)^2)/(n^*)^\kappa$

$\alpha = 3.3 \ \times 10^7, \ \beta = 0, \ \gamma = 1300, \ \kappa = 5.8$

increased by a factor of around 500 over that which would be expected by a pure photoionisation process. However comparison of figures 6.1 and 6.32, between the ion yields obtained in the proportional counter with and without the buffer gas, suggests that the collisional enhancement of the ionisation may not be as large as 500. Nevertheless, Whitaker et al (1981) demonstrated an enhancement of a factor of 200, by a direct comparison of the photoionisation yield with the collisional ionisation yield of highly excited rubidium atoms.

6.8 RESONANT IONISATION OF RUBIDIUM IN A QUADRUPOLE MASS SPECTROMETER

INTRODUCTION

The quadrupole mass spectrometer was sensitive enough to detect the resonant ionsation of rubidium atoms when in the vapour phase at room temperature. The major disadvantage in using the mass spectrometer, instead of the proportional counter, was in the calibration of the detected signals. When operating at its best, and with maximum gain from the secondary electron multiplier, the mass spectrometer should be able to just detect single ions above the background noise. (The background noise was electrical and came from the amplifier pickup of the RF applied to the quadrupoles.) This single ion detection ability was thought unrealistic. Prolonged use of the SEM without adequate cleaning degrades its performance, as does operation at pressures much above 5×10^{-6} torr. Allied to this was the affect on the ion transmission efficiency, resulting from the modifications made to the mass spectrometer which enabled it to be used with the existing laser ionisation chamber. The detection efficiency was estimated to be ~1% ie. 1% of the ions of one mass created in the ion cage were detected.

At 300 K rubidium has a saturated vapour pressure of 4×10^{-7} torr, and the pressure of Rb_2 molecules is approximately 2.4×10^{-11} torr, figures extrapolated from Samson (1966) and Granneman et al (1976). The ratio of molecular rubidium dimers, Rb_2, to atomic rubidium at 300 K is 6×10^{-5}. These pressures correspond to number densities of 1.4×10^{10} cm^{-3} for Rb atoms and 8×10^5 cm^{-3} for Rb_2 molecules. In an unfocussed laser beam of dimensions 1.5 mm x 1.5 mm x 20 mm, there are then approximately 6×10^8 atoms and 4×10^4 molecules, and in a focussed beam of dimensions 0.13mm x 0.13mm x 10mm there are 2×10^6 atoms and 10 molecules.

However, as in the proportional counters, if impurities are outgassed from the walls of the mass spectrometer they may react with rubidium, and effectively lower its vapour pressure. The proportional counter was essentially bolted on to the mass-spectrometer and, if impurities were outgassing from the walls, a reduction in the vapour pressure of rubidium could be expected. These values therefore give the maximum number of atoms and molecules that may be detected.

With the use of a quadrupole mass spectrometer the importance of the ionisation in a proportional counter caused by collisions with the buffer gas became apparent. This can be readily seen by comparing the three-photon ionisation spectra of rubidium vapour shown in figures 6.37 and 6.38 taken between 620 nm and 660 nm. The resonances correspond in wavelength to the two photon excitation of s and d states in atomic rubidium, the fine structure of the lowest d level just being resolved, (figure 6.39). The first spectrum (figure 6.37) was taken in a proportional counter filled with counter gas to a pressure of 100 torr, while the second (figure 6.38) was taken in the quadrupole mass spectrometer in which the ambient pressure was less than 3×10^{-5} torr. The photon fluxes in both spectra were similar at around, 7×10^{26} photons cm^{-2} sec^{-1}, and were obtained by focussing the laser with a 25 cm lens. The ionisation of the s states relative to the d states is considerably diminished in the spectrum taken in the quadrupole mass spectrometer at the lower pressure.

If rubidium atoms are similar to caesium atoms, then the two photon excitation cross-sections from the ground state to the s states and to the d states will be of similar size, but the ionisation cross-sections of the s states will be orders of magnitude smaller than the d states, (Pindzola 1984a). In the absence of a buffer gas the relative sizes of the ionisation signals from the s and d levels should reflect this difference in the ionisation cross-sections. For example at a pressure of 2.3×10^{-5} torr the ionisation ratio for 9s/7d in figure 6.37 was found to be 4.6×10^{-3} at a flux of 4×10^{26} photons cm^{-2} sec^{-1}, and for the 10s/8d states the ratio was 1.7×10^{-3} at a similar flux. A plot of the ratio of the ionisation yield for the 10s/8d states, against the buffer gas pressure, is shown in figure 6.40, with the pressures ranging from 1000 torr to 1 torr. At a pressure of 1000 torr the ratio is 0.5 and this falls to a ratio of 0.015 at 2 torr. The n+2s/nd ratios were used rather than the ns/nd ratios because the photon flux was constant over this wavelength range. The ratios plotted in 6.40 weighted in favour of the 10 s level due to a degree of saturation of the 8 d level.

The absolute level of ionisation from both states also fell as the pressure was reduced, although a quantitative figure for the ion yield could not be obtained at low pressures due to noise obscuring the ^{55}Fe calibration signal.

The enhancement of the ionisation of the s states, and to a lesser extent of the d states,
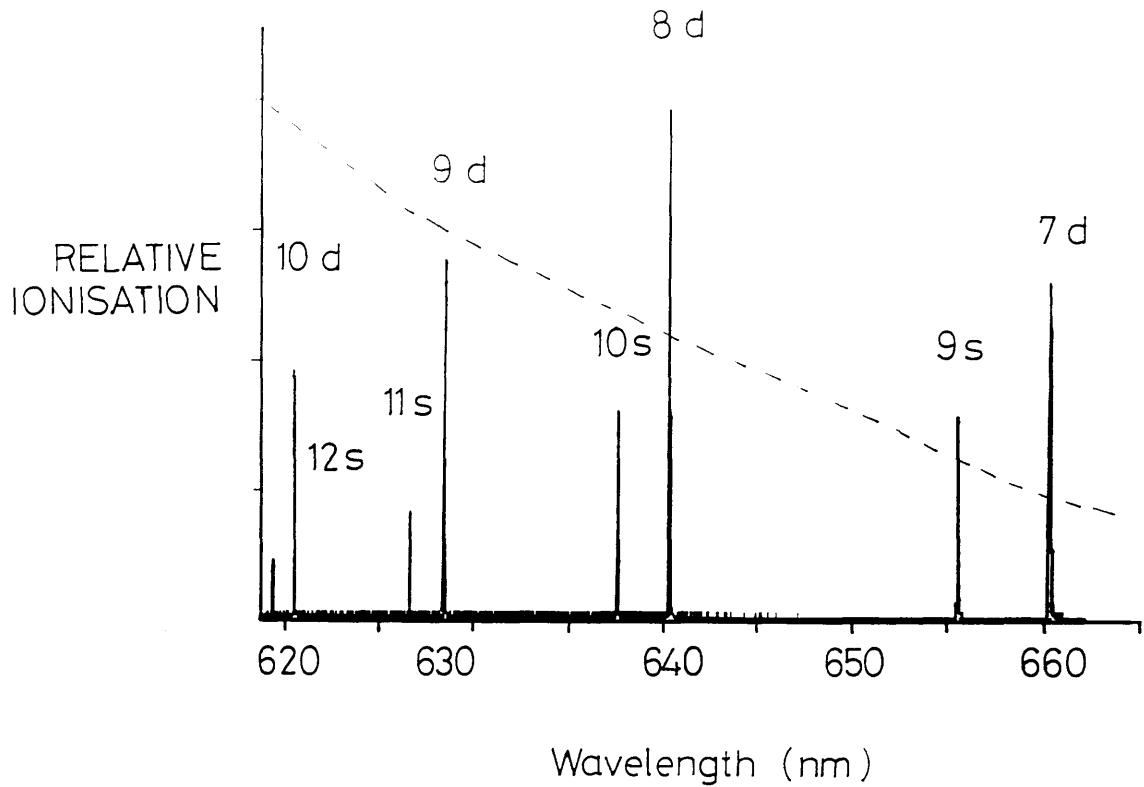
Fig 6.37 Three photon ionisation spectrum of rubidium vapour in a proportional counter filled to 100 torr with buffer gas. The resonances are the two photon $5s_{1/2}$-$ns_{1/2}$, $5s_{1/2}$-$nd_{5/2,3/2}$ transitions.
(focussed, flux $= 7 \times 10^{26}$ photons cm^{-2} sec^{-1})
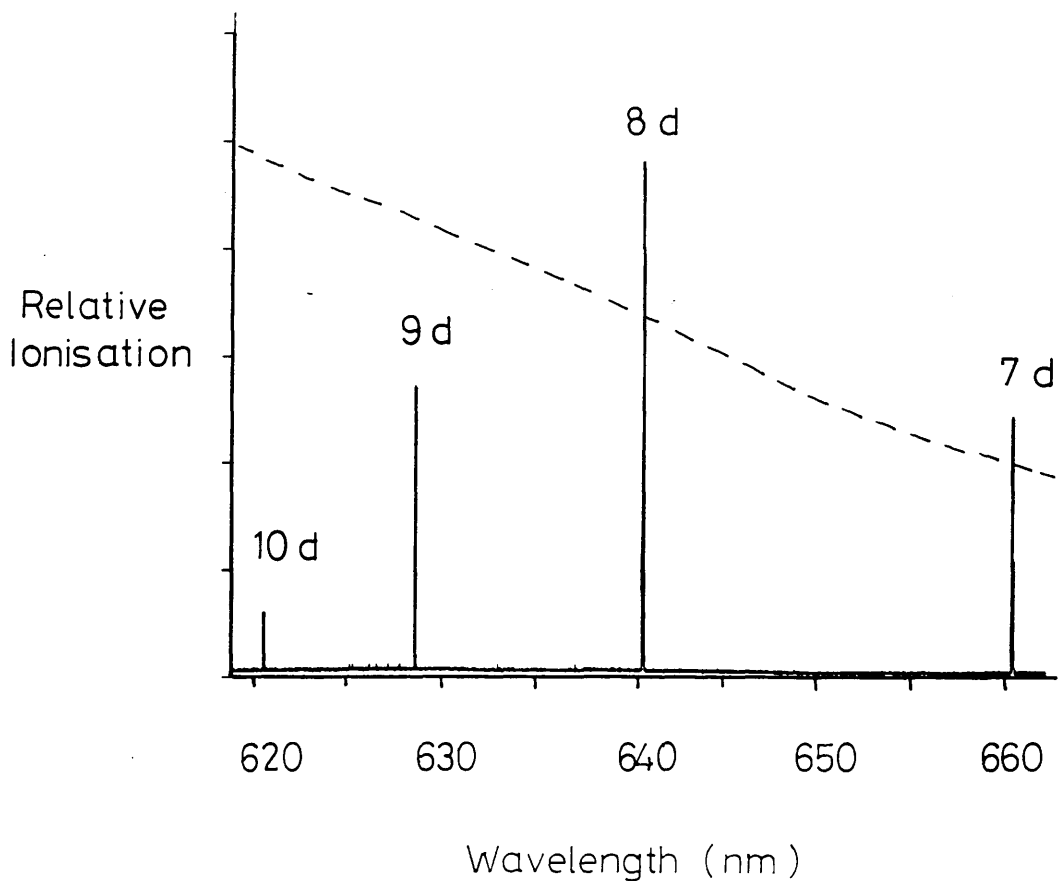
Fig 6.38 Three photon ionisation spectrum of rubidium vapour in quadrupole mass spectrometer. The resonances are the two photon $5s_{1/2}$-$nd_{5/2,3/2}$ transitions.The $5s_{1/2}$-$ns_{1/2}$ resonances are not evident.
(focussed, flux $= 7 \times 10^{26}$ photons cm^{-2} sec^{-1})
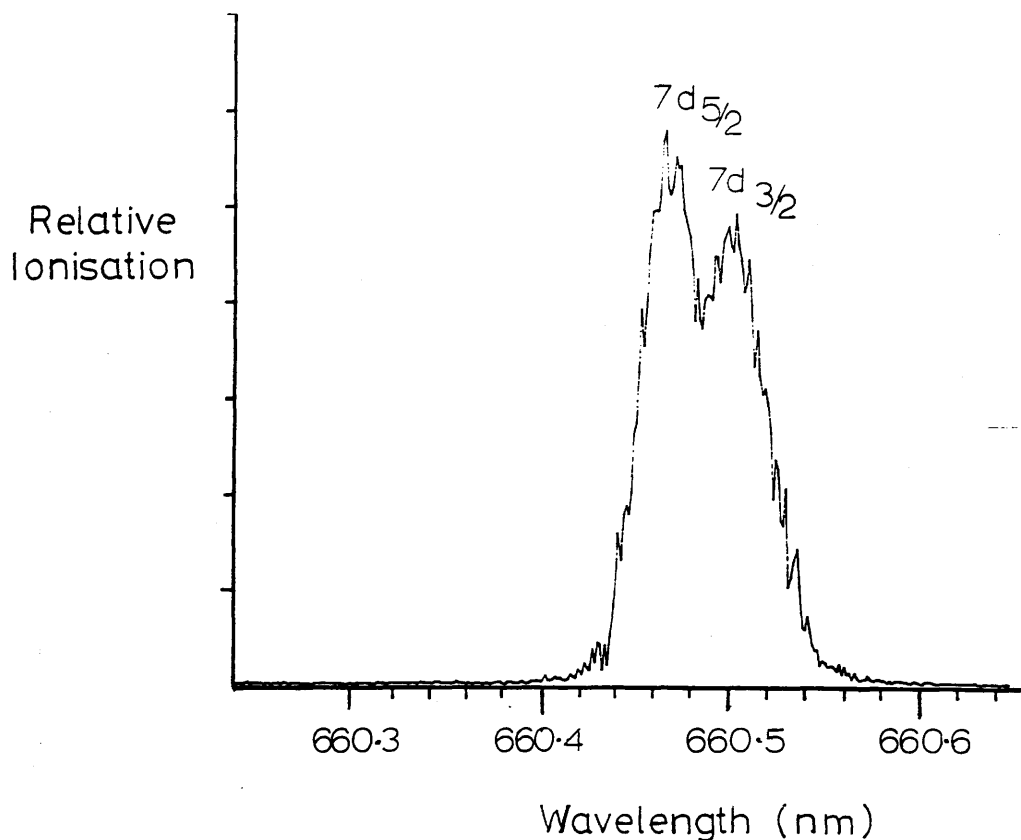
Fig 6.39 Fine structure of the 7d level in atomic rubidium
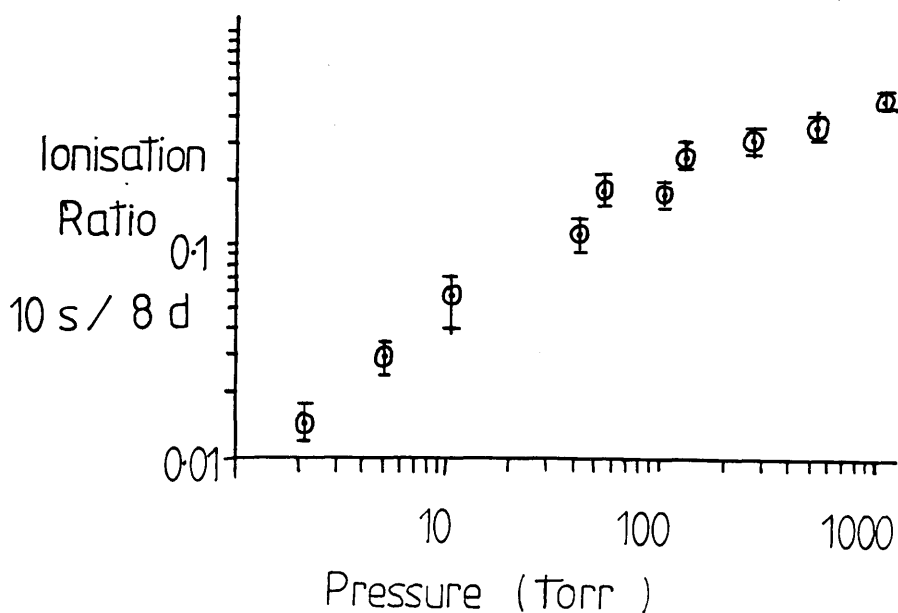
Fig 6.40 Ratio of the 10s/8d ion yields for atomic rubidium against buffer gas pressure in proportional counter.

by the presence of the buffer gas is further illustrated in figures 6.41 and 6.42. These plot the dependence of the ionisation with laser power taken in the proportional counter for the s and d states at both high and low pressure. At a pressure of 100 torr the ionisation of the s state is quadratically dependent at all laser powers, whilst the d state shows a cubic dependence at low laser power and begins to saturate at high laser power. At a pressure of 5 torr the ionisation of the 10s state is still quadratically dependent on laser flux while that of the 8d state is cubically dependent except at the very highest flux. This would indicate that collisional ionisation of the s state is still the dominant mechanism at 5 torr buffer gas pressure, while photoionisation is the dominant mechanism for the d state. However the 9s level in rubidium lies about 0.4 eV below the continuum and the direct collisional ionisation by argon atoms would be unlikely. When the temperature of the rubidium is reduced to 300 K, and with an ambient pressure of less than 2×10^{-5} torr in the mass spectrometer, the d state is cubically dependent on photon flux at all laser powers, (figure 6.44), which would indicate that there was little collisional ionisation at this pressure. A mass spectrum is shown in figure 6.43 when the laser is resonant with the two photon transition $5\,s_{1/2} - 8\,d_{5/2}$ at a wavelength of 640.6nm. There is no evidence of any ionisation of Rb_2 molecules.

Figure 6.45 is a spectral and mass three photon ionisation spectrum of atomic rubidium over the two photon $5s_{1/2}-7d_{5/2,3/2}$ transition, and figure 6.46 plots the ratio of the $^{85}Rb^+/^{87}Rb^+$ ionisation yields. The ratio was calculated by integrating the individual ^{85}Rb and ^{87}Rb mass peaks at each wavelength. The isotope splitting of the 5s level is expected to be around 0.05 cm^{-1}, (Gross 1974), which is much smaller than the ~2.5 cm^{-1} laser line width. No isotopic selectivity would be expected therefore. The error bars in figure 6.46 are a measure of the fluctuation in the background signal detected at all masses. On the two resonances the ratio drops which may be indicative of saturation of the electronics for large ion signals. The naturally occuring isotope ratio, $^{85}Rb/^{87}Rb$ is ~2.59 and this is indicated on figure 6.46.
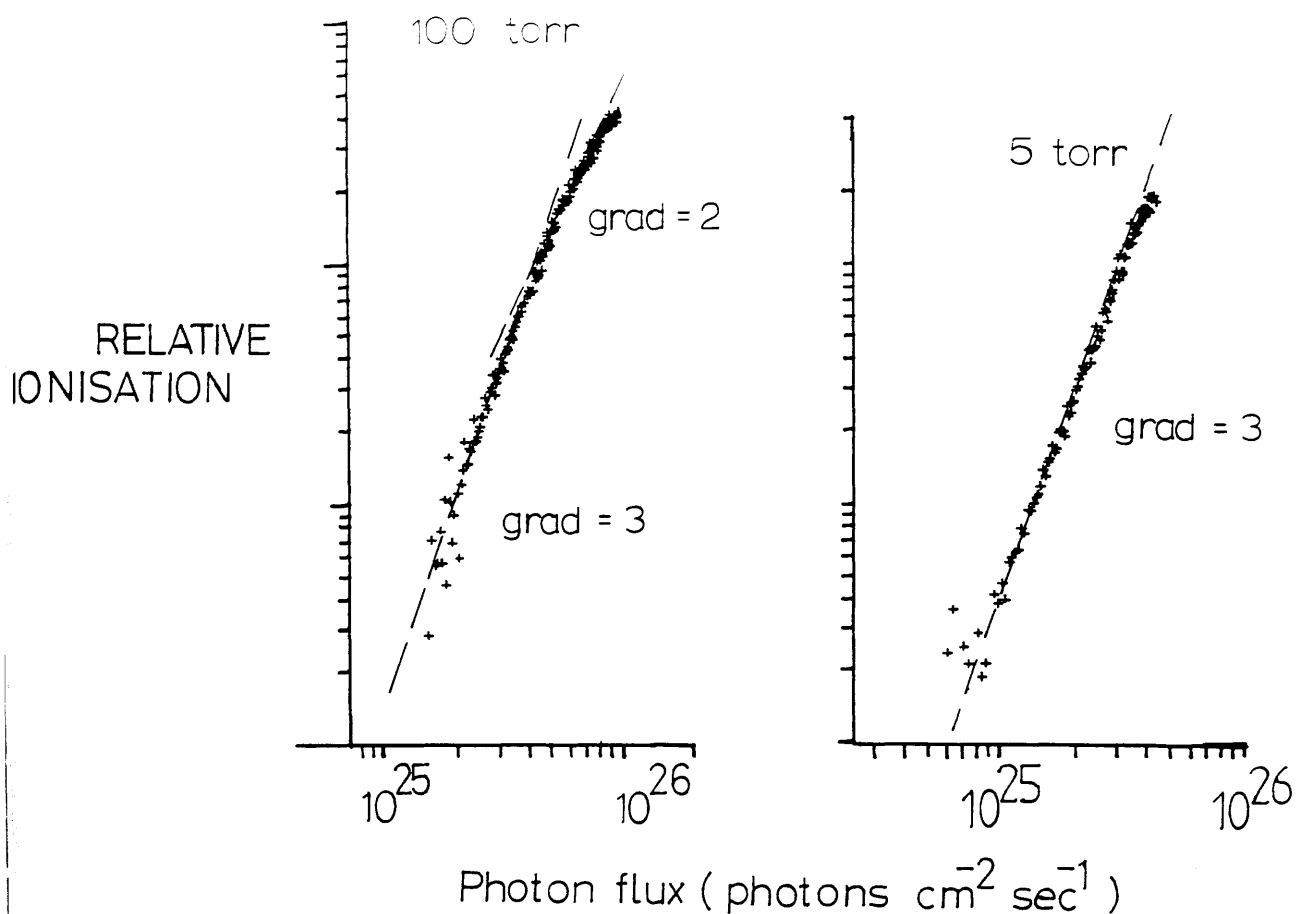
Fig 6.41 Dependence of the three photon resonant ionisation on photon flux in rubidium vapour at two different buffer gas pressures in the proportional counter
(λ = 640.56 nm, $5s_{1/2}$ - $8d_{5/2}$)
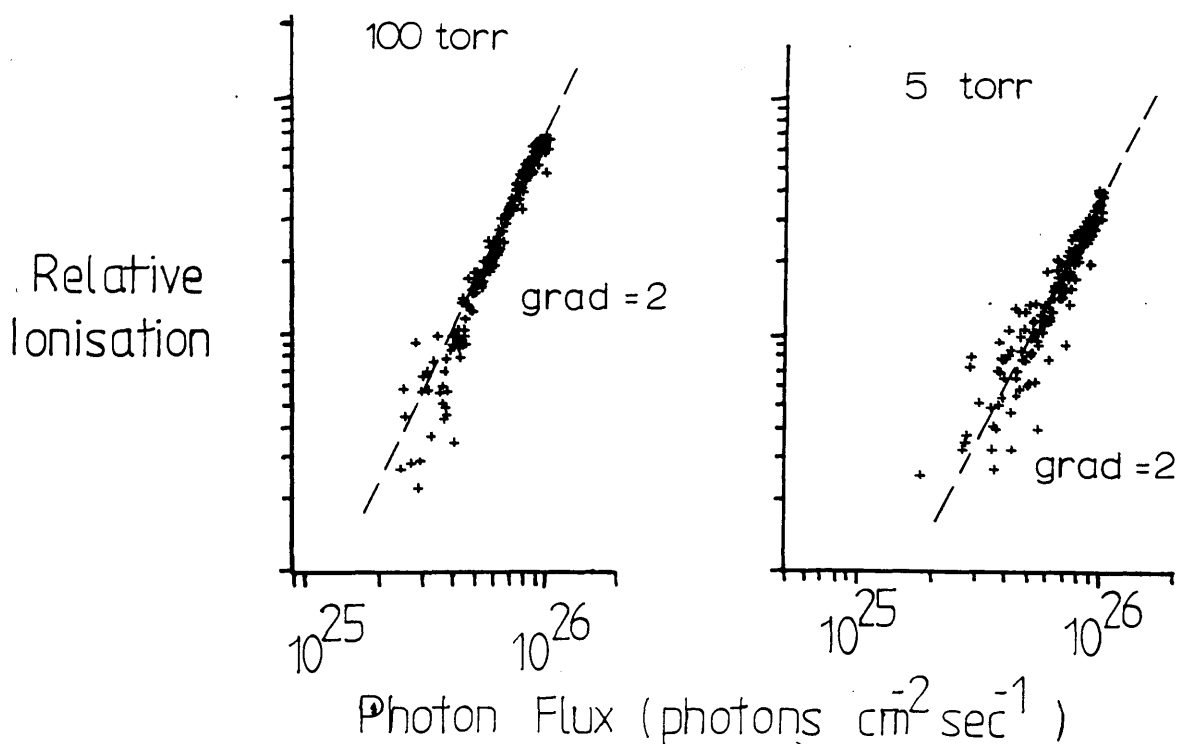
Fig 6.42 Dependence of the three photon resonant ionisation on photon flux in rubidium vapour at two different buffer gas pressures in the proportional counter
(λ = 655.76 nm, $5s_{1/2}$ - $9s_{1/2}$)
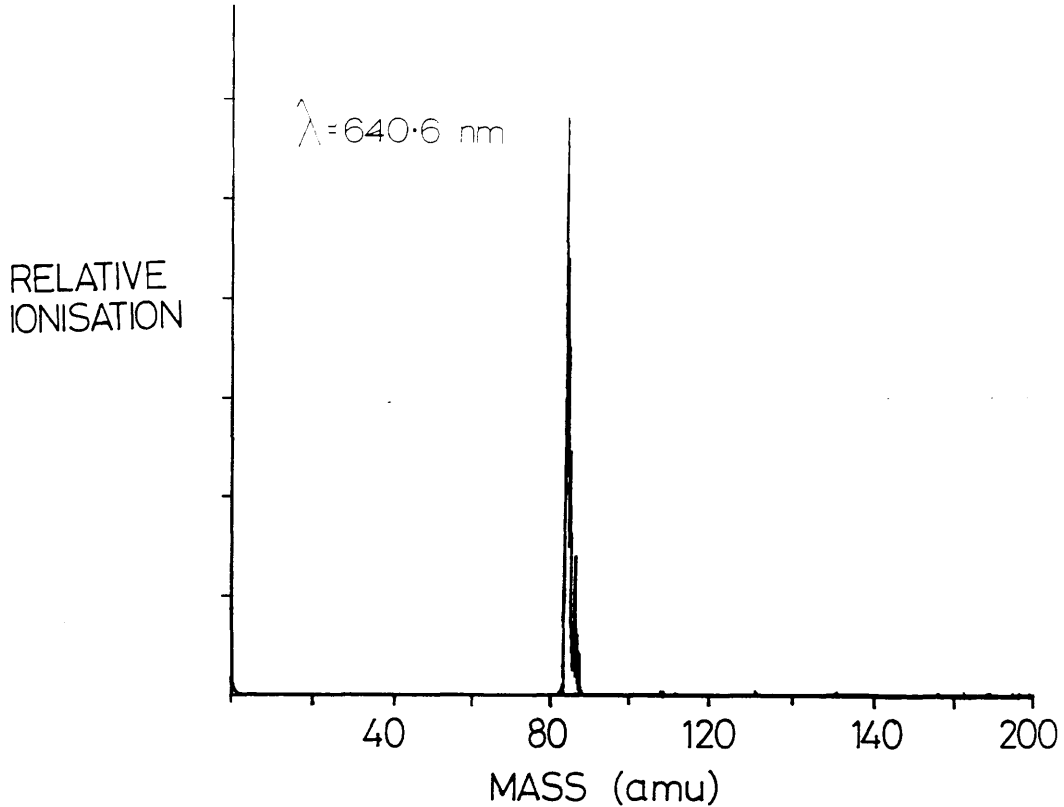
Fig 6.43 Mass spectra of ionisation in rubidium vapour with focussed laser
(λ = 640.6 nm, $5s_{1/2}$ - $8d_{5/2}$)
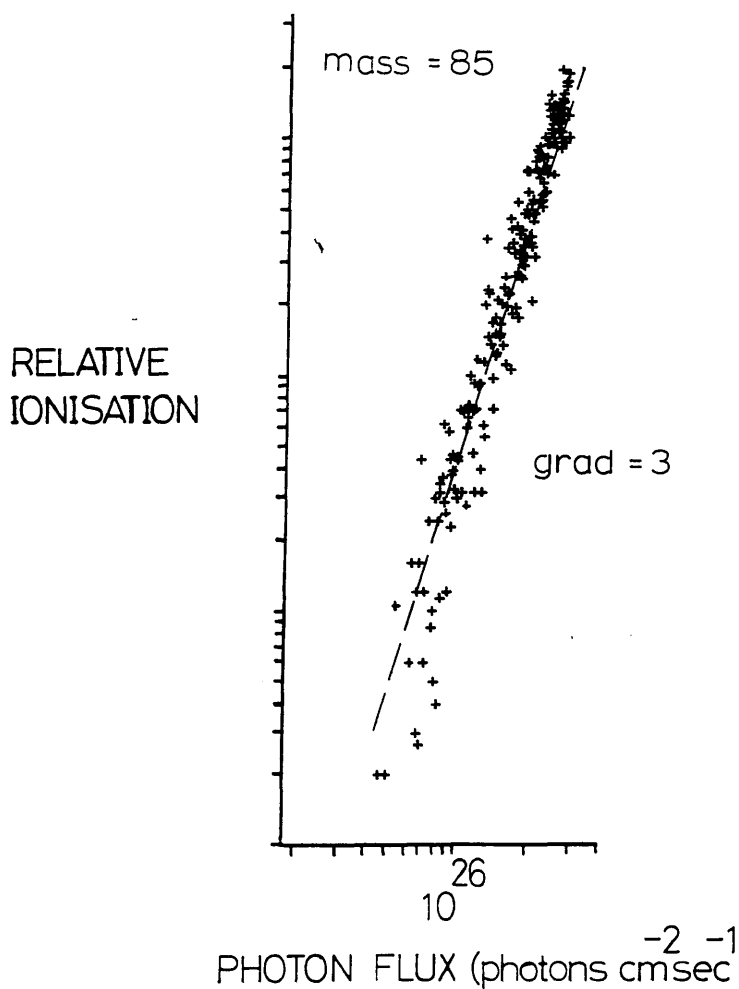
Fig 6.44 Dependence of the three photon resonant ionisation on photon flux in
rubidium vapour in the quadrupole mass spectrometer, at mass 85 amu
(λ = 640.6 nm, $5s_{1/2}$ - $8d_{5/2}$)
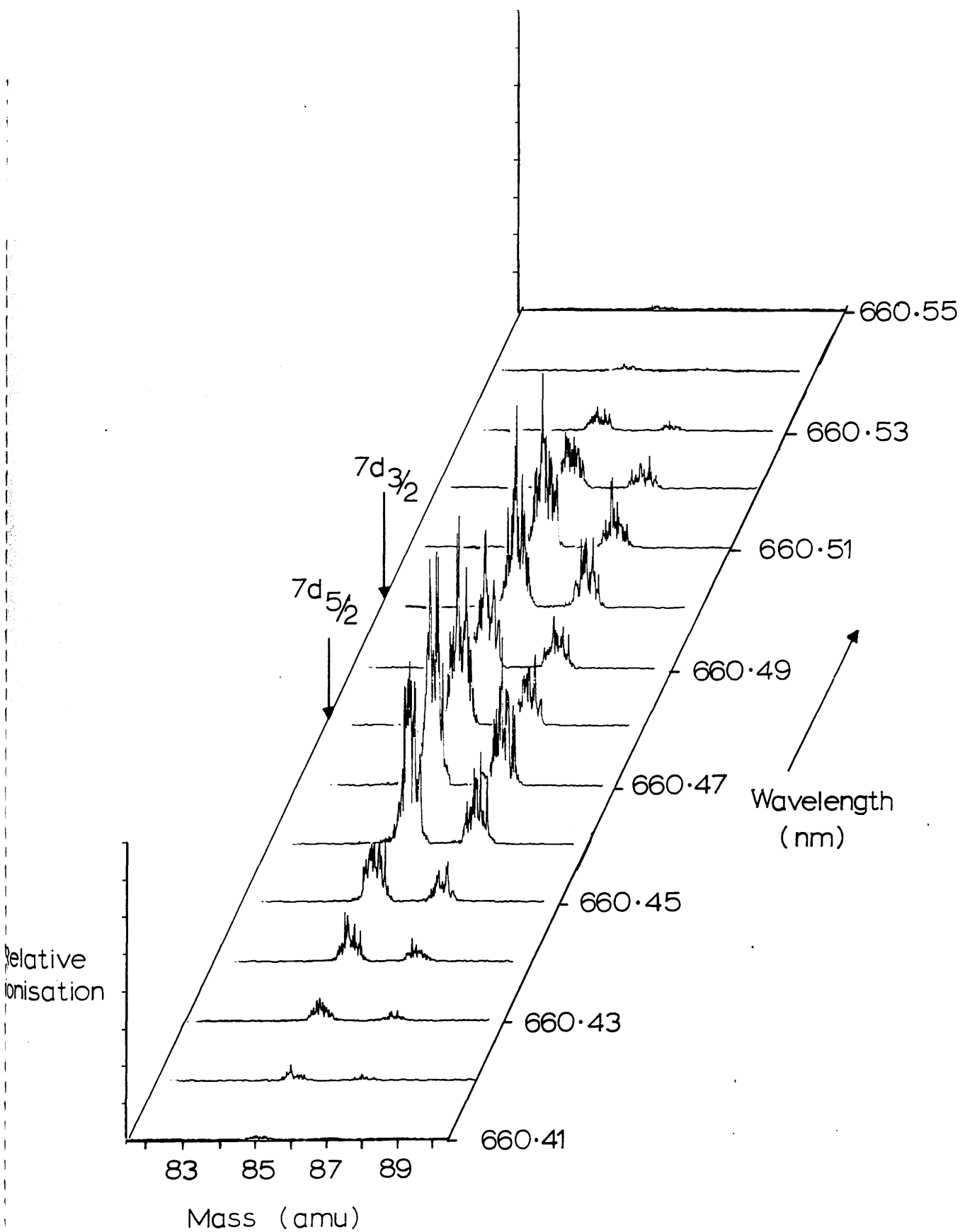
Fig 6.45   Mass and wavelength dependence of the ionisation of atomic rubidium over the 5s-7d doublet transition
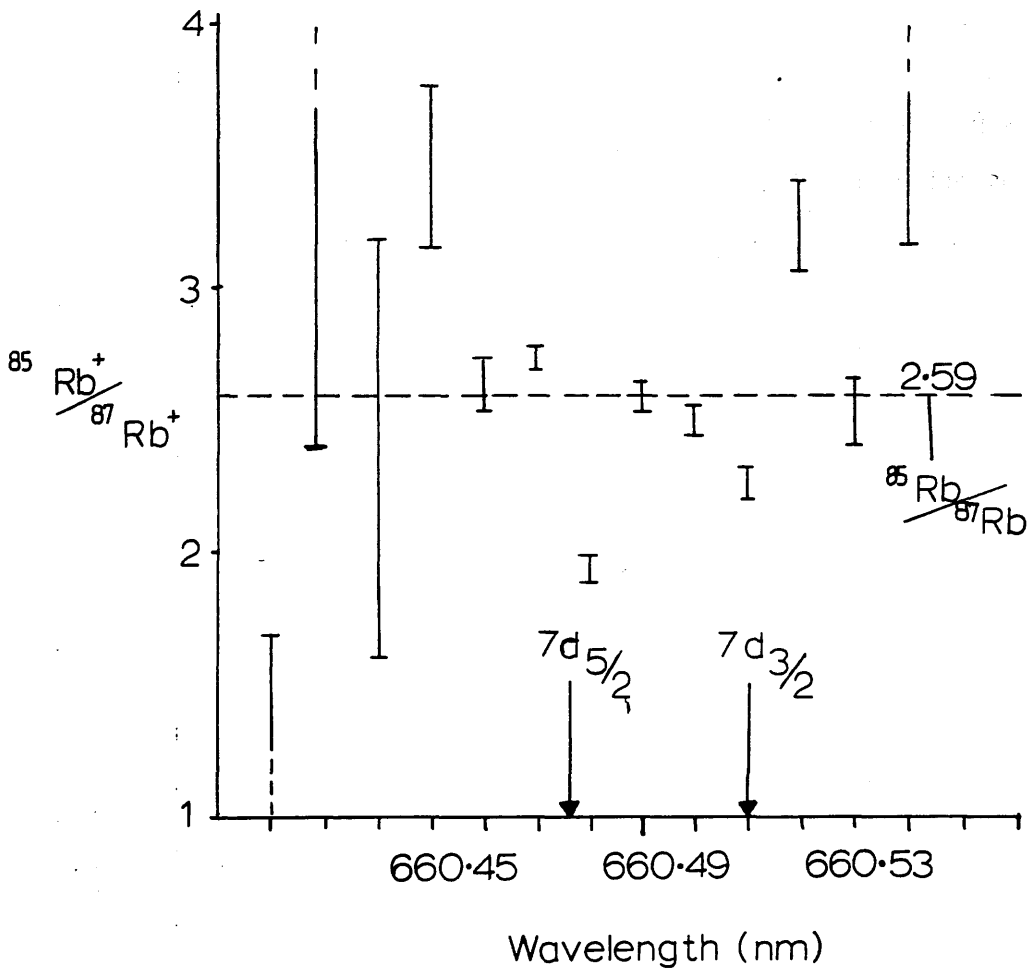
Fig 6.46   Dependence of the $^{85}Rb^+/^{87}Rb^+$ ionisation ratio on wavelength over
the 5s-7d doublet transition

TWO PHOTON IONISATION OF RUBIDIUM VAPOUR

ATOMIC IONISATION

Figure 6.47 is an ionisation spectrum taken at low laser power (5×10^{21} photons cm^{-2} sec^{-1}) showing the $5s_{1/2}$-$6p_{3/2}$ and $5s_{1/2}$-$6p_{1/2}$ resonant transitions in atomic rubidium. From calculations based on Burgess and Seaton (1960), the photoionisation cross section σ_i of the $6p_{3/2}$ state, at a wave-length of 420.3 nm, is 4×10^{-18} cm^2, and the spontaneous decay rate of the $6p_{3/2}$ state, A_{12}, is 2.3×10^6 sec^{-1}. (Ambartsumyan et al (1976) quotes a value of 1.9×10^{-18} cm^2 for the photoionisation cross-section of this state using an ionising wavelength of 347 nm.) Saturation of the photoionisation step would therefore require a fluence of around $1/\sigma_i$ = 5×10^{17} photons cm^{-2}, (Letokhov 1987). Assuming a laser line width v_L of 10^{11} sec^{-1}, an estimate of the excitation cross-section of the transition, σ_{exc}, and of the photon flux Φ_{sat} required to saturate it ($\Phi_{sat} = 1/2\ \sigma_{exc}$) can be made at 4×10^{-15} cm^{-2} and 1.2×10^{22} photons cm^{-2} sec^{-1} respectively, (Tuosunov et al 1985). At the laser power level in figure 6.47 therefore the excitation step is not saturated. This is bourne out in figures 6.48a and 6.48b which record the ionisation yield at the two resonant wavelengths as a function of laser flux. In both transitions saturation begins at a flux of $\sim 4 \times 10^{22}$ photons cm^{-2} sec^{-1}. The laser power used to produce the spectrum shown in figure 6.47 is indicated on the graphs, and at this point the ionisation yield is quadratic with laser power.

NONRESONANT IONISATION

It was necessary to focus the laser in order to bring the background nonresonant ionisation above the noise. A mass scan of the nonresonant ionisation obtained with a focused laser of power 6.5×10^{25} photons cm^{-2} sec^{-1}, at a wavelength of 430 nm, is shown in figure 6.49. Figure 6.50 shows the quadratic dependence of this ionisation at mass 85 on the laser power. There is again no evidence of any molecular dimer signal in figure 6.49, nor any evidence in the power dependence curve of any saturation which would be expected if the ionisation signal was molecular in origin and resulted from the two photon ionisation/dissociation of Rb_2.

The two photon non resonant ionisation cross section for atomic rubidium at a
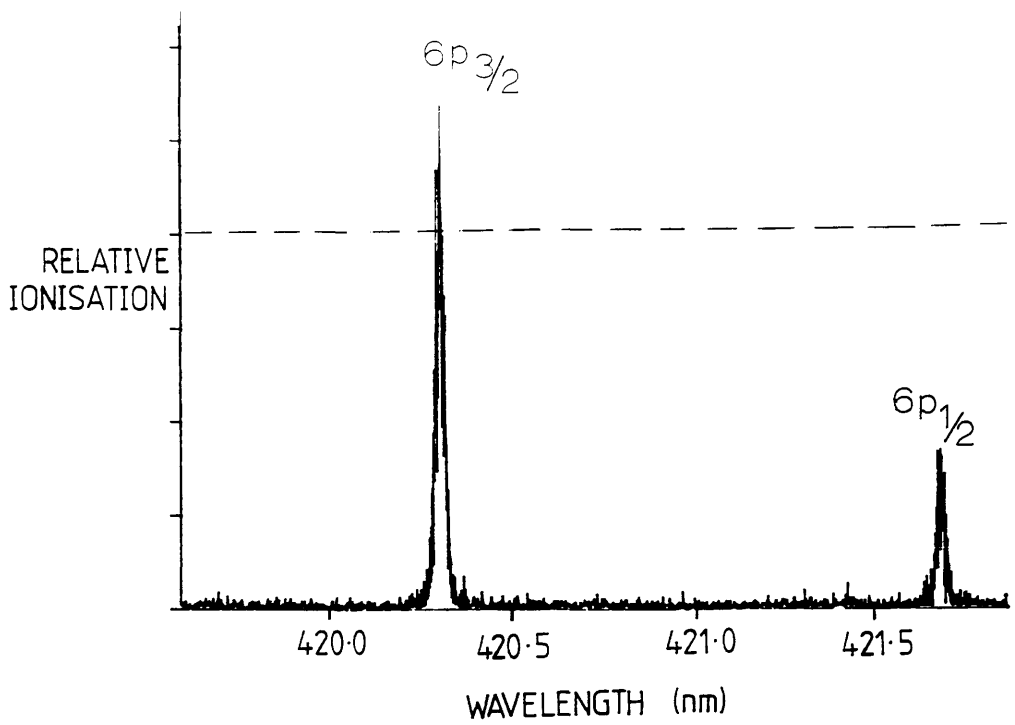
Fig 6.47 Two photon ionisation spectrum of atomic rubidium at mass 85, via the single photon $5s_{1/2}$-$6p_{3/2,1/2}$ transition.
(not focussed, flux = 5 x 10^{21} photons cm^{-2} sec^{-1})
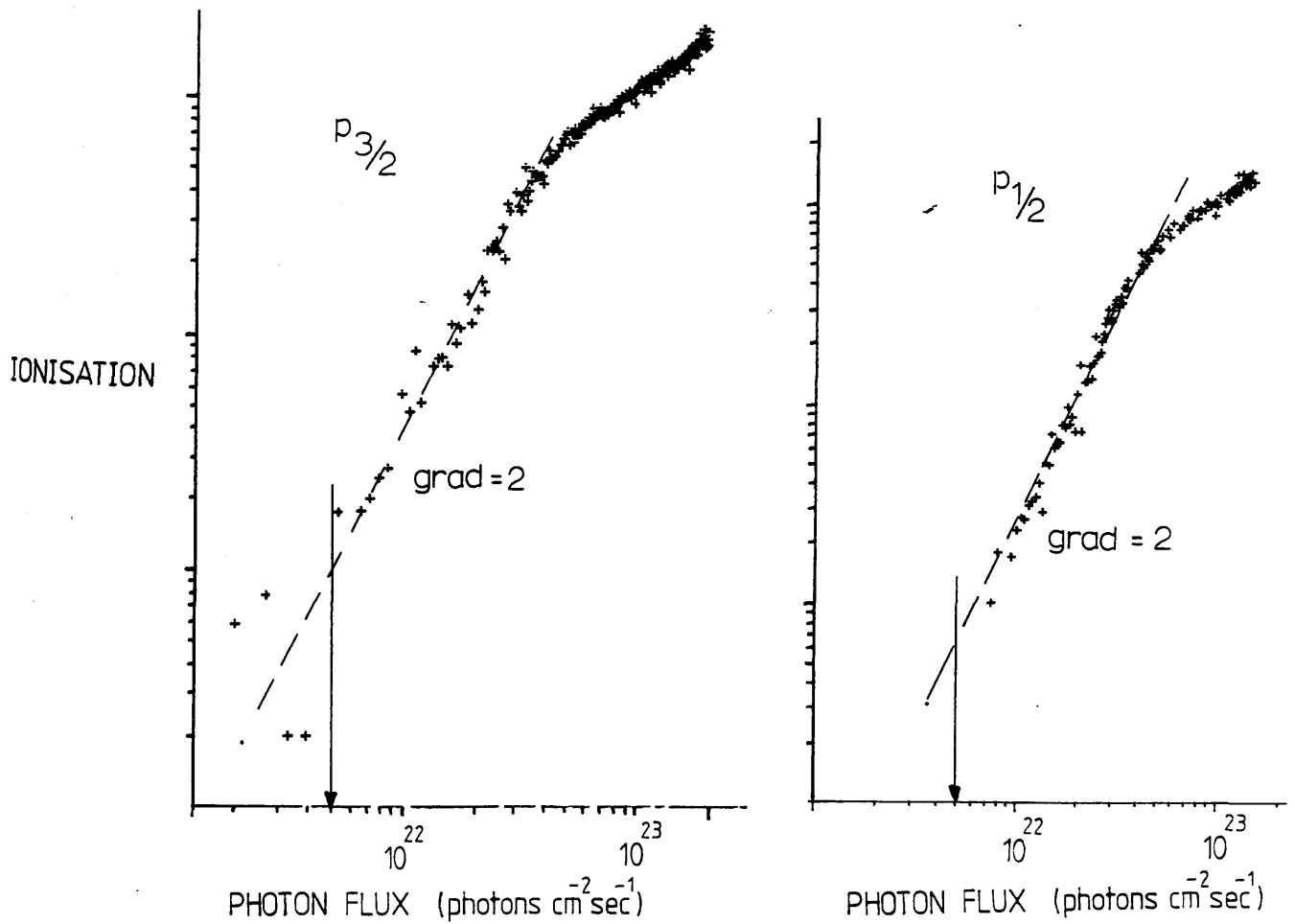
Fig 6.48 Dependence of the resonant ionisation on photon flux in rubidium vapour at mass 85
a) resonant with the $5s_{1/2}$- $6p_{3/2}$ transition
b) resonant with the $5s_{1/2}$- $6p_{1/2}$ transition
Flux of 5 x 10^{21} photons cm^{-2} sec^{-1} is indicated
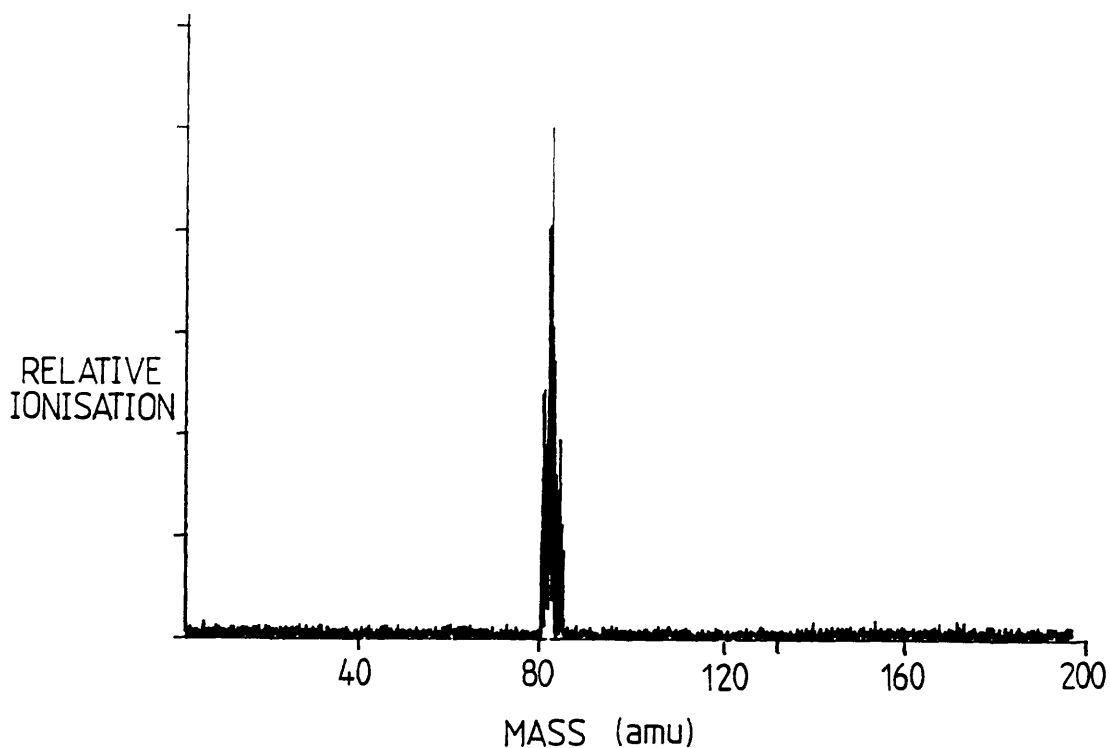
Fig 6.49 Mass spectrum of nonresonant ionisation in rubidium vapour at λ = 430 nm
(focussed, flux = 6.5×10^{25} photons cm^{-2} sec^{-1})
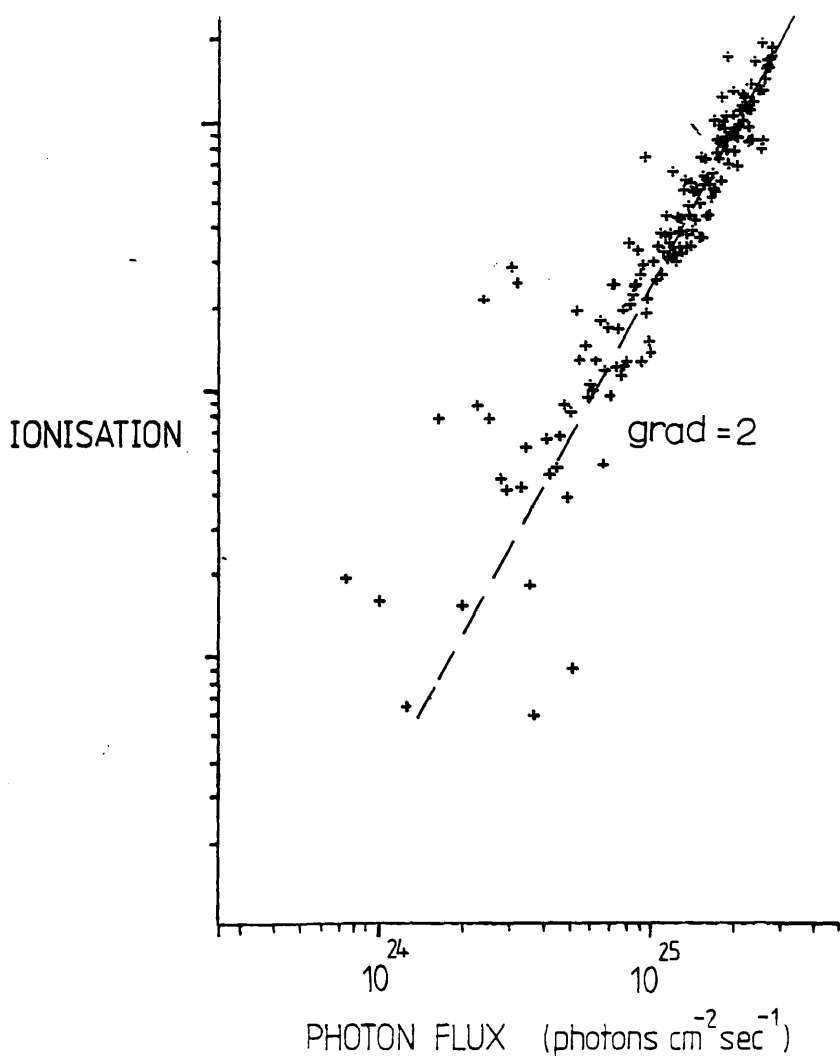
Fig 6.50 Dependence of the nonresonant ionisation on focussed photon flux in rubidium vapour at mass 85 amu
(λ = 430 nm)

wavelength of 488 nm is 9×10^{-49} cm^4 sec (Granneman et al 1976). At a wavelength of 430 nm it is not expected to vary by more than a couple of orders of magnitude from this value, (Hurst et al 1979a, Bebb 1966). Therefore the number of ions formed can be estimated from (Normand and Morellec 1980),

$$N_i = N_0\, \sigma_T \Phi^2 \tau v$$

where N_i is the number of ions, N_0 is the number of neutral atoms in the interaction volume v, σ_T is the total ionisation cross-section, Φ is the photon flux and τ is the interaction time which can be approximated to the laser pulse length. The interaction volume can be estimated at the focussed laser volume = 1.7×10^{-4} cm^3. Using values for the number of atoms in the focussed laser volume, $N_0 = 2 \times 10^6$, the interaction time $\tau = 10^{-8}$ sec (the laser pulse length), photon flux of 6.5×10^{25} photons cm^{-2} sec^{-1} and total ionisation cross-section of 10^{-48} cm^4 sec^1, the number of ions produced is ~100 and may vary by one or two orders of magnitude. With a detection efficiency of 1% the quadrupole may not detect this ionisation. However evidence for the atomic ionisation being the cause of the nonresonant ionisation came from a direct comparison of the levels of ionisation on and off resonance. By extrapolating the quadratic dependence of the nonresonant rubidium ionisation from the high flux needed to observe it (around 10^{25} photons cm^{-2} sec^{-1}) down to the low flux levels at which the unsaturated resonant rubidium ionisation could be observed (around 10^{21} photons cm^{-2} sec^{-1}), the ratio of the resonant ionisation to the nonresonant ionisation at the low flux was found to be 2×10^7. The two photon resonant ionisation cross-section of rubidium via the $5s_{1/2}$-$6p_{3/2}$ transition can be estimated at 1.6×10^{-41} cm^4 sec^1, from the photoexcitation cross-section 4×10^{-15} cm^2, the photoionisation cross-section 4×10^{-18} cm^2 and the interaction time 10^{-8} sec, (Granneman et al 1976). The ratio of the approximate resonant/non resonant two photon ionisation cross-sections for rubidium given above is $1.6 \times 10^{-40} / 10^{-48} = 1.6 \times 10^8$ which is within a factor of 10 of the experimental ratio of 2×10^7.

Therefore it is assumed that the background signal is due to the nonresonant two photon ionisation of rubidium atoms.

A low resolution mass scan, designed to maximise the ion transmission, at a laser power of 5×10^{21} photons cm^{-2} sec^{-1}, and wavelength of 420.78 nm, resonant with the $6s_{1/2}$-$7p_{3/2}$ transition, is shown in figure 6.51. The two naturally occuring isotopes of rubidium (^{85}Rb and ^{87}Rb) can just be resolved (insert to figure 6.51), but there is no evidence of any molecular dimer ions of rubidium which have masses of 170 amu (^{85}Rb + ^{85}Rb) , 172 amu (^{85}Rb + ^{87}Rb), and 174 amu (^{87}Rb + ^{87}Rb). Even at a much higher power level (5×10^{22} photons cm^{-2} sec^{-1}, figure 6.52) there is little evidence for the Rb$_2$ dimer ions.

This is attributed to the very small number of Rb$_2$ molecules in the unfocused laser beam, (2×10^4), and to the low transmission efficiency (~1%) of the quadrupole mass-spectrometer. The two photon ionisation of Rb$_2$ at a wavelength of 430 nm proceeds via the excited D state of the molecule (figure 6.53a) and continues to either an excited ionic level or to a dissociative ionic ground state level as indicated below, (Granneman et al 1976)

(ground state) $\quad$ Rb$_2$ + $h\nu$ -----> Rb$_2^*$ (D state) $\quad$ .... 1.

(D state) Rb$_2^*$ + $h\nu$ -----> Rb$^+$ + Rb + e$^-$ $\quad$ .... 2(a)

(D state) Rb$_2^*$ + $h\nu$ -----> Rb$_2^+$ + e$^-$ $\quad$ .... 2(b)
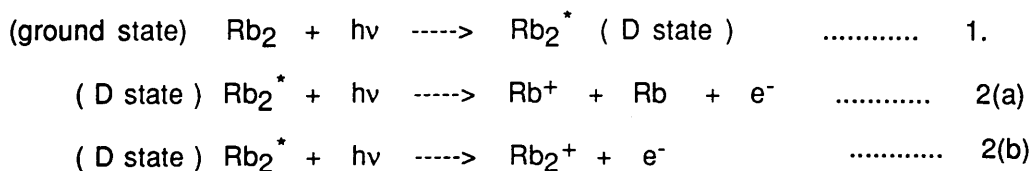
The overall ionisation cross section is of the order 10^{-43} cm^4 sec, (Granneman et al 1976), and little ionisation of Rb$_2$ is likely at the laser powers used in the mass-spectra of figures 4 and 5. There is nothing to be gained from focussing the laser since the absolute number of molecules irradiated is reduced proportionately (there are at most 100 molecules in a focused beam of 0.13mm x 0.13mm x 10mm).

When the temperature of the arm holding the rubidium reservoir was raised to 410 K the molecular component of the ionisation became evident. At this temperature the saturated vapour pressure of rubidium atoms is 5×10^{-4} torr (2×10^{13} atoms cm^{-3}) and the Rb$_2$ molecule pressure is around 2×10^{-7} torr (7×10^9 molecules cm^{-3}).

Figure 6.54 is an ionisation spectrum at mass 170 with a focused laser. The overall
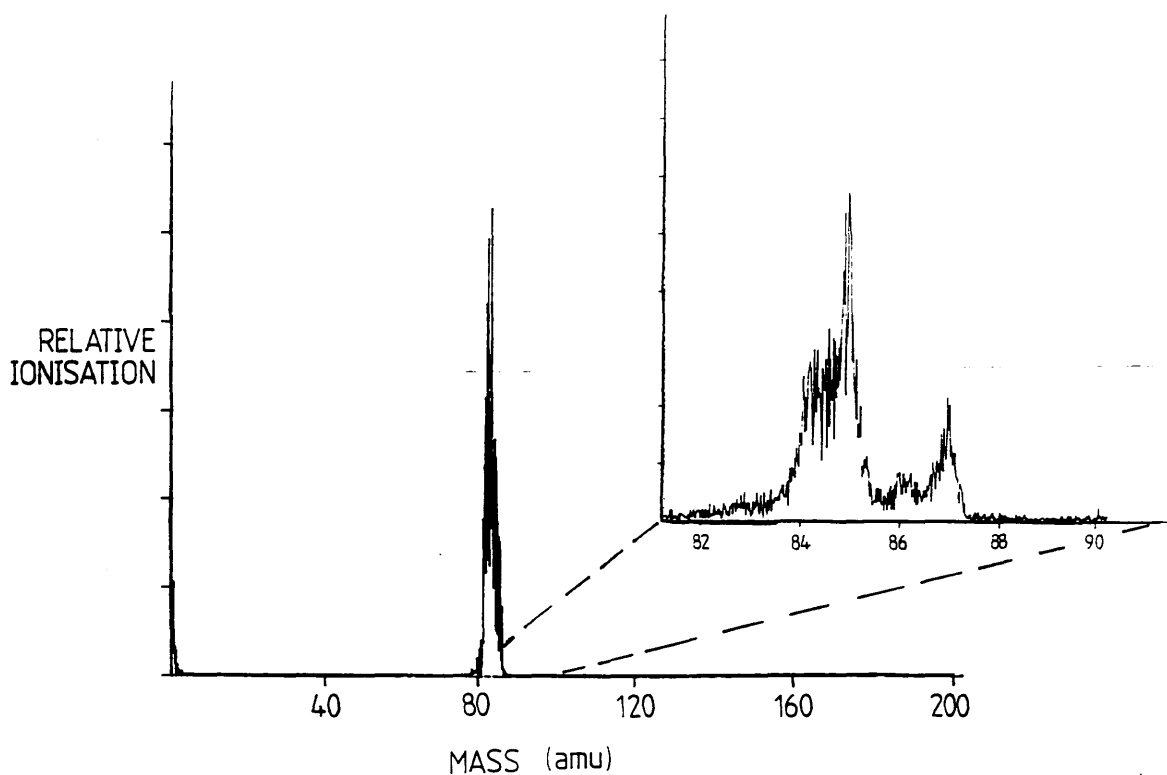
Fig 6.51   Mass spectrum of ionisation in rubidium vapour at λ = 420.78 nm resonant with the $5s_{1/2}$-$6p_{3/2}$ transition.
(not focussed, flux = 5×10^{21} photons cm^{-2} sec^{-1})
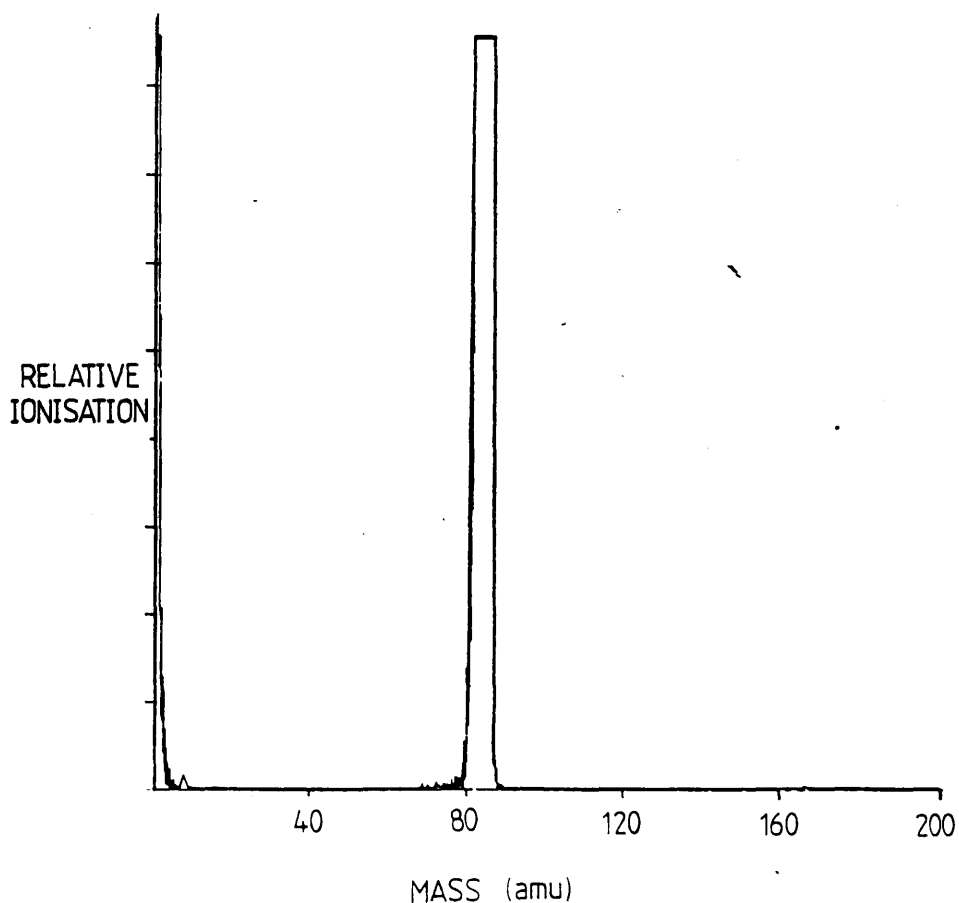
Fig 6.52   Mass spectrum of ionisation in rubidium vapour at λ = 420.78 nm resonant with the $5s_{1/2}$-$6p_{3/2}$ transition.
(not focussed, flux = 5×10^{22} photons cm^{-2} sec^{-1})
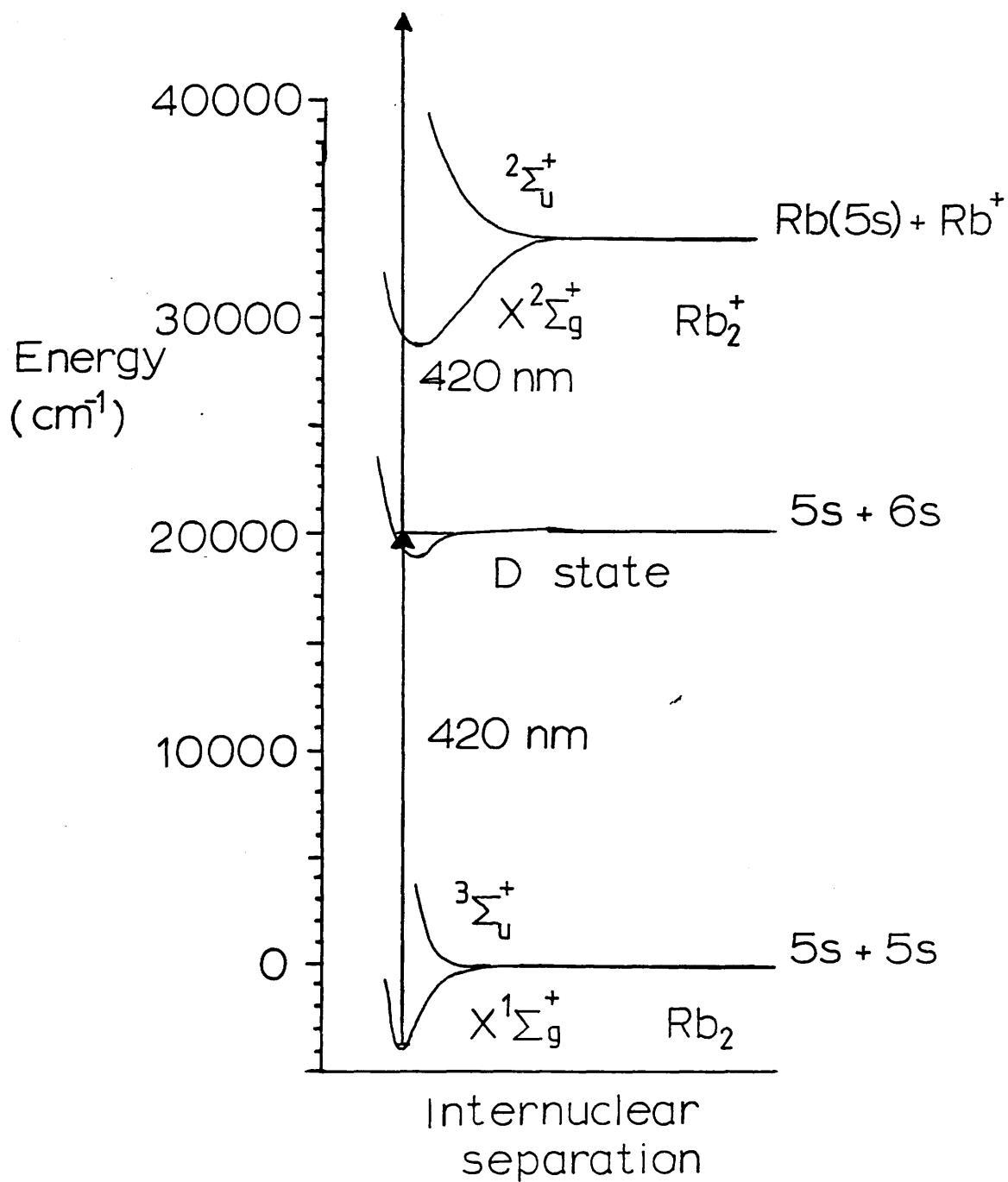
Fig 6.53a Energy levels of Rb$_2$ molecule at 420 nm showing two photon ionisation

shape of the spectrum is mainly a function of the laser power variation with wavelength, although the Rb_2 molecule has an absorption band centred on 430 nm, as indicated above, (Gupta et al 1978). The resonance in this spectrum is assigned to single photon absorption from the ground state molecule to the excited D state molecule. The excited molecule is then photoionised to an excited state of the Rb_2^+ ion (reaction 2(b)). Reaction 2(a), which gives an atomic Rb^+ signal from the photo-dissociation of the D state molecule, has not been investigated yet.

A plot of the ionisation yield at mass 170 with laser power is given in figure 6.53 with a tentative line of gradient 2 drawn through the points. The small number of ions formed is evident from the wide variation in ionisation at similar laser power levels.

The most interesting feature of the spectrum are the two "dips" which correspond in wavelength to the atomic rubidium transitions $5s_{1/2}\text{-}6p_{3/2}$ and $5s_{1/2}\text{-}6p_{1/2}$. When the laser is tuned to these atomic transitions the formation of molecular ions is almost completely supressed, evidenced from the ionisation at the bottom of these wells dropping off almost to the background level.

One simple explanation for this relates to the equilibrium position in the atom/molecule reaction in the rubidium vapour.

$$Rb\,(5\,S_{1/2}) \;+\; Rb\,(5\,S_{1/2}) \;\;\mathrel{<\text{-----}>}\;\; Rb_2\;(\text{ground state})$$
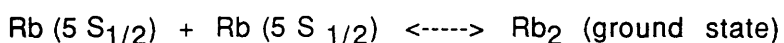
The particular ratio of molecules to atoms is dependent on temperature. As the temperature is increased up to 1000 K, the molecule/atom ratio increases. When the laser is tuned to an atomic resonance, and if saturation of this transition occurs (ie. all or most of the ground state atoms are excited), the equilibrium position will shift in favour of the dissociation of the molecule, with the result that there will be few ground state molecules available to be ionised. When the laser is tuned off the atomic resonance, the excitation of the molecular component will saturate, most of the ground state atoms will not be excited (only nonresonant two photon ionisation of the atoms will occur), the equilibrium position will shift towards the formation of the molecule, and the molecular ion signal will increase. From the ratio of the number of molecular ions formed on and off the atomic resonances, it is clear that either the formation of most of the molecules detected has occured, or that dissociation of most of the molecules already
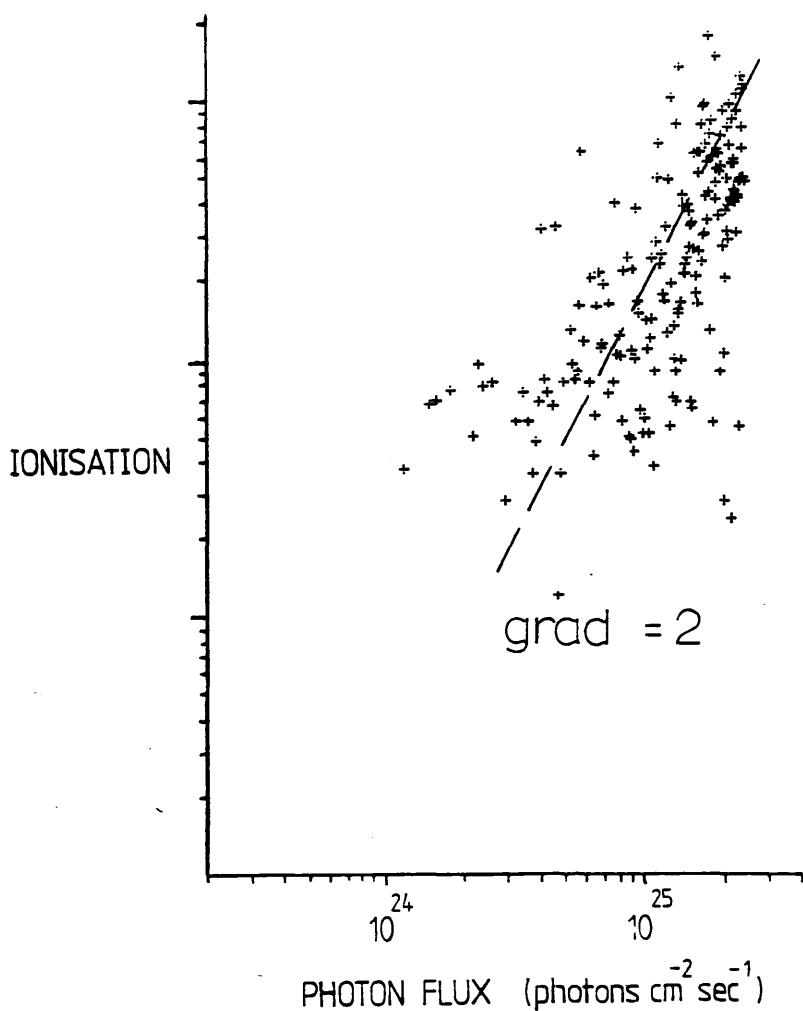
Fig 6.53 Dependence of the ionisation on focussed photon flux in rubidium vapour at mass 170 amu
(λ = 427.1 nm, Two photon ionisation of Rb_2 molecules)
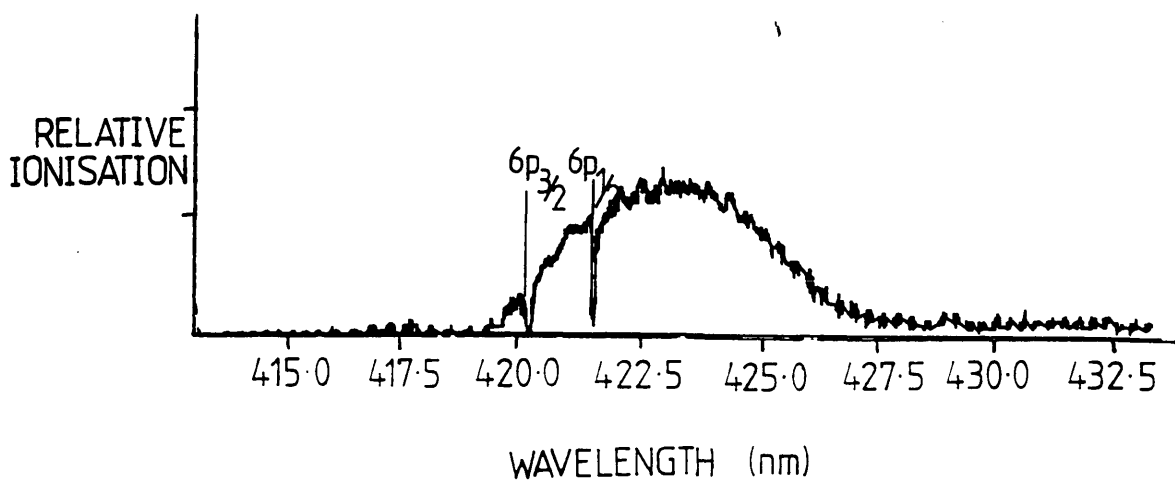
Fig 6.54 Ionisation spectrum of rubidium dimers (mass = 170 amu) with focussed laser. The positions of the atomic 5s-6p transitions are indicated.

present has occured, during the laser pulse length of 10 nanoseconds.

Another explanation (Bronch-Bruevich et al 1976, 1977) requires that the radiation field exerts considerable influence in the formation of an excited state molecule during the collision of a pair of atoms.

$$Rb\ (5\ S_{1/2}) \ + \ Rb\ (5\ S_{1/2}) \ + \ h\nu \ \ ---\!\!-\!\!> \ \ Rb_2^*$$
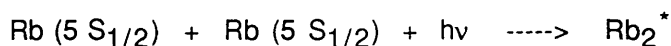
In this case the formation of the excited Rb_2^* molecule is directly proportional to the intensity of the laser flux. The drop in ionisation yield when the laser is tuned to the atomic resonance is essentially due to the same reason, namely depletion of the number of ground state atoms available for this reaction.

PROBLEMS ASSOCIATED WITH MOLECULAR ALKALI DIMERS

The tendency of alkali metals to form clusters of atoms, primarily diatomic molecules but also tri-atomic etc., increases with temperature. These molecules have broad absorption spectra in the visible region of the spectra (Gupta 1978) and may thus be resonantly ionised over a wide range of wavelengths, (Granneman et al 1976). They may also be photodissociated over broad spectral regions, as was shown with caesium in the proportional counter. In resonant ionisation mass spectrometers these molecular ions could interfere isobarically with atomic ions and limit the sensitivity of the mass spectrometer at specific masses. At low temperatures the molecule/atom ratio will be small and molecular ionisation may be negligible. However at higher temperatures (up to 1000 K) the ratio will increase and dimer ionisation may become more noticeable. Furthermore ion sputtering and laser ablation techniques, used to vapourise the sample, may enhance the formation of dimers. Kimock (1984) has suggested that up to 10% of the sputtered particles using ion ablation will be in the form of dimers and larger clusters. Laser ablation may have a similar effect. This aspect was investigated in the time of flight mass spectrometer. Other factors which heighten the problem are isotopic considerations, (ie. there are three Rb_2^+ masses), and the possibility of mixed dimers, such as RbCs and NaRb which may form if more than one alkali metal is present (Kappes et al 1985). Little is known of the absorption spectra of these hetronuclear alkali dimers. Table 6.2 lists some of these with their ionisation potentials.

TABLE 6.2   IONISATION POTENTIALS OF ALL ALKALI DIMERS (Kappes et al 1985)

ATOM	NO. OF ISOTOPES (naturally occuring)	MASS (amu)	ALKALI DIMERS (ionisation potential eV)
Lithium	2	6 (7.5%) 7 (92.5%)	Li_2 (5.145); LiNa (5.05); LiK (4.57); LiRb (4.31); LiCs (4.1)
Sodium	1	23	Na_2 (4.89); NaK (4.41); NaRb (4.32); NaCs (4.05)
Potassium	3	39 (93.2581%) 40 (0.0117%) 41 (6.7302%)	K_2 (4.06); KRb (3.91); KCs (3.9)
Rubidium	2	85 (72.17%) 87 (27.83%)	Rb_2 (3.91); RbCs (3.7)
Caesium	1	133	Cs_2 (3.7)

In order to try to establish the conditions relating to the laser power which would warrant the use of population rate equations to model this two photon ionisation process, the line width of the $5s_{1/2}$-$6p_{3/2}$ transition was measured at different laser powers.

In general for population rate equations to apply power broadening should not be the dominant cause of line broadening (Hurst et al 1979a, Ackerhalt et al 1977)

Figure 6.55 illustrates the increase in the observed transition line width as the laser power is increased by a factor of 100 from 2.7 mJ cm^{-2} to 0.22 J cm^{-2}. The linewidth increases approximately with the square root of the laser energy flux. There may be saturation of the ionisation step ($\sigma_i = 4 \times 10^{-18}$ cm^2) at the highest powers used.

On resonance at high laser powers the line width should be proportional to the square root of the laser intensity. The Rabi frequency on resonance, between states a and b, R_{ab} (equation 2.66) is,

$$R_{ab} = <a|\underline{r}|b> eE_0/2\hbar$$

From Sobelman (1979) the oscillator strength of the $5s_{1/2}$-$6p_{3/2}$ absorption transition in rubidium is ~0.01. The cycle averaged energy flux of the laser I (J cm^{-2} sec^{-1}) is related to the electric field strength E_0 (V m^{-1})of the EM wave,

$$I = \varepsilon_0 E_0 c/2$$

where ε_0 is the permitivity of free space and c is the velocity of light. For an unfocussed laser of power 1 mJ cm^2 per 10 nsec pulse, $E_0 = 8.6 \times 10^5$ V m^{-1}. The Rabi frequency is thus 1.35×10^{10} sec^{-1} and the broadening ($4R_{ab}$) is ~5.5×10^{10} sec^{-1}, which is much less than the laser line width $\Delta\omega_L \sim 5 \times 10^{11}$ sec^{-1}. For a focussed laser of power 0.1 J cm^{-2} in a 10 nsec pulse the broadening is ~5.5×10^{11} sec^{-1} which is of the same order as the laser line width. Therefore power broadening should only be noticeable above this level. The observed line broadening and estimated power broadening are plotted in figure 6.56 as a function of laser power. The observed broadening is about a factor of 10 greater than the estimated power broadening.
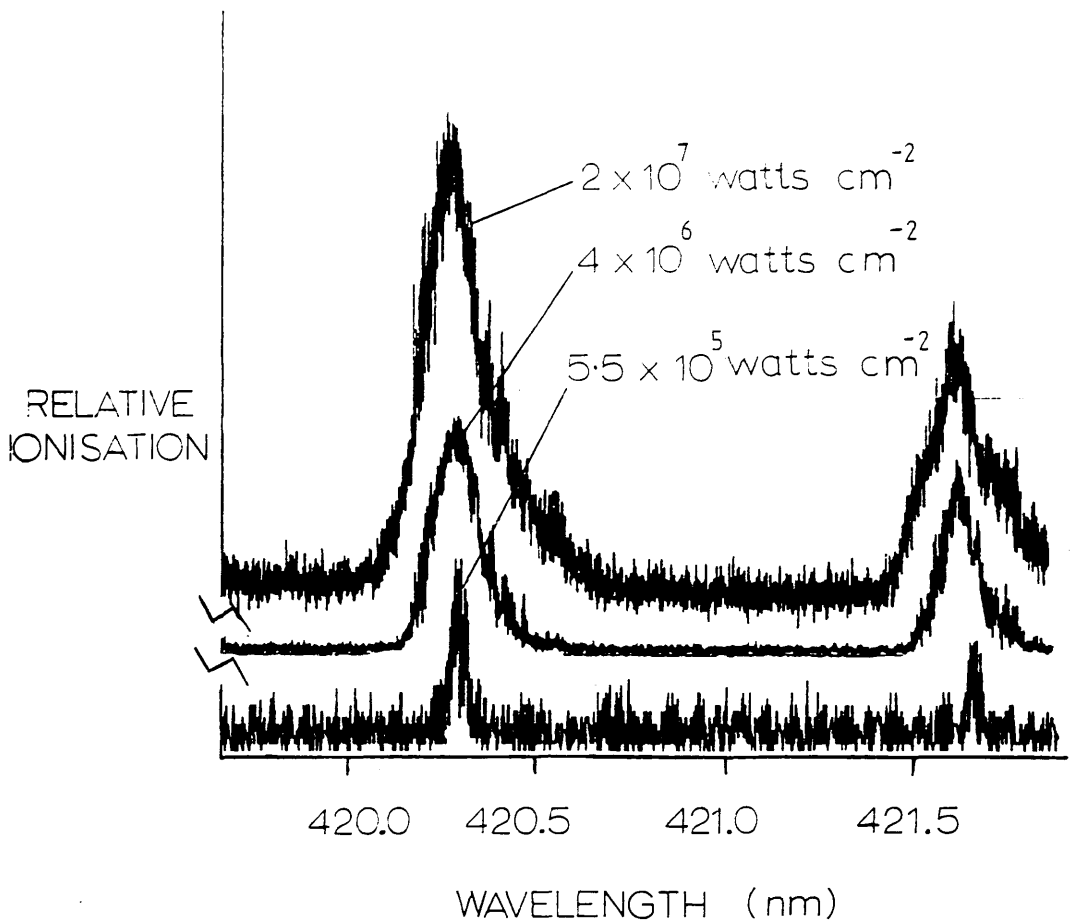
Fig 6.55 Broadening of the 5s-6p transition width in atomic rubidium with increasing laser power
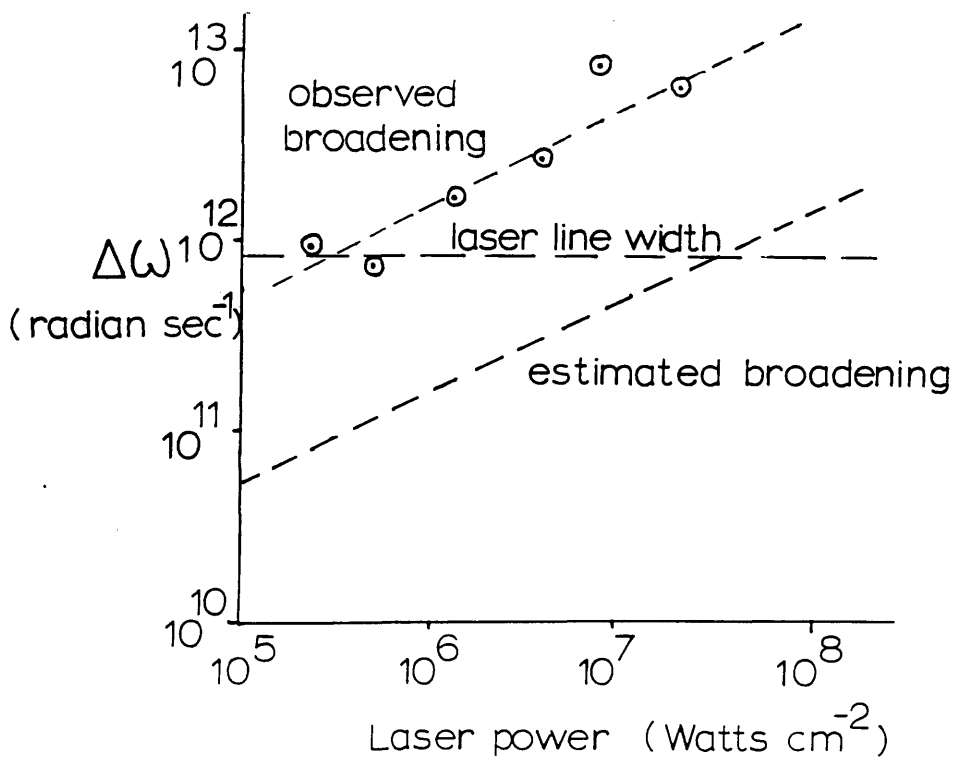
Fig 6.56 Dependence of observed broadening and estimated power broadening, of the two photon ionisation of rubidium via the single photon 5s-6p transition, on laser power. The observed broadening is about a factor of 10 greater in magnitude.

One explanation for the much larger observed width of the transition compared to the expected value is that the spectral profile of the dye laser may have sidebands which could resonantly excite the transition, ionisation of the excited level being due to the main frequency band of the laser, (Nogar and Keller 1985). There is some evidence for this in the structure that can be discerned in the resonant profile of the laser transition. Peaks are evident, separated by ~0.05 nm. Similar structure can be observed in both pairs of the doublet transitions. A similar effect was also noticeable in the resonant ionisation of rubidium in the time of flight mass spectrometer, which suggests that the phenomenon may be common. These sidebands are thought to originate in the amplifier cell of the dye laser, or be due to an interaction between the amplifier cell and grating, (Nogar and Keller 1985). Their presence and ability to strongly excite resonant transitions, when the main frequency band of the laser is tuned off resonance, could reduce the selectivity of the resonant ionisation process.

CHAPTER 7

INITIAL RESULTS OF LASER INDUCED IONISATION IN TIME OF FLIGHT MASS SPECTROMETER

7.1 LASER ABLATION/IONISATION OF RUBIDIUM AND ALKALI CHLORIDE SALTS

This chapter reports the initial results from the time of flight mass spectrometer, and also examines the potential sensitivity of the instrument using a pulsed ion gun to vapourise the sample.

The detection of rubidium ions was thought to be a good means to physically align the time of flight system and optimise its performance. It was also hoped to determine the magnitude of the rubidium dimer ion signal, relative to the atomic signal, sputtered from the sample surface, and to investigate the resonant laser ionisation of these dimers.

Rather than use rubidium metal, which would be difficult to introduce into the mass spectrometer, a sample of rubidium chloride was chosen. This was deposited on a conducting graphite substrate to ensure that charge would not build up on the sample stub. Positive charge from the argon ions could build up on the stub, lowering the potential difference between the ion gun and the stub, thereby reducing the effective energy of the incident ions and lowering the sputter yield. One other undesirable consequence of a build up of charge on the sample stub would be its effect on the electric field in the extraction region of the ion optics. The pulse to pulse strength of the extraction field may vary leading to a time jitter in the detected signal. Conducting samples are therefore highly desirable. The concentration of rubidium in the sample was of the order of parts per ten.

The resonant transition selected was the $5s_{1/2}$ - $6p_{3/2,1/2}$ doublet transition around 420 nm enabling the two photon ionisation of rubidium using one laser. Due to the pulse generator in the ion gun breaking down, the initial results were obtained using the dye laser to ablate and resonantly ionise the rubidium atoms. The laser was focussed

on to the sample at an angle of ~85° incidence from the normal to the sample stub, and at the focal point the energy density was approximately 5 J cm^{-2}. Figure 7.1 illustrates an ionisation spectrum, at mass 85, obtained with this resonant ablation technique in which both the ablation and resonant ionisation take place place during a single laser pulse. The resonant transitions can be distinguished. The nonresonant ionisation of rubidium is from rubidium ions ablated directly from the sample. Figure 7.2 is an ionisation spectrum at mass 170 taken over the same wavelengths and using the same technique. Ions are seen at all wavelengths. They are formed from the two photon resonant ionisation of Rb_2 molecules and from the nonresonant sputtering of molecular ions. The three rubidium dimers could be resolved in the mass spectrometer and were approximately 10% of the size of $^{85}Rb^+$ signal. With a different sample containing rubidium at a much lower concentration, (parts per thousand), the dimer signal could not be detected. This is illustrated in figure 7.3, again using the ablation/ionisation technique with the laser at 420 nm. The sample was made up from a mixture of NaCl, KCl and RbCl deposited on a conducting graphite substrate. The concentration of Na, K and Rb in the sample was estimated at the parts per thousand level. The naturally occuring isotopes of lithium, potassium and rubidium were detected but no alkali dimer signal of any species was detected.

Dimers will also occur in other elements apart from the alkali metals. Figure 7.4 illustrates a mass spectrum showing the ablation/ionisation of lead and its dimers at a wavelength of 355 nm. The dimer signal is approximately 10% of the atomic signal.

Only at very high concentrations of rubidium in a sample were dimer signals a significant proportion (~10%) of the atomic signal. At lower concentrations the dimer signal is negligible, at least using the technique of laser ablation/ionisation.

7.2 CONTINUOUS ARGON ION SPUTTERING AND RESONANT IONISATION OF RUBIDIUM

The formation of dimers by ion sputtering could not be investigated since the argon ion gun could only be operated continuously. Figure 7.5a is a resonant ionisation spectrum of the same 5s-6p doublet transition in rubidium, but using instead a DC argon ion gun to ablate and vapourise the RbCl sample. Figure 7.5b is a mass spectrum showing the two rubidium isotopes. The dimer signal was not seen in this spectrum, but this may have been due to the large secondary ion background obscuring the signal. In both
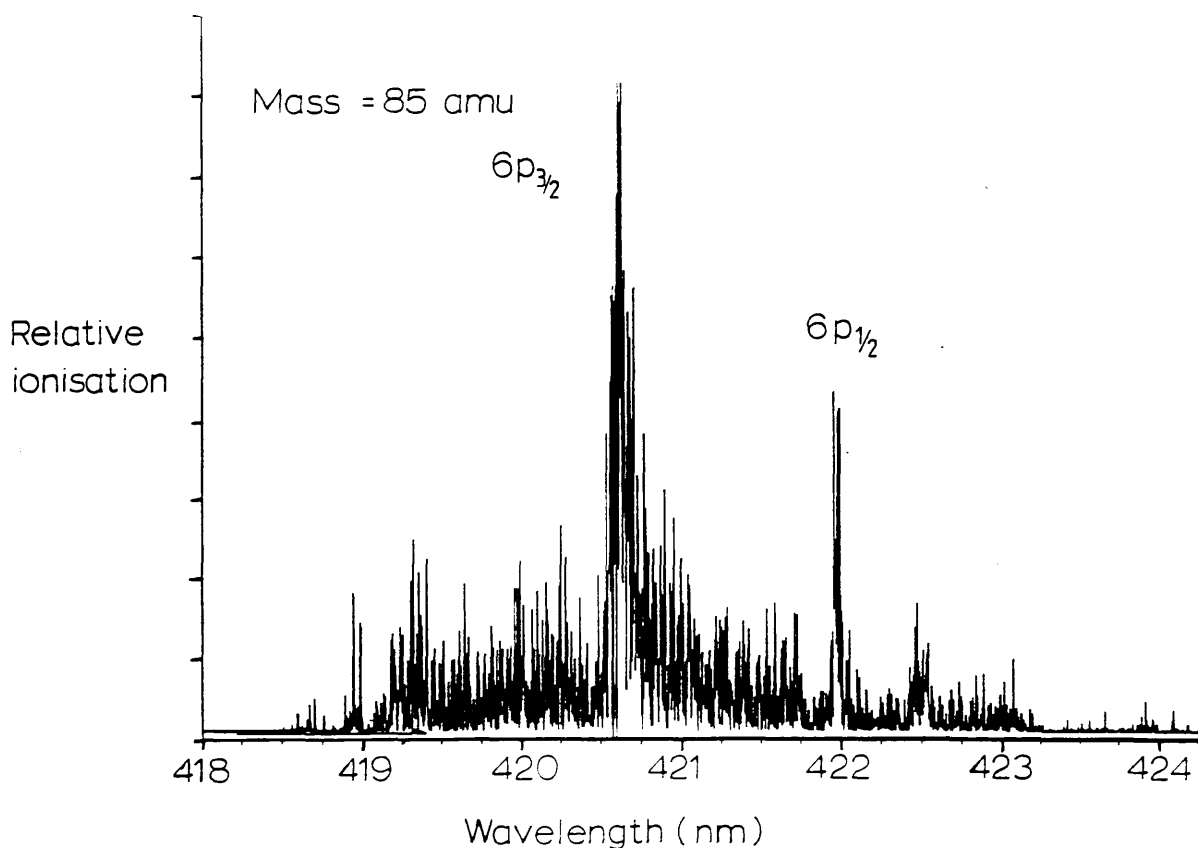
Fig 7.1   Ionisation spectrum by laser ablation/ionisation, at mass 85, of a
sample of rubidium chloride doped onto a conducting graphite matrix.
The $5s_{1/2}$-$6p_{3/2,1/2}$ doublet transition can be resolved. The off
resonance ionisation is from the photo-dissociation and ionisation of
Rb_2 molecules and from rubidium ions ablated directly from the
sample at all wavelengths.
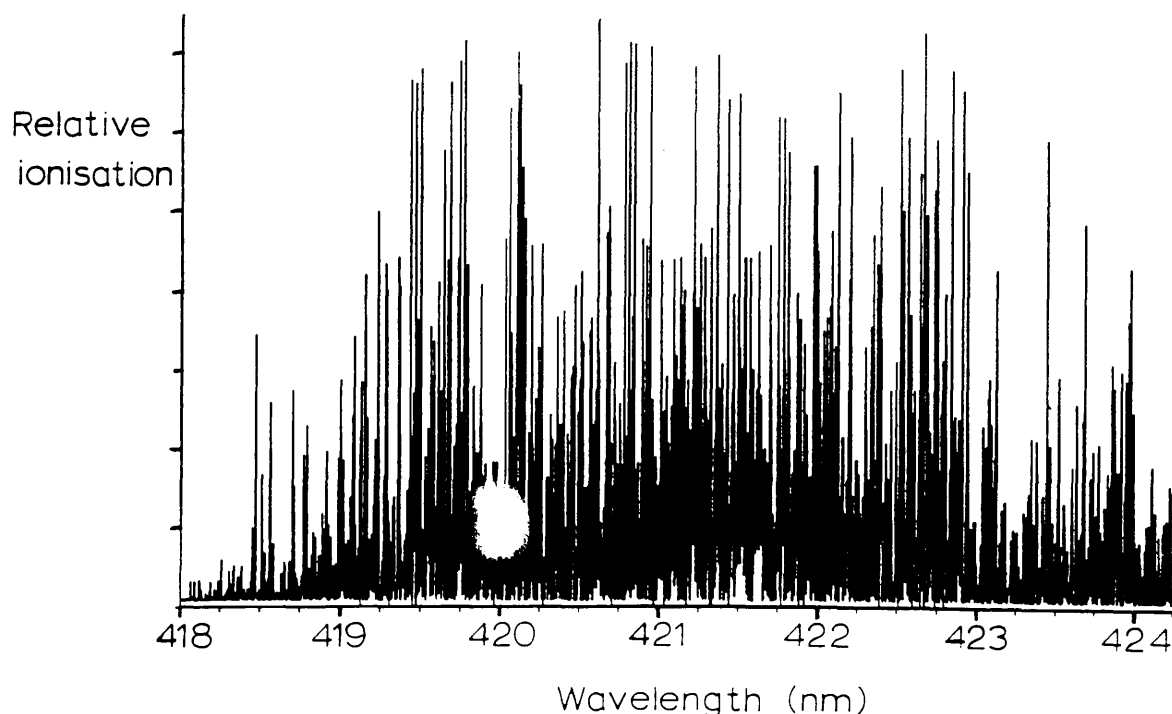
Fig 7.2   Ionisation spectrum by laser ablation/ionisation, at mass 170 (Rb_2),
of a sample of rubidium chloride doped onto a conducting graphite
matrix.
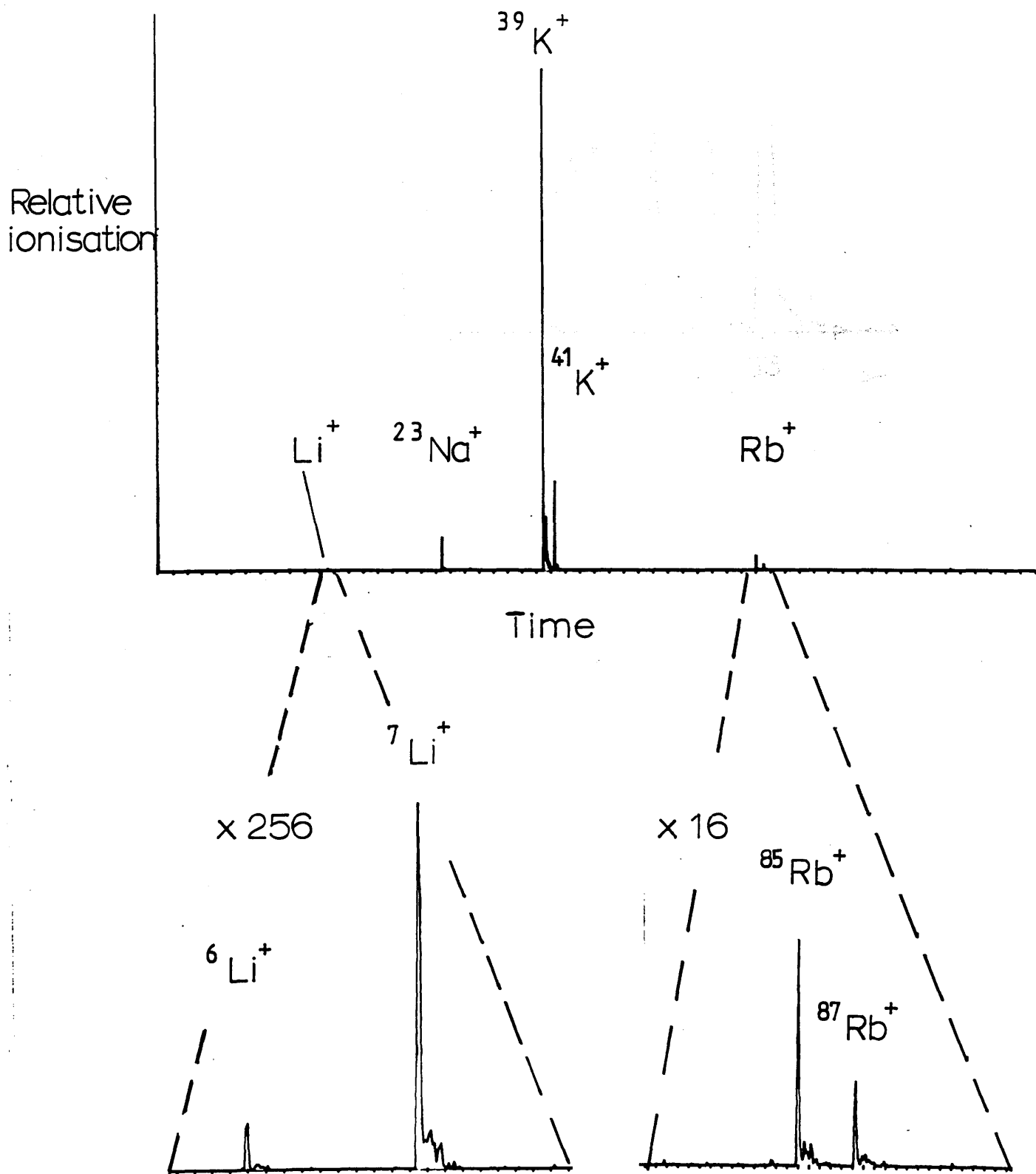
Fig 7.3   Mass spectrum by laser ablation/ionisation at 420 nm of a mixture of alkali salts (NaCl, KCl, RbCl) in a graphite matrix. The concentration of the alkali metals in the sample matrix is of the order of parts per thousand. The laser was focussed with a power of 100 μJ in the focal area. No alkali dimers of any kind are evident.
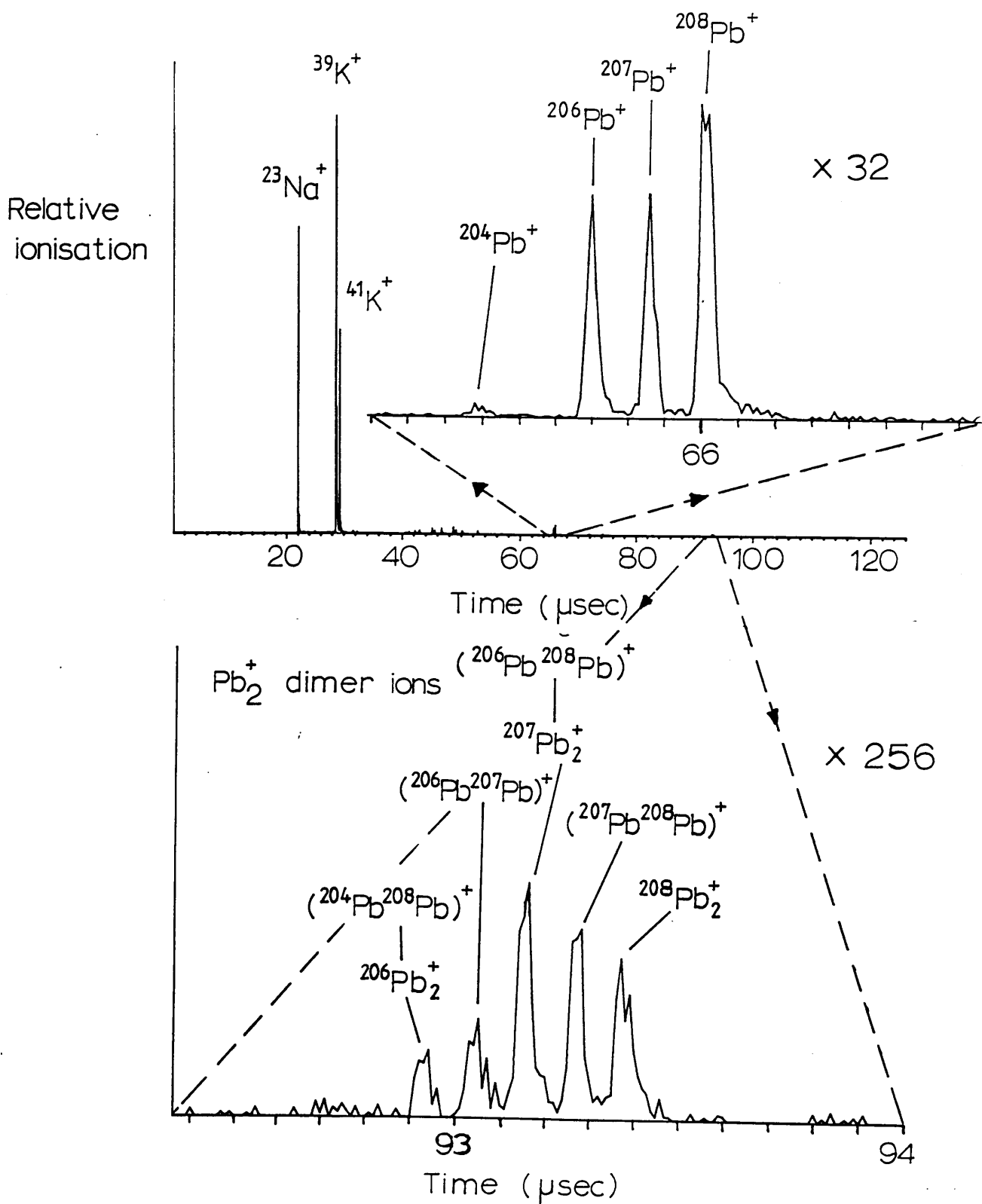
Fig 7.4   Mass spectrum by laser ablation/ionisation at 355 nm of a solid
sample of lead. The Pb_2^+ signal is approx imately 10% of the Pb^+
signal. The Na^+ and K^+ ions are contaminants from a previous sample.

spectra the laser was unfocussed with beam dimensions 2.5 mm x 2.5 mm, and power 10 mJ cm^{-2}.
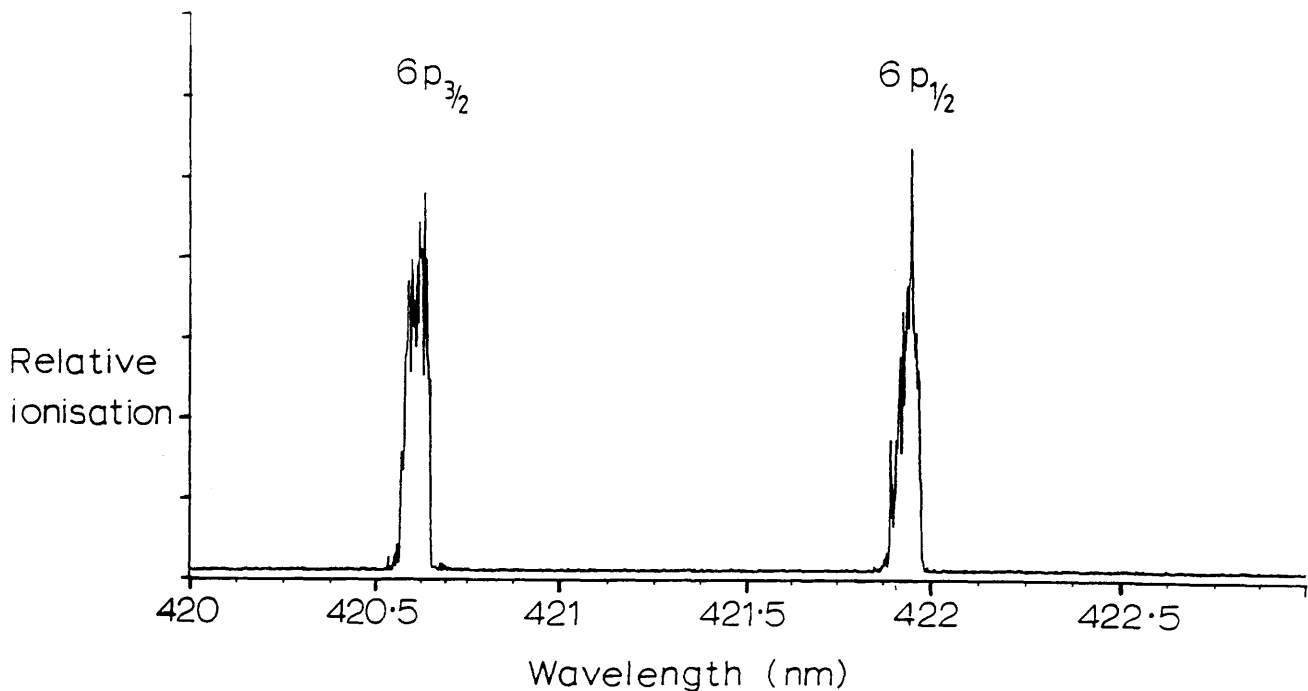
Fig 7.5a Two photon resonant ionisation spectrum of ^{85}Rb, using continuous argon ion sputtering of a sample of rubidium chloride doped onto a conducting graphite matrix, showing the single photon $5s_{1/2}-6p_{3/2,1/2}$ doublet transitions.
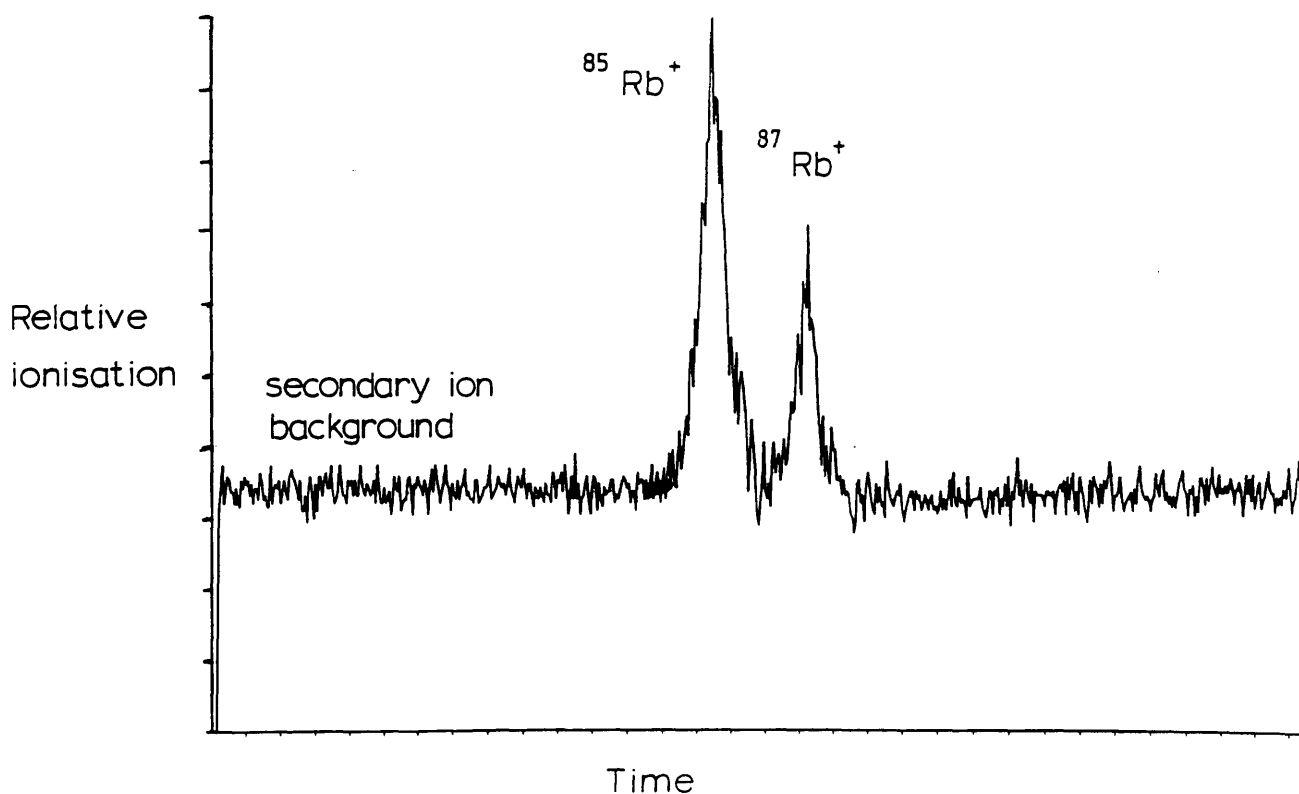
Fig 7.5b Mass spectrum using continuous argon ion sputtering of a sample of rubidium chloride doped onto a conducting graphite matrix. The laser was at 420.6 nm, resonant with the $5s_{1/2}-6p_{3/2}$ transition. No Rb_2^+ ions were seen in this spectrum, but they may have been obscured by the large secondary ion background.

7.3 PROJECTED SENSITIVITY WITH PULSED ION SPUTTERING OF A SOLID SAMPLE.

The TOF mass spectrometer is a purpose built instrument designed for the laser induced ionisation of ablated and sputtered samples, ablation using a pulsed laser and sputtering using a pulsed argon ion gun. A lower limit of the concentration of trace elements which may be detected, using the pulsed ion source to vapourise the sample, has been established at around 10 parts per billion (ppb). The determination of this lower limit is quite straightforward and is important in that areas may be identified in which significant improvements can be made.

The analysis can be split up into three steps: sputtering, resonant ionisation and detection. Each step will be looked at in turn.

SPUTTERING

Sputtering is defined as the removal of atoms (and molecules) from a surface by bombardment with fast ions or neutrals. This is an effective method of vapourising the surface of a solid sample. With the current instrument argon ions are used for the bomdardment, and the ion beam can be pulsed or applied continuously. The need for a pulsed ion beam comes from the quite stringent condition of saturation of the resonant ionisation process. Currently avaliable dye lasers, used for resonant ionisation, will only operate at high flux (the saturation condition) when pulsed at around 30Hz, with a pulse length of ~10 nsec. Therefore for efficient utilisation of a sample a pulsed ion beam is necessary, synchronised to sputter the sample just before the pulsed lasers are fired. Smaller samples may then be used. Present day continuous wave lasers have neither sufficient power to saturate the resonant ionisation step, nor operate strongly in the near UV wavelengths, a necessary requirement for the excitation of many atoms.

VELOCITY DISTRIBUTION OF SPUTTERED ATOMS

Atoms sputtered from a sample surface will have kinetic energies spread over a wide range (up to keV) but peaked sharply around the surface binding energy of the target atom, which is of the order of a few eV. An example of the spread in energies from a sample of gold atoms bomdarded with 20 keV argon ions is illustrated in figure 7.6, (Townsend et al 1976). Binding energies depend on the atom and on the surrounding sample matrix. Kimock et al (1984) quotes a value of 5 eV for the surface binding
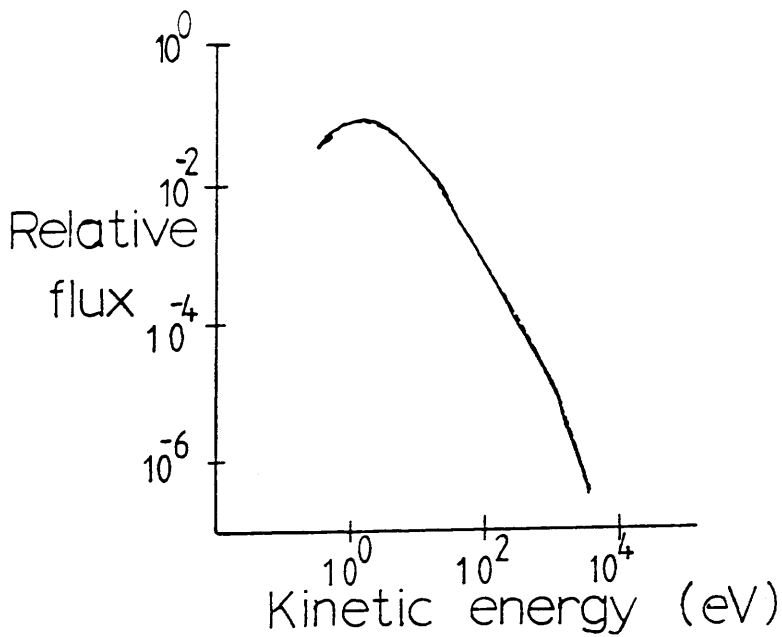
Fig 7.6   Kinetic energy distribution of ions sputtered from a sample of gold by 20 keV argon ions, (Townsend et al 1976).
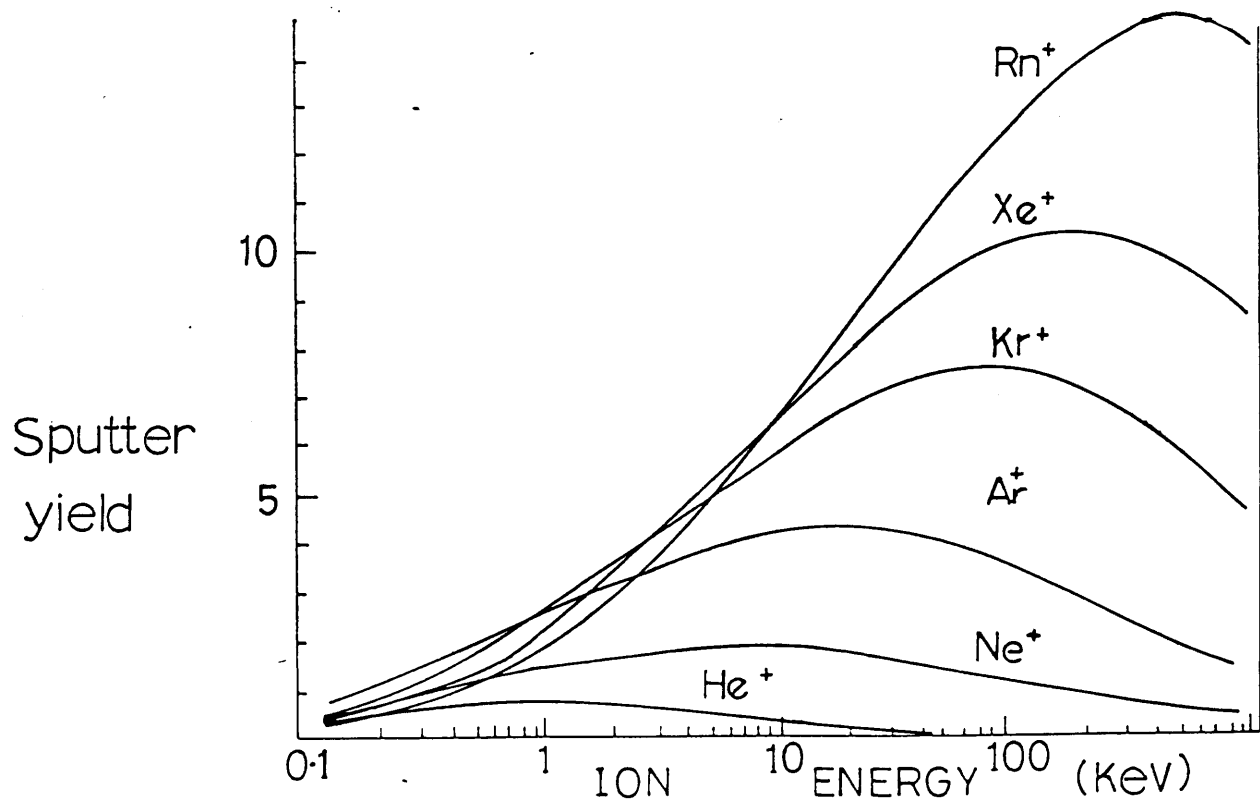
Fig 7.7   Variation of sputter yield from sample surface with increasing incident energy of noble gas ions, (Townsend et al 1976).

energy of indium in a matrix of silicon.

The laser pulse is of the order of 10 nsec and the atoms are effectively frozen during this time. Only a fraction of the sputtered atoms will therefore be in the laser pulse, those travelling too fast or too slow being outside the laser beam dimensions.

This energy spread may introduce unwanted mass descrimination. For example, assuming that all masses are sputtered with a range energies centred around 5eV then, at the end of a 3 μsec ablation pulse, atoms of mass 1 amu will have a distribution peak approximately 9 mm from the target, whilst atoms of mass 100 amu will have a distribution peak 0.9mm from the target. A narrow diameter beam of diameter ~2 mm would not illuminate a representative mixture of the constituents in the original sample surface layers.

SPUTTER YIELD

The number of atoms sputtered per incident ion is termed the sputter yield and is dependent on factors such as the incident energy and incident angle of the ion, the mass of the incident and target atoms and the binding energy of the target atom. This is illustrated in figure 7.7 which illustrates the calculated sputtering yields for aluminium as a function of ion energy and ion mass. The most effective angle of incidence has been established at between 45° and 60° to the sample normal, (Townsend et al 1976). However if crystalline samples are used the incident angle may be along a crystal plane resulting in a sharp drop in the sputter yield at particular angles. From figure 7.7, a 5 keV argon ion incident on a target at 55° to the normal will sputter around 5 atoms from the sample

MATRIX EFFECTS

It is believed that matrix effects, of the preferential sputtering of one species of atom or molecule over another, may not be too severe or at least not as severe as in secondary ionisation mass spectrometry, (Becker et al 1984, Kimock et al 1983, Parks 1983). The basis for this assumption is that the number of sputtered neutrals is much larger than the number of sputtered ions (10^2-10^4) resulting in the sputter yield being less sensitive to the particular target atom. Atoms with higher sputter yields are in general preferentially sputtered over those with lower sputter yields, (Kimock et al 1984).

Matrix effects severely hamper the quantitative interpretation of results from secondary ionisation mass spectrometers, (Morrison 1981).

The optimum pulse length of the ion beam is a balance between having the maximum number of atoms in the laser beam and not wasting the sample unnecessarily. The pulse length of the Glasgow instrument can be varied between 0.2 μsec and 3 μsec. For a 15 μA continuous argon ion beam of energy 3 keV, pulsed at 10Hz (the Nd:YAG laser repetition rate), with a 3 μsec pulse length, and with a sputter yield of 5, the number of atoms sputtered will be 10^{10} per second.

RESONANCE IONISATION

SELECTED STATE OF SPUTTERED NEUTRALS

Neutral atoms of the same species sputtered from the sample surface may be in different energy states. Resonance ionisation requires that they are in a known energy state and preferably the ground state. Thus only the fraction of atoms which are in the ground state (or known state) will be resonantly ionised. This fraction will be dependent on the particular atom selected, but averaged over all elements in the periodic table it is suggested that 50% of all yield atoms will be in the ground state, (Young et al 1987).

GEOMETRICAL OVERLAP BETWEEN THE SPUTTERED VAPOUR PLUME AND LASER BEAMS

The sputtered plume is interrogated by the laser beam. During the laser pulse of 10 nsec the atoms are effectively spatially frozen, and the fraction of sputtered ions in the beam can be estimated from simple geometrical considerations. These include the diameter and position of the laser beam, the diameter of the ablation beam impacting on the sample and the time delay between the ablation and laser beams. Enlarging the laser beam so as to maximize the overlap lowers the laser flux and may decrease the ionisation probability. Large beam diameters will also decrease the mass resolution of the time of flight mass spectrometer. The diameter of the ion beam should be kept less than the laser ionisation beam, but as the incident current increases, space charge effects in the ion beam tend to limit the minimum focussed spot size, (Kimock 1984). The optimum time delay between the sputtering pulse and ionisation pulses is only critical in that, if the ion pulse has a long "tail", nonresonant sputtered ions will be

121

mixed in with resonant laser induced ions. As outlined previously some mass discrimination may take place due to the timing consideration.

The number of atoms in the laser beam will thus vary depending on the ionisation scheme used, and the mass resolution required. The maximum number will be around 25% for large diameter beams of around 6mm diameter close to the sample with atoms coming from a point source (Kimock et al 1984). Parks et al (1985), using a 1mm diameter beam centred 3 mm from the surface sample estimated a 10% geometrical overlap factor, and a timing factor of 15%, giving an overall 1.5% of sputtered atoms which are in the laser beam.

IONISATION EFFICIENCY

Resonant ionisation by single photon steps can be 100% efficient in that every irradiated atom in a selected state can be ionised, if the statistical weights of each level are ignored. Resonant multiphoton Ionisation via virtual states requires a much higher flux to saturate and non-resonant multiphoton ionisation of the same order an even higher flux. The ionisation probability will therefore depend on the particular ionisation scheme used and a value of 10% ionisation is estimated, (Becker et al 1985).

DETECTION EFFICIENCY

Modern time of flight mass spectrometers are very efficient at transmitting ions to the detector. The inclusion of an ion mirror may lower this to around 10%, (Price et al 1984). The multichannel plate ion detector is around 80% efficient. The total detection and transmission efficiency will thus be approximately 10%.

OVERALL SENSITIVITY

The lowest concentration in a matrix at which the target atom could be detected at a rate of 1 ion per second is 1 part in 10^8, assuming 100% ionisation, 10% geometrical overlap, a 10% transmission and detection efficiency and with 10^{10} atoms sputtered per second.

As a comparison Parks et al (1985) have claimed the ability to detect impurities at the 0.1 ppb level in an analysis time of 5 minutes, using sputter initiated RIS in a

magnetic sector mass spectrometer. The actual detection of 2 ppb of boron in silicon was reported using this apparatus. Their 100 fold increase in sensitivity over the projected sensitivity of the Glasgow time of flight instrument, is mainly due to their ability to detect only 100 ions of a particular mass in the analysis time of ~10,000 seconds. The time of flight mass spectrometer, which has a gated detector, has an estimated detection limit of ~1 ion per second, a factor of 100 less sensitive.

INCREASING THE SENSITIVITY

The sensitivity of the current instrument is limited to around the 10 p.p.b. limit. The two main factors determining this limit are the low duty cycle imposed by the 10 Hz repetition rate of the Nd:YAG pumped dye laser system, and the low current flux from the argon ion gun.

Excimer pumped dye lasers can operate up to 1000 Hz, and copper vapour lasers up to 10 kHz, (Peuser et al 1985). This would lower the detection limit by between 2 and 3 orders of magnitude. Brighter argon ion sources of up to 1mA continuous beam and with ion energies up to 30 keV are available, and would increase the number of sputtered atoms by around the same magnitude, again lowering the detection limit, (Kimock et al 1983).

The ionisation probability is largely determined by the final photoionisation step from the excited state of an atom. Photoionisation cross-sections are typically 3 orders of magnitude smaller than the excitation cross-sections. To saturate the photoionisation step requires much higher laser powers than are necessary to saturate the photoexcitation steps. If the photoionisation step could be eliminated or be made more efficient the laser flux necessary to saturate the total ionisation process could be reduced. Larger laser beams would then be available with a proportionate increase in the geometrical overlap between the laser beam and the sputtered atom plume. One other advantage would be that with a less intense laser beam the background nonresonant ionisation would be less likely.

There are three main schemes which have been mooted as more efficient alteratives to photoionisation to the continuum. These are collisional ionisation from highlying Rydberg levels, field ionisation from Rydberg levels and transitions to autoionisation states of the atom or molecule. As has been demonstrated with caesium and rubidium

vapours, collisions between highly excited atoms and buffer gas atoms can ionise the excited atoms very efficiently and can enhance the ionisation over photoionisation by up to two orders of magnitude, (Whitaker et al 1981). However collisional ionisation would not be feasible in a mass spectrometer operating at ~10^{-8} torr. Pulsed electric fields above a threshold field strength and applied just after the photoexcitation step(s), will ionise highly excited atoms with unit probability, (Letokhov 1987). Autoionisation states effectively lie in the continuum and can be excited by transitions from levels below the continuum. The autoionisation cross-sections can be around two orders of magnitude greater than the normal nonresonant photoionisation cross-sections, and can thus be saturated more easily, (Bekov et al 1978a). However it is not a suitable process for those atoms such as the alkali metals, which have second ionisation potentials of around 20 eV. The spectral position of these states is also not well tabulated.

For example if a copper vapour laser operating at 6.5 kHz were used instead of the Nd:YAG laser, and an ion beam of primary current 10 mA, at 25 keV energy and with a pulse length of 5 μsec, the number of ions sputtered per second would be ~2×10^{15}, assuming a sputter yield of 10 neutral atoms per incident ion. The detection limit would be increased by 5 orders of magnitude, if the other parameters such as the resonant ionisation probability stayed the same.

It would not be too surprising if the detection limits are found to vary by one or two orders over the elements in the periodic table, since this will depend strongly on the resonant ionisation schemes that are available, and on the mass resolution required which may vary from element to element. The general detection limits quoted for these instruments must be viewed in this light. Much of the work at Glasgow will be spent on obtaining reproducible quantitative results in the sub ppm regime.

7.4 A POTENTIAL APPLICATION - LOW LEVEL COUNTING OF RADIOACTIVE ATOMS

Mass spectrometers, which detect the parent or daughter isotope, would seem to be better suited to the detection of long lived radionuclides than conventional radiometers, which monitor the decay event. Furthermore the conventional radiometric analysis of low-energy β⁻ emmiters is difficult and requires a specific activity of around 1 picocurie per gram of a sample (3.7×10^{-2} Bq g⁻¹), (Halverson 1984). The detection of long lived but low energy β⁻ emitters is thus an example of a potential

application of resonant ionisation mass spectrometry which could be carried out with the present time of flight instrument at Glasgow. These radioactive nuclides, which are currently discharged into the sea from nuclear power and reprocessing plants, may be of considerable environmental importance in that the specific ionisation in biological matter is greatest for low energy β^- particles, (Baxter 1983).

In order to assess which radioactive isotopes could be detected, the specific activity of 1 pC per gram can be converted to a concentration of that element per gram of sample, that is a function of the elements half-life. Assuming a gram of an environmental sample to contain around 10^{22} atoms, the concentration of important radionuclides of varying half-lives is shown below (table 7.1), assuming all the activity to come from one radionuclide.

The projected sensitivity of the mass spectrometer at Glasgow University might enable ^{129}Iodine to be detected at around the 1 ppb level. The detection of ^{135}Cs and ^{99}Te would certainly require a higher degree of sensitivity, possibly by the use of some of the methods outlined, such as a brighter ion sputtering source, or a pre-enrichment of the sample.

TABLE 7.1

Z	A	Element	Half life (years)	No of Atoms per gram	Concentration
38	90	Strontium	28	3.26×10^7	3.26×10^{-15}
43	99	Technetium	2.13×10^5	2.48×10^{11}	2.48×10^{-11}
48	113	Cadmium	14.6	1.7×10^7	1.7×10^{-15}
53	129	Iodine	1.57×10^7	1.83×10^{11}	1.83×10^{-9}
55	135	Caesium	2.06×10^6	2.4×10^{12}	2.4×10^{-10}
55	137	Caesium	30.17	3.5×10^7	3.5×10^{-15}
61	147	Prometium	2.62	3.05×10^6	3.05×10^{-16}

CHAPTER 8

CONCLUSIONS

8.1 BACKGROUND IONISATION OF HYDROCARBON IMPURITIES

The resonant ionisation of hydrocarbon or organic molecules with low ionisation potentials could limit the sensitivity of all types of resonance ionisation spectrometers. The molecules have ionisation structure which may interfere with the resonant signal of interest in proportional counters, whilst photodissociation of the parent molecule into many different masses may interfere with the sample ion in mass spectrometers. As the wavelength is increased from 300 nm to 330 nm the ionisation of these organic molecules in proportional counters is reduced by a factor of more than 10^3. This reduction in the background ionisation with increasing wavelength is also noticeable in the time of flight mass spectrometer. Figures 8.1a and 8.1b are mass spectra with laser ablation/ionisation of a sample of alkali salts, (NaCl, KCl, RbCl), doped onto a conducting graphite matrix. The laser was operated at two different wavelengths, 266 nm and 355 nm. Ions are formed in the ablation process itself and from the nonresonant multiphoton ionisation of ablated neutral atoms. There is a marked decrease in the number and intensity of hydrocarbon (organic) ion masses at the longer wavelength, indicating both a reduction in the ionisation of these molecules and in their photofragmentation. By using wavelengths greater than ~330 nm for the resonant excitation and ionisation steps, the ionisation of organic impurities should be made negligible.

In proportional counters the impurities may be inherent in the materials from which the counter is constructed, they may be introduced during the initial cleaning of the counter, or they may be in the buffer gas itself.

Organic impurities may also come from vacuum pump oil. Figures 8.2a and 8.2b illustrate background ionisation mass spectra at 266 nm in the time of flight mass spectrometer, at a pressure of 10^{-8} torr. The ionisation is from organic molecules in the ionisation region which are thought to be from the diffusion pump oil. This oil is a poly-phenol molecule with a molecular weight of 446 amu. As the laser is focussed the
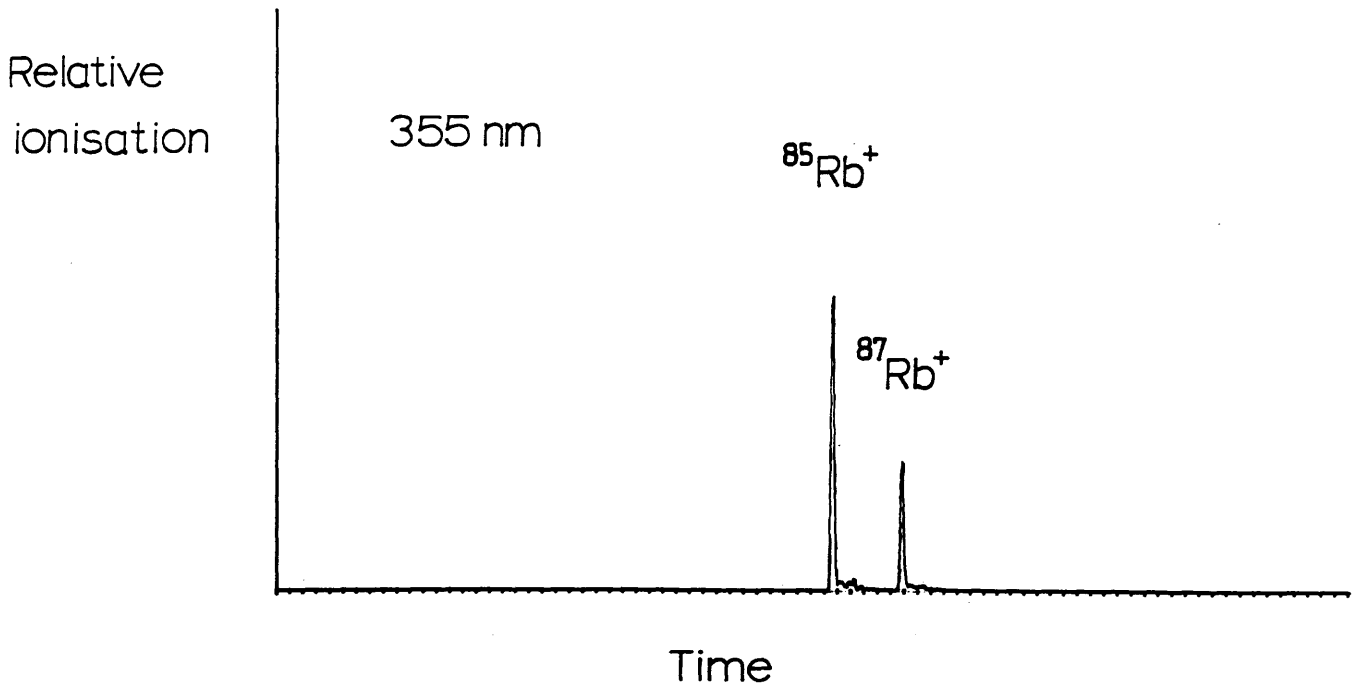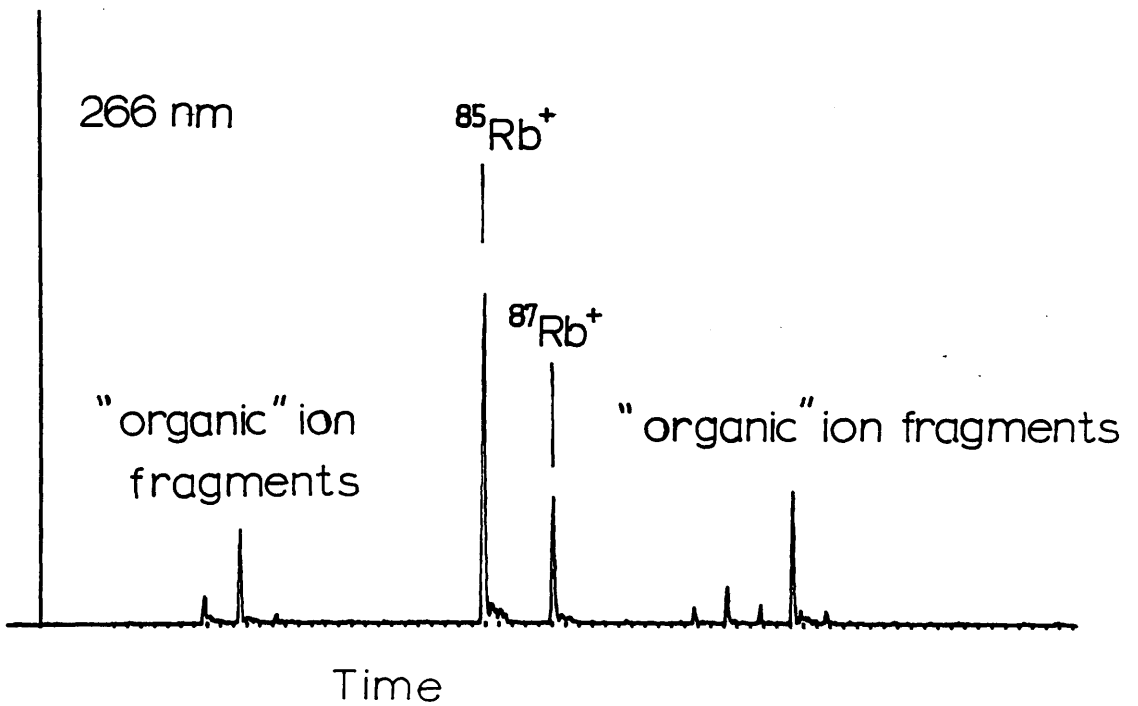
Fig 8.1   Laser ablation/ionisation at 355 nm (a), and 266 nm (b), of a mixture of alkali chlorides (NaCl, KCl, RbCl) doped onto a conducting graphite matrix. Organic ion fragments, probably from the graphite matrix, are only evident at 266 nm.

a.

focussed laser

Relative
ionisation

H^+

C^+

C_2^+

C_3^+

C_4^+

Time

b.

unfocussed laser

Relative
ionisation

H^+

C^+

C_2^+

C_3^+

C_4^+

C_5^+

$C_6H_5^+$
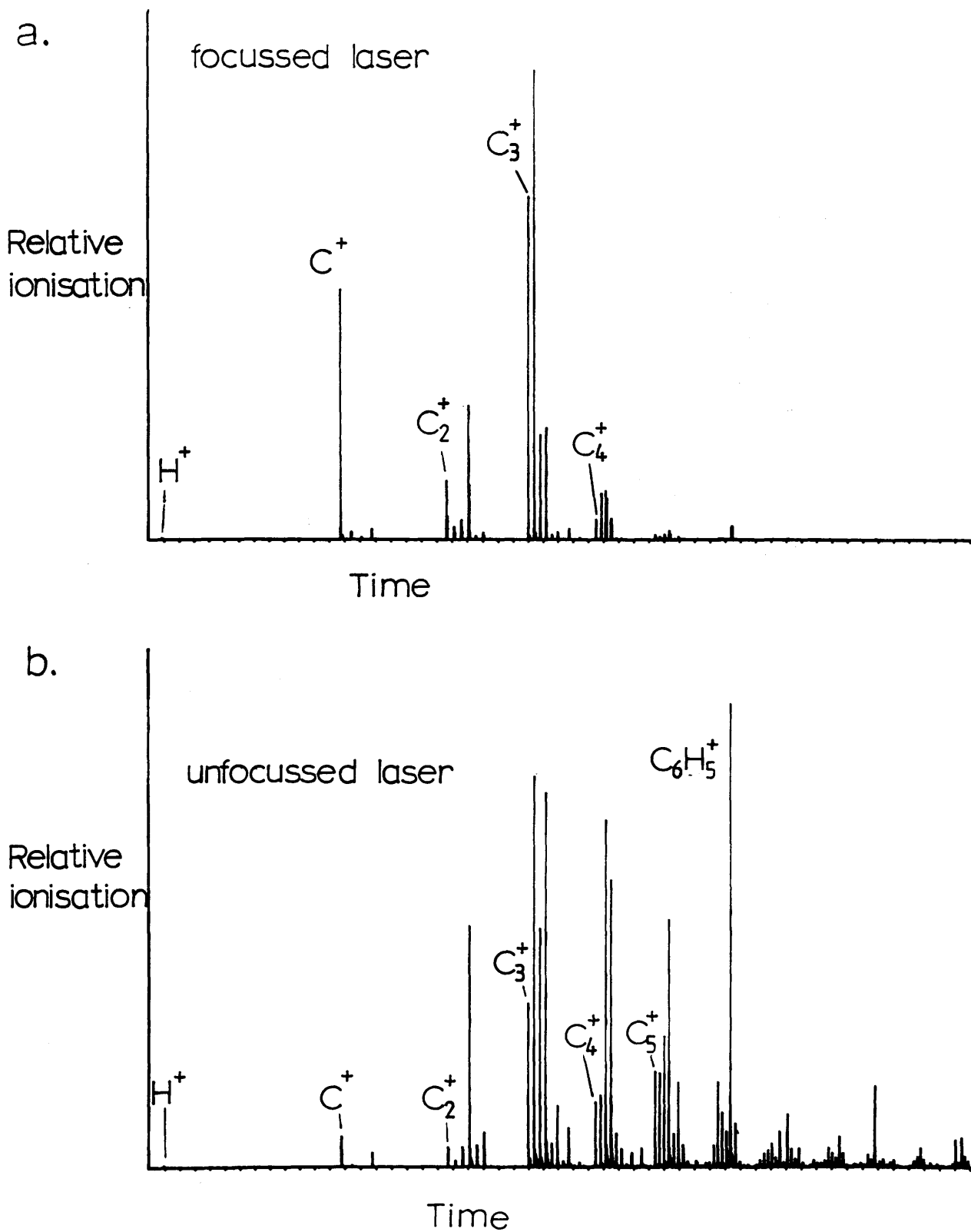
Time

Fig 8.2   Organic ion fragments formed in the ionisation region of the time of flight mass spectrometer when irradiated with laser at 266 nm, focussed (a) and unfocussed (b). Focussing the beam increases the fragmentation. The major parent molecule is thought to be diffusion pump oil which is a poly-phenol molecule of weight 446 amu.

frqgmentation of the hydrocarbons increases, evidenced by the much larger size of the C^+ ion relative to the higher $C_nH_m^+$ ion clusters.

8.2 RESONANT IONISATION OF CAESIUM

Caesium can be detected in a proportional counter at concentrations below 1 part in 10^9, by two photon resonant ionisation via the $6s_{1/2}$-$7p_{3/2}$ transition, (Houston 1986). Alternatively the atoms can be resonantly excited to high lying Rydberg p levels and be collisionally ionised with unit probability. Photoionisation from Rydberg levels is very inefficient and collisional ionisation of these states may enhance the ion yield by a factor of 500. The relative merits of these two techniques ie. photoionisation via the resonant excitation of low lying levels as opposed to the collisional ionisation of highly excited Rydberg levels, has not been investigated. This would require a comparison to be made of the ion yields obtained from both processes when saturation conditions are obtained. The realisation of ionisation saturation is not trivial and may be dependent on the different wavelengths and thus different dyes used for the two processes, (Kimock 1984).

The spectral structure of the three photon resonant ionisation of atomic caesium shows evidence of a large quasi-molecular ionisation component, arising from the photodissociation of caesium dimers to a ground state and an excited state atom. The excited atom is then two photon resonantly ionised. This technique can be used to nonresonantly excite caesium atoms from the ground state to higher lying p and d states effectively extending the single photon resonant spectroscopy to a two step process. Use can also be made of the photodissociation to map out the energy levels of Cs_2 molecules, (Collins et al 1981a, 1981b).

8.3 RESONANT IONISATION OF RUBIDIUM

The resonant ionisation in a proportional counter of particular transitions in rubidium was found to be strongly dependent on the pressure of the proportional counter gas. This pressure induced ionisation makes modelling the resonant ionisation more difficult and may also limit the effectiveness of proportional counters for analytical work, in that it will be difficult to draw direct comparisons between the ionisation spectra and known transition cross-sections. Proportional counters can be operated with no buffer gas and thus no amplification, but the sensitivity of the resonant ionisation detection is greatly

reduced.

The two photon ionisation of Rb_2 molecules occurs over a wide spectral range (~10 nm) and has a much larger cross-section than the two photon resonant ionisation of rubidium atoms. In a mass spectrometer the dimer signals from all the alkali metals may cause significant interference with atomic signals at the same mass. At a temperature of ~100° C the Rb_2 ion signal was found to be less than 1% of the atomic Rb signal when detected in the quadrupole mass spectrometer. The use of pulsed laser ablation and ion sputtering techniques to vapourise samples may enhance the formation of these dimers, and this was demonstrated in the laser ablation/ionisation of rubidium chloride in the time of flight mass spectrometer. With a rubidium sample of parts per ten the Rb_2 ionisation was approximately 10% of the atomic signal, although at low concetrations of alkali metals (< parts per thousand) dimer ions were not evident. The sputtering of dimers from ion bombardment was not detected, although the signal may have been obscured by a large secondary ion background. Kimock et al (1984) has estimated that up to 10% of the sputtered sample may be in the form of clusters of atoms.

The broadening of the 5s-6p resonant transition was found to be roughly proportional to the square root of the laser flux. The cause was tentatively suggested as being due to spectral irregularities in the dye laser pulse (Nogar et al 1985). This broadening may limit the selectivity of the resonant ionisation process at high laser powers.

8.4 FUTURE EXPERIMENTS

Proportional counters operating at atmospheric pressures are extremely sensitive detectors of electrons, and can be calibrated absolutely in that the number of initially formed ion/electron pairs can be determined. They are thus ideally suited to resonant ionisation spectroscopy. However at these high buffer gas pressures the resonant transitions are broadened considerably and the spectral separation of isotope transitions is not feasible. Also the resonant ionisation may be dependent, especially for highly excited states, on the pressure of the buffer gas, which complicates the quantitative analysis of the ionisation process. The present combination of proportional counter and quadrupole mass spectrometer with a single excimer pumped dye laser, is potentially a powerful instrument for the spectroscopic analysis of resonant ionisation. The quadupole mass spectrometer serves two purposes, mass separation of the ions

making spectroscopic analysis much simplier, and the elimination of the buffer gas, thus rendering possible the measurement of resonant ionisation yields. Preliminary tuning of the time of flight mass spectrometer is still in progress, and trace element detection will shortly be attempted.

ATOMIC AND MOLECULAR SPECTROSCOPY

The proportional counter may be used to determine the position of autoionisation states in multielectron atoms. These states may increase the photoionisation cross-section of such atoms, increasing the efficiency of their detection. Atoms with two valence electrons and low ionisation potentials would be the most suitable elements with which to begin these studies. Magnesium, calcium and barium have ionisation potentials below 8 eV. However the temperature of these atoms would need to be raised to around 350° C in order to detect their ions in the proportional counter, which would require the addition of a low temperature oven ($\sim500^{\circ}$ C).These elements may also be detected in the time of flight instrument with vapourisation by laser ablation or high energy ion sputtering.

Molecules of toluene have been detected in the proportional counter at concentrations of the order of 1 part in 10^8, (Towrie et al 1986). The detection of other organic molecules at low concentrations, such as trinitrotoluene, is of considerable interest. Work is under way at Glasgow to design a proportional counter to obtain the two photon resonant ionisation spectra of molecules which have very low vapour pressures at room temperature. These spectra may provide identifiable "finger prints" of such molecules. A laser will be used to ablate and vapourise the molecular sample if it is found that the room temperature vapour pressure is not high enough to detect its ionisation.

Proportional counters may also be used as reference chambers with which to calibrate the wavelength of the dye lasers used in the time of flight mass spectrometer. In trace analysis with small samples it would be desirable if the dye lasers could be accurately set to the resonant transitions of the sample in question. This could be achieved by putting a much larger amount of the sample in a proportional counter, using this counter to set the wavelengths of the dye lasers so as to maximise the resonant ionisation.

Singhal (1988b) has shown that population rate equations can predict, to within a factor of ~4, the saturation conditions experimentally determined by Bekov et al (1978a), for the three photon resonant excitation plus field ionisation of ytterbium. Similar calculations, to determine the validity of population rate equations as a model of resonant ionisation for the simpler two and three level cases will be attempted. This will require knowing the ion yields for the process, as well as parameters such as the spectral, spatial and temporal profiles of the laser pulses. The quadrupole mass spectrometer could be used to determine the ion yields of the two photon resonant ionisation of atoms. The laser parameters have not been determined accurately at present, but experiments are underway to measure these.

A major problem lies in the calibration of the quadrupole mass spectrometer, that is in determining, from the output signal from the channeltron ion detector, the number of ions created by the laser in the ion cage. An attempt was made at this, using the proportional counter as the standard, the assumption being that, at a given laser flux, the number of ions created in the ion cage could be the same for the proportional counter and the mass spectrometer. However this calibration was not conducted at high enough laser powers to saturate the ionisation, and no account was taken of the effect of the buffer gas on the ionisation in the proportional counter. If the proportional counter is to be used to calibrate the quadrupole mass spectrometer, a better understanding of collisional ionisation is needed. The modelling of the ionisation of Rydberg states, as shown in chapter 5, is an example of how a simple theory of collisional ionisation can be applied to future experiments. The dependence of Rydberg ionisation on the pressure of the buffer gas and on different constituents of the buffer gas could be investigated. The mass spectrometer would enable efficient detection of the ions at very low pressures. With a more realistic model of collisional ionisation in the proportional counter the degree of collisional enhancement of the ionisation of Rydberg levels could be determined, and the detection efficiency of the quadrupole mass spectrometer more accurately calibrated.

MODIFICATIONS TO THE PROPORTIONAL COUNTER/QUADRUPOLE MASS SPECTROMETER

The versatility of the instrument would be enhanced if a more effective means was used to vapourise the sample. Presently atoms are emitted into the ionisation volume from

the bulk of the sample at saturated vapour pressure at room temperature, or slightly above (100° C). This is not suitable for atoms or molecules which have low vapour pressures near room temperatures. An electrically heated oven, thermally insulated from the rest of the instrument, and operating up to around 500° C, would increase the number of different species of atoms that could be detected in both the proportional counter and mass spectrometer. It could also be used to control the pressure of the sample.

This method would not be suitable for less stable molecules, which would require the more costly approach of vapourisation by laser or ion ablation. The time of flight instrument which has this facility, and also has a much greater mass range, would thus be more suitable for resonant ionisation mass spectroscopy of molecules with low vapour pressures and high masses.

TIME OF FLIGHT MASS SPECTROMETER

This instrument has been designed for the detection of small numbers of atoms sputtered from solid samples, and future experiments will be based on this. However with two independently tunable dye lasers many more elements can be resonantly ionised, and spectroscopic experiments will also be carried out. Suitable experiments include the search for autoionisation levels in two electron atoms, and the investigation of so called isotope effects in resonant ionisation. An isotope effect is the preferential ionisation of one isotope over another which may occur even with saturated ionisation using broad band lasers. Recent studies have suggested that preferential ionisation may occur, which could invalidate the important assumption of equal ionisation probabilities for all isotopes using broad band lasers, (Fairbank et al 1988).

The current sensitivity of the time of flight mass spectrometer, in pulsed ion sputtering mode, has been estimated at 10 ppb, for those elements that can be resonantly ionised using single photon steps. Further studies using NBS coal samples will attempt to realise this limit. The detection of long-lived low energy β^{-} emitters such as ^{129}Iodine may then be attempted.

Ackerhalt J.R., Eberly J.H.,; Phys. Rev. A, 14, 1976, p1705

Ackerhalt J.R.,Shore B.W.; Phys. Rev. A, 16, 1977, p277

Agostini P., Barjot G., Bonnal J.F., Mainfray G., Manus C., Morellec J.; IEEE J. Quant. Electronics, QE-4, 1968, p667

Ambartsumyan R.V., Kalinin V.N., Letokhov V.S.; Sov. Phys. JETP Lett., 13 1971, p217

Ambartsumyan R.V., Letokhov V.S.; Applied Optics, 11, 1972, p354

Ambartsumyan R.V., Bekov G.I., Letokhov V.S., Mishin V.I.; Sov. Phys. JETP Lett., 21, 1975, p279

Ambartsumyan R.V., Apatin A.M., Letokhov V.S., Makarov A.A.,Mishin V.I., Puretskii A.A., Furzikov N.P.; Sov. Phys. JETP, 43, 1976, p866

Antonov V.S., Knyazev I.N., Letokhov V.S., Matuik V.M., Movshev V.G., Potapov V.K.; Optics Letters, 3, 1978, p37

Austin W.E., Holme A.E., Leck J.H.; Quadrupole Mass Spectrometry, (chapter 4), Elsevier Science Publishers 1976

Bates D.R. and Damgaard A.; Phil. Trans. A, 242 ,1949, p101

Bayfield J.E. and Koch P.M.; Phys. Rev. Lett., 33, 1974, p258

Baxter M.S.; Marine Pollution Bulletin, 14, 1983, p126

Bebb H.B., Gold A.; Phys. Rev., 143, 1966, p1

Bebb H.B.; Phys. Rev., 149, 1966, p25

Bebb H.B.; Phys. Rev., 153, 1967, p23

Becker C.H. and Gillen K.T.; Anal. Chem., 56, 1984, p1671

Becker C.H. and Gillen K.T.; J. Opt. Soc. Am. B, 2, 1985, p1438

Beekman D.W., Callcott T.A., Kramer S.D., Arakawa E.T., Hurst G.S., Nussbaum E.; Int. J. Mass Spectrom. Ion Phys., 34, 1980, p89

Bekov G.I., Letokhov V.S., Matveev O.I., Mishin V.I.; Optics Letters, 3, 1978a, p159

Bekov G.I., Letokhov V.S., Matveev O.I., Mishin V.I.; Sov. Phys. JETP, 48, 1978b, p1052

Bekov G.I., Yegorov A.S., Letokhov V.S., Radaev V.N.; Nature, 301, 1983a, p410

Bekov G.I. and Letokhov V.S.; Appl. Phys. B, 36, 1983b, p161

Bekov G.I., Letokhov V.S., Radaev V.N.; J. Opt. Soc. Am. B, 2, 1985, p1554

Bekov G.I., Kudryavtsev Y.A., Auterinen I., Likonen J.; Resonance Ionisation Spectroscopy 1986, Inst. Phys. Conf. Ser. No. 84.

Bethe H.A., Jackiw R. Intermediate Quantum Mechanics, Benjamin Cummings Publishing Company 1986

Bjorkholm J.E., Liao P.F.; Phys. Rev. Lett., 33, 1974, p128

Boerner H., 1985, (private communication)

Boesl U., Neusser H.J., Schlag E.W.; J. Chem. Phys., 72, 1980, p4327

Boesl U., Neusser H.J., Weinkauf R., Schlag E.W.; J. Phys. Chem., 86, 1982, p4857

Bonch-Bruevich A.M., Przhibelskii S.G., Federov A.A., Khromov V.V.; Sov. Phys. JETP, 44, 1976, p909

Bonch-Bruevich A.M., Przibelskii S.G., Khromov V.V.; Sov. Phys. JETP, 45, 1977, p912

Bransden B.H., Joachaim C.J., Physics of atoms and Molecules, Longman Group Ltd 1983

Brophy J.H., Rettner C.T., Chem. Phys. Lett., 69, 1979, p351

Brunnee C.; Int. J. Mass. Spectro. Ion. Proc., 76, 1987, p507

Burgess A. and Seaton M.J.; Mon. Not. R. astr. Soc., 120, 1960, p121

Cannon B.D., Bushaw B.A., Whitaker T.J.; J. Opt. Soc. Am. B, 2, 1985, p1542

Chen C.H., Hurst G.S.,Payne M.G.; Chem.Phy.Lett., 75,1980, p473

Chin S.L., Lambropoulos P., Multiphoton Ionisation of Atoms, Academic Press 1984

Clark C.W., Fassett J.D., Lucatorto T.B., Moore L.J., Smith W.W.; J. Opt. Soc. Am. B, 2, 1985, p891

Collins C.B., Johnson B.W., Popescu D., Musa G., Pascu M.L., Popescu I.; Phys. Rev. A, 8, 1973, p2197

Collins C.B., Johnson B.W., Mirza M.Y., Popescu D., Popescu I.; Phys. Rev. A, 10, 1974, p813

Collins C.B., Curry S.M., Johnson B.W., Mirza M.Y., Chellehmalzadeh M.A., Anderson J.A., Popescu D., Popescu I.; Phys. Rev. A., 14, 1976, p1662

Collins C.B., Lee F.W., Anderson J.A., Vicharelli P.A., Popescu D, Popescu I.; J. Chem. Phys., 74, 1981a, p1067

Collins C.B., Anderson J.A., Popescu D., Popescu I.; J. Chem. Phys., 74, 1981b, p1053

Compton R.N., Stockdale J.A. Cooper C.D., Tang X., Lambopoulos P.; Phys. Rev. A, 30, 1984a, p1776

Compton R.N.,Klots C.E., Stockdale J.A.D., Cooper C.D.; Proc. 2nd. Topical Meeting on Laser Techniques in the Extreme Ultra-Violet, A. J. P., 119, 1984b, p101

Crance M.; J. Phys. B; Atom. Molec. Phys., 13, 1980, p101

Dermtroder W., Laser Spectroscopy, Springer-Verlag 1982

Dobryshin V.E., Karpov N.A., Kotochigova S.A., Krynetskii B.B., Mishin V.A., Stelmakh O.M., Shustryakov V.M.; Opt Spectrosc. (USSR), 54, 1983, p244

Dodhy A., Stockdale J.A., Compton R.N., Tang X., Lambropoulos P., Lyras A.; Phys. Rev. A, 35, 1987, p2878

Donohue D.L., Young J.P., Smith D.H.; Int. J. Mass Spectrom. Ion Phys.,43, 1982, p293

Donohue D.L., Smith D.H., Young J.P., McKown H.S., Pritchard C.A.; Anal. Chem., 56, 1984, p379

Drummond D.L., Schlie L.A.; J. Chem. Phys., 65, 1976, p2116

Drysdale S.L.T., Ledingham K.W.D., Raine C., Smith K.M., Smyth M.H.C., Stewart D.T., Houston C.M., Towrie M.; Nucl. Inst. and Meth., A252, 1986, p521

Ducas T.W., Littman M.G., Freeman R.R., Kleppner D.; Phys. Rev. Lett., 35, 1975, p366

Duman E.L., Shmatov I.P.; Sov. Phys. JETP, 51, 1980, p1061

Edelstein S. A. and Gallagher T.F.; Advances in Atomic and Molecular Physics, 14, 1978, p365

Fassett J.D., Travis J.C., Moore L.J., Lytle F.E.; Anal. Chem.,55, 1983, p765

Fassett J.D., Moore L.J., Shidler R.W., Travis J.C.; Anal. Chem. 56, 1984a, p203

Fassett J.D., Powell L.J., Moore L.J.; Anal. Chem., 56, 1984b, p2228

Fairbank Jr W.M., Hansch T.W., Schawlow A.L.; J. Opt. Soc. Am., 65, 1975, p199

Fairbank Jr W.M., Hutchinson J.M.R., Inn K.G.W., Parks J.E., Spaar M.T., Proc. 4th. Int. Symposium on Resonance Ionisation Spectroscopy and Applications 1988, (to be published)

Filipovicz P., Meystre P., Rempe G., Walther H.; Optica., 32, 1985, p1105

Feneuille S., Jaquinot P.; Advances in Atomic and Molecular Physics, 17, 1981, p99

Gallagher T.F., Edelstein S.A., Hill R.M.; Phys. Rev. Lett., 35, 1975, p644

135

Gallagher T.F., Humphrey L.M., Cooke W.E., Hill R.M., Edelstein S.A.; Phys. Rev. A, 16, 1977, p1098

Gallas J.A., Leuchs G., Walther H., Figger H.; Advances in Atomic and Molecular Physics, 20, 1985, p413

Gold A. and Bebb H.B.; Phys. Rev. Lett., 14, 1965, p60

Gontier Y. and Trahin M.; J.Phys. B: Atom. Mol. Phys., 11, 1978, pL131

Gontier Y. and Trahin M.; Phys. Rev. A, 19, 1979, p264

Gontier Y. and Trahin M.; J. Phys. B: Atom. Molec. Phys., 13, 1980, p259

Goppart-Mayer M., Ann. Physik, 9, 1931, p273

Granneman E.H.A., Klewer M., Nygaard K.J., Van der Wiel M.J.; J. Phys. B; Atom. Molec. Phys., 9, 1976, p865

Gross R.W.F.; Proc. Soc. Photo-Opt. Instrum. Eng., 49, 1974, p135

Grossman L.W., Hurst G.S., Payne M.G., Allman S.L.; Chem. Phys. Lett., 50, 1977, p70

Gupta R., Happer W., Wagner J., Wennmyr E.; J. Chem. Phys. 68, 1978, p799

Halverson J.E.; Nucl. Inst. and Meth., 223, 1984, p349

Handbook of Chemistry and Physics 53th ed., Chemical Rubber Publishing Co. 1973

Harvey K.C., Stoicheff B.P.; Phys. Rev. Lett., 38, 1977, p537

Hecht E., Zajac A.; Optics, Addison-Wesley Publishing Company 1974

Held B., Mainfray G., Manus C., Morellec J.; Phys. Lett., 35A, 1971, p257

Held B., Mainfray G., Manus C., Morellec J.; Phys. Rev. Lett., 28, 1972, p130

Held B., Mainfray G., Manus C., Morellec J., Sanchez F.; Phys. Rev. Lett., 30, 1973, p423

Heitler W., Quantum Theory of Radiation, Oxford University Press, 1954

Herzberg G., Molecular Spectra and Molecular Structure I., D. Van Nostrand Company Inc. 1957

Houston C.M., Drysdale S.L.T., Jennings R., Land A.P., Ledingham K.W.D., Singhal R.P., Smyth M.H.C., Stewart D.T., Towrie M.; 1988   (to be published)

Houston C.M., Glasgow University, Ph.D. thesis 1986

Hubricht G., Kleinknect K., Muller E., Pollman D., Teupe E.; Nucl. Inst. and Meth., 228, 1985, p327

Hurst G.S., Payne M.G., Nayfeh M.H., Judish J.P., Wagner E.B.; Phys. Rev. Lett., 35, 1975, p82

Hurst G.S., Nayfeh M.H., Young J.P.; Appl. Phys. Lett., 30, 1977, p229

Hurst G.S., PayneM.G., Kramer S.D., Young J.P.; Rev. Mod. Phys., 51, 1979a, p767

Hurst G.S., Kramer S.D., Payne M.G., Young J.P.; IEEE Transactions on Nuclear Science, NS-26, 1979b, p133

Hurst G.S., Resonance Ionisation Spectroscopy 1986, Inst. Phys. Conf. Ser No. 84

Johnson P. M. and Otis C.E.; Ann. Rev Phys. Chem., 32, 1981, p139

Kappes M.M., Schar M., Schumacher E.; J. Phys. Chem., 89, 1985, p1499

Kaulakys B. and Svedas V.; J. Phys. B: At. Mol. Phys., 20, 1987a, L565

Kaulakys B., Ciziunas A.; J. Phys. B: At. Mol. Phys., 20, 1987b, p1031

Keldysh L.V.; Sov. Phys. JETP 20, 1965, p1306

Kimock F.M., Baxter J.P., Winograd N., Surf. Sci. 124, 1983, pL41

Kimock F.M., Baxter J.P., Pappas D.L., Kobrin P.H., Winograd N.; Anal. Chem., 56, 1984, p2782

Kliger D.S., Ultrasensitive Laser Spectroscopy, Academic Press 1983

Klots C.E. and Compton R.N.; Phys. Rev. A, 31, 1985, p525

Kronert U., Bonn J., Kluge H.J., Ruster W., Wallmeroth K., Peuser P., Trautmann N.; Appl. Phys. B, 38, 1985, p65

Ledingham K.W.D., Raine C., Smith K.M., Smyth M.H.C., Stewart D.T., Towrie M., Houston C.M.; Nucl. Inst. Meth. A241, 1985, p441

Lee Y.T., Mahan B.H.; J. Chem. Phys., 42, 1965, p2893

Letokhov V.S., Chebotayev V.P.; Laser Analytical Spectroscopy, Springer-Verlag, 4, 1977

Letokhov V.S.; Laser Photoionisation Spectroscopy, Academic Press 1987

Levenson M.D., Introduction to Non-linear Laser Spectroscopy, Academic Press 1982

Liberman S. and Pinard J.; Phys. Rev. A., 20, 1979, p507

Loudon R.; The Quantum Theory of Light, Clarendon Press, 1973

Luc-Koenig E., Liberman S., Pinard J.; Phys. Rev. A, 20, 1979, p519

137

Mamyrin B.A., Karataev V.I., Shmikk D.V., Zagulin V.A.; Sov. Phys. JETP, <u>37</u>, 1973, p45

Meyerand Jr., R.G. and Haught A.F.; Phys. Rev. Lett., <u>11</u>, 1963, p401

Meyerand Jr., R.G. and Haught A.F.; Phys. Rev. Lett., <u>13</u>, 1964, p7

Miller C.M., Nogar N.S., Gancarz A.J., Shields W.R.; Anal. Chem., <u>54</u>, 1982, p2377

Miller C.M., Engleman R., Keller R.A.; J. Opt. Soc. Am. B, <u>2</u>, 1985, p1503

Mihajlov A.A., Janev R.K.; J. Phys. B: At. Mol. Phys., <u>14</u> , 1981, p1639

Moore L.J., Fassett J.D., Travis J.C.; Anal. Chem., <u>56</u>, 1984, p2770

Moore L.J., Fassett J.D., Travis J.C., Lucatorto T.B., Clark C.W.; J. Opt. Soc. Am. B <u>2</u>, 1985, p1561

Morellec J., Normand D., Petite G.; Phys. Rev. A, <u>14</u>, 1976, p300

Morellec J., Normand D., Mainfray G., Manus C.; Phys. Rev. Lett., <u>44</u>, 1980, 1394

Morrison G.H., Secondary Ion Mass-Spectrometry SIMS III, Springer-Verlag <u>19</u> 1981 p224

Niemax K.; Appl. Phys. B, <u>32</u>, 1983, p59

Nogar N.S., Keller R.A.; Analytical Chemistry, <u>57</u>, 1985, p2992

Normand D., Morellec J.; J. Phys. B: Atom. Molec. Phys., <u>13</u>, 1980, p1551

Otis C.E., Johnson P.M.; Chem Phys. Lett., <u>83</u>, 1981, p73

O'Shea D.C., Callen W.R., Rhodes W.T., An Introduction to Lasers and their Applications, Addison-Wesley Publishing Company 1978

Palmer B. A., Engleman R. Jnr., Keller R.A.; An Atlas of Uranium Emission Intensities in a Hollow Cathode Discharge, Los Alamos Scientific Laboratory Report, LA-8251-MS, July 1980

Parks J.E., Schmitt H.W., Hurst G.S., Fairbank Jr. W.M., Laser Based Ultrasensitive Spectroscopy and Detection, Proc. SPIE 426, 1983, p32

Parks J.E., Beekman D.W., Schmitt H.W., Spaar M.T.; "Ultrasensitive Elemental Analysis of Materials using Sputter Initiated Resonance Ionization Spectroscopy", Talk presented to the 1985 Spring Meeting of Materials Research Society, at the Golden Gateway Holiday Inn, San Francisco, California, April 15-18 1985

Peach G.; Mem. R. astr. Soc. <u>71</u>, 1967, p13

Peuser P., Herrmann G., Rimke H., Sattelberger P., Trautmann N., Ruster W., Ames F., Bonn J., Kluge H.J., Kronert U., Otten E.W.; Appl. Phys. B, <u>38</u>, 1985, p249

Pichler G.; J. Quant. Spectrosc. Radiat. Transfer, 16, 1976, p147

Pindzola M.S.; Proc. 2nd. Topical Meeting on Laser Techniques in the Extreme Ultra-Violet, A. J. P., 119, 1984a, p150

Pindzola M.S., Glasser A.H., Payne M.G.; Phys. Rev. A, 30, 1984b, p1800

Pindzola M.S.; Phys. Rev. A, 32, 1985, p1883

Price D. and Milnes G.J.; Int. J. Mass Spectrom. Ion Proc., 60, 1984, p61

Raine C., Ledingham K.W.D., Smith K.M., Nucl. Instr. and Methods, 217, 1983, p305

Samson J.A.R.; Advances in Atomic and Molecular Physics, 2, 1966, p240

Sansonetti C.J., Lorenzen C.J.; Phys. Rev. A, 30, 1984, p1805

Singhal R.P., 1988a   (to be published)

Singhal R.P., 1988b   (to be published)

Singhal R.P., Land A.P., Ledingham K.W.D., Towrie M.; Proc. 4th. Int. Symposium on Resonance Ionisation Spectroscopy and Applications 1988c,   (to be published)

Sobelman I.I., Atomic Spectra and Radiative Transitions, Springer-Verlag 1979

Stebbings R.F., Latimer C.J., West W.P., Dunning F.B., Cook T.B.; Phys. Rev. A, 12, 1975, p1453

Thompson D.C., Weinberger E., Xu G.X., Stoicheff B.P.; Phys. Rev. A, 35, 1987, p690

Townsend P.D., Kelly J.C., Hartley N.E.W.; Ion Implantation, Sputtering and their Applications, Academic Press 1976

Towrie M., Cahill J.W., Ledingham K.W.D., Raine C., Smith K.M., Smyth M.H.C., Stewart D.T., Houston C.M.; J. Phys. B: At. Mol. Phys., 19, 1986, p1989

Towrie M., Glasgow University, Ph.D. thesis 1987

Towrie M., Drysdale S.L.T., Jennings R.,Land A.P.L., Ledingham K.W.D., McCombes P., Singhal R.P., Smyth M.H.C., Stewart D.T., Proc. 4th. Int. Symposium on Resonance Ionisation Spectroscopy and Applications 1988,   (to be published)

Tursunov A.T. and Eshkobilov N.B.; Opt. Spectrpsc. (USSR) 58,1985, p607

Ultraviolet Atlas of Organic Compounds; London : Butterworths; Weinheim: Verlag-Chemie 1966

Voronov G.S. and Delone N.B.; Sov. Phys. JETP Lett., 1, 1965, p66

Wagner G. S., Isenor N.R.; Can. J. Phys., 63, 1985, p976

Weber K.H., Sansonetti C.J.; Phys. Rev. A, 35, 1987, p4650

Weiner J., Boulmer J.; J. Phys. B; At. Mol. Phys., 19, 1986, p599

Weise W.L., Martin G.A.; Wavelengths and Transitions for Atoms and Atomic Ions, NSRDS-NBS 68, National Bureau of Standards 1980

Whitaker T.J.; Bushaw B.A.; Chem. Phys. Lett., 79, 1981, p506

Winograd N., Baxter J.P., Kimock F.M.; Chem. Phys. Lett., 88, 1982, p581

Woodgate G.K., Elementary Atomic Structure, Clarendon Press 1983

Young C.E., Pellin M.J., Calaway W.F., Jorgensen B., Schweitzer E.L., Gruen D.M.; Nucl. Inst. and Meth. B, 27, 1987, p119

Zakheim D.S., Johnson P. M.; Chem. Phys., 46, 1980, p263

Zandee L., Bernstein R.B., Lichtin D.A.; J. Chem. Phys., 69, 1978, p3427

Zandee L., Bernstein R.B.; J. Chem. Phys., 71, 1979, p1359

Zhang J.Y.; Resonance Ionisation Spectroscopy 1986, Inst. Phys. Conf. Ser., No. 84, 1986, p195